Durham E-Theses

Nonlinear optical characterisation of organic chromophores and aspects of molecular aggregation

Hackman, Nancy-Ann

How to cite:

Hackman, Nancy-Ann (2001) *Nonlinear optical characterisation of organic chromophores and aspects of molecular aggregation*, Durham theses, Durham University. Available at Durham E-Theses Online: http://etheses.dur.ac.uk/3822/

Use policy

The full-text may be used and/or reproduced, and given to third parties in any format or medium, without prior permission or charge, for personal research or study, educational, or not-for-profit purposes provided that:

- a full bibliographic reference is made to the original source
- a link is made to the metadata record in Durham E-Theses
- the full-text is not changed in any way

The full-text must not be sold in any format or medium without the formal permission of the copyright holders.

Please consult the full Durham E-Theses policy for further details.

Academic Support Office, Durham University, University Office, Old Elvet, Durham DH1 3HP
e-mail: e-theses.admin@dur.ac.uk Tel: +44 0191 334 6107
http://etheses.dur.ac.uk

Nonlinear Optical Characterisation of Organic Chromophores and Aspects of Molecular Aggregation

A thesis submitted for the degree of
Doctor of Philosophy

The copyright of this thesis rests with the author. No quotation from it should be published in any form, including Electronic and the Internet, without the author's prior written consent. All information derived from this thesis must be acknowledged appropriately.

by

Nancy-Ann Hackman

University of Durham
Department of Physics

April 2001

17 SEP 2001

Abstract

The work presented in this thesis describes an investigation into the properties and behaviour of a new class of nonlinear optical organic chromophores. This study contributes to the optimisation of nonlinear optical molecules through an improved understanding of the relationships between the molecular nonlinear optical properties and the measured macroscopic quantities.

A series of highly dipolar non-linear optical chromophores with absorption typically in the range of 350-500 nm have been synthesised by the reactions of amines with tetracyanoquinodimethane (TCNQ). One of the advantages of these materials is the large molecular figure of merit ($\mu\beta$, where μ is the molecular dipole moment and β is the second order polarisability), which theoretically allows large nonlinear optical coefficients to be obtained.

The molecular dipole moments of these chromophores were determined both experimentally and theoretically, and were found to agree. The nonlinear optical properties of these compounds in solution were studied using an electric field induced second harmonic generation (EFISH) technique. The measurements of $\mu\beta$ at 1064 nm and 1907 nm in chloroform and acetone are presented. Moderate $\mu\beta$ values were obtained but β is found to be unexpectedly small in chloroform and shows unusual dispersion characteristics in this solvent compared to acetone. Further concentration investigations revealed features that suggest the presence of aggregates within solution. Optical spectroscopy measurements provide evidence of new species whose presence and conformation were found to be solvent-dependent. The results of this work highlight the need for an entire concentration range to be studied if accurate determination of molecular properties of highly dipolar molecules is required.

Guest-host polymer films of these materials have been corona poled using a constant current corona triode. Detailed characterisation studies of the second order nonlinearities using second harmonic generation (SHG) were compared to a less dipolar molecule. These investigations showed that the highly dipolar TCNQ derivatives show severe aggregation within the polymer films. The magnitude of the SHG that can be obtained from such systems is therefore limited by this aggregation.

Declaration

I hereby declare that work reported in this thesis has not previously been submitted for any degree and is not being currently submitted in candidature for any other degree.

Signed.....

Candidate

The work reported in this thesis was carried out by the candidate. Any work not carried out by the candidate is acknowledged in the main text.

Signed.....

PhD Supervisor

Signed.....

Candidate

Statement of Copyright

The copyright of this thesis rests with the author. No quotation should be published without her prior written consent and information derived from it should be acknowledged.

Acknowledgements

As my graduate education nears its conclusion, I wish to express my deepest appreciation to those who have contributed to this thesis. There are a large number of people who should be thanked for their help, support and encouragement.

Firstly, I would like to thank my supervisor, Dr. Graham Cross for his guidance and patience throughout the course of this work. His supervisory style has allowed me to learn and develop my understanding of the details of this work in particular, and science in general. I would also like to thank Professor David Bloor for his helpful discussions, advice and attention throughout the research project.

I am very grateful to Professor Joseph Zyss for allowing me to work in his group, LPQM, at the Ecole Normale Supérieur in Cachan, Paris. During my time in Paris, I worked closely with Isabelle Ledoux-Rak and Sandrine Deveau. I would like to thank them and the whole group for welcoming me wholeheartedly and helping me with my research. I would also like to thank Dr. Robert Blum of Professor Eich's group in Germany for providing measurements on our poled samples and for his advice and enthusiasm about my work.

I would like to thank the Physics Faculty Heads of Department for allowing me to use the facilities for my research, Professor Mike Pennington and Professor Brian Tanner. A big thank you must go to the technical staff at the Physics department as their help as been invaluable. Norman Thompson and Davey Patterson have always been very kind, and have always found time to help me. The electronic workshop has been very patient and helpful, and the mechanical workshop has also provided assistance and expertise and I would like to thank them all.

I would like to thank EPSRC and Corning (formerly BICC) for providing funding.

Dr. Marek Szablewski has provided ongoing support throughout my time in Durham that is deeply appreciated. I have welcomed and enjoyed our many discussions about my work and materials. I have had numerous discussions with him and his wife, Lucy, and am grateful for their kindness to me. I would like to thank him for his advice, enthusiasm, kindness and patience. In addition to this, he and Dr. Ravi Mosurkal have

made the crucial contribution of synthesising the molecules for this work and I wish to thank them both for their perseverance and patience of my pleading for more quantities of materials!

I would like to thank the outgoing and incoming members of the group. The group fosters a lively, friendly spirit. The daily interaction of with my coworkers provided me with an enjoyable atmosphere in which to work as well as many interesting discussions and speculations about the work. Dr. Maria Farsari, Dr. Marek Szablewski, Dr. Phil Thomas, Dr. Anna Thornton, Dr. Yasu Kagawa, Dr. Yitao Ren and Christoph Renger welcomed me into the group when I first joined. During the course my research, Dr. Paul Laughlin, Dr. Naveed Zaidi, Dr. Ravi Mosurkal, Dr. Lars-Olof Pålsson, Dr. Marcus Swann, Dr. Kenny Donnelly and Phil Hands have all made my life more interesting and enjoyable as part of this group as well as being a great help to me, and I thank them all. Akira Masutani has shown immeasurable kindness and patience with me and I would like to thank him for being my friend and a computer expert!

In addition I would like to thank my other friends and colleagues who are members of the Physics Department for contributing to the enjoyable atmosphere in the research labs. The friends I have made during my time in Durham have supported me and helped me to retain some sanity, and I would like to say a big thank you to them, Daniel Azzopardi, Tom Bennett, Anthony Bimbi, Jeremy Bull, Rebecca Collis, Andrew Clydesdale, Stuart Dailey, Ian Daniel, Robert Gregson, Sharon Fairless, Brian Fulthorpe, Tom Hase, Amanda Hunter, Peter Jarvis, Isobel Johnson, Catherine McKenner, Mark Leeson, Sarah and John Maguire, Rachel Pick, Dan Read, Michael Swinhoe, Rachel Swinhoe, Jonathan Terry, and Colin Weir.

I would also like to thank my close friends Sarah Edenbrow and Adèle Duperouzel for their support, love and friendship during my time in Durham.

I wish to express my deepest gratitude to my family, my brother and in particular my parents, without whom completion of this thesis would have been impossible. I would like to thank them for their love and continual encouragement. They have offered support of every kind throughout the course of my entire education and have always been extremely understanding, especially at times when I have needed it most.

"Nothing in life is to be feared.
It is only to be understood."

Marie Curie- Skłodowska

TABLE OF CONTENTS

LIST OF FIGURES

Chapter 1

Chapter 2

Chapter 3

Chapter 4

Chapter 5

LIST OF TABLES

Chapter 1 : Introduction

The mid to late 70's saw the arrival of telecommunications using optical fibres. The possibility to use photons instead of electrons to collect, store, process and transmit data was seen to be a key technology for future devices. Since then, the increased demand of high speed computing in daily life has lead to the birth of the optical information highway. The development of the information highway requires the production of high-speed modulators and switches. Optical fibre telecommunication networks have now been installed worldwide and play a major role in the information infrastructure. Although optical networks are becoming a major component of the information infrastructure from global to consumer premises, there are remaining issues regarding technological and economical breakthroughs. Future networks must meet the requirements of multimedia nature and wideband traffic. This has proved to be a significant stimulus for the explosion of effort into research of nonlinear optics, (NLO) during the last thirty years and it is now an established area of research.

Nonlinear optics is the study of the interaction of electromagnetic fields and matter in which the material's polarisation responds in a nonlinear manner. This is in contrast with the usual optical properties, such as absorption and refractive index, in which the polarisation response is a linear function of the applied field. When an intense coherent optical beam, such as that from a laser is incident on a material, the microscopic polarisation response is proportional to both the input field, and proportional to higher orders of the input field. The proportionality factors are the susceptibilities ($\chi^{(n)}$, where n is an integer) from which macroscopic polarisabilities are observed. The nonlinear response may result in changes in phase, frequency or other propagation characteristics of the incident beam. The manipulation of the beam in this manner, known as photonics technology, is extremely useful in the telecommunication industry.

Nonlinear optical devices are likely to be a key component for optical data transmission processes [1]. The primary focus of nonlinear optics has been the development of nonlinear optical materials with large nonlinearities at the telecommunication transmission wavelengths of 1.3 and 1.5 μm. The fundamental processes that govern

NLO effects have been widely investigated in order to deepen the general understanding of the origins of the NLO processes and so support the development of devices [2-7].

Initially, inorganic materials were investigated for their NLO properties [8-11] and currently, inorganic materials are used for most devices. For example, lithium niobate, $LiNbO_3$, is used for electro-optic modulators (with electro-optic coefficients of $r_{33} = 30.9\ pmV^{-1}$ and $r_{13} = 9.6\ pmV^{-1}$ [12]) where the phase of the light beam is modulated. Nuclear motion is responsible for the NLO effect in $LiNbO_3$, which results in a relatively slow response. Conversely, conjugated organic materials show fast responses with highly polarisable $\pi-$electrons [4]. In addition, organic compounds show great improvements in NLO properties when strong donor-acceptor groups can be coupled with each other [13], and when the molecules are well ordered in the medium. Organic materials are promising candidates for future devices because of their potential low cost and ease of fabrication, together with the possibility of offering higher bandwidths and faster modulation speeds than their inorganic counterparts. Thus, organic materials have been the subject of a great deal of investigation [14-26], including the work in this thesis, for photonic applications.

The single mode silica fibre that is already utilised in the trunk network is not necessarily suitable media for short network distances because the small core diameters of the single mode fibre requires accurately designed optical devices and connectors, which increases the total system cost. Currently data from the trunk network is generally converted into electrical signals and distributed to end users by means of local area networks (LAN's) using copper wire. An alternative approach that is becoming more popular is the polymer optical fibre (POF) that overcomes fibre distributing and connecting problems [27]. In general, POF's have high attenuation in the infra-red but adequate transmission at shorter wavelengths used in LAN's (650 nm). As the optical data network is extended ever closer to end users, the demand for inexpensive LAN's based on POF's is expected to increase. Therefore POF's are expected to become a large market since the telecommunications industry requires low cost, mass produced fibres and devices. To achieve low voltage operation of high frequency modulators requires devices with higher electro-optic coefficients than presently available. It was hoped that the organic chromophores studied here would meet this requirement when incorporated into a polymer matrix.

1.1 Aims of this Thesis

This research initiates a study into a class of organic materials with the ultimate goal of their application to opto-electronic devices in local area networks. These materials are derivatives of 7,7,8,8 tetracyanoquinodimethane (TCNQ) and have large optical nonlinearities. These materials provide good optical transmission at wavelengths longer than 500 nm and good thermal stability with decomposition temperatures in the range of 260 to 300 °C.

Evidence has shown that the properties of molecules, such as the dipole moment and polarisability, are very sensitive to molecular environment [28, 29]. This result suggests that the values of dipole moment and hyperpolarisability measured in solution may not be considered a reliable representation of their values in the solid state. In addition, it has recently been suggested that molecular interactions that occur at higher number densities of chromophore may result in a decrease in the overall nonlinearity of the system [30]. In view of the fact that most future devices are likely to be manufactured using thin film technology containing large number densities of NLO molecules, it is therefore important to investigate the nature of the response of chromophores at high number densities in both the solid and solution states. It is clear that this approach must be taken if the properties and behaviour of thin polymer films are to be characterised accurately with a view to device operation. The subject of the studies reported in the body of this work is therefore concerned with the nonlinear optical characterisation of molecules as guests doped into polymer thin films as well as dissolved in solutions.

The aim of this thesis is to understand the behaviour of a particular class of organic materials, where the molecular nonlinear properties are expected to be large. This study attempts to characterise these materials and ascertain the behaviour of the NLO properties compared to those predicted by determining the dipole moment, first hyperpolarisability in solutions, second order NLO susceptibilities, in-situ poling in films and optical spectroscopy of both the solution and solid state. Often, in practice, high macroscopic nonlinearities are not achieved from chromophores with large molecular nonlinearities due to chromophore-chromophore interactions. This effect is

probed in this work by studies of nonlinearities as a function of concentration to elucidate the nature of the reduced signals.

1.2 Outline of Thesis

With the aims of the study having been outlined in the previous section, the following section begins with an introduction of the fundamental concepts of NLO and second order effects in particular. There are a number of excellent reviews and text books on the subject of nonlinear optics and this thesis merely introduces the necessary concepts for this work [1, 2, 4, 5, 12, 26, 31-33]. A brief historical overview of the field is given to set the scene for the work contained in this thesis. This is not an exhaustive list but a representation of just some of the important works in the field of NLO. The features necessary for optimisation of the nonlinearities is described in the remains of this chapter together with an outlook for potential devices.

Chapter 2 introduces the theoretical concepts necessary for the data analysis later in the thesis. To this end the molecular and macroscopic origins of NLO are described. Various models significant to the work are discussed and the relationship between the macroscopic and microscopic nonlinearities is described in terms of conventional thermodynamic models. Molecular interactions are also introduced.

Chapter 3 describes the experimental methods, including details of the laser and detection system useful for a variety of experiments, together with sample preparation and characterisation techniques. A detailed description of the poling rigs that were used to align the dipolar molecules is included. The constant current corona triode had extensive modifications to enable successful poling and these are described. The in-situ rig was designed and built as part of the work of this thesis.

Chapter 4 reports the results of the molecular studies in solution. The results from solvent-dependent electric field induced second harmonic experiments are presented. The data is compared to that expected for these molecules and concentration dependent studies are carried out to investigate the effect of intermolecular interactions on the macroscopic nonlinearity. A novel "zero-fringe" calculation is applied to derive the molecular product, $\mu\beta$. In addition optical spectroscopy as a function of concentration is performed on solutions.

In Chapter 5, the evolution of the bulk susceptibilities with concentration is presented. In-situ poling studies were undertaken to investigate the temporal stability of the poled films and these results are presented in this chapter. The films are also characterised by refractive index measurements. This leads finally to Chapter 6 where the conclusions of the investigations are made. Various aspects of the thermodynamic model approach to the translation of microscopic to macroscopic nonlinearities are also discussed.

1.3 Fundamental Concepts of Nonlinear Optics and Second Order Effects

When a beam of electromagnetic radiation is projected into a material, absorption of the energy causes the charges within the atoms to oscillate. In a linear material, the amount of charge displacement is proportional to the instantaneous magnitude of the electric field. The charges oscillate at the same frequency as that of the incident light. Either the oscillating charges radiate light at that frequency or the energy is transferred into non-radiative modes resulting in material heating or other energy transfer mechanisms.

For an isotropic and homogeneous material, the emitted light travels in the same direction as the incident light beam [34]. The light is effectively "bound" to the material. The light excites charges that re-radiate light that then excites more charges. As a result, the light travels through the material at a lower velocity (exhibiting a phase change) than it does in vacuum. Thus the linear refractive index of a material, n, is defined as the ratio of light speed in vacuum, c, to the speed of light in the material, v. If the motion of some of the charges within the material decays without emitting light, some of the light intensity is lost from the incident beam by scattering and absorbance. The absorbance is defined as the ratio of light exiting a material to the light incident into the material divided by the material thickness. Both the absorbance and refractive index are linear optical properties of a material for low intensity incident light. In the linear regime, measurements of the index of refraction or dielectric constant probe molecular dipole moments and polarisabilities.

In a nonlinear optical material, the displacement of charge from its equilibrium value is a nonlinear function of the electric field. All materials, when exposed to a high enough light intensity show a nonlinear response. A nonlinear optical response can be understood using a simple classical picture. Figure 1.1 shows a plot of the potential

energy and effective polarisation response within a hypothetical material. For small potentials, $U(x)$, the displacement of the charge, x, is small and is approximated by a harmonic potential shown as the smooth curve Figure 1.1 and a linear polarisation response. When the displacement away from equilibrium is large, the harmonic approximation breaks down and the polarisation is no longer a linear function of the applied field, E as shown by the dotted curves in Figure 1.1. In general, nonlinear optical effects are considered to result from nonlinearities in the polarisation response of the medium to incident fields. For a slowly varying electric field, the induced molecular polarisation, p, can be expanded as a power series in the applied electric field, E,

$$p = \mu + \alpha E + \beta\, E \cdot E + \gamma\, E \cdot E \cdot E + \quad \cdots$$

Equation 1.1

where μ is the permanent dipole moment, α is the linear polarisability, and β and γ are the second and third order polarisability (or hyperpolarisability) respectively. The term α describes the linear optical properties of the molecule while β and γ account for the second and third order response of the molecule. For the macroscopic description of the interaction of a medium with light, an analogous power series may be written for the macroscopic polarisation, P, induced in the material by an applied field, E,

$$P = P^0 + \chi^{(1)} E + \chi^{(2)} E \cdot E + \chi^{(3)}\, E \cdot E \cdot E + \quad \cdots$$

Equation 1.2

where P^0 is the permanent polarisation of the medium and $\chi^{(1)}$ is the linear susceptibility and $\chi^{(2)}$ and $\chi^{(3)}$ are the second and third order nonlinear susceptibilities of the material, respectively. Equation 1.1 and Equation 1.2 are introduced here in an *ad hoc* fashion and are described more rigorously with frequency dependence in Chapter 2.

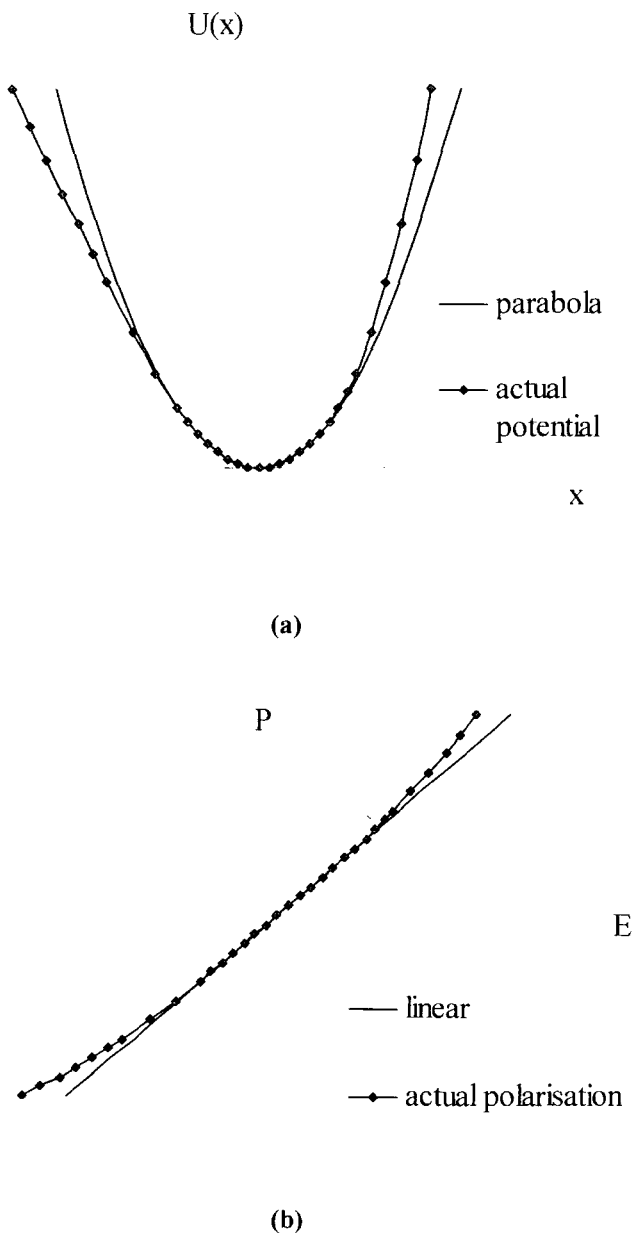

Figure 1.1: Schematic plot of the potential energy function (a) and the polarisation response (b) of a second order NLO material

Second harmonic generation (SHG) or frequency doubling is a nonlinear optical effect, and is an example of a second order response resulting from the molecular β in Equation 1.1 and the $\chi^{(2)}$ susceptibility Equation 1.2, where the response is proportional to the square of the electric field. Symmetry requirements impose the condition that second order effects vanish for centrosymmetric electronic structures. Therefore, to observe second order effects, or indeed any "even order effect" where the response is

proportional to an even power of the applied field, the molecular structure must be asymmetric.

To a first approximation, it is possible to infer the nonlinear optical properties of the bulk medium from those of the constituent molecules and vice versa. The arguments regarding the symmetry of the medium extend to the macroscopic NLO coefficients $\chi^{(2)}$ and are characteristic of the medium. Only if electric dipoles are contributing to the nonlinear effect in non-centrosymmetric media, can bulk SHG be observed.

1.4 Historical Overview of Nonlinear Optics

Although nonlinear optical phenomena can be described by Maxwell's and Schrödinger's equations, it was not until the advent of the laser in 1960 that most nonlinear optical phenomena were discovered [35], with a few notable exceptions. In 1845, Faraday observed a magnetic dependent refractive index; in 1875, the DC Kerr effect was first observed, and in 1893, Pockels studied the linear electro-optic effect, now also known as the "Pockels effect" [34]. Kerr applied a constant voltage across a dielectric medium and found that the polarization angle of a light beam exiting the dielectric depended on the voltage. This is a third-order nonlinear optical effect because the birefringence in the index of refraction depends quadratically on the applied field. The Pockels effect is a linear electro-optic effect as the induced birefringence is proportional to the first power of the applied electric field. However, the introduction of the laser led to the discovery of a wide variety of nonlinear responses at optical frequencies.

Production of second harmonic light was first observed by Franken and co-workers in 1961 [36]. The beam from a ruby laser ($\lambda = 694$ nm) was passed through a quartz crystal and ultraviolet second harmonic generation ($\lambda = 347$ nm) was observed. Since then, researchers have confirmed large numbers of nonlinear optical effects, including second and third harmonic generation, electro-optic effects and optical rectification and have applied them to many practical uses [4, 12, 32, 37].

In 1962, Kleinman studied the theoretical nonlinear dielectric polarization in ionic crystals and predicted that the linear electro-optic coefficients (r) are related to the nonlinear susceptibility tensor, ($\chi^{(2)}$) [38]. Peticolas *et al* were the first to observe

two-photon processes in organic materials [39]. They studied two-photon excitation of a number of polycyclic aromatic molecules by using a ruby laser for the excitation and measuring the fluorescence. Only a year later, Heilmer *et al* experimentally verified Kleinman's prediction that the second harmonic coefficient ($\chi^{(2)}$) and the electro-optic coefficient (r) were directly related in hexamine crystals [40]. This leads to the now well-known conclusion that nonlinear optical effects in organic molecules are almost exclusively electronic in origin. In 1964 Rentzepis and Pao observed the first second harmonic generation from organic crystals [41]. In this study, crystals of 3,4 benzpyrene, 1,2 benzanthracene and anthracene were irradiated with light from a ruby laser. Second harmonic generation was observed for the asymmetric 3,4 benzpyrene and 1,2 benzanthracene crystals but could not be detected from the symmetric anthracene crystals. These studies indicate that absorbing molecular crystals may emit second harmonic generation provided it is allowed by crystal symmetry.

A key advance in the field of NLO was made by Kurtz and Perry by the introduction of the powder SHG technique to estimate the optical nonlinearity of the material [42]. In this method, a laser beam is focused onto a crushed crystalline sample and the intensity of the generated second harmonic light detected. In this way, a measure of the macroscopic second order susceptibility of the crystals is obtained. The results require a powder with a well-determined grain size for an accurate analysis to be obtained. The SHG also depends on the phase-matching and absorption properties of the material. Because of the complicated interpretation of results, this technique is mainly used as a rough screening tool to select materials for further study. When used in this way and provided an accurate determination of the second order susceptibility is not required, this is an extremely quick experiment with facile sample preparation. For this reason, powder SHG experiments are commonly used today to find suitable organic materials for more detailed investigation without the need to grow large crystals.

Following this, Maker observed a fringe pattern of the second harmonic intensity when a thin plane-parallel quartz platelet was rotated in the fundamental beam [9]. These fringes result from dispersion effects from the phase sensitivity of the energy flow between the fundamental and harmonic wave. Thus, if the two waves are non-phasematched, the refractive index dispersion at the fundamental and harmonic frequencies causes light to propagate at different velocities at the two frequencies. As the harmonic light propagates through the medium, overlapping the fundamental wave,

energy flows back and forth between these waves, depending on their phase relationship and this results in different intensities of harmonic light depending on the distance of propagation through the material. These are now known as "Maker fringes" and Jerphagnon and Kurtz analysed the optical arrangement to relate the second harmonic coefficient to the observed intensity variations [43]. They illustrated their method from results of quartz plates. The basis of their mathematical equations are often used today to extract $\chi^{(2)}$ coefficients from angular scans of SHG. This theory was later refined by Herman and Hayden to include reflection of the second harmonic wave from the film-substrate interface, absorption at both the fundamental and second harmonic frequencies and the dispersive nature of the medium [44]. This analysis is used in this thesis and will be discussed in more detail in Chapter 5.

In 1970, Davydov *et al* reported a connection between the second harmonic generation and the nature of the electronic transitions of the molecules [45]. The correlation between the efficiency of second harmonic generation with charge transfer was demonstrated by measuring many organic compounds with different charge transfer characteristics. The largest nonlinearities were seen for organic molecules containing donor and acceptor groups at either end of a conjugated π-electron system. From these experiments, the Russian scientists concluded that charge transfer in molecules enhanced second harmonic generation.

Following this, further experiments were developed to investigate the molecular properties necessary to produce large macroscopic nonlinearities. In particular, the technique of electric field induced second harmonic generation, (EFISH), was developed to determine the molecular hyperpolarisability, β. This method employs a pulse of electric field applied across a solution containing the NLO active chromophores to partially align the molecules and remove the centrosymmetric arrangement. Under such conditions, any hyperpolarisability present can result in the generation of second harmonic signal. This solution technique has been refined and applied to a number of molecules by Levine and Bethea [17, 46-50] and Oudar [13, 25, 51]. Since this technique involves an electric field acting on the dipole moment, μ, of the molecules, the result of the experiment is the molecular product $\mu\beta$. If the molecular hyperpolarisability, β, is required, the dipole moment must be determined through other experiments.

In 1975 the two level model was proposed by Oudar and Chemla to account for the dispersion of the molecular hyperpolarisability [52]. This is a simple model for molecules with intramolecular charge transfer and has been extremely useful in the synthetic design of new NLO systems. Subsequently Lalama and Garito discuss the origin of the second order susceptibility of substituted benzene molecules in terms of a molecular Hartree-Fock calculations [18]. The success of these calculations on predicting the molecular susceptibility arises from the dominant contribution of the valence electrons to the susceptibility. This contribution takes place through the difference between the ground state, and first excited state, dipole moments.

More recently, a model based on the bond length alternation has been introduced to relate the structure of the molecule to nonlinear optical properties [21]. In this work, a description of the linear and nonlinear polarisability is presented in terms of the average differences in length between alternating single and double bonds.

It has been shown that organic materials containing delocalised π-electrons together with electronic asymmetry, such as the class investigated in this work, possess exceptional nonlinear responses compared to inorganic crystals in use today [18, 53, 54]. Besides optimised donor-acceptor groups [55, 56], the hyperpolarisability shows a marked dependence on the conjugation length [57-60] and planarity of the molecule. Model materials that have been investigated consist of benzene derivatives with electron donors and acceptor moieties substituted on either end of the benzene ring. Such crystals are intrinsically noncentric and include *m*-nitroaniline (m-NA) [61] and 2-methyl-4-nitroaniline (MNA) [50]. Crystals of these materials however are difficult to grow and attention has been turned to incorporating the chromophores into polymeric systems.

Chromophores may be incorporated into polymer systems by guest-host systems [62-64], by chemically attaching to a polymer side chain [65-67] or main chain [65, 68], or by using cross-linked polymeric structures [69]. Of these, the simplest method is to disperse the guest chromophores throughout the polymer matrix. This is easily achieved by using a common solvent to dissolve both the guest molecules and the polymer. Since this technique allows simple sample preparation, it is often the technique of choice when characterisation of chromophores in the solid state is required.

The first observation of second order nonlinear effects from poled polymers occurred in 1982 when Meredith and co-workers observed second harmonic generation in a molecularly doped thermoplastic liquid crystal polymer [62]. Two models were applied to describe the orientation induced by poling, the Isotropic and Ising models. After the poling field was removed, the polar order of the material was found to be short lived.

Four years later, Singer *et al* demonstrated second harmonic generation from a poled chromophore doped polymer [70]. The guest-host system of a poly(methyl methacrylate) (PMMA) thin film doped with disperse red 1 (DR1) chromophore was poled above the glass transition temperature, T_g, of the system and cooled under field in an attempt to stabilise the orientation. Corona poled copolymers have also shown second order nonlinear optical properties [71, 72]. One of the copolymers that has been investigated is a side chain polymer of PMMA with covalently attached dicyanovinyl moiety. The susceptibilities were found to be higher than those previously measured due to the increased number density afforded by the incorporation of the chromophore to the side-chain of the polymer. Moreover, the side chain polymer was found to have a more stable orientation relaxation than guest-host systems previously studied.

A thermodynamic theory of chromophore orientation in response to poling fields was developed by Singer, Kuzyk and Sohn [73], known as the SKS model. They were able to demonstrate that this model may be successfully applied to both second harmonic generation and electro-optic measurements. Such thermodynamic models predict enhancement in the magnitude of second order NLO susceptibilities of a chromophore doped polymer when the NLO active chromophore concentration is increased, and consequently, later studies focused on methods of electric-field poling and material doping.

The orientational stability of poled polymers was addressed by Hampsch and co-workers using SHG as a probe [74]. These researchers were able to measure the SHG intensity as a function of time after poling had been completed. Combined with further work, it was found that the molecular orientational stability was a function of processing conditions, including physical ageing and temperature [75].

Eich and co-workers at IBM studied the poling dynamics in-situ of an amorphous polymer containing *p*-nitroanaline NLO-active side group covalently attached to a

polyethylene-type backbone [76]. The corona field was turned on and off just below the T_g of the system and the extrapolated relaxation SHG data exhibited multiple exponential behaviour with an average decay time that is longer than predicted by Williams-Landel-Ferry (WLF) type behaviour. This group also demonstrated the use of the cross linking process during corona poling for the first time [77].

It became clear that a better understanding of relaxation and poling dynamics was required to improve the stability of poled polymer films for nonlinear optics. Furthermore, since the poled lifetimes of new polymer systems was increasing it was necessary to define accelerated experiments for predicting the relaxation from a short-time measurement. In this vein, Köhler *et al* were the first to correlate second harmonic generation signals with thermally stimulated discharge results [78]. In this type of study, the SHG from a poled polymer is monitored simultaneously with current across the sample as the system is heated. The results suggested that the trapped charge from corona poling is released at temperatures higher than the temperature of total polarisation relaxation and the two contributions could be easily distinguished by this method. The decay was also found to be consistent with a distribution of relaxation times as modelled with WLF theory. In the same year, others were investigating models for the orientational order of the poled films. The Maier-Saupe theory for liquid crystals was extended by van der Vorst and Picken to describe the electric field poling of polymers with π-conjugated donor-acceptor molecules as pendant side groups [79].

Recently, refinements to the SKS theory were made by Ghebremichael and co-workers in 1998 [80]. This work involves calculations relating the microscopic to the macroscopic polarisations for second order nonlinear optical properties of dye-doped polymers. The extra correction terms arise from expressing the order parameter that translates the microscopic nonlinearity to the measured nonlinearity in terms of Legendre polynomials. These refinements include extra higher order terms in the orientational averaging that are neglected by Singer *et al* and are not likely to contribute substantially to simple one-dimensional-like molecular dopant systems.

Dalton *et al* have recently investigated the attenuation of the second order coefficients with number density [81]. In this work, accentric order is optimised by consideration of chromophore-chromophore electrostatic interactions. All intermolecular interactions are neglected in the SKS model since the order parameter used to translate the

microscopic ordering to the macroscopic nonlinearities is independent of the number density. Dalton *et al* have extended the SKS model to include a modified order parameter that comprises extra terms to account for these interactions. The interactions considered are van der Waal type electrostatic interactions. The origins of such interactions are discussed in Chapter 2.

In addition to poled polymers the NLO properties of Langmuir-Blodgett films [82-88], polymeric photorefractive materials [89-91] and polymers incorporated in sol-gel matrices [92, 93] have been extensively investigated.

Thus over the last thirty years, the search for new materials has been accompanied by the elucidation of the origin of the nonlinear responses. A large part of this thesis discusses how second harmonic generation may be used as a probe to provide information on the arrangement of the molecules in the system.

1.5 Measurement Techniques

In this section a brief overview of the different techniques that are commonly used for the measurement of nonlinear optical effects is given. More detail may be found in later Chapters for the experiments particularly relevant to this thesis.

1.5.1 Linear Electro-optic Measurements

The linear electro-optic effect or Pockels effect is the linear change in refractive index of a system in the presence of an external field [1, 12]. The small changes in refractive index are measured by detecting phase shifts of the light traversing the material. In practice, the general principle involves an electric field applied to the material that is situated between two crossed polarisers. The intensity change as a function of the applied field is measured to establish the electro-optic coefficient of the material. Thus, the operating system allows the birefringence to be varied electronically by means of a controlled applied electric field [94-96]. The retardance can be altered as desired, thereby changing the state of polarisation of the incident beam, and the system may function as a polarisation modulator [97-101].

1.5.2 Electric Field Poling

As described in section 1.3, second order effects are prohibited by symmetry if a material possesses a centre of inversion. When guest chromophores are introduced into a polymer matrix, they will occupy random positions relative to each other within the system. Such a random arrangement of molecules is a centrosymmetric orientational distribution. Therefore, order may be imparted to such systems by the technique of electric field poling in order to align the guest dipolar chromophores within a host polymer matrix.

A high static electric field is applied while the polymer is heated to a state of high mobility close to its glass transition temperature, T_g. The dipole moments of the guest molecules may then align in the field direction. The polymer is then cooled whilst maintaining the electric field in order to lock in the dipolar alignment. The major difficulty in using such a poling process is the serious risk of dielectric breakdown caused by film defects as well as the increasing conductivity of the polymer near the glass transition. Damage to the sample from such breakdown or even small pinhole damages from singular electrical discharges are unacceptable for integrated devices as they could introduce additional scattering losses inside the waveguide active region. However, for research purposes a small amount of damage may be tolerated.

There are two main poling methods commonly employed; contact poling and corona poling. A third, less common technique is internal field poling.

Contact poling involves the evaporation of thin metal electrodes onto the insulating polymer film and the required electric field is applied directly. The electrode configurations may either be parallel plate [70] or in-plane (coplanar) [102]. This technique allows the use of the same electrodes for the fabrication and operation of electro-optic devices. In addition, if optical transparency is required, the film may be sandwiched between two ITO coated glass slides, or patterned ITO coplanar electrodes. Although these techniques are simple, the processing must usually be carried out in a clean room environment to ensure the highest purity of the samples to prevent charge injection and catastrophic short-circuiting, destroying the device. In addition, the poling fields that can be achieved are generally lower than those achieved using other techniques.

The internal field poling method employs a ferroelectric polymer as the host and utilizes the high internal electric fields generated by such hosts. Efforts were made to exploit the high fields to induce the alignment in guest host systems and copolymers containing a pendant NLO chromophore [103, 104]. The main advantage of this poling technique is that relatively low external fields may be applied to generate large ferroelectric polarization fields within the polymer host and thus allowing a greater degree of chromophore alignment. However, concentrations of the guest chromophore must be kept low since the degree of order in the crystalline regions (from where the high electric fields are generated) is disrupted by the inclusion of guest molecules. This is clearly a major disadvantage when trying to increase the total non-linearity of the system by increasing the number density of the NLO chromophores.

Corona poling utilizes the ions generated from a corona discharge to create very high electric fields when deposited on the polymer surface. Such a discharge may be formed when a sufficiently high potential difference exists between an asymmetric electrode arrangement, such as a needle and plate conformation. This technique was used to pole the materials in this study.

1.5.3 Second Harmonic Generation (SHG)

The phenomenon of frequency doubling or second harmonic generation may be observed when intense electromagnetic radiation from a laser is directed through a NLO material. As mentioned in section 1.3, there is an important symmetry constraint for the observation of second order NLO effects; these effects are only possible in noncentrosymmetric systems. In a gaseous or liquid state where random fluctuations create a centre of symmetry, alignment of the molecules using an external field is required to break the centre of inversion and observe coherent second order effects. In chromophore doped polymer systems, the alignment must also be induced through electric field poling [66, 70, 105]. In this case, the measurement of the nonlinearity often utilizes the Maker fringe technique [9]. The Maker fringe method provides a powerful tool for making accurate relative measurements of NLO coefficients. The reference material is usually a standard NLO material such as quartz. SHG is one of the main experimental techniques used in this thesis and will be discussed in detail in Chapter 3.

1.5.4 Solvatochromism

The "solvatochromic method" developed by Paley and Harris [106], for the determination of the molecular first hyperpolarisability, β, is not a true NLO measurement, but rather an estimation based on the two level model [13] using spectroscopic data. Solvatochromism is the solvent dependence of the UV-visible absorption spectrum of a molecule. Within the two level model (see Chapter 2) the molecular hyperpolarisability is related to the frequencies of the optical fields, the oscillator strength of the transition between the ground and excited state and the dipole moment difference between these two states. Absorption data readily provides information about the oscillator strength directly from the integration of the frequency spectrum [107]. In addition, the spectral shift in the absorption spectrum with solvent polarity can be used to determine the dipole moment difference between the ground and excited states [106]. Highly polarisable molecules create frequency shifts in the optical absorption spectra when dissolved in solvents of different polarities due to the presence of a reaction field. The dissolved molecule will distort the electronic distribution of the solvent molecules and if the solvent molecules are dipolar, cause them to orient. These oriented polarised dipolar molecules in turn exert an electric field, the reaction field, on the dissolved solute molecule, which tends to increase the dipole moment. The two level model and reaction field are described in more detail in Chapter 2.

1.5.5 Electric Field Induced Second Harmonic Generation (EFISH)

Electric field induced second harmonic generation (EFISH) is a standard technique often used to measure the magnitude of the molecular hyperpolarisability, β [16, 108]. The general principle involves a high voltage static electric field applied across a cell containing a solution of the NLO chromophore under investigation. The pulsed electric field aligns the dipolar molecules and breaks the symmetry of the solution. The SHG is then probed using a synchronously pulsed laser beam, often from a Nd:YAG laser. A pulsed rather than DC source is used to minimise problems associated with electrolysis of the cell containing the solution. The cell usually contains a wedge shape cavity and is mounted on a translation stage that can be stepped or driven laterally with respect to the laser beam such that fringes associated with the phase mismatch between the nonlinear polarisation of the fundamental propagating wave and the second harmonic wave are observed. In practice, a long focal length lens is used to focus the

fundamental beam into the cell to avoid significant beam divergence and intensity does not vary in the cell. The Maker fringe signal is then compared to the fringes from a known substance, as this is a relative measurement. The ratio of the two signals then serves as the basis of the data analysis and the extraction of β.

1.5.6 Hyper-Rayleigh Scattering (HRS)

Hyper-Rayleigh scattering is a powerful technique to extract the molecular hyperpolarisability of organic chromophores. In these experiments, a fundamental laser beam is incident on a cell containing a solution of the NLO molecule. Microscopic fluctuations in chromophore orientation and density give rise to incoherently scattered second harmonic radiation that has intensity proportional to the square of the fundamental intensity. This incoherent second harmonic light scattering from a disordered system was first observed by Terhune *et al* [109]. The magnitude of the second harmonic intensity scattered from a solution with known concentration of sample chromophore can be related to the chromophore β value. Since HRS is an incoherent effect and light is scattered in all directions and care must be taken with the analysis and interpretation of the data because the scattered light cannot be separated spatially from fluorescence contributions [110, 111]. However, this technique does not involve an orienting electric field so that the experimental set up is relatively simple compared to EFISH. Moreover, nonpolar molecules, such as octopolar nonlinear species, and ionic molecules may also be assessed that cannot be measured using EFISH because they are unable to orient in an electric field [112]. In addition, this technique has the advantage that it yields the first hyperpolarisability alone without the need for calculating any other molecular parameters such as the dipole moment.

1.6 Optimisation of Systems for Second Order Effects

Molecular properties relate to bulk effects of the medium. According to the SKS theory [73], the magnitude of the macroscopic nonlinear effect, $\chi^{(2)}$ responsible for SHG and EFISH is linearly proportional to the product $NE\mu\beta$, the number density, electric field, molecular hyperpolarisability and dipole moment respectively and inversely related to $5kT$. In addition, the degree of non-centrosymmetric orientational order plays a role in

the determination of $\chi^{(2)}$. This relation will be discussed in more detail in the next chapter but here the possible approaches to optimisation of $\chi^{(2)}$ will be summarised.

1.6.1 Molecular Design

Molecular properties may be optimised based on structure property relationships obtained from a combination of experimental and theoretical work [4, 13, 21, 54, 113-115]. Properties to be optimised include molecular hyperpolarisabilities, together with optical properties such as transparency, mechanical properties of flexibility and tensile strength and chemical properties such as solubility, stability against photo-oxidation or temperature decomposition. In addition, when guest-host polymer systems are studied for second order effects, a high dipole moment, μ is required to assist the alignment in the applied electric field. Therefore, essentially the product $\mu\beta$ is required to be optimised for these systems. To produce high $\mu\beta$ is a mission for molecular design and synthesis. A dominant contribution to β arises from the charge transfer properties of the molecule. That is β may be defined in terms of the optical transition strength, the excited state energy and the dipole moment difference between the ground and excited states of the molecule [13, 116]. A classic structure comprises an electron donor linked to an electron acceptor through a π-conjugated system and results in chromophores with high $\mu\beta$. The simplest example is *p*-nitroaniline that contains asymmetry in the polarisation of electrons within the π system leading to a dipole. The class of materials studied in the work are highly polarisable dipolar molecules leading to large ground state dipole moments and a high figure of merit, $\mu\beta$.

1.6.2 Increase Poling Field

The poling field strength is limited due to electrical break down of polymers. An increase in molecular mobility when a guest host system is poled above the glass transition temperature, T_g, is the mechanism responsible for increased poling efficiency. Electrical break down may result from high current densities that also accompany an increase in the molecular mobility. The risk of breakdown is further increased if the impurity concentration is high, as this will further increase the current density of the sample. Corona poling is often preferred over fixed electrode poling because corona

poling reduces the risk of electrical break down since the absence of a top electrode ensures that electrical breakdown remains localized.

1.6.3 Increase Number Density

The number density of NLO molecules in a guest-host polymeric system is limited by phase-separation caused by poor solubility of the chromophore. Studies in the past have indicated that, in guest host systems, doping of NLO molecules is also limited due to a reduction of the T_g of the host polymer in proportion to the doping level due to the plasticising effect [63]. Incorporating the NLO moiety as a side chain on a polymer backbone allows an increase in number density by preventing the phase separation of the dye [72].

1.7 Theoretical Modelling

Many quantum-chemical methods have been developed for the calculation of the electronic structure and molecular properties. These methods may be classified into ab-initio and semi-empirical methods. Ab-initio methods are extremely demanding on computation time and are therefore limited to moderate size molecules. However, generally ab-initio methods have the advantage of reduced arbitrariness while semi-empirical methods are generally less demanding, require substantially less computational resources and produce results that may include molecular orbital diagrams that may be interpreted in an intuitive chemical manner. Ab-initio software packages are widely available, such as GAUSSIAN available through CS Chem 3D Pro [117], to perform electronic structure calculations. Semi-empirical calculations are a simplification compared to ab-initio since empirical functions are used instead of exact numerical integrals in the electronic structure calculations. The inner electrons are taken as a fixed core potential and only the valence electrons are considered explicitly. This method is widely used and in particular, the algorithms are readily available in the MOPAC [118] software package.

1.8 Devices

Nonlinear optical effects are widely used in optoelectronic devices that have many applications in telecommunications including fast switches, optical computing, optical data storage and optical information processing. The nonlinear devices include harmonic generators, electro-optic modulators and optically bistable devices.

In the development of devices, the suitability of a material for applications is not only determined by the requirement for a large nonlinearity. Other factors may adversely affect device performance and these are important in the design and realisation of practical devices. Materials must also be efficient and stable under extreme conditions of storage and operation. In addition, low operating voltages are required for modulator devices. Other constraints of the material for devices include low absorption loss at the required wavelength and high damage thresholds.

Recent advances in polymeric electro-optic materials and device fabrication techniques have significantly increased the potential for incorporation of these materials and devices into modern high bandwidth telecommunications and information processing. The photonics industry is expected to fully exploit the rich variety of nonlinear optical effects and materials, with organic materials in particular a promising candidate for future devices.

1.9 References

1. Prasad, P.N. and Williams, D., *Introduction to nonlinear optical effects in molecules and polymers.* 1991, New York: Wiley-Interscience. 306.

2. Walker, A.C., *Tutorial review: A comparison of optically nonlinear phenomena in the context of optical information processing.* Optical Computing and Processing, 1991. **1**(1): p. 91-106.

3. Marks, T. and Ratner, M., *Design, synthesis, and properties of molecule-based assemblies with large 2nd-order optical nonlinearities.* Angewandte Chemie-International Edition in English, 1995. **34**(2): p. 155-173.

4. Chemla, D.S. and Zyss, J., *Nonlinear optical properties of organic molecules and crystals.* Quantum Electronics - Principles and Applications, ed. D.S. Chemla and J. Zyss. Vol. 1 and 2. 1987, New York: Academic Press. 482.

5. Williams, D.J., *Organic polymeric and non-polymeric materials with large optical nonlinearities.* Angewante Chemie International Edition in English, 1984. **23**: p. 690-703.

6. Moylan, C.R., McComb, I.H., Miller, R.D., Lee, V.Y., Twieg, R.J., Ermer, S., Lovejoy, S.M., and Leung, D.S., *Defeating tradeoffs for nonlinear optical materials.* Molecular Crystals and Liquid Crystals Science and Technology Section a-Molecular Crystals and Liquid Crystals, 1996. **283**: p. 115-118.

7. Dalton, L.R., Steier, W.H., Robinson, B.H., Zhang, C., Ren, A., Garner, S., Chen, A.T., Londergan, T., Irwin, L., Carlson, B., Fifield, L., Phelan, G., Kincaid, C., Amend, J., and Jen, A., *From molecules to opto-chips: organic electro-optic materials.* Journal Of Materials Chemistry, 1999. **9**(9): p. 1905-1920.

8. Boyd, G.D., Miller, R.C., Nassau, K., Bond, W.L., and Savage, A., *$LiNbO_3$: An efficient phase matchable nonlinear optical material.* Applied Physics Letters, 1964. **5**(11): p. 234-236.

9. Maker, P.D., Terhune, R.W., Nisenoff, M., and Savage, C.M., *Effects of dispersion and focusing on the production of optical harmonics.* Physical Review Letters, 1962. **8**(1): p. 21-22.

10. Jerphagnon, J. and Kurtz, S.K., *Optical nonlinear susceptibilities: Accurate relative values for quartz, ammonium dihyrogen phosphate, and potassium dihydrogen phosphate.* Physical Review B, 1969. **1**(4): p. 1739-1744.

11. Peterson, G.E., A.A., B., Lenzo, P.V., and Bridenbaugh, P.M., *Electro-optic properties of $LiNbO_3$.* Applied Physics Letters, 1964. **5**(3): p. 62-64.

12. Boyd, R.W., *Nonlinear Optics.* 1992, London: Academic Press Inc. 427.

13. Oudar, J.L. and Chemla, D.S., *Hyperpolarisabilities of the nitroanilines and their relations to the excited state dipole moment.* The Journal of Chemical Physics, 1977. **66**(6): p. 2664-2668.

14. Ahlheim, M., Barzoukas, M., Bedworth, P.V., BlanchardDesce, M., Fort, A., Hu, Z.Y., Marder, S.R., Perry, J.W., Runser, C., Staehelin, M., and Zysset, B., *Chromophores with strong heterocyclic acceptors: A poled polymer with a large electro-optic coefficient.* Science, 1996. **271**(5247): p. 335-337.

15. Bosshard, C., Sutter, K., Schlesser, R., and Gunter, P., *Electrooptic effects in molecular-crystals.* Journal of the Optical Society of America B-Optical Physics, 1993. **10**(5): p. 867-885.

16. Teng, C.C. and Garito, A.F., *Dispersion of the nonlinear second-order optical susceptibility of organic systems.* Physical Review B, 1983. **28**(12): p. 6766-6773.

17. Levine, B.F. and Bethea, C.G., *Second and third order hyperpolarizabilitlies of organic molecules.* The Journal of Chemical Physics, 1975. **63**(6): p. 2666-2682.

18. Lalama, S.J. and Garito, A.F., *Origin of the nonlinear second-order optical susceptibilities of organic systems.* Physical Review A, 1979. **20**(3): p. 1179-1193.

19. Nahata, A., Wu, C., and Yardley, J.T., *Electrooptic characterization of organic media.* IEEE Transactions on Instrumentation and Measurement, 1992. **41**(1): p. 128-131.

20. Boldt, P., Bourhill, G., Brauchle, C., Jim, Y., Kammler, R., Muller, C., Rase, J., and Wichern, J., *Tricyanoquinodimethane derivatives with extremely large second- order optical nonlinearities.* Chemical Communications, 1996(6): p. 793-795.

21. Marder, S.R., Gorman, C.B., Meyers, F., Perry, J.W., Bourhill, G., Bredas, J.L., and Pierce, B.M., *A unified description of linear and nonlinear polarization in organic polymethine dyes.* Science, 1994. **265**(5172): p. 632-635.

22. Szablewski, M., *Novel reactions of TCNQ: formation of zwitterions for nonlinear optics by reactions with enamines.* The Journal of Organic Chemistry, 1994. **59**: p. 954-956.

23. Kaino, T. and Tomaru, s., *Organic materials for nonlinear optics.* Advanced Materials, 1993. **5**(3): p. 117-123.

24. Ravi, M., *Optical second harmonic generation studies on a new class of molecular materials: diaminodicyanoquinodimethanes*, in *School of Chemistry.* PhD, 1997, University of Hyderabad: Hyderabad. p. 216.

25. Oudar, J.L., *Optical nonlinearities of conjugated molecules. Stilbene derivatives and highly polar aromatic compounds.* The Journal of Chemical Physics, 1977. **67**(2): p. 446-457.

26. Zyss, J., *Nonlinear organic materials for integrated optics: a review.* Journal of Molecular Electronics, 1985. **1**: p. 25-45.

27. Groh, W., Lupo, D., and Sixl, H., *Polymer optical fibers and nonlinear optical-device principles.* Angewandte Chemie-International Edition in English, 1989. **28**(11): p. 1548-1559.

28. Meyers, F., Marder, S.R., Pierce, B.M., and Brédas, J.L., *Tuning of large second hyperpolarizabilities in organic conjugated compounds.* Chemical Physics Letters, 1994. **228**: p. 171-176.

29. Szablewski, M., Thomas, P.R., Thornton, A., Bloor, D., Cross, G.H., Cole, J.M., Howard, J.A.K., Malagoli, M., Meyers, F., Bredas, J.-L., Wenseleers, W., and Goovaerts, E., *Highly dipolar, optically nonlinear adducts of tetracyano-p-quinodimethane: synthesis, physical characterisation and theoretical aspects.* Journal of the American Chemical Society, 1997. **119**(13): p. 3144-3154.

30. Dalton, L.R., Harper, A.W., and Robinson, B.H., *The role of London forces in defining noncentrosymmetric order of high dipole moment high hyperpolarizability chromophores in electrically poled polymeric thin films.* Proceedings of the National Academy of Sciences of the United States of America, 1997. **94**(10): p. 4842-4847.

31. Butcher, P.N. and Cotter, D., *The elements of nonlinear optics.* Cambridge studies in modern optics: 9, ed. P.L. Knight and W.J. Firth. Vol. 9. 1990, Cambridge: Cambridge University Press. 344.

32. Zernike, F. and Midwinter, J.E., *Applied nonlinear optics.* Pure and Applied Optics. 1973, New York: John Wiley and sons.

33. Burland, D.M., Miller, R.D., and Walsh, C.A., *Second-order nonlinearity in poled-polymer systems.* Chemical Reviews, 1994. **94**(1): p. 31-75.

34. Hecht, E. and Zajac, A., *Optics.* Seventh ed. 1982, Massachusetts: Addison-Wesley. 565.

35. Maiman, T.H., *Stimulated optical radiation in ruby.* Nature, 1960. **187**(4736): p. 493-494.

36. Franken, P.A., Hill, A.E., Peters, C.W., and Weinreich, G., *Generation of optical harmonics.* Physical Review Letters, 1961. **7**(4): p. 118-119.

37. Franken, P.A. and Ward, J.F., *Optical harmonics and nonlinear phenomena.* Review of Modern Physics, 1963. **35**(1): p. 23-39.

38. Kleinman, D.A., *Nonlinear dielectric polarization in optical media.* Physical Review, 1962. **126**(6): p. 1977-1979.

39. Peticolas, W.L., Goldsborough, J.P., and Rieckhoff, K.E., *Double photon excitation in organic crystals.* Physical Review Letters, 1963. **10**(2): p. 43-45.

40. Heilmeier, G.H., Ockman, N., Braunstein, R., and Kramer, D.A., *Relationship between optical second harmonic generation and electro-optic effects in the molecular crystal hexamine.* Applied Physics Letters, 1964. **5**(11): p. 229-230.

41. Rentzepis, P.M. and Pao, Y.H., *Laser-induced optical second harmonic generation in organic crystals.* Applied Physics Letters, 1964. **5**(8): p. 156-158.

42. Kurtz, S.K. and Perry, T.T., *A powder technique for the evaluation of nonlinear optical materials.* Journal of Applied Physics, 1968. **39**(8): p. 3798-3813.

43. Jerphagnon, J. and Kurtz, K., *Maker fringes: detailed comparison of theory and experiment for isotropic and unixial crystals.* Journal of Applied Physics, 1970. **41**(4): p. 1667-1681.

44. Herman, W.N. and Hayden, L.M., *Maker fringes revisited - 2nd-harmonic generation from birefringent or absorbing materials.* Journal of the Optical Society of America B-Optical Physics, 1995. **12**(3): p. 416-427.

45. Davydov, B.L., Deracheva, L.D., Dunina, V.V., Zhabotinskii, M.E., Zolin, V.F., Koreneva, L.G., and Samokhina, M.A., *Connection between charge transfer and laser second harmonic generation.* JFTP Letters, 1970. **12**: p. 16-18.

46. Levine, B.F. and Bethea, C.G., *Molecular hyperpolarisabiliies determined from conjugated and nonconjugated organic liquids.* Applied Physics Letters, 1974. **24**(9): p. 445-447.

47. Levine, B.F. and Bethea, C.G., *Hyperpolarisability of the pyridine-iodine charge transfer complex.* The Journal of Chemical Physics, 1976. **65**(6): p. 2439-2442.

48. Levine, B.F. and Bethea, C.G., *Effects on hyperpolarisabilities of molecular interactions in associating liquid mixtures.* The Journal of Chemical Physics, 1976. **65**(15): p. 2429-2438.

49. Levine, B.F. and Bethea, C.G., *Second order hyperpolarisability of a polypeptide α–helix: Poly-γ-benzyl-L-glutamate.* The Journal of Chemical Physics, 1976. **65**(5): p. 1989-1993.

50. Levine, B.F., Bethea, C.G., Thurmond, C.D., Lynch, R.T., and Bernstein, J.L., *An organic crystal with an exceptionally large optical second harmonic coefficient: 2-methyl-4-nitroananline.* Journal of Applied Physics, 1979. **50**(4): p. 2523-2527.

51. Oudar, J.L., Chemla, D.S., and Batifol, E., *Optical nonlinearities of various substituted benzene molecules in the liquid state, and comparison with solid state nonlinear susceptibilities.* The Journal of Chemical Physics, 1977. **67**(4): p. 1626-1635.

52. Oudar, J.L. and Chemla, D.S., *Theory of second-order optical susceptibilities of benzene substituents.* Optics Communications, 1975. **13**(2): p. 164-168.

53. Lalama, S.J., Singer, K.D., Garito, A.F., and Desai, K.N., *Exceptional second-order nonlinear optical susceptibilities of quinoid systems.* Applied Physics Letters, 1981. **39**(12): p. 940-942.

54. Lambert, C., Stadler, S., Bourhill, G., and Brauchle, C., *Polarized π-electron systems in a chemically generated electric field: Second-order nonlinear optical properties of ammonium borate zwitterions.* Angewandte Chemie-International Edition in English, 1996. **35**(6): p. 644-646.

55. Marder, S.R., Beratan, D.N., and Cheng, L.T., *Approaches for optimizing the first electronic hyperpolarizability of conjugated organic molecules.* Science, 1991. **252**(5002): p. 103-106.

56. Zyss, J., *Hyperpolarisabilities of substituted conjugated molecules. III. Study of a family of donor-acceptor disubstituted phenyl-polenes.* Journal of Chemical Physics, 1979. **71**(2): p. 909-916.

57. Gorman, C.B. and Marder, S.R., *Effect of molecular polarization on bond-length alternation, linear polarizability, first and second hyperpolarizability in donar-acceptor polyenes as a function of chain length.* Chemical Materials, 1995. **7**: p. 215-220.

58. Dulcic, A., Flytzanis, C., Tang, C., Pepin, D., Fetizon, M., and Y., H., *Length dependence of the 2nd-order optical nonlinearity in conjugated hydrocarbons.* Journal of Chemical Physics, 1981. **74**(3): p. 1559-1563.

59. Huijts, R. and Hesselink, G., *Length dependence of the second-order polarizability in conjugated organic-molecules.* Chemical Physics Letters, 1989. **156**(2-3): p. 209-212.

60. Cheng, L.T., Tam, W., Marder, S.R., Stiegman, A.E., Rikken, G., and Spangler, C.W., *Experimental investigations of organic molecular nonlinear optical polarizabilities .2. A study of conjugation dependences.* Journal of Physical Chemistry, 1991. **95**(26): p. 10643-10652.

61. Bergman, J.G. and Crane, G.R., *Nonlinear optical susceptibilities of triphenylbenzene, resorcinol, and metanitroanaline.* The Journal of Chemical Physics, 1977. **66**(8): p. 3803-3805.

62. Meredith, G.R., Vandusen, J., G, and Williams, D., J, *Optical and nonlinear optical characterization of molecularly doped thermotropic liquid crystalline polymers.* Macromolecules, 1982. **15**: p. 1385-1389.

63. Stähelin, M., Burland, D.M., Ebert, M., Miller, R.D., Smith, B.A., Twieg, R.J., Volksen, W., and Walsh, C.A., *Reevaluation of the thermal-stability of optically nonlinear polymeric guest-host systems.* Applied Physics Letters, 1992. **61**(14): p. 1626-1628.

64. Hampsch, H.L., Yang, J., Wong, G.K., and Torkelson, J.M., *Second harmonic-generation in doped glassy polymer-films as a function of physical aging and dopant size.* Polymer Communications, 1989. **30**(2): p. 40-43.

65. Hagen, R., Zobel, O., Sahr, O., Biber, M., Eckl, M., Strohriegl, P., Eisenbach, C.D., and Haarer, D., *Poling and orientational relaxation: Comparison of nonlinear optical main-chain and side-chain polymers.* Journal of Applied Physics, 1996. **80**(6): p. 3162-3166.

66. Hayden, L.M., Sauter, G.F., Ore, F.R., Passillas, P.L., Hoover, J.M., Lindsay, G.A., and Henry, R., A, *Second order nonlinear optical measurements in guest host and side chain polymers.* Journal of Applied Physics, 1990. **68**(2): p. 456-465.

67. Brower, S.C. and Haydon, M.L., *Activation volumes associated with chromophore reoroientation in corona poled guest-host and side chain polymers.* Journal of Polymer Science Part B: Polymer Physics, 1995. **33**(2391-2404).

68. Weder, C., Neuenschwander, P., Suter, U.W., Prêtre, P., Kaatz, P., and Günter, P., *Orientational relaxation in electric-field poled films from main chain nonlinear optical polyimides.* Macromolecules, 1995. **28**: p. 2377-2382.

69. Bewsher, J.D. and Mitchell, G.R., *Study of the nonlinear optical properties of a crosslinkable chromophore for use in guest host polymer films.* Optical Engineering, 1997. **36**(1): p. 167-174.

70. Singer, K.D., Sohn, J.E., and Lalama, S.J., *Second harmonic generation in poled polymer films.* Applied Physics Letters, 1986. **49**(5): p. 248-250.

71. Hill, J.R., Pantelis, P., Abbasi, F., and Hodge, P., *Demonstration of the linear electro-optic effect in a thermopoled polymer film.* Journal of Applied Physics, 1988. **64**(5): p. 2749-2751.

72. Singer, K.D., Kuzyk, W.R., Sohn, J.E., Lalama, S.J., Comizzoli, R.B., Katz, H.E., and Schilling, M.L., *Electro-optic phase modulation and optical second-harmonic generation in corona-poled polymer films.* Applied Physics Letters, 1988. **53**(19): p. 1800-1802.

73. Singer, K.D., Kuzyk, M.G., and Sohn, J.E., *Second-order nonlinear-optical processes in orientationally ordered materials: relationship between molecular and macroscopic properties.* Journal of the Optical Society of America B, 1987. **4**(6): p. 968-976.

74. Hampsch, H.L., Yang, J., Wong, G.K., and Torkelson, J.M., *Orientation and second harmonic-generation in doped polystyrene and poly(methyl methacrylate) films.* Macromolecules, 1988. **21**(2): p. 526-528.

75. Hampsch, H.L. and Torkelson, J.M., *Second harmonic generation in corona poled, doped polymer films as a function of corona processing.* Journal of Applied Physics, 1990. **67**(2): p. 1037-1041.

76. Eich, M., Sen, A., Looser, H., Bjorklund, G.C., Swalen, J.D., Twieg, R., and Yoon, D.Y., *Corona poling and real-time second-harmonic generation study of a novel covalently functionalised amorphous nonlinear optical polymer.* Journal of Applied Physics, 1989. **66**(6): p. 2559-2567.

77. Eich, M., Reck, B., Yoon, D.Y., Willson, C.G., and Bjorklund, G.C., *Novel second-order nonlinear optical polymers via chemical cross- linking-induced vitrification under electric-field.* Journal of Applied Physics, 1989. **66**(7): p. 3241-3247.

78. Köhler, W., Robello, D.R., Dao, P.T., Willand, C.S., and Williams, D.J., *Second harmonic-generation and thermally stimulated current measurements - a study of some novel polymers for nonlinear optics.* Journal of Chemical Physics, 1990. **93**(12): p. 9157-9166.

79. van der Vorst, C.P.J.M. and Picken, S.J., *Electric field poling of acceptor-donor molecules.* Journal of the Optical Society of America B, 1990. 7(3): p. 320-325.

80. Ghebremichael, F., Kuzyk, M.G., Singer, K.D., and Andrews, T.H., *Relationship between the second-order microscopic and macroscopic nonlinear optical susceptibilities of poled dye- doped polymers.* Journal of the Optical Society of America B-Optical Physics, 1998. **15**(8): p. 2294-2297.

81. Harper, A.W., Sun, S., Dalton, L.R., Garner, S.M., Chen, A., Kalluri, S., Steier, W.H., and Robinson, B.H., *Translating microscopic optical nonlinearity into macroscopic optical nonlinearity: the role of chromophore-chromophore electrostatic interactions.* Journal of the Optical Society of America B-Optical Physics, 1998. **15**(1): p. 329-337.

82. Ashwell, G.J., Dawnay, E.J.C., Kuczynski, A.P., Szableweski, M., Sandy, I.M., Bryce, M.R., Grainger, A.M., and Hasan, M., *Langmuir-Blodgett alignment of zwitterionic optically non-linear D-π-A materials.* Journal of the Chemical Society of Faraday Transactions, 1990. **68**(7): p. 1117-1121.

83. Ashwell, G.J., Jefferies, G., Rees, N.D., Williamson, P.C., Bahra, G.S., and Brown, C.R., *Centrosymmetric chromophores: Second-harmonic generation from Langmuir-Blodgett and spun-coated films of hydroxy-substituted squaraines.* Langmuir, 1998. **14**(10): p. 2850-2856.

84. Cross, G.H., Girling, I.R., Peterson, I.R., and Cade, N.A., *Linear pockels response of a monolayer langmuir-blodgett-film.* Electronics Letters, 1986. **22**(21): p. 1111-1112.

85. Girling, I.R., Cade, N.A., Kolinsky, P.V., Jones, R.J., Peterson, I.R., Ahmad, M.M., Neal, D.B., Petty, M.C., Roberts, G.G., and Feast, W.J., *2nd-Harmonic generation in mixed hemicyanine - fatty-acid langmuir-blodgett monolayers.* Journal of the Optical Society of America B-Optical Physics, 1987. **4**(6): p. 950-955.

86. Schildkraut, J.S., Penner, T.L., Willand, C.S., and Ulman, A., *Absorption and second harmonic generation of monomer and aggregate hemicanine dye in langmuir-blodgett films.* Optics Letters, 1988. **13**(2): p. 134-136.

87. Anderson, B.L., Hoover, J.M., Lindsay, G.A., Higgins, B.G., Stroeve, P., and Kowel, S.T., *Second harmonic generation in langmuir-blodgett multilayers of stilbazolium chloride polyethers.* Thin Solid Films, 1989. **179**: p. 413-421.

88. Swalen, J.D., *Linear and non-linear optical and spectroscopic properties of langmuir-blodgett films.* Thin Solid Films, 1988. **160**(1-2): p. 197-208.

89. Sandalphon, Kippelen, B., Meerholz, K., and Peyghambarian, N., *Ellipsometric measurements of poling birefringence, the pockels effect, and the kerr effect in high-performance photorefractive polymer composites.* Applied Optics, 1996. **35**(14): p. 2346-2354.

90. Chen, Z., Wang, F., Huang, Z., Gong, Q., Chen, Y., Zhang, Z., and Chen, H., *An optimised nonlinear optical chromophore in a low-glass-transition-temperature photorefractive polymer.* Journal of Physics D: Applied Physics, 1998. **31**: p. 2245-2248.

91. Marder, S.R., Kippelen, B., Jen, A.K.Y., and Peyghambarian, N., *Design and synthesis of chromophores and polymers for electro- optic and photorefractive applications.* Nature, 1997. **388**(6645): p. 845-851.

92. Zhang, Y., Prasad, P.N., and Burzynski, R., *Second-order nonlinear optical-properties of n-(4-nitrophenyl)- (s)-prolinol-doped sol-gel-processed materials.* Chemistry of Materials, 1992. **4**(4): p. 851-855.

93. Jeng, R.J., Chen, Y.M., Jain, A.K., Kumar, J., and Tripathy, S.K., *Second-order optical nonlinearity on a modified sol-gel system at 100-degrees-C.* Chemistry of Materials, 1992. **4**(5): p. 972-975.

94. Chollet, P.A., Gadret, G., Kajzar, F., and Raimond, P., *Electrooptic coefficient determination in stratified organized molecular thin-films - application to poled polymers.* Thin Solid Films, 1994. **242**(1-2): p. 132-138.

95. Khanarian, G., Sounik, J., Allen, D., Shu, S.F., and Walton, C., *Electro-optic characterization of nonlinear-optical guest-host films and polymers.* Journal of the Optical Society of America B-Optical Physics, 1996. **13**(9): p. 1927-1934.

96. Teng, C.C. and Man, H.T., *Simple reflection technique for measuring the electrooptic coefficient of poled polymers.* Applied Physics Letters, 1990. **56**(18): p. 1734-1736.

97. Bauer, S., *Poled polymers for sensors and photonic applications.* Journal of Applied Physics, 1996. **80**(10): p. 5531-5558.

98. Chen, A., Chuyanov, V., Garner, S., Zhang, H., Steier, W.H., Chen, J.H., Zhu, J.S., Wang, F., He, M.Q., Mao, S.S.H., and Dalton, L.R., *Low-V-π electro-optic modulator with a high-mu beta chromophore and a constant-bias field.* Optics Letters, 1998. **23**(6): p. 478-480.

99. Dalton, L., Harper, A., Ren, A., Wang, F., Todorova, G., Chen, J., Zhang, C., and Lee, M., *Polymeric electro-optic modulators: From chromophore design to integration with semiconductor very large scale integration electronics and silica fiber optics.* Industrial & Engineering Chemistry Research, 1999. **38**(1): p. 8-33.

100. Steier, W.H., Chen, A., Lee, S.S., Garner, S., Zhang, H., Chuyanov, V., Dalton, L.R., Wang, F., Ren, A.S., Zhang, C., Todorova, G., Harper, A., Fetterman,

H.R., Chen, D.T., Udupa, A., Bhattacharya, D., and Tsap, B., *Polymer electro-optic devices for integrated optics.* Chemical Physics, 1999. **245**(1-3): p. 487.

101. Mohlmann, G.R. and Horsthuis, W.H.G., *Optically nonlinear oplymeric switches and modulators.* SPIE Nonlinear Optical Properties of Organic Materials III, 1990. **1337**: p. 215-225.

102. Stähelin, M., Walsh, C.A., Burland, D.M., Miller, R.D., Twieg, R.J., and Volksen, W., *Orientational decay in poled 2nd-order nonlinear-optical guest-host polymers - temperature-dependence and effects of poling geometry.* Journal of Applied Physics, 1993. **73**(12): p. 8471-8479.

103. Tsutsumi, N., Tsuyoshi, O., and Tsuyoshi, K., *Internal electric field and second harmonic generation on the blends of vinylidene flouride-triflouroethylene copolymer and poly(methyl methacrylate) with a pendant nonlinear optical dye.* Macromolecules, 1993. **26**: p. 5447-5466.

104. Tsutsumi, N., Fujii, I., Ueda, Y., and Kiyotsukuri, T., *Second harmonic generation from and nlo dye aligned by the Internal electric field in a blend of poly(vinylidene flouride) and poly(methyl methacrylate).* Macromolecules, 1995. **28**(4): p. 950-955.

105. Mortazavi, M.A., Knoesen, A., Kowel, S.T., Higgins, B.G., and Dienes, A., *Second-harmonic generation and absorption studies of polymer dye films oriented by corona-onset poling at elevated-temperatures.* Journal of the Optical Society of America B-Optical Physics, 1989. **6**(4): p. 733-741.

106. Paley, M.S. and Harris, J.M., *A solvatochromic methos for determining second-order polarisabilities of organic molecules.* Journal of Organic Chemistry, 1989. **54**: p. 3774-3778.

107. Atkins, P.W., *Physical Chemistry.* Fourth ed. 1990, Oxford: Oxford University Press. 992.

108. Singer, K.D. and Garito, A.F., *Measurements of molecular second order optical susceptibilities using dc induced second harmonic generation.* Journal of Chemical Physics, 1981. **75**(7): p. 3572-3580.

109. Terhune, R.W., Maker, P.D., and Savage, C.M., *Measurement of nonlinear light scattering.* Physical Review Letters, 1965. **14**(17): p. 681-684.

110. Stadler, S., Bourhill, G., and Brauchle, C., *Problems associated with hyper-rayleigh scattering as a means to determine the second-order polarizability of organic chromophores.* Journal of Physical Chemistry, 1996. **100**(17): p. 6927-6934.

111. Flipse, M.C., De jonge, R., Woudenberg, R.H., Marsman, A.W., Van Walree, C.A., and Jenneskens, L.W., *The determination of first hyperpolarizabilities-beta using hyper-rayleigh scattering - a caveat.* Chemical Physics Letters, 1995. **245**(2-3): p. 297-303.

112. Zyss, J. and Ledoux, I., *Nonlinear optics in multipolar media: theory and experiments.* Chemical Review, 1994. **94**: p. 77-105.

113. Kogej, T., Meyers, F., Marder, S.R., Silbey, R., and Bredas, J.L., *Nonlinear optical properties of π-conjugated compounds incorporating a saturated spacer group.* Synthetic Metals, 1997. **85**(1-3): p. 1141-1142.

114. Cheng, L.T., Tam, W., Stevenson, S.H., Meredith, G.R., Rikken, G., and Marder, S.R., *Experimental investigations of organic molecular nonlinear optical polarizabilities .1. Methods and results on benzene and stilbene derivatives.* Journal of Physical Chemistry, 1991. **95**(26): p. 10631-10643.

115. Brédas, L.J., *Molecular geometery and nonlinear optics.* Science, 1994. **263**: p. 487-488.

116. Kanis, D.R., Ratner, M.A., and Marks, T.J., *Design and construction of molecular assemblies with large second order optical nonlinearities. Quantum chemical aspects.* Chemical Reviews, 1994. **1994**(94): p. 195-242.

117. www.camsoft.com, *CS Chem 3D Pro*, 1999, Cambridge Soft: Cambridge.

118. MOPAC, *CS MOPAC PRO: Semi-empirical computation*, 1993-1997, Fujitsu Limited.

Chapter 2 : Theoretical Aspects

Many studies have focussed on understanding the origin of the nonlinear susceptibilities of molecules with the hope of the production of better materials for photonics applications. These include two and three state models [1], symmetry models and bond length alternation [2]. These models have helped to enable the prediction of classes of structures that give rise to high optical nonlinearities. Therefore, the main focus of research has constituted fine tuning the design of organic structures [3-8] and until recently, there has been comparatively little attention to the problem of macroscopic ordering of these molecules [9, 10].

2.1 Molecular Origins of NLO

As previously mentioned in Chapter 1, the microscopic polarisation response is proportional to the input field and also proportional to higher orders of the input field. However in that phenomenological description, it was implicitly assumed that the nonlinear polarisation response follows the applied field instantly, so that the susceptibilities were quoted as independent of frequency. For opitcal frequencies this is not a good approximation as the electronic excitation frequencies of the molecules are typically of the same order of magnitude and this means that dispersion and resonance effects are significant. Thus, the linear and nonlinear optical properties can be discussed using a frequency dependent power series expansion of the induced dipole moment, μ, in powers of the electric field [11-13],

$$p_i(\omega) = \mu_i + \alpha_{ij}(\omega_0)E_j(\omega_0) + \beta_{ijk}(-\omega_0;\omega_1,\omega_2)E_j(\omega_1)E_k(\omega_2) + \gamma_{ijkl}(-\omega_0;\omega_1,\omega_2,\omega_3)E_j(\omega_1)E_k(\omega_2)E_l(\omega_3) + \cdots$$

Equation 2.1

where the subscripts i, j, k, l refer to the molecular coordinate system and E_j, E_k etc denote the components of the applied field and repeated indices are summed over following the Einstein convention [12] that will be used throughout this work. The first term in the expansion, α_{ij} is the linear polarisation, the first nonlinear term, β_{ijk} is the

second order polarisability or hyperpolarisability tensor and γ_{ijkl} is the third order hyperpolarisability. The negative sign represents a photon that is "emitted" and a positive sign indicates an "absorbed photon", where the energy of the emitted photon is the sum of those absorbed.

Symmetry constraints may now be considered directly from Equation 2.1. Analysis of the tensorial nature of the polarisation leads to the conclusion that second order effects are only present in media that have a non-centrosymmetric molecular structure: In centrosymmetric molecules, an inversion of the electric field, E $\rightarrow$ -E, results in a polarisation, $p \rightarrow -p$. Considering the second order term of Equation 2.1 and neglecting the frequency dependence leads to the following expression,

$$-p_i = \beta_{ijk}(-E_j)(-E_k) = \beta_{ijk}(E_j)(E_k)$$

Equation 2.2

This condition is only possible if $\beta_{ijk} = 0$ and therefore in centrosymmetric molecules, only linear and odd order effects will be observed.

2.2 Macroscopic Origins of NLO

The nonlinear response of a material is directly related to the response of the individual constituent molecules of the system. The polarisation induced in the bulk medium may be expanded out in terms of powers of the applied electric field, in a similar manner to the microscopic polarisation resulting in the following parallel expression to Equation 2.1 [13] (in Gaussian or cgs system of units),

$$\begin{aligned} P_I(-\omega_0) = P_I^0 + \chi_{IJ}^{(1)}(-\omega_0;\omega_0)E_J(\omega_0) + \chi_{IJK}^{(2)}(-\omega_0;\omega_1,\omega_2)E_J(\omega_1)E_K(\omega_2) \\ + \chi_{IJKL}^{(3)}(-\omega_0;\omega_1,\omega_2,\omega_3)E_J(\omega_1)E_K(\omega_2)E_L(\omega_3) + \cdots \end{aligned}$$

Equation 2.3

where the subscripts *I*, *J* and *K* refer to the Cartesian co-ordinate system of the bulk material in the laboratory frame of reference and E_J, E_K and E_L are the components of the externally applied field. P^0 is the permanent polarisation in the material and the proportionality factors, $\chi^{(n)}$ are the molecular susceptibilities from which macroscopic polarisabilities are observed. $\chi^{(1)}$ is the linear susceptibility of the material, $\chi^{(2)}$ and $\chi^{(3)}$

are the second and third order nonlinear susceptibilities respectively. $\chi^{(2)}$ is a third rank tensor and $\chi^{(3)}$ is a fourth rank tensor.

2.3 Organic Material Requirements

Organic materials in particular have several potential attractive properties over inorganic materials. Organic materials are generally suitable for inexpensive mass production, have the ability to chemically tailor physical and optical properties and possess low dielectric constants. In addition, large nonlinearities may be provided through the electron systems giving rise to faster switching speeds.

A variety of different organic material systems are available for NLO, including single crystals [14-16], molecular Langmuir-Blodgett (LB) films [17, 18], liquid crystals [19-21] or polymeric systems [22, 23]. The growth of large pure crystals is difficult, expensive and time consuming. Moreover, since NLO materials often contain large dipole moments, such molecules have a strong tendency to align in antiparallel pairs with oppositely oriented dipoles, and in most cases form centrosymmetric crystals. Strategies to hinder the dimerisation process and promote crystallisation into noncentrosymmetric crystals include substitution of the NLO chromophores with bulky side groups, or with chiral groups, or with functional groups that form specific intermolecular bonds such as hydrogen bonds. LB films can suffer from difficult preparation conditions such as slow deposition and non-ideal alignment problems. In contrast, a promising approach is the use of amorphous polymers that are relatively inexpensive, simple and easy to process and fabricate into thin films for device applications.

The general form of an organic molecule consists of a number of carbon and hydrogen atoms that are bonded to each other by covalent "sharing" of electrons in the upper electronic orbital of the atoms. The types of bonding and subsequent electronic orbital overlap determine the atomic arrangement, molecular geometry and physical properties of the system.

Conjugated organic systems are comprised of alternating single and double carbon bonds. Thus the bonding in conjugated systems is a result of the formation of hybridised orbitals and unsaturated multiple bonds. Carbon-carbon single bonds or,

σ-bonds are formed by the "sharing" of one electron in the outer shell of each atom. Although the σ-bonds form a significant contribution to the properties of an organic molecule, they are highly localised and therefore are only slightly perturbed under the application of an electric field. In contrast, π-bonds, formed by the interaction of remaining *p*-orbitals of the atom, are highly delocalised and are greatly perturbed under the influence of an electric field. The formation of a π and σ bond in a system creates a carbon-carbon double bond. Many of the unique features of organic materials originate from the π electrons within the systems. The delocalisation of π-electrons enables the movement of charge along the molecule under the influence of an applied electric field, allowing molecules to have larger dipole moments, polarisabilities and hyperpolarisabilities than would be possible with purely σ-bonded molecules [24].

In addition to being highly polarisable, molecules for second order nonlinear optics must possess an asymmetric charge distribution. This is achieved in practice by introducing electron donating groups and accepting groups at either end of the conjugated molecule. The nonlinearity arises from the fact that it is more difficult for charge to move from the electron deficient acceptor, *A*, to electron rich donor, *D*, to than to move from the donor to the acceptor. Thus model organic molecules with a second order response usually consist of three fundamental moieties, as *D*-π conjugated system-*A*. These molecules are often termed charge transfer (CT) molecules.

2.4 Bond Length Alternation Model (BLA)

The bond length alternation (BLA) model allows insight into the structure-property relationships that govern the nonlinear optical (NLO) properties of organic conjugated molecules. The main aspects of the model are introduced here, but for a more detailed description the reader is referred to the literature [2, 8, 25-28].

The extent of charge separation and the electronic distribution in the ground state depends primarily on the molecular structure and on the nature of the surrounding medium. For example, the charge separation may be influenced not only by different donor or acceptor moieties of the structure but also on the polarity of the medium surrounding the molecule.

BLA is defined as the average difference in length between adjacent carbon-carbon bonds in a conjugated polyene chain. The degree of charge separation in the ground state or the degree of polarisation of ground state is related to β through the BLA parameter. Polyenes have alternating single and double bonds, with bond lengths 1.34 Å and 1.45 Å respectively. Closely related to the BLA is the bond order parameter; a bond order of 1 would arise for a single carbon-carbon bond, and a bond order of 2 would arise for a double bond and hence a bond order of 1.5 is midway between the two. This is a similar case to that of benzene where the bond can be considered either as a single bond plus half a bond or as a resonance hybrid between two forms, for example two Kekulé structures in the case of benzene.

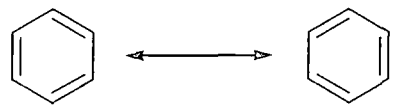

(a)

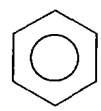

(b)

Figure 2.1: (a) Kekulé or resonance structures of benzene where the double headed arrow indicates that the actual structure lies between the two representations, (b) delocalised representation

The dipole moment, μ, of a molecule is seen to increase with increasing applied fields and eventually saturates as shown in Figure 2.2. Thus the value of dipole moment increases as the field is increased. The left hand side of Figure 2.2 shows that at low fields the BLA is conventionally taken to be positive indicating a non-polar or quinoidal type structure. The BLA ranges from a positive value through zero at the "cyanine" limit, the point at which the average difference between the lengths of alternating carbon-carbon bonds is zero. The BLA also exhibits negative values, where the structure tends towards a charge separated form. In contrast the polarisability is maximum at the cyanine limit where the BLA is zero and the charges are evenly distributed between the atoms. The extremes of BLA are therefore less polarisable since the charges are more localised between the atoms. The evolution of the second

order polarisability also reflects the changes in the electronic structure of the molecules as the field is applied. Thus molecules with negative β are found on the right hand side of Figure 2.2 when BLA is negative, indicating the structure tends towards a charge-separated ground state. Although this model only strictly applies to polyenes, the general ideas and concepts may be extended to encompass general conjugated organic systems.

The microscopic polarisation may be expressed in the form of a Taylor series expansion of the dipole moment as derivative with respect to the applied field, as [2, 29],

$$\begin{aligned} p_i &= \mu_i^{E=0} + \alpha_{ij}E_j + \beta_{ijk}E_jE_k + \gamma_{ijkl}E_jE_kE_l + \cdots \\ &= \mu_i^{E=0} + \left.\frac{\partial \mu_{ij}}{\partial E_j}\right|_{E=0} E_j + \frac{1}{2!}\left.\frac{\partial^2 \mu_{ijk}}{\partial E_j \partial E_k}\right|_{E=0} E_jE_k + \frac{1}{3!}\left.\frac{\partial^3 \mu_{ijkl}}{\partial E_j \partial E_k \partial E_l}\right|_{E=0} E_jE_kE_l + \cdots \end{aligned}$$

Equation 2.4

where i, j, k and l are the usual molecular frame tensorial indices, E_i is the local microscopic field applied to the molecule and $\mu^{E=0}$ is the molecular dipole moment without any applied field, such that $\mu = qd$ [30], where q is the charge and d is the charge separation. α_{ij}, is the polarisability that is proportional to the derivative of the dipole with respect to field. Correspondingly the β_{ijk} and γ_{ijkl} are the second and third order hyperpolarisabilities that are proportional to the second and third order derivatives of dipole moment with respect to the field. This picture of evolution of the polarisabilities with the field has been confirmed by quantum-mechanical calculations and subsequent experimental observations for polyene-like molecules [1, 2, 25, 26].

The wavefunction of the electronic ground state may be considered to be a linear combination of two limiting resonance structures; a neutral form characterised by positive BLA and a charge separated form characterised by negative BLA [2]. Thus the BLA can be considered to be a mixing function of the two states. The charge-separated state may be stabilised by the influence of the donor-acceptor strength [28, 31], or through solvent mediated polarisations [28]. Thus the applied field in Equation 2.4 may be considered to be an effective field acting on the molecule to influence the degree of mixing of the two limiting wavefunctions.

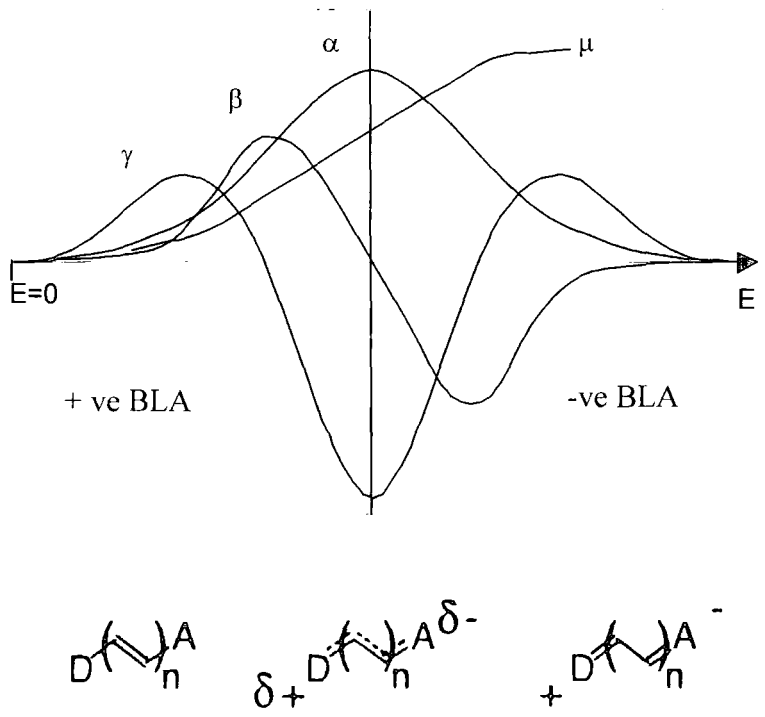

Figure 2.2: Schematic plot of α, β, γ and μ of a conjugated polyene as function of applied field to demonstrate BLA

2.5 Two Level Model

The two level model is a special case of the sum over states approach to modelling NLO systems. The sum over states approach is derived from perturbation theory and yields expressions for the hyperpolarisabilities in terms of excited state energies and dipole matrix elements [32]. Thus to predict hyperpolarisabilities using these expressions, the electronic structure of the ground state together with a large number of excited states must be calculated. Although this is a very powerful method as it automatically yields frequency dependence of the hyperpolarisabilities, it can be time consuming. In 1977 Oudar introduced the two level model by considering the special case where only transitions involving two levels are involved, and assuming that the transition dipole moments lie parallel to each other, and only a single diagonal matrix element of the charge transfer transition dominates the contribution to β [33]. Following this analysis, the contribution to the hyperpolarisability in the z-direction, β_{zzz} may then be approximated as [11, 12, 29, 33],

$$\beta_{zzz}(-2\omega;\omega,\omega) \approx \frac{3e^2\hbar^2}{2m} \frac{\omega_{eg} f_{osc} \Delta\mu}{(\omega_{eg}^2 - \omega^2)(\omega_{eg}^2 - 4\omega^2)}$$

Equation 2.5

where ω_{eg} is the angular frequency of an energy transition and $\Delta\mu$ is the difference between the ground and excited state dipole moments of the molecule. The oscillator strength, f_{osc}, of the charge transfer transition relates to the transition dipole, μ_{eg} by the equation [34],

$$f_{osc} = \frac{8\pi^2}{3} \frac{m_e \omega_{eg}}{\hbar e^2} \mu_{eg}^2$$

Equation 2.6

In practice the two-level model is often used to extrapolate the zero frequency component, β_0 value from the measurement of $\beta(\omega)$ in order to allow relatively easy comparisons between hyperpolarisabilities of different molecules obtained at different wavelengths or with different measurement techniques [29]. To this end, Equation 2.5 may be divided into two parts with the aid of Equation 2.6 into the frequency independent term, β_0, and dispersion term, $F(\omega)$ which is dependent on the relation of the transition frequency to the fundamental and second harmonic frequencies [35];

$$\beta_{---}(-2\omega;\omega,\omega) = \beta_0 F(\omega)$$
$$= \frac{3\mu_{eg}^2 \Delta\mu}{2\varepsilon_0 \hbar \omega_{eg}^2} \frac{1}{\left(1 - \left(\frac{\omega}{\omega_{eg}}\right)^2\right)\left(1 - \left(\frac{2\omega}{\omega_{eg}}\right)^2\right)}$$

Equation 2.7

Equation 2.7 shows how the hyperpolarisability increases rapidly as the energy of either the fundamental or harmonic incident radiation approaches that of the molecular transition. This effect is known as resonant enhancement. In practice, molecular absorption of energy also increases, leading to a transparency-efficiency trade off. The operation wavelength needs to be close enough to a molecular absorption band to obtain some resonant enhancement but far enough away that absorption does not have an adverse effect.

2.6 Second Harmonic Generation (SHG)

The origin of second harmonic generation may be readily understood by considering a system which is subject to a strong oscillating electric field of the form $E=E_0cos(\omega t-kz)$, where ω is the frequency of oscillation, k is the propagation constant of the wave propagating in the z direction through the NLO material. Substitution of this sinusoidal field into the second order term of the polarisation expansion, Equation 2.3, reveals the contribution to the bulk second order polarisation,

$$P_I^{(2)} = \frac{1}{2}\chi_{Izz}^{(2)} E_0^2 \left(1 + \cos(2\omega t - 2kz)\right)$$

Equation 2.8

The polarisation response at 2ω results in a harmonic oscillation of the dipolar species at twice the frequency, 2ω, of the incident fundamental wave. The dipoles act as sources of electromagnetic radiation in the medium at the new frequency that propagate with twice the fundamental propagation constant value without energy loss to the medium. Thus, the second harmonic polarisation leads to the propagation of second harmonic light [29, 36, 37].

The intensity of the second harmonic beam oscillates as it travels through a thick sample [32]. This is due to the natural dispersion of the material that occurs because the refractive index at the second harmonic frequency is different from that at the fundamental frequency. The contributions to the second harmonic field generated at different positions will have different phases. Thus the second harmonic and fundamental wave propagate at different phase velocities, and consequently interfere constructively or destructively. The distance between one intensity maximum and the next is known as the coherence length of the material, $l_c = \lambda / \left| (n_\omega - n_{2\omega}) \right|$. This intensity modulation gives rise to an interference pattern known as Maker fringes [38], when materials thicker than the coherence length are rotated in a beam. The propagation of the second harmonic will be discussed in more detail in the appropriate experimental configurations in Chapter 5.

2.7 Poling

Second order nonlinear optical properties of chromophores doped into polymeric materials have been a field of interest due to their potential application as electro-optic and frequency conversion devices [12, 18, 29]. Polymers provide an easily processable host of high optical quality for the incorporation of nonlinear optical chromophores. These materials are isotropic however, and so are intrinsically centrosymmetric and incapable of exhibiting second order nonlinear optical effects.

In order to induce polar order to guest-host systems, the technique of electric field poling may be employed [19]. Electric field poling utilises the dipolar nature of the chromophores by application of a DC electric field in order to preferentially align the chromophores in the direction of the applied field. At room temperature, orientational motion of the dipolar guest moieties is inhibited by steric interactions with the polymer host. As the temperature is raised, orientational motion increases until near the glass transition temperature, the mobility state becomes very high and the NLO molecules may easily orient under the influence of an electric field. Once the alignment has reached equilibrium, the soft polymer is then cooled with the applied field to freeze in the alignment of the chromophores. The poling imparts an alignment predicted by the Boltzmann distribution and the film gains $C_{\infty V}$ symmetry. For this particular symmetry group there are two nonvanishing nonlinear coefficients, $\chi_{zzz}^{(2)}$ and $\chi_{zxx}^{(2)}$ [12, 37].

There are several ways in which the electric field is applied to achieve electrical poling of polymer films and these have been outlined in Chapter 1. Probably the most versatile technique for polymer films is corona poling: When a sufficiently high potential difference exists between a pair of unsymmetrical electrodes, such as a needle and plate arrangement, shown in Figure 2.3, a corona discharge of electrical ions is produced.

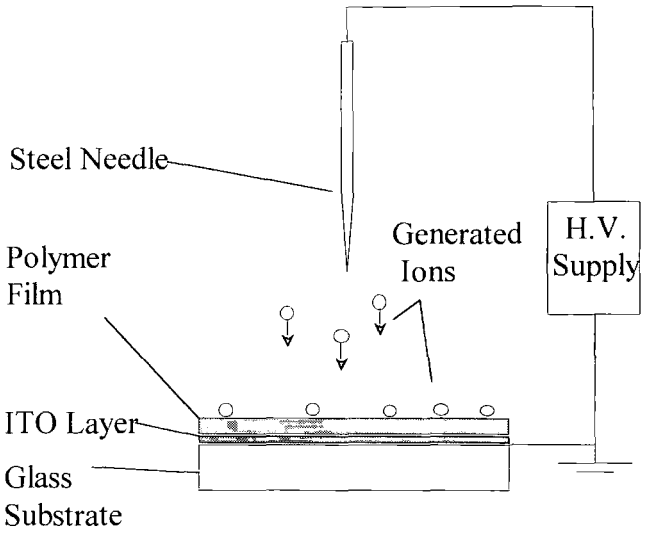

Figure 2.3: Schematic of corona poling. ITO is an indium tin oxide, transparent conducting layer

The ions are of the same polarity as the needle tip and will tend to drift towards regions of lower potential. In this way, ions become deposited on the sample surface, where some will be trapped. In this manner a field is established across the sample thickness. The field strength is only limited by the dielectric strength of the material and the availability of surface traps at the poling temperature. More discussion on electric poling techniques and the corona poling method in particular may be found in Chapter 4.

2.7.1 Relationship between Macroscopic and Microscopic Nonlinearities in Poled Polymers

Macroscopic optical properties can be described in terms of the microscopic properties when appropriately summed and averaged over all contributing constituents. In this section the relationships of microscopic and macroscopic polarizations are addressed. Specifically, the polarization of a static-field-oriented system that results in second harmonic light is considered. When a static field is applied to an otherwise isotropic material, the permanent dipole moments tend to align with the field. This alignment breaks the material symmetry making SHG possible. The amount of alignment or orientation (and reorientation) monitored through the intensity of second harmonic light generated by the material sheds light on the micro-environment of the molecule and its vicinity.

The transformation from the molecular microscopic level to the macroscopic level can be achieved using an orientated rigid gas model. This model describes the orientational

distribution of independent dipoles under the influence of an applied field [39]. In this model it is assumed that the molecules preserve all their properties, and interactions with the host are accounted for by the introduction of parameters such as local field correction factors. However, all intermolecular interactions are neglected.

In a rigid gas model, the second order susceptibility responsible for SHG in a material is,

$$\chi^{(2)}_{IJK}(-2\omega;\omega,\omega) = N\left\langle \beta^{*}_{ijk}(-2\omega;\omega,\omega)\right\rangle_{IJK}$$

Equation 2.9

where I, J and K are the laboratory coordinates, i, j and k describe the molecular coordinates, the asterisk, (*), indicates the local field corrected hyperpolarisability, and N is the number density of contributing molecules. $<\beta_{ijk}>_{IJK}$ is the ijk^{th} component of the orientational average of the molecular second order susceptibility. The transformation from the molecular coordinate system to the laboratory system is achieved by the consecutive rotation of the axes in terms of the standard Euler angles, $\Omega = (\psi, \phi, \theta)$, which relate the two sets of axes as shown in Figure 2.4. The transform matrix relating the two axes can be expressed by [40],

$$a = \begin{pmatrix} \cos\theta\cos\phi\cos\psi - \sin\phi\sin\psi & \cos\theta\sin\phi\cos\psi + \cos\phi\sin\psi & -\sin\theta\cos\psi \\ -\cos\theta\cos\phi\sin\psi - \sin\phi\cos\psi & -\cos\theta\sin\phi\sin\psi + \cos\phi\cos\psi & \sin\theta\sin\psi \\ \sin\theta\cos\phi & \sin\theta\sin\phi & \cos\theta \end{pmatrix}$$

Equation 2.10

The transformation is simplified when a molecule with only one dominant polarization axis is considered. If the direction of the permanent dipole moment, μ and the polarization are chosen in the same direction, say the z-axis, then the only contributing terms in a are, for fixed z,

$$a_{iz} = (\sin\theta\cos\phi, \sin\theta\sin\phi, \cos\theta)$$

Equation 2.11

where the angles are shown in Figure 2.4.

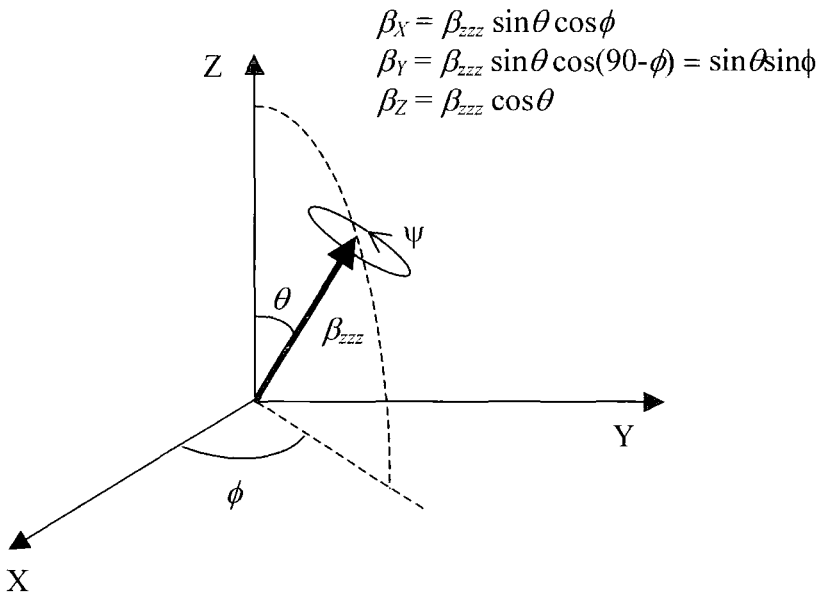

Figure 2.4: Diagram to show coordinate axes of transformation

2.7.2 Orientational Field Distributions

A simple classical molecular theory first developed by Keilich [41] is presented which considers the interaction between electric fields on dipolar species randomly distributed in a naturally isotropic medium.

The statistical average for an azimuthal symmetric molecule (one-dimensional) will be independent of ϕ and, ψ and the first hyperpolarisability can be written as,

$$\left\langle \beta^*_{zzz} \right\rangle_{IJK} = \int_0^{\pi} \beta^*_{zzz} a_{iz} a_{jz} a_{kz} G \sin\theta \quad d\theta$$

Equation 2.12

where G is the orientation distribution function. If the system is ordered by a thermal process, such as electric field poling at elevated temperatures, $G(\theta)$ is the thermodynamic, statistical distribution function. When the fundamental signal is polarized in the plane of incidence, using Equation 2.9 to Equation 2.12, the non-zero components of β for one-dimensional molecules are given by:

$$\begin{aligned}\left\langle \beta^{*}_{zzz} \right\rangle_{XXX} &= \int_0^{\pi} \beta^{*}_{zzz} a_{Xz} a_{Xz} a_{Xz} G \sin\theta \quad d\theta \\ &= \beta^{*}_{zzz} \int_0^{\pi} \left[\sin^2\theta\cos\theta\right] G \sin\theta \quad d\theta \\ &= \beta^{*}_{zzz} \left\langle \sin^2\theta\cos\theta \right\rangle \\ &= \beta^{*}_{zzz} \left\langle \cos\theta - \cos^3\theta \right\rangle\end{aligned}$$

Equation 2.13

Similarly,

$$\begin{aligned}\left\langle \beta^{*}_{ZZZ} \right\rangle_{ZZZ} &= \int_0^{\pi} \beta^{*}_{ZZZ} a_{Zz} a_{Zz} a_{Zz} G \sin\theta \quad d\theta \\ &= \beta^{*}_{ZZZ} \int_0^{\pi} \left[\cos^3\theta\right] G \sin\theta \quad d\theta \\ &= \beta^{*}_{ZZZ} \left\langle \cos^3\theta \right\rangle\end{aligned}$$

Equation 2.14

In this work, the macroscopic system is assumed to exhibit uniaxial symmetry and as such the Boltzmann distribution function of the molecules is only dependent on the polar angle θ between the molecular dipole axis and the poling axis, as follows,

$$G = \frac{\int_0^{\pi} \exp(p\cos\theta)\, d\theta}{\int_0^{\pi} \exp(p\cos\theta)\sin\theta\, d\theta}$$

Equation 2.15

where,

$$p = \frac{\mu_z E_z^{loc}}{kT_p}$$

Equation 2.16

k is the Boltzmann constant, T_p is the poling temperature, E_z^{loc} is the component of the local field in the z-direction and μ is the local permanent dipole moment of the molecule.

It follows from Equation 2.14 that,

$$\left\langle \cos^3\theta \right\rangle = \int_0^{\pi} G(\theta)\cdot\cos^3\theta\cdot\sin\theta\, d\theta$$

Equation 2.17

Therefore by substituting Equation 2.15 and Equation 2.16 into Equation 2.17 gives

$$\begin{aligned}\left\langle \cos^3\theta \right\rangle &= \frac{\int_0^{\pi}\cos^3\theta\exp(p\cos\theta)\sin\theta\, d\theta}{\int_0^{\pi}\exp(p\cos\theta)\sin\theta\, d\theta} \\ &= L_3(p)\end{aligned}$$

Equation 2.18

where $L_3(p)$ is the solution to the integrals in Equation 2.18 and is known as the third order Langevin function. The n^{th} order Langevin functions are given by [41]:

$$\begin{aligned}L_1(p) &= \coth p - \frac{1}{p} \\ &\approx \frac{p}{3} - \frac{p^3}{45} + \frac{2p^5}{945} + \cdots\end{aligned}$$

Equation 2.19

$$L_2(p) = 1 + \frac{2}{p^2} - \frac{2}{p}\coth p$$

Equation 2.20

$$\begin{aligned}L_3(p) &= \left(1 + \frac{6}{p^2}\right)L_1(p) - \frac{2}{p} \\ &\approx \frac{p}{5} - \frac{p^3}{105} + \frac{4p^5}{4725}\cdots\end{aligned}$$

Equation 2.21

For low values of p (implying low dipole moment or field), the odd order Langevin functions are essentially linear in p but saturate for higher values. Thus in the low field limit the first term of the expansions of the Langevin function are valid. In general [12, 39, 42, 43],

$$L_n(p) = \langle \cos^n \theta \rangle = \frac{\int_0^{\pi} \exp(p\cos\theta) \cos^n \theta \sin\theta \, d\theta}{\int_0^{\pi} \exp(p\cos\theta) \sin\theta \, d\theta}$$

Equation 2.22

Therefore, by combining Equation 2.9, Equation 2.14 and Equation 2.18 the second order nonlinear susceptibility for SHG may be expressed as follows:

$$\chi^{(2)}_{ZZZ} = N\beta^*_{zzz} L_3(p)$$

Equation 2.23

In the limit of low poling fields and low dipole moments, Equation 2.23 takes the relatively simple form,

$$\chi^{(2)}_{ZZZ} = \frac{N\beta^*_{zzz} E^{loc}_z \mu_{zzz}}{5kT_p}$$

Equation 2.24

The nonlinear susceptibility is therefore a function of the number density, N, the local dipole moment, μ, and the local "field addressed" hyperpolarisability, β *, (see section 2.7.3) and the poling temperature, T_p.

2.7.3 Local Field Factors

In a dielectric medium containing polarisable molecules, the fields experienced by the individual molecules differs from the externally applied fields (optical, $E^{(\omega)}$, and DC, $E^{(0)}$), due to the presence of the dipole fields generated by the surrounding medium. The local field is not the same as the externally applied field because the local field includes the total field acting on a molecule due to all external sources and the applied field. Thus the externally applied fields must be modified by "local field factors" to account for the local field effects. The local field problem, even for a dielectric with an idealised linear response is quite difficult to solve. It has received the attention of many theoreticians over decades, although this has yielded practical results in only a few simple cases [30, 44].

The classical approach, first established over eighty years ago by Lorentz, is commonly used today [11, 30, 44]. The chromophore is assumed to be embedded in a uniformly polarisable medium. The model assumes an ideal dipole in the centre of a spherical cavity. For atoms or nonpolar molecules with tightly bound electrons, the local field may be expressed as,

$$f_{\omega}^{L} = \frac{n_{\omega}^{2} + 2}{3}$$

Equation 2.25

where f_{ω}^{L} is the Lorenz local field factor and n_{ω}^{2} is the refractive index of the medium at the relevant frequency, ω, which is related to the dielectric constant at optical fields by $\varepsilon \approx n_{\omega}^{2}$. Thus the Lorentz correction factor results from the effects of induced dipoles in the medium from electronic polarization. However, external fields, especially static fields can orient molecules with permanent electric-dipole moments. A refinement of the Lorentz local field may be made when orientational reactive forces are accounted for.

The local fields may be considered to be composed of a "self-field" from the dipole moment and a reaction field. The field of the polarisable dipole in such a cavity polarises the surrounding material, and the resulting inhomogeneous polarisation of the environment will cause a field at the dipole, which is known as the reaction field, R. The presence of a reaction field has important consequences on the electronic properties of guest molecules. The reaction field interacts with the molecule causing a perturbation of the electronic distribution. Therefore, the molecular properties such as the dipole moment, μ and second order polarisability, β that are extremely sensitive to changes in electronic distribution will evolve with R [2]. The reaction field may also induce a dipole in a non-dipolar species [30].

Since the reaction field is brought about by polarizations in the surrounding media, a dipole moment can be expected to change when placed in different environments [45]. In general, increases in the dielectric constant of a medium enhance the dipole moment. In a similar manner, the molecular nonlinear polarisabilities will also be affected by the environment [8, 46] resulting in a dependence of nonlinear properties on the host media. Since these effects change the ground state dipole moment, the transition

energy of the molecule is also dependent on the dielectric constant of the environment, resulting in the effect known as solvatochromism [47].

The reaction field is included in the Onsager model that described the local fields in terms of two components, the cavity field and the reaction field and results in the often-used "Onsager local field factor" [45, 48],

$$f_{\omega}^{0} = \frac{\varepsilon(n_{\omega}^{2} + 2)}{2\varepsilon + n_{\omega}^{2}}$$

Equation 2.26

where the polarisable host medium permittivity is given by ε and the cavity is occupied by a medium of permittivity, n_{ω}^{2}.

Both Equation 2.25 and Equation 2.26 are the usual corrections exploited to relate gas-phase computations and solution or solid phase measurements; in particular, for static (or DC) electric field the local factor is often given by the Onsager expression. Thus, if these local field factors are combined with Equation 2.24, the following result for the second order susceptibility is obtained [35]:

$$\chi_{ZZZ}^{(2)} = NE^{p}f^{o}f^{\omega}f^{\omega}f^{2\omega}\frac{\mu_{zzz}\beta_{zzz}}{5kT}$$

$$= NE^{p}\left(\frac{\varepsilon_{0}\left(n_{\omega}^{2} + 2\right)}{2\varepsilon_{0} + n_{\omega}^{2}}\right)\left(\frac{n_{\omega}^{2} + 2}{3}\right)^{2}\left(\frac{n_{2\omega}^{2} + 2}{3}\right)\frac{\mu_{zzz}\beta_{zzz}}{5kT}$$

Equation 2.27

The validity of this approach rests on the hypothesis that the polarization within the medium is uniform and also depends on the shape of the cavity employed. It has been shown that the distribution of local fields is sensitive to the microstructure of the local medium [49]. Both equations are derived for spherical cavities and do not account for molecular anisotropy. A spherical cavity may not necessarily be the best shape approximation for the molecules considered in this work. It may be more appropriate to represent guest molecules by ellipsoidal cavity shapes [50]. However, when such volumes are used, the semi-principle axes must be calculated together with the polarisability. Modelling packages exist to calculate molecular properties [51] such as polarisability and molecular dimensions; however, these packages only calculate gas phase values and cannot calculate local values. As has been mentioned, the reaction

field has a considerable effect on the electronic properties of a molecule, including polarisability. Therefore, field factor calculations that are more complex may introduce further errors into the computation of susceptibilities and for the sake of simplicity; the relatively straightforward form of Equation 2.27 has been employed.

2.8 Electric Field Induced Second Harmonic Generation (EFISH)

The time-averaged molecular orientation in liquids or solution will be completely isotropic. This random fluctuation of the orientation of molecules in solutions will result in average cancellation of macroscopic even-order polarisation effects. In order to access the molecular second order susceptibility, $\Gamma^{2\omega}{}_{IJKL}$, in isotropic media, a static electric field is applied to the sample along the direction of polarisation of the fundamental beam. The application of the electric field breaks the symmetry of the medium introducing a bias orientational distribution of the electric dipoles in the direction of the field. Thus the technique of electric field induced second harmonic generation, (EFISH) enables the generation of second harmonic fields. Since the experiments generate a field at 2ω from the interaction of three waves (two at the fundamental frequency and one at dc), the induced nonlinear polarisation must operate through a third order process.

The polarisation, $P_I^{(\omega)}$, at the second harmonic for EFISH is given by [12, 29, 41],

$$P_I^{(2\omega)} = \chi_{IJKL}^{(2\omega)} E_J^{\omega} E_K^{\omega} E_L^{0} = \Gamma_{IJKL}^{2\omega} E_J^{\omega} E_K^{\omega} E_L^{0} = d_{IJK}^{eff} E_J^{\omega} E_K^{\omega}$$

Equation 2.28

where E_J^{ω} and E_K^{ω} are the applied fundamental optical fields and E_L^{0} is the static field. The susceptibility is related to the susceptibility in Equation 2.3 through the expression,

$$\Gamma_{IJKL}^{2\omega} = \chi_{IJKL}^{(2\omega)} = \chi_{IJKL}^{(3)}(-2\omega;\omega,\omega,0)$$

Equation 2.29

This susceptibility possesses several general symmetry properties. Firstly, $\Gamma^{2\omega}{}_{IJKL} = \Gamma^{2\omega}{}_{IKJL}$ since E_J and E_K are interchangeable. Choosing a propagation direction because the medium is isotropic can restrict $\Gamma^{2\omega}{}_{IJKL}$. Thus assuming the direction of propagation of plane polarised waves is in the $x = 1$ direction, different

combinations of the various components of β_{ijk} will be measured by different components of $\Gamma^{2\omega}$. However, the focus here is on E^{ω} and E^{0} having a common polarisation in the z direction, leading to,

$$P_z^{2\omega} = \Gamma_{zzzz}^{2\omega} E_z^{\omega} E_z^{\omega} E_z^{0}$$

Equation 2.30

The second harmonic microscopic polarisation, $P^{2\omega}{}_{ijkl}$ of a molecule under the influence of static and optical fields is given by,

$$\begin{aligned} p_i^{2\omega} &= \beta_{ijk}^{2\omega} E_j^{\omega} E_k^{\omega} + \gamma_{ijkl}^{2\omega} E_j^{\omega} E_k^{\omega} E_l^{0} \\ &= \left(\frac{\beta_{ijk}^{2\omega}}{E_l^{0}} + \gamma_{ijkl}^{2\omega} \right) E_j^{\omega} E_k^{\omega} E_l^{0} \end{aligned}$$

Equation 2.31

where $(\beta^{2\omega}{}_{ijk}/E^{0}{}_{l}) + \gamma^{2\omega}{}_{ijkl} = \gamma^{TOT}$ represents the total third order nonlinearity at the second harmonic frequency including contributions from electronic, vibrational, and rotational motions. It should be noted that this γ^{TOT} is not the same as in Equation 2.1, since the polarisation expansion only contains terms relating to the electronic distortion. Thus for a single molecule, the second harmonic polarisation may be written as [52],

$$p_i^{2\omega} = \beta_{ijk}^{2\omega} E_j^{\omega} E_k^{\omega} + \left(\gamma_{ijkl}^{e} + \gamma_{ijkl}^{v} \right) E_j^{\omega} E_k^{\omega} E_l^{0}$$

Equation 2.32

where, $\gamma^{e}{}_{ijkl}$ and $\gamma^{v}{}_{ijkl}$ are the electronic and vibrational contributions to the nonlinearity. In order to relate Equation 2.32 to experiment, $P^{2\omega}{}_{i}$ must be averaged over all possible orientations of the molecules. Since contributions to μ and β are dominated by charge transfer interactions this implies that the largest contributions are along the charge transfer direction of the molecule. Thus if the charge transfer axis is along the z-direction the contributions to μ and β in the x- and y- directions are small compared to the z-direction. For this reason, all the fields are chosen along the z-direction. The application of a static field in EFISH experiments orients the dipoles so that the average macroscopic dipole moment lies in the direction of the external field. Thus if μ and β are parallel to each other and in the z-direction, an average

component of β is measured. A Boltzmann distribution of averaging is used to yield the following [52]:

$$\left\langle P_{ZZZZ}^{2\omega} \right\rangle = \gamma_{ZZZZ} E_Z^0 \left(E_Z^{\omega}\right)^2$$

Equation 2.33

where,

$$\gamma_{ZZZZ} = \gamma = \gamma^e + \gamma^r + \gamma^v$$
$$\approx \gamma^e + \frac{\mu\,\beta}{5kT}$$

Equation 2.34

where γ_{ZZZZ} is the average total hyperpolarisability, γ^e is the average electronic contribution, γ^v is the average vibrational nonlinearity that is often neglected as shown in Equation 2.34, and $\gamma^r = \mu\beta/5kT$ is the average dipolar rotational contribution. For centrosymmetric molecules, this rotation term will vanish because μ and β are zero.

The three contributions to γ have different response times; the purely electronic contribution has a frequency response in the ultra violet ($\tau \sim 10^{-15}$ s), the molecular vibrations occur in the infrared ($\tau \sim 10^{-13}$ s), while the dipole rotation response γ^r is in the mm region ($\tau \sim 10^{-11}$ s). Levine and Bethea have shown that the vibrational contribution, γ^v to the hyperpolarisability is negligible compared to the electronic contribution, γ^e [52]. In addition measurements of γ^e using four-wave mixing have been performed on a variety of highly conjugated molecules, indicating the effect of γ^e will usually be 10% of the rotational term in these systems [53]. Thus, in practice, the electronic contribution is also often neglected because this contribution is much smaller than the rotational contribution, particularly for molecules with large dipole moments [12, 48, 53, 54]. Within the experimental accuracy, it is also reasonable to neglect γ^e in this work in line with these other studies of conjugated molecules.

2.9 Intermolecular Forces

Forces that arise between particles may be classified into four categories: gravitational, electromagnetic, strong nuclear and weak nuclear forces. The gravitational force is extremely long range and of small magnitude. Conversely, the strong and weak nuclear forces are electromagnetic forces responsible for the binding of neutrons and protons inside the nucleus, and consequently the range over which they are significant is of the order of 10^{-15} m. Since typical molecular dimensions are of the order 5×10^{-11} m, electromagnetic forces are the source of intermolecular interactions. Consequently, intermolecular forces are electrostatic forces that exist between molecules that cause one molecule to influence another. Such forces will cause a gas to deviate from ideal gas behaviour ($PV = RT$) and are stronger in the liquid and solid state. The ideal gas law arises from the fact that the pressure, P, and temperature, T, are both related to the motion of the molecules through the gas constant, R. The pressure is due to the force that molecules exert on the walls of the container of volume V, by virtue of their collisions with the walls and the temperature is a measure of the average kinetic energy of the molecules.

In an attempt to explain this deviation, the Dutch physicist, J.D. van der Waals was one of the first to consider the effect of attractive forces between molecules and arrived at the famous equation of state for gases and liquids [55-57]. This was a modification to the ideal gas law to account for the finite size of the molecules (by subtracting a term, b, from the volume) and an extra term was added, a/V^2 to the pressure to account for the attractive intermolecular forces, now known as van der Waal forces:

$$\left(P + \frac{a}{V^2}\right)(V - b) = RT$$

Equation 2.35

Some thirty years later, in 1903, Mie proposed an interaction "pair potential" of the form,

$$U(r) = -\frac{A}{r^n} + \frac{B}{r^m}$$

Equation 2.36

where A and B are constants, $m > n$ and r is the intermolecular separation. This was a semi-empirical expression that, for the first time, included a repulsive short range term together with an attractive long range term. The potential exhibits a single minimum that represents the closest approach of atoms to their neighbours. This was successfully able to account for a wide range of properties. The Lennard-Jones potential was developed in 1924 and is a special case of the Mie potential with $n = 12$ and $m = 6$. The repulsive potential falls at $1/r^{12}$ represents the decay of atomic wavefunctions at large distances, and hence the overlap that is responsible for repulsion. These are simplified representations of the potential energy where the details are ignored and the general features are represented by a few adjustable parameters. Indeed the attractive component of the Lennard-Jones potential is theoretically based on the dispersion energy contribution, whilst the form of the repulsive term is derived from the fact that atoms may not be infinitely close since electron clouds may not overlap. Nonetheless, such representations having the considerable advantage of relative simplicity are successfully and widely used today.

The long-range attractive component of intermolecular forces is most significant when distances are such that the probability of overlap of electron clouds of different molecules is small. There are three main types of force that contribute to the attractive van der Waals interactions depending on the nature of the interacting molecules; dipole-dipole interactions, dispersion interactions and induced-dipole induced-dipole interactions. These will be considered separately in the following sections in more detail. In certain instances other types of attractive interactions are observed and are often of great importance.

In particular, hydrogen bonding interactions are forces that exist between molecules that have a hydrogen atom bonded to a highly electronegative atom such as oxygen, nitrogen, or fluorine. This represents a strong partial dipole in the molecule that will have the hydrogen end (positive) attracting the negative end (O, N, or F) of other molecules. In the bonds N-H, O-H, and F-H the shared electron pair is shifted towards the N, O and F so that these bonds have a permanent strong dipole $X^{\delta-}—H^{\delta+}$. Hydrogen bonding between ammonia molecules, between water molecules, and between hydrogen fluoride molecules is responsible for their high boiling points and the liquids are said to be highly associated [34]. Carbon and hydrogen have very similar electronegativity and C-H bonds are almost non-polar and thus methane has a much

lower boiling point than ammonia, water and hydrogen fluoride. Hydrogen bonds are responsible for forming the open framework lattice of ice in which each oxygen atom forms two intramolecular covalent bonds to hydrogen and two intermolecular hydrogen bonds to hydrogen atoms in neighbouring water molecules.

2.9.1 Dipole-dipole (Keesom) Interactions

This is one of the interactions that contribute to van der Waals interactions and is often termed the orientation or Keesom interaction. Dipole-Dipole interactions are forces that exist between polar molecules where the partial positive end of one molecule attracts the partial negative charge of another molecule. Only polar molecules can exhibit this type of Van Der Waals and the strength of the force increases with an increase in the polarity of the molecule.

Consider a pair of molecules, *1* and *2*, separated at large distances, *r*, compared to the molecular dimensions as shown in Figure 2.5; in the absence of quadrupole or higher order mulitpoles, the direct electrostatic interaction energy, $U(r, \theta_1, \theta_2, \phi)$, may be expressed in terms of the separation, *r* and relative orientation [56] as described in Equation 2.37,

$$U(r,\theta_1,\theta_2,\phi) = -\frac{\mu_1\mu_2}{(4\pi\varepsilon_0)r^3} f(\theta_1,\theta_2,\phi)$$

Equation 2.37

where μ_1 and μ_2 are the dipole moments of molecules 1 and 2 respectively.

The function $f(\theta_1, \theta_2, \phi)$ contains the orientation dependence of the energy and has the form [55]:

$$f(\theta_1,\theta_2,\phi) = -(\sin\theta_1 \sin\theta_2 \cos\phi - 2\cos\theta_1 \cos\theta_2)$$

Equation 2.38

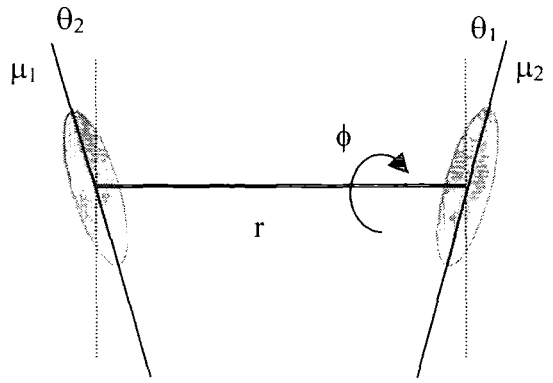

Figure 2.5: Schematic to show the geometry of a dipole-dipole interaction

Thus, it can be seen that the dipole-dipole interaction energy is proportional to r^{-3} for a fixed configuration of the molecules, and that it is strongly dependent on orientation, varying from attractive to repulsive as one molecule is rotated.

If the two molecules are free to rotate as they are in the gas phase or in solution, the dipole-dipole energy averaged over all possible orientations is required. If all relative orientations were equally possible, then this average would lead to zero interaction energy. However, such averaging is unrealistic since not all relative orientations are equally probable. Preferential weighting results from the introduction of the Boltzmann averaging which accounts for temperature effects and favours configurations with lower energy relative to those with higher energy. In general, the angle-averaged free energy, *U(r)*, of the instantaneous orientation-dependent energy, *U(r, Ω)*, is given by the potential distribution theorem,

$$\exp\left[\frac{-U(r)}{kT}\right] = \frac{\int U(\omega)\exp\left[\frac{-U(r,\Omega)}{kT}\right]\, d\Omega}{\int d\Omega} = \left\langle \exp\left[\frac{-U(r,\Omega)}{kT}\right] \right\rangle$$

Equation 2.39

where T is the temperature and the instantaneous orientation-dependent free interaction energy, $U(r, \Omega)$, arises from Equation 2.37 and $d\Omega$ corresponds to the polar and azimuthal anlges, θ and ϕ as in Figure 2.5 and integration over angular space.

When the potential energy of the interaction of the two dipoles is very small compared with the energy of thermal motion, the exponential in Equation 2.39 may be expanded to give,

$$\exp\left[\frac{-U(r)}{kT}\right] = 1 - \frac{U(r)}{kT} + \cdots$$
$$= \left\langle 1 - \frac{U(r,\Omega)}{kT} + \frac{1}{2}\left(\frac{U(r,\Omega)}{kT}\right)^2 \right\rangle$$

Equation 2.40

Consequently,

$$U(r) \approx \left\langle U(r,\Omega) - \frac{U(r,\Omega)^2}{2kT} \right\rangle$$

Equation 2.41

Therefore, using Equation 2.41 and Equation 2.37 the angle-averaged free energy of a dipole-dipole interaction is

$$U(r) = -\frac{\mu_1^2 \mu_2^2}{3(4\pi\varepsilon_0\varepsilon)^2 kTr^6} \qquad for \quad kT > \frac{\mu_1\mu_2}{(4\pi\varepsilon_0\varepsilon)r^3}$$

Equation 2.42

Noting the spatially averaged values of angles;

$$\langle \cos^2\theta \rangle = \frac{1}{4\pi}\left[\int_0^\pi \cos^2\theta \sin\theta \, d\theta\right] \cdot \int_0^{2\pi} d\phi = \frac{1}{3}$$
$$\langle \sin^2\theta \rangle = \frac{1}{4\pi}\left[\int_0^\pi \sin^2\theta \sin\theta \, d\theta\right] \cdot \int_0^{2\pi} d\phi = \frac{2}{3}$$
$$\langle \sin^2\phi \rangle = \langle \cos^2\phi \rangle = \frac{1}{2}$$
$$\langle \sin\theta \rangle = \langle \cos\theta \rangle = 0$$

Equation 2.43

So far the interactions have implicitly assumed to occur at constant volume and hence free energies have been stated. In order relate the free energy, A, to the total energy, U^{TOT}, of the system, the thermodynamic, Gibbs-Helmholtz relation may be used:

$$U^{TOT} = A + TS$$
$$= -T^2 \frac{\partial}{\partial T}\left(\frac{A}{T}\right)$$

Equation 2.44

where S is the entropy of the system and T is the temperature. Thus the total energy for the angle averaged dipole-dipole interaction is,

$$U = \frac{2\mu_1^2\mu_2^2}{3(4\pi\varepsilon_0\varepsilon)^2 kTr^6}$$

Equation 2.45

The Boltzmann-angle averaged interaction between two permanent dipoles, the dipole-dipole interaction, varies with the inverse sixth power of distance as shown in Equation 2.45.

2.9.2 Dispersion (London) Forces

London dispersion forces are the attractive forces that exist between all molecules as a result of the electrostatic attraction of the positive nuclei of one molecule to electrons of another molecule. The electronic distribution of a molecule at a given instant in time may not be perfectly symmetrical as shown in Figure 2.6. In this case, the centres of gravity of the positive and negative charge distributions do not coincide and the atom would have a transient dipole. A close neighbouring atom will be influenced by this apparent dipole and thus due to electron repulsion, a temporary dipole on one atom can induce a similar dipole in a neighbouring atom and cause an attraction between the two atoms. All molecular substances exhibit London dispersion forces and these are the weakest of the van der Waals forces. Often the greater the polarisability of a molecule, the easier it is to induce a momentary dipole (alter the electron distribution) and the stronger the dispersion forces.

(a)

The time-averaged electron density distribution around a nucleus. The shaded area represents the electron cloud and the dark dot represents the nucleus

(b)

Representation of instantaneous dipole-induced dipole interaction

Figure 2.6: Scematic to show dispersion interaction

The dispersion energy is purely quantum mechanical in origin and so cannot be described in terms of classical mechanics. Fritz London first described the dispersion force in terms of an oscillator model [58] in 1936. For two identical molecules, the dispersion interaction energy is,

$$U(r) = \frac{-C_{disp}}{r^6} = -\frac{3}{4}\frac{\alpha^2 h\nu}{(4\pi\varepsilon_0)^2 r^6}$$

$$= -\frac{3}{4}\frac{\alpha^2 I}{(4\pi\varepsilon_0)^2 r^6}$$

Equation 2.46

where r is the distance between the atoms, α is the static polarisability, and I is the ionisation potential.

And for two dissimilar molecules:

$$U(r) = -\frac{3}{2}\frac{\alpha_1\alpha_2}{(4\pi\varepsilon_0)^2 r^6}\frac{I_1 I_2}{(I_1 + I_2)}$$

Equation 2.47

This simple model has been superseded by more rigorous and complicated quantum mechanical calculations that lead to expressions of the same form as Equation 2.46 with different values for $C_{disp.}$ For the purposes of this work, Equation 2.46 is relied upon to give values that contribute to the total van der Waal interactions.

2.9.3 Induction (Debye) Forces

When a molecule is placed in an electric field, there is a redistribution of the electronic charge distribution, known as polarisation. Consequently, a dipole moment is induced in the molecule. The polarising electric field need not necessarily be externally applied. Since a neutral molecule possessing a permanent dipole moment, μ, gives rise to an electrostatic potential Φ and consequently and electric field, $E = -\delta\Phi/\delta r$, this electric field maybe responsible for the induction of a dipole moment in a second molecule which is nearby, whether the second molecule is itself polar or not. In general, the treatment of induction forces is complex partly because for many molecules the polarisability is not isotropic but is tensorial in character. Furthermore, higher-order multipoles in polar molecules can induce higher order multipoles in other molecules.

For the simple case of a fixed dipole, μ, oriented at an angle, θ, to the line joining it to a polarisable molecule, with polarisability α, as in Figure 2.7, the interaction energy is given by [55, 57],

$$U(r,\theta)_{ind} = -\frac{1}{2}\alpha E^2 = -\mu^2\alpha\frac{\left(1+3\cos^2\theta\right)}{2(4\pi\varepsilon_0\varepsilon)^2 r^6}$$

Equation 2.48

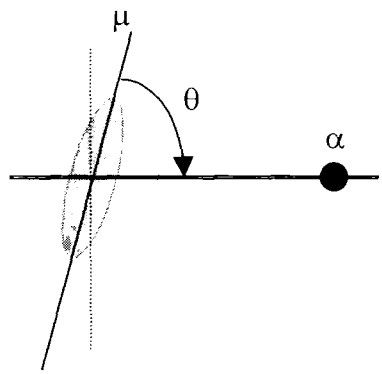

Figure 2.7: Schematic diagram of interaction between a dipole, μ and a polarisable molecule with polarisability, α

Typically, the strength of this interaction is not sufficient to mutually orient molecules, as may occur in strong dipole-dipole interactions. The effective interaction is the angle-averaged energy. Thus if each orientation is weighted with the Boltzmann factor, $exp(-U_{ind}/kT)$, the average energy of the interaction at sufficiently high temperatures becomes,

$$U(r) = -\frac{\mu^2\alpha}{(4\pi\varepsilon_0\varepsilon)^2 r^6}$$

Equation 2.49

While more generally, for two molecules each possessing permanent dipole moment, μ_1 and μ_2 and polarisabilities, α_1 and α_2, the net dipole-induced dipole energy is [55],

$$U(r) = -\frac{\left(\mu_1^2\alpha_2 + \mu_2^2\alpha_1\right)}{(4\pi\varepsilon_0\varepsilon)^2 r^6}$$

Equation 2.50

Thus it can be seen that the Debye interaction constitutes another of the three inverse sixth power contributions to the total van der Waals interaction energy between

molecules. However, unlike the dipole-dipole interaction energy, the induction interaction is not temperature dependent.

This model is considerably simplified. In general, the static polarisability is not isotropic so it must be represented by a second rank tensor, α. The elements of this tensor relate the dipole moment component induced in one direction to a field component in another direction. Furthermore, even if the polarisability is isotropic, such as in the case of a molecule with spherical geometry, nonlinearities between the induced dipole and the field can occur. In addition, higher order multipole moments may be induced by the electric field. Each of these factors may contribute to the induction energy between two molecules.

2.9.4 Solvent Effects

In general, the interactions of an isolated pair of molecules are not the same when the molecules are surrounded by solvent molecules in a medium. Interactions with the surrounding medium may cause complex repulsive and attractive forces such as steric forces, solvation forces and electrostatic forces.

The interaction energy is modified by the intervening medium through the dielectric constant of the solvent, ε_s. This is reflected in the oriented gas model described in this chapter by employing local field factors. In addition, the solvent structure will be disturbed by the presence of solute molecules as the solvent-solvent interactions are replaced by solvent-solute interactions resulting in a change in the net energy of the system. These interactions are often called solvation forces. Moreover, local rearrangements of molecules may cause a significant entropy change of the system. Consequently, the ideal model should consider interactions involving the average of all possible configurations of the solvent molecules relative to the solute. Finally, the electronic distribution of the solute molecules will become distorted from the free space distribution because of interactions between the solute molecules in the solvent, and this in turn will modify the solute-solute and solute-solvent interactions.

2.9.5 Modified Orientated Gas Model

It is known that for small, polar molecules, the dipole-dipole and induced dipole interactions discussed in 2.9.1 and 2.9.3 respectively, comprise approximately 20% of the long-range attractive energy [56]. The third contribution to the attractive van der Waals interactions consists of the dispersion energy.

Nevertheless, all of the molecular interactions described in this section are often neglected when translating microscopic properties of nonlinearities to macroscopic nonlinearities in nonlinear optical materials. As has been shown through Equation 2.45, Equation 2.50 and Equation 2.47, this electrostatic interaction becomes stronger the larger the dipole moments and polarisabilities of the molecules concerned. Since nonlinear optics intrinsically requires molecules to have large dipole moments and polarisabilities, the neglect of these interactions is not likely to be strictly valid. Recently, Dalton *et al* [59] have proposed a model that includes these intermolecular interactions in the poling of thin films and this model has been extended to describe EFISH results of this thesis.

The competition between chromophore-chromophore electrostatic interactions and chromophore-applied electric field interactions is modelled using a theory based on Van der Waals interactions and is termed a modified "London theory". London's famous expression (Equation 2.46) for the dispersion interaction energy between two identical neutral atoms is [58],

$$U(r) = \frac{-C_{disp}}{r^6} = -\frac{3\alpha^2 I}{4(4\pi\varepsilon_0)^2 r^6}$$

Equation 2.51

where r is the distance between the atoms, α is the static polarisability, and I is the ionisation potential. This interaction is essentially quantum mechanical in nature, arising from instantaneous but fluctuating dipole moments of neutral atoms and thus it retains some electrostatic character. Indeed the $1/r^6$ dependence of the force is the same as that for the two other polarisation interactions (the Keesom and Debye forces) that contribute to the net van der Waals force. As discussed previously in sections 2.9.1 to 2.9.3, there are three distinct types of force that contribute to the total long-range interaction between polar molecules, collectively known as the van der Waals force: namely the interactions of dispersion (or London forces), induction (or Debye forces)

and orientational (or Keesom forces). So for two dissimilar polar molecules the interaction energy may be written as:

$$W_{VDW}(r) = -\frac{C_{VDW}}{r^6} = -\frac{1}{r^6}\left[C_{ind} + C_{orient} + C_{disp}\right]$$
$$= -\frac{1}{r^6}\left[\frac{\left(\mu_1^2\alpha_2 + \mu_2^2\alpha_1\right)}{(4\pi\varepsilon_0)} + \frac{2\mu_1^2\mu_2^2}{3kT(4\pi\varepsilon_0)^2} + \frac{3\alpha_1\alpha_2 I}{4}\right]$$

Equation 2.52

Where μ_1 and μ_2 are the dipole moments of molecules 1 and 2 respectively and r is the average distance between chromophores. It is this statistically averaged potential energy for the chromophore-chromophore interaction that is used in model described by Dalton *et al.* Assuming spherically symmetrical chromophores and averaging over the relative orientation of one chromophore with respect to another leads to the energy term,

$$U = \mu F \cos\theta - W_{VDW}\cos\phi$$

Equation 2.53

Where F contains all the local field factors, θ describes the average angle between a chromophore, W_{VDW} is the interaction energy associated with the van der Waals force and the poling field direction and two chromophores are related to each other by the angle ϕ. This energy term is then used in the usual orientational average $<\cos^3\theta>$ term when translating microscopic to macroscopic nonlinearities, as described in section 2.7.1 [9],

$$\chi^{(2)} = NF\beta < \cos^3\theta >$$
$$= NF\beta\left[\frac{\mu E_p}{5kT}\left(1 - L_1^2\left(\frac{W_{VDW}}{kT}\right)\right)\right]$$

Equation 2.54

Where L_1 is the first order Langevin function as given by the following:

$$
\begin{aligned}
L_1(p) &= <\cos p> \\
&= \coth(p) - \frac{1}{p} \\
&= \frac{\int_0^{\pi} \cos\theta \cdot \exp(p \cdot \cos\theta) \cdot \sin\theta \, \partial\theta}{\int_0^{\pi} \exp(p \cdot \cos\theta) \cdot \sin\theta \, \partial\theta}
\end{aligned}
$$

Equation 2.55

Strictly speaking, the $\mu E_p F/5kT$ term in Equation 2.54 is derived from the approximation of the third order Langevin function as described in section 2.7.2. Dalton's modified oriented gas model for polymer films is now adapted to model EFISH data. The third order susceptibility can be related to the microscopic properties by,

$$
\begin{aligned}
\Gamma &= \chi^{(3)} \\
d_{ijk} &= \Gamma_{ijk} E_I^0 \\
&= N\gamma\beta f_0 f_\omega^2 f_{2\omega} \\
&= N\beta <\cos^3\theta> f_0 f_\omega^2 f_{2\omega}
\end{aligned}
$$

Equation 2.56

where N is the number density of the nonlinear optical molecule, f_0, f_ω^2 and $f_{2\omega}$ are the local field factors. Equation 2.56 shows that the susceptibility Γ depends on constant field factors, the constant molecular property of β, the number density and a term relating to the average orientation of the chromophores in the applied electric field, $<\cos^3\theta>$. So if the orientational average term takes on a simple form the nonlinearity, Γ would be expected to be a linear function of number density, N. However, if the functional form of $<\cos^3\theta>$ term is more complex and depends on factors such as the distance between particles (and therefore the number density), the dependence of Γ on N may not be so straightforward. Thus, if the attractive van der Waals interactions are taken into account as in Equation 2.54, the third order non-linearity may be expressed as,

$$
\Gamma = N f_\omega^2 f_{2\omega} \beta L_3(p) \left[1 - L_1^{\,2} \left(\frac{W_{VDW}}{kT} \right) \right]
$$

Equation 2.57

where p is the ratio of the poling orientation energy to thermal energy, $\mu f_0 E_p / kT$.

Since the energy, W_{VDW} is proportional to N^2, Equation 2.57 shows that the total nonlinearity is no longer a linear function of the number density of active NLO species. The long-range van der Waals forces associated with polar and neutral molecules defines the form of this model.

2.10 References

1. Meyers, F., Marder, S.R., Pierce, B.M., and Brédas, J.L., *Electric field modulated nonlinear optical properties of donar-acceptor polyenes: sum-over-states investigation of the relationship between molecular polarizabilities (α, β, and γ) and bond length alternation.* Journal of the Chemical Society, 1994. **116**: p. 10703-10714.

2. Marder, S.R., Gorman, C.B., Meyers, F., Perry, J.W., Bourhill, G., Bredas, J.L., and Pierce, B.M., *A unified description of linear and nonlinear polarization in organic polymethine dyes.* Science, 1994. **265**(5172): p. 632-635.

3. Kamada, K., Ueda, M., Nagao, H., Tawa, K., Sugino, T., Shmizu, Y., and Ohta, K., *Molecular design for organic nonlinear optics: polarisability and hyperpolarisabilities of furan homologues investigated by ab initio molecular orbital method.* Journal of Physical Chemistry, 2000. **A 104**: p. 4723-4734.

4. Blanchard-Desce, M., Alain, V., Midrier, L., Wortmann, R., Lebus, S., Glania, C., Krämer, P., Fort, A., Muller, J., and Barzoukas, M., *Intramolecular charge transfer and enhanced quadratic optical non-linearities in push-pull polyenes.* Journal of Photochemsitry and Photobiology A: Chemistry, 1997. **105**: p. 115-121.

5. Wang, F., Harper, A.W., Lee, M.S., Dalton, L.R., Zhang, H., Chen, A.T., Steier, W.H., and Marder, S.R., *Progress toward device-quality second-order NLO materials: 3. Electrooptic activity of polymers containing E,E,E-[4-(N,N-dialkylamino)-phenyl] pentadienylidene-3-phenyl-5-isoxazolone chromophores.* Chemistry Of Materials, 1999. **11**(9): p. 2285.

6. Wang, P., Zhu, P., Wu, W., Kang, H., and Ye, C., *Design of novel nonlinear optical chromophores with mulitple substitutions.* Physical Chemistry Chemical Physics, 1999. **1**: p. 3519-3525.

7. Verbiest, T., Houbrechts, S., Kauranen, M., Clays, K., and Persoons, A., *Second-order nonlinear optical materials: recent advances in chromophore design.* Journal of Materials Chemistry, 1997. **7**(11): p. 2175-2189.

8. Meyers, F., Marder, S.R., Pierce, B.M., and Brédas, J.L., *Tuning of large second hyperpolarizabilities in organic conjugated compounds.* Chemical Physics Letters, 1994. **228**: p. 171-176.

9. Dalton, L.R., Harper, A.W., and Robinson, B.H., *The role of London forces in defining noncentrosymmetric order of high dipole moment high hyperpolarizability chromophores in electrically poled polymeric thin films.* Proceedings of the National Academy of Sciences of the United States of America, 1997. **94**(10): p. 4842-4847.

10. Dalton, L.R., *Polymeric electro-optic materials: optimization of electro- optic activity, minimization of optical loss, and fine-tuning of device performance.* Optical Engineering, 2000. **39**(3): p. 589-595.

11. Boyd, R.W., *Nonlinear Optics*. 1992, London: Academic Press Inc. 427.

12. Prasad, P.N. and Williams, D., *Introduction to nonlinear optical effects in molecules and polymers*. 1991, New York: Wiley-Interscience. 306.

13. Williams, D.J., *Organic polymeric and non-polymeric materials with large optical nonlinearities.* Angewante Chemie International Edition in English, 1984. **23**: p. 690-703.

14. Jerphagnon, J. and Kurtz, K., *Maker fringes: detailed comparison of theory and experiment for isotropic and unixial crystals.* Journal of Applied Physics, 1970. **41**(4): p. 1667-1681.

15. Ravi, M., Szablewski, M., Hackman, N.-A., Cross, G.H., Bloor, D., Goeta, A.E., and Howard, J.A.K., *Crystal structures of amino substituted dicyanoquinodimethanes with potential nonlinear optical applications.* New Journal of Chemistry, 1999. **23**: p. 841-844.

16. Bosshard, C., Sutter, K., Schlesser, R., and Gunter, P., *Electrooptic effects in molecular-crystals.* Journal of the Optical Society of America B-Optical Physics, 1993. **10**(5): p. 867-885.

17. Ashwell, G.J., Dawnay, E.J.C., Kuczynski, A.P., Szableweski, M., Sandy, I.M., Bryce, M.R., Grainger, A.M., and Hasan, M., *Langmuir-Blodgett alignment of zwitterionic optically non-linear D-π-A materials.* Journal of the Chemical Society of Faraday Transactions, 1990. **68**(7): p. 1117-1121.

18. Bosshard, C.H., Sutter, K., Prêtre, P.H., Hulliger, J., Flörsheimer, M., Kaatz, P., and Günter, P., *Organic nonlinear optical materials*. Advances in nonlinear optics, ed. A.F. Garito and F. Kajzar. Vol. Volume I. 1995, Postfach: Gordon and Breach.

19. Meredith, G.R., Vandusen, J., G, and Williams, D., J, *Optical and nonlinear optical characterization of molecularly doped thermotropic liquid crystalline polymers.* Macromolecules, 1982. **15**: p. 1385-1389.

20. Körner, H., Shiota, A., Bunning, T.J., and Ober, C.K., *Orientation-on-demand thin films: curing of liquid crystaline networks in ac electric fields.* Science, 1996. **272**: p. 252-255.

21. Grell, M., Bradley, D.D.C., Inbasekaran, M., and Woo, E.P., *A glass-forming conjugated main chain liquid crystal polymer for polarised electroluminescence applications.* Advanced Materials, 1997. **9**(10): p. 799-803.

22. Singer, K.D., Kuzyk, W.R., Sohn, J.E., Lalama, S.J., Comizzoli, R.B., Katz, H.E., and Schilling, M.L., *Electro-optic phase modulation and optical second-harmonic generation in corona-poled polymer films.* Applied Physics Letters, 1988. **53**(19): p. 1800-1802.

23. Kaino, T. and Tomaru, s., *Organic materials for nonlinear optics.* Advanced Materials, 1993. **5**(3): p. 117-123.

24. Sutton, L.E., *The significance of the differences between the dipole moments of saturated and unsaturated substances.* Proceedings of the Royal Society (London), 1931. **133**: p. 668-695.

25. Marder, S.R., Perry, J.W., Bourhill, G., Gorman, C.B., Tiemann, B.G., and Mansour, K., *Relation between bond-length alternation and 2nd electronic hyperpolarizability of conjugated organic-molecules.* Science, 1993. **261**(5118): p. 186-189.

26. Marder, S.R., Cheng, L.-T., Tiemann, B.G., Friedli, A.C., Blanchard-Desce, M., Perry, J.W., and Skindhoj, J., *Large first hyperpolarizabilities in push-pull polyenes by tuning of the bond length alternation and aromaticity.* Science, 1994. **263**: p. 511-514.

27. Brédas, L.J., *Molecular geometery and nonlinear optics.* Science, 1994. **263**: p. 487-488.

28. Bourhill, G., Bredas, J.L., Cheng, L.T., Marder, S.R., Meyers, F., Perry, J.W., and Tiemann, B.G., *Experimental demonstration of the dependence of the 1st hyperpolarizability of donor-acceptor-substituted polyenes on the ground-state polarization and bond-length alternation.* Journal of the American Chemical Society, 1994. **116**(6): p. 2619-2620.

29. Chemla, D.S. and Zyss, J., *Nonlinear optical properties of organic molecules and crystals*. Quantum Electronics - Principles and Applications, ed. D.S. Chemla and J. Zyss. Vol. 1 and 2. 1987, New York: Academic Press. 482.

30. Böttcher, C.J.F., *Theory of electric polarisation.* Dielectrics in static fields, ed. O.C. van Belle, P. Bordewijk, and A. Rip. Vol. volume I. 1993, Amsterdam: Elsevier. 377.

31. Lambert, C., Stadler, S., Bourhill, G., and Brauchle, C., *Polarized π-electron systems in a chemically generated electric field: Second-order nonlinear optical properties of ammonium borate zwitterions.* Angewandte Chemie-International Edition in English, 1996. **35**(6): p. 644-646.

32. Armstrong, J.A., Bloembergen, N., Ducuing, J., and Pershan, P.S., *Interactions between light waves in a nonlinear dielectric.* Physical Review, 1962. **127**(6): p. 1918-1939.

33. Oudar, J.L. and Chemla, D.S., *Hyperpolarisabilities of the nitroanilines and their relations to the excited state dipole moment.* The Journal of Chemical Physics, 1977. **66**(6): p. 2664-2668.

34. Atkins, P.W., *Physical Chemistry*. Fourth ed. 1990, Oxford: Oxford University Press. 992.

35. Burland, D.M., Miller, R.D., Reiser, O., Tweig, R.J., and Walsh, C.A., *The design, synthesis, and evaluation of chromophores for second-harmonic*

generation in a polymer waveguide. Journal of Applied Physics, 1992. **71**(1): p. 410-417.

36. Yariv, A., *Optical Electronics.* Third ed. 1985, New York: The Dryden Press, Saunders College Publishing. 552.

37. Butcher, P.N. and Cotter, D., *The elements of nonlinear optics.* Cambridge studies in modern optics: 9, ed. P.L. Knight and W.J. Firth. Vol. 9. 1990, Cambridge: Cambridge University Press. 344.

38. Maker, P.D., Terhune, R.W., Nisenoff, M., and Savage, C.M., *Effects of dispersion and focusing on the production of optical harmonics.* Physical Review Letters, 1962. **8**(1): p. 21-22.

39. Singer, K.D., Kuzyk, M.G., and Sohn, J.E., *Second-order nonlinear-optical processes in orientationally ordered materials: relationship between molecular and macroscopic properties.* Journal of the Optical Society of America B, 1987. **4**(6): p. 968-976.

40. Singer, K.D., *Orientational order, poling, and relaxation in second-order nonlinear optical polymers*, in *Organic thin film for waveguiding nonlinear optics*, F. Kajzar and F. Swalen, Editors. 1996, Gordon and Breach: Amsterdam. p. 193-220.

41. Kielich, S., *Optical Second Harmonic Generation by electrically polarised isotropic media.* IEEE Journal of Quantum Electronics, 1969. **QE-5**(12): p. 562-568.

42. Page, R.H., Jurich, M.C., Reck, B., Sen, A., Twieg, R.J., Swalen, J.D., Bjorklund, G.C., and Willson, C.G., *Electrochromic and optical waveguide studies of corona-poled electro-optic polymer films.* Journal of the Optical society of America B, 1990. **7**(7): p. 1239-1250.

43. Harper, A.W., Sun, S., Dalton, L.R., Garner, S.M., Chen, A., Kalluri, S., Steier, W.H., and Robinson, B.H., *Translating microscopic optical nonlinearity into macroscopic optical nonlinearity: the role of chromophore-chromophore electrostatic interactions.* Journal of the Optical Society of America B-Optical Physics, 1998. **15**(1): p. 329-337.

44. Hill, N.E., Vaughan, W.E., Price, A.H., and Davies, M., *Dielectric Properties and molecular behaviour.* The Van Nortrand Seies in physical chemistry, ed. T.M. Sugden. 1969, London: Van Noetrand Reinhold company. 480.

45. Onsager, L., *Electric moments of molecules in liquids.* Journal of the American Chemical Society, 1936. **58**: p. 1486.

46. Albert, I.D.L., Dibella, S., Kanis, D.R., Marks, T.J., and Ratner, M.A., *Solvent effects on the molecular quadratic hyperpolarizabilities*, in *Polymers For Second-Order Nonlinear Optics.* 1995, American Chemical Society: Washington. p. 57-65.

47. Reichardt, C., *Solvatochromic dyes as solvent polarity indicators.* Chemical Reviews, 1994. **94**(8): p. 2319-2358.

48. Teng, C.C. and Garito, A.F., *Dispersion of the nonlinear second-order optical susceptibility of organic systems.* Physical Review B, 1983. **28**(12): p. 6766-6773.

49. Chen, Z. and Shen, P., *Local fields in random dielectrics: Distribution characteristics and the effects of microstructure.* Physical Review B, 1991. **43**(7): p. 5735-5746.

50. Thomas, P.R., *The molecular properties of zwitterionic, non-linear optical molecules and their evolution and their evolution with molecular environment*, in *Department of Physics*. Ph.D, 1998, University of Durham: Durham. p. 235.

51. MOPAC, *CS MOPAC PRO: Semi-empirical computation*, 1993-1997, Fujitsu Limited.

52. Levine, B.F. and Bethea, C.G., *Second and third order hyperpolarizabilitlies of organic molecules.* The Journal of Chemical Physics, 1975. **63**(6): p. 2666-2682.

53. Oudar, J.L., *Optical nonlinearities of conjugated molecules. Stilbene derivatives and highly polar aromatic compounds.* The Journal of Chemical Physics, 1977. **67**(2): p. 446-457.

54. Ledoux, I. and Zyss, J., *Influence of the molecular environment in solution measurements of the second-order optical susceptibility for urea and derivatives.* Chemical Physics, 1982. **73**: p. 203-213.

55. Israelachvili, *Intermolecular and surface forces.* Second ed. 1992, London: Academic Press. 450.

56. Rigby, M., Smith, E.B., Wakeham, W.A., and Maitland, G.C., *The forces between molecules.* 1986, Oxford: Clarendon Press. 232.

57. Maitland, G.C., Rigby, M., Smith, E.B., and Wakeham, W.A., *Intermolecular forces. Their origin and determination.* 1981, Oxford: Clarendon Press.

58. London, F., *The general theory of molecular forces.* Transactions of the Faraday Society, 1936. **33**: p. 8-26.

59. Robinson, B.H. and Dalton, L.R., *Monte Carlo statistical mechanical simulations of the competition of intermolecular electrostatic and poling-field interactions in defining macroscopic electro-optic activity for organic chromophore/polymer materials.* Journal of Physical Chemistry, 2000. **A 104**: p. 4785-4795

Chapter 3 : Experimental

3.1 Introduction

The techniques used for the preparation and characterisation of thin polymer films and chromophore solutions are explained in this chapter. The equipment used for EFISH measurements is described. It is necessary to induce a non-centrosymmetric structure in the polymer samples and hence the dipolar molecules were aligned by poling using applied DC fields. The poling was carried out using a constant current corona triode, (CCCT) and an outline of this set up is described in section 3.5.2. The polar alignment and the second order nonlinear optical coefficients of the molecular species were determined by second harmonic generation (SHG) measurements and this is described in section 3.6. The molecular figure of merit, $\mu\beta$, was determined by EFISH measurements, described in section 3.3. Photoluminescence and absorption experiments were used to investigate the aggregation properties of the chromophores.

3.2 Sample Preparation and Characterisation

Thin polymer films were prepared by spin coating. This study uses a guest-host system where the guest nonlinear optical molecules are dispersed throughout the polymer matrix. This method requires that the polymer and guest material can be dissolved in a common solvent. Solutions were prepared and usually stirred overnight to ensure complete dissolution. To ensure that high optical quality films were produced, the solutions were filtered through a 0.45 μm pore size Millipore in-line filter (Millex SLHV 025 NS, syringe driven PVDF filter unit) directly onto the cleaned substrate immediately before spinning. Following the coating process, excess solvent was removed from the samples by drying in a vacuum oven at a suitable temperature governed by the properties of both the solvent and the film.

3.2.1 Substrate Preparation

Glass substrates with a transparent conducting coating, indium tin oxide (ITO), were patterned to give a circular ground plane area of diameter 18 mm with a surrounding guard ring, as described in section 3.5.2, to ensure accurate definition of the area and hence current density. ITO coated glass sheets (Merck Display Technologies, Resistivity ~120 Ohms/square) were cut into 25 x 25 mm squares and washed with acetone. The substrates were covered in a photo-resist through a mask pattern. The substrates were then etched, before being cleaned prior to sample preparation. The photo-resist patterning procedure together with the ITO etching and cleaning procedures can be found in Appendix I.

Experiments were undertaken to investigate the effect of ITO resistivity on poling field strengths. Substrates with high (~120 Ohms/square) and low (~15 Ohms/square) ITO resistivities were tested in the CCCT poling rig (described in section 3.5.2). However, no appreciable difference in the poling fields was observed. To investigate the effect of ITO resistivity, a standard NLO material, 4-(N,N-dimethylamino)-3-acetamidonitrobenzene, DAN, was doped into poly(bisphenol A carbonate) to a weight loading of 20%. Both samples produced the same d_{33} value when the SHG was measured. The readily available 120 Ohms/square ITO was therefore used throughout this study.

3.2.2 Spin Coating

The solution was filtered directly onto the substrate and complete coverage was produced. The substrate was then rotated at 2000 rpm to produce a highly uniform coating and the excess solution was removed. The viscosity of the solution, angular velocity and time of spinning govern the thickness of the film and careful control of these factors can lead to uniform films with thickness ranging from sub-micron to tens of microns. Studies were made to investigate the parameters required to produce films of the required thickness. Less volatile solvents tend to produce films of a high optical quality but this does result in long drying times at high temperatures.

Typically 1 g of polymer, such as poly(bisphenol A carbonate) (PC) (Aldrich Cat. No.18, 162-5) was co-dissolved with the required weight loading of chromophore in

6 ml of 1,1,2-2 tetrachloroethane (Aldrich Cat. No. 10,653-4, bp=147°C). This choice of solvent was the only one found that was able to dissolve the polymer, whilst also being suitable for spin coating. After stirring overnight, the samples were prepared by spin coating on cleaned ITO or quartz substrates (as described in Appendix I). Spin speeds of 2000 rpm for 10 seconds gave a film thickness of around 3 μm. The films were then left to dry in a vacuum oven at 80 °C for several days to ensure the complete removal of solvent.

3.2.3 Electrical Contacts

Electrodes were attached to the samples to enable measurement of the sample current during poling. Following removal of an appropriate amount of the polymer film, the wires (which had the coating removed from the ends using a flame and wire wool) were attached using conducting silver paint (RS Cat No. 186-3600). The paint was allowed to dry for 12 hours before cyanoacrylate adhesive was carefully applied to protect the contact and the copper guard shield was added.

3.2.4 Thickness

Film thickness was determined using an Alpha Step 200 surface profiler (Tencor Instruments). This instrument requires that a groove be created between the substrate surface and the film surface such that the stylus can be vertically displaced when traversing across the step. Grooves were made by scratching away a thin section of the polymer film using a scalpel blade. The difference in the levels is represented graphically and numerically and so the film thickness can be determined.

3.2.5 Refractive Index

The refractive index is an intrinsic property of any optical medium and governs the ability of the material to refract light. The oscillating electric and magnetic fields of a light wave produce oscillating motion of charges in the material. These oscillating charges produce their own oscillating magnetic and electric fields. This induced electromagnetic wave combines with the original to create a light wave with a velocity

slower than the velocity of light in a vacuum. The exact arrangement of charges in the material determines the speed of light within that material. The definition of refractive index, n, is given by the ratio between the speed of light in a vacuum and the speed of light in the medium.

$$n = \frac{\text{speed of light in a vacuum}}{\text{speed of light in medium}} = \frac{c}{v}$$

Equation 3.1

The magnitude of the oscillations produced by the incident light depends on the wavelength and hence the refractive index is wavelength dependent. This wavelength dependence is known as dispersion. In general, normal dispersion requires that the refractive index of a material increases as the wavelength becomes shorter. In addition to refraction, the intensity of light can decrease as it travels through the material due to absorption and scattering of the incident electromagnetic wave.

The refractive index of the polymer films was measured using prism coupling [1]. This method requires that a waveguide mode of the film be excited by radiation coupled into the film using a prism arrangement as shown in Figure 3.1. The materials are chosen such that the refractive index of the prism, n_p, is larger than the refractive index of the film, n_f, which in turn has a larger refractive index than the substrate, n_s, to ensure that all the possible waveguide modes in the film can be excited.

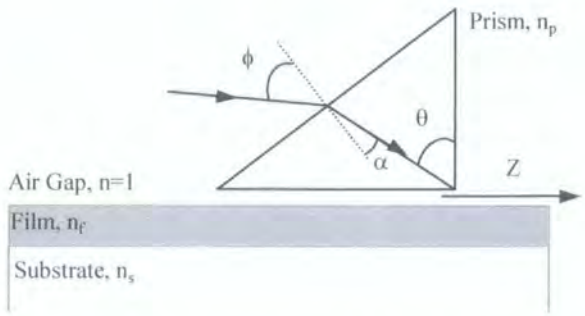

Figure 3.1: Geometrical arrangement for prism coupling experiment

The incident laser beam is totally internally reflected at the base of the prism, allowing an evanescent wave to be established. Providing the air gap is small enough this wave extends below the prism base and into the film. In order to excite one of the waveguide modes in the film, the phase matching condition must be satisfied. This means that the

horizontal component of the wavevector of the evanescent field must match the horizontal component of the wavevector of the film. When this boundary condition is satisfied, energy from the incident beam is coupled exclusively into individual waveguide modes. The number of modes a film can support is related to the thickness, with thicker films containing more modes. The propagation constant for the m^{th} mode is defined as:

$$\beta_m = k_0 n_{eff} = k_0 n_p \sin\theta$$

Equation 3.2

where n_{eff} if the effective refractive index for the mode, $k_0 = 2\pi/\lambda$ is the wavevector in a vacuum and λ is the wavelength of the incident radiation. Provided the refractive indices of the prism, the substrate, the angle of the prism and the wavelength of the laser are all known, the refractive index of each mode can be calculated by measuring the coupling angles, ϕ of the incident laser beam [2].

3.2.6 Refractive Index Experimental Procedure

In practice two prism coupling is used to measure the coupling angles; a second prism is clamped along the waveguide in an opposite direction to the first. This technique may only be used when there is very little or no absorption at the measurement wavelength. Two right-angled prisms were attached to U shaped mounts and clamped directly onto the film and substrate. If good optical contact is achieved between the prisms and the film, a coupling spot on the base of the prism can be observed through the prism. This coupling spot takes the form of an area that is silvery in appearance and becomes larger and smoother as the film surface quality improves and the coupling efficiency of the laser beam increases.

The experimental arrangement is shown in Figure 3.2. Experiments were carried out at four different wavelengths, (632.8 nm, 1300 nm, 940 nm, 780 nm) using a HeNe laser (5 mw) and a selection of laser diodes. The power supply (Spears Robertson) was operated in current mode, supplying around 30-40 mA to the laser diodes such that a pale spot could be viewed on an IR detection card. All of the films were prepared on silica substrates (n = 1.457018 at 632.8 nm) by spin coating. Tests were carried out to achieve the correct film thickness to support at least three guided modes. A narrow air

gap between the film surface and the base of the prism is present due to dust particles or the uneven surface of the film. The two prisms each have an angle of 60° and are made from SF6 glass (n = 1.79883 at 632.8 nm).

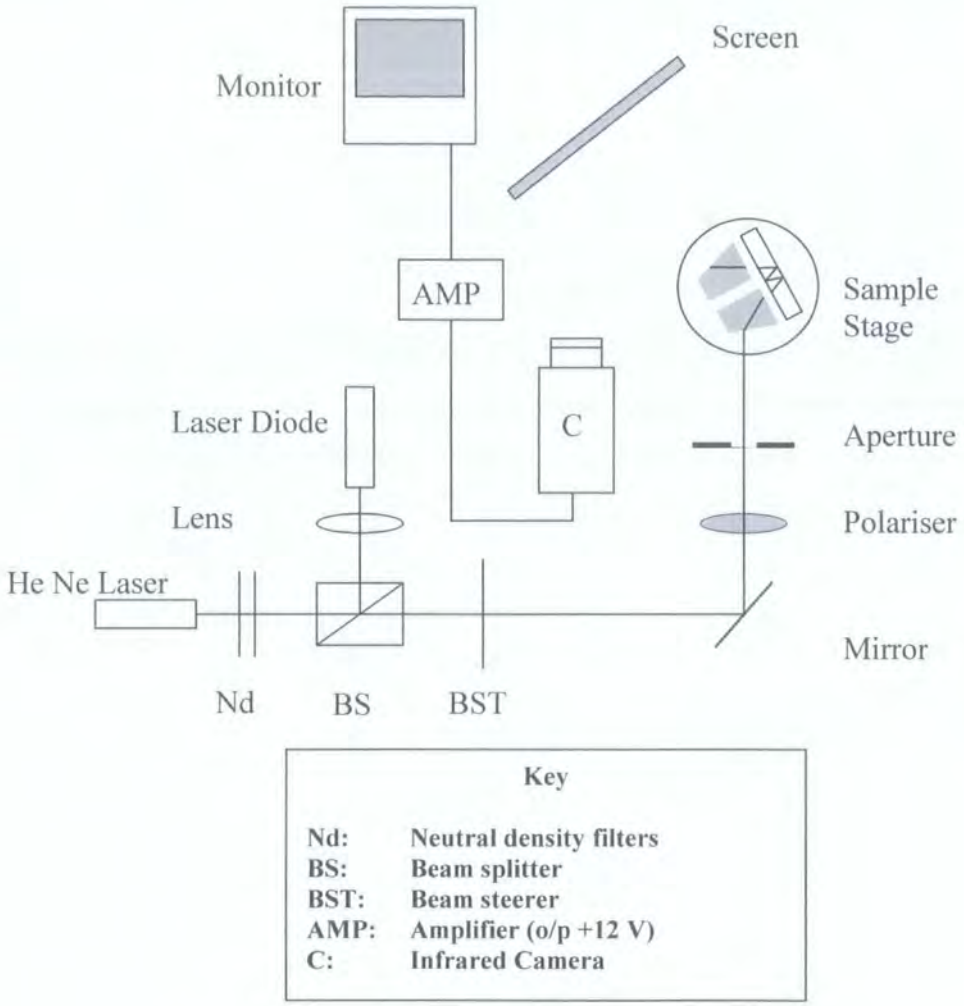

Figure 3.2: Experimental arrangement for refractive index measurements.

The visible laser beam was used to align the components for the IR laser beams. The beam was aligned through a polariser to strike the centre of the rotation stage to ensure a constant coupling efficiency as the stage is carefully rotated backwards and forwards. The polariser allows TE (parallel to the plane of incidence of the film) or TM (perpendicular to the plane of incidence of the film) guided modes to be excited in the waveguide. The first prism was positioned to align the coupling spot with the corner of the prism and the centre of the laser beam. The second prism was clamped a small distance away to allow light to couple out of the waveguide. The normal incidence

angle was determined by rotating the stage so that the incident beam and the beam reflected from the sloping face of the first prism had coincident paths. This angle reading was recorded and all subsequent coupling angles were referenced from the normal incidence angle.

The guided modes coupled out via the second prism were monitored directly on a screen or by using a monitor and camera (Microviewer, Electrophysics model 7290) as shown in Figure 3.2. After the reference angle has been measured, the stage is tuned roughly clockwise and anti-clockwise until patterns of light, which represent guided modes, were observed on the screen. These patterns take the form of several bright vertical lines of light, the brightest of which represents the guided mode. Other modes can also be seen due to scattering within the waveguide film, and surface roughness. Good quality films gave bright sharp lines. Fine-tuning of the rotation stage was used to determine the optimum position that produced lines of maximum intensity on the screen or monitor for each mode. Angles were recorded from tuning clockwise and then anticlockwise to monitor any play in the rotation stage. The optimised angle was recorded as the mode angle. The external coupling angles, ϕ, were calculated according to:

$$\phi = \text{Normal Incident Angle} - \text{Mode Angle}$$

Equation 3.3

These coupling angles, the refractive indices of the prisms and the substrate, and the wavelength of the laser used were input into a computer program [3] that calculated the refractive index and film thickness using the equations described by Kogelnik and Ramaswamy [2]. The results were presented in the form of a curve of film thickness as a function of refractive index over which the waveguide mode can be supported. When more than one mode of a film is measured, several curves are produced which intersect and hence the unique film thickness and refractive index can be determined. Generally, three modes were measured so that the error could be estimated easily. In addition, the film thickness was measured as described previously to ensure agreement with the calculated values. Figure 3.3 shows a typical set of curves from this measurement. In this case the sample was a 7-(2,6,dimethylmorpholino)-7-(4-methyl piperdino)-8,8,-dicyanoquinodimethane (MORPIP) doped bisphenol A-polycarbonate (PC) film to 1% weight loading. The program gave a thickness of $t = 4.88$ μm and $n = 1.58288$.

The film thickness was found to be t = 4.89 μm when measured with the Tencor surface profiler which is in good agreement in the program.

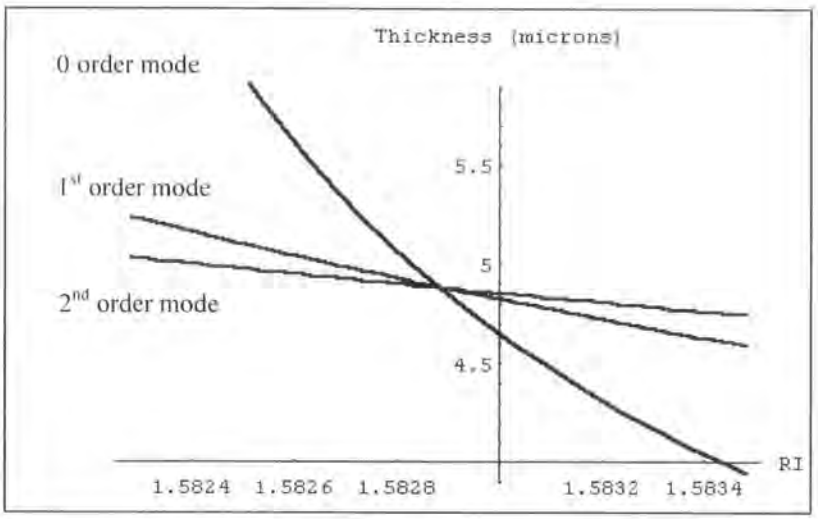

Figure 3.3: Graph showing a typical set of curves of refractive index and thickness for a MORPIP doped PC (1 % wt) polymer film.

3.2.7 Optical Spectroscopy

The absorption spectra of the film and solution samples were measured using a commercial Perkin-Elmer Lambda 19 absorption spectrometer. Photoluminescence emission and excitation spectra were recorded using a commercial Flouromax spectrometer. Solution samples were filtered, if necessary, through a 0.45 μm filter (Millex SLHV 025 NS, syringe driven filter unit) before optical measurements were performed. For solutions of high concentrations, short path length cells of 0.1 mm (Starna, 31/Q/0.1) or 1 mm were used, and for extremely low concentrations a cell of path length 100 mm was used. All other solution measurements were made using standard 1 cm^2 quartz cuvettes.

3.3 Electric Field Induced Second Harmonic Generation (EFISH)

The nonlinear optical molecular figure of merit ($\mu\beta$) for several chromophores was measured using the electric field induced second harmonic generation (EFISH) technique [4, 5]. These measurements were carried out using equipment at the Laboratoire de Photonique Quantique et Moléculaire in Paris. As explained in Chapter 1, the EFISH technique utilizes an electric field to break the symmetry of the medium and induce a macroscopic third order non-linearity, Γ_L, into a sample in solution. The Maker Fringe technique [4-8] was used to measure Γ_L.

The experimental arrangement is shown in Figure 3.4. The EFISH cell consists of a stainless steel container with two quartz optical windows that define a wedge shape cavity for the solution within the cell. The quartz windows are polished along the sides that are normal to the incident radiation and placed between two electrodes. The angle between the wedges is roughly 1°. If the solution absorbs at either the fundamental or the second harmonic wavelength then the signal may not be detected over long path lengths, hence the average interaction distance is limited to 2 mm. The uppermost electrode is connected to a high voltage supply via an isolated stainless steel rod situated above the cavity. The lower electrode is situated under the quartz windows and is connected to the high voltage supply by means of an isolated stainless steel cylinder. The interelectrode distance is 2 mm, giving a static electric field of approximately 40 $kVcm^{-1}$. The cell was mounted on an electrically isolated translation stage such that the cell could be translated horizontally relative to the indent beam to produce Maker Fringes. A computer controlled stepping motor produced a translation resolution of 1 μm.

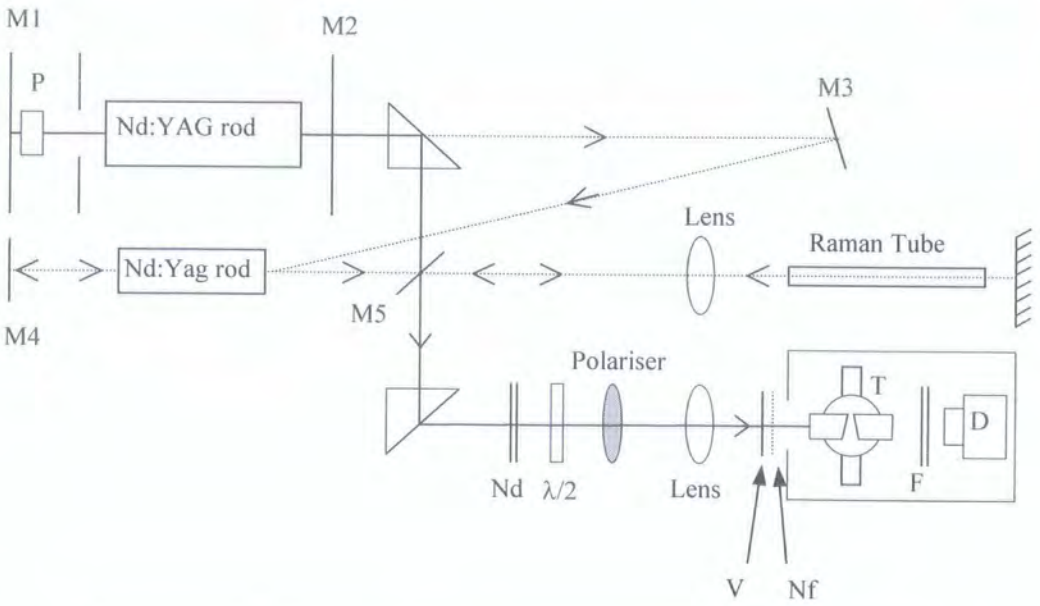

Key

M1, M3, M4: Mirrors for 1064 nm

M2: Partial mirror for 1064 nm

M5: One-way mirror for 1907 nm (transparent to 1064 nm)

Nd: Neutral density filters

V: Visible blocking filter

Nf: 1064 nm blocking filter

λ/2: Half wave plate

D: Detector (Photomultiplier tube, PMT)

F: Filters including neutral density, 532 or 954 nm band pass filters and 1064 or 1907 nm blocking filters

T: Translation stage containing the EFISH cell with quartz windows forming a wedge shape cavity

Figure 3.4: Experimental arrangement for EFISH experiments. The solid and dotted lines show the path of 1064 nm and 1907 nm light respectively.

The experiment employs an actively Q-switched Nd^{3+}:YAG (Yttrium Aluminum Garnet) laser rod to pump a second Nd^{3+}:YAG rod amplifier operating at 1064 nm and 10 Hz. The output pulse has a duration of 20 ns, which provides a peak power of

300 kW. An electronic circuit is used to synchronously time the high voltage pulse with the optical laser pulse. A Glan polariser was used to vertically polarize the fundamental with respect to the electrodes, i.e. parallel to the applied electric field. The beam was then weakly focused using a 40 cm focal length lens to give a 0.5 mm beam waist. The harmonic emission was detected using an uncooled photomultiplier and was synchronously sampled and averaged using a box-car (Stanford Research Systems Ltd.).

Maker fringes are produced when the EFISH cell is translated horizontally with respect to the fundamental "*p*-polarised" beam. The second harmonic, which is also "*p*-polarised" is detected and analysed according to Oudar [4].

3.4 Dipole Moment Measurements

The molecular dipole moments were determined from the measurement of the dielectric constant increment for solutions of varying concentrations of the molecules under investigation. The experimental method and capacitance cell used for the measurement of the dielectric constant has been developed at Durham by Thomas as part of his PhD [9]. The LCR meter (Hewlett Packard, HP4278a) used to measure capacitance of the solution was operated at 1 MHz, which is well away from any resonance points. As a precaution, the dielectric loss was monitored for all the solutions and was found to be very low in every case. Since capacitance depends on the temperature, humidity and conditions of measurement, the capacitance of the empty cell was measured prior to each experiment. The capacitance meter was switched on at least half an hour before measurements were taken. Typical values for the empty cell were found to be 14.62 ± 0.1 pF. A stock solution of typical concentration 10^{-4}-10^{-3} mol l^{-1} was prepared. This solution was then successively diluted using 50 ml volumetric flasks such that two orders of magnitude in concentration were traversed during the experiment. The capacitance of each solution was then measured and recorded and the solution returned to the flask, starting with the most dilute solution. In an attempt to eliminate any errors caused by changes in temperature during the measurements, the solutions were then measured in the order of the highest concentration to the lowest concentration. The dielectric constant of the solution was determined by dividing each capacitance measurement by the capacitance of the empty cell (air). Graphs of solution

dielectric constant as a function of concentration (mol l^{-1}) were plotted and the gradient was calculated. A program written by Thomas in Mathematica [3] was used to extract the chromophore dipole moment [9].

3.5 Electrical Poling

Electric field poling was used to align the guest dipolar chromophores within the host polymer matrix. The technique of poling involves heating the polymer to a state of high mobility close to its glass transition temperature, T_g and simultaneously applying a high electric field. The dipole moments of the guest molecules may then align in the field direction. The polymer is then cooled whilst maintaining the electric field in order to lock in the dipolar alignment. In particular, corona poling utilizes the ions generated from a corona discharge to create very high electric fields when deposited on the polymer surface. This technique was used to pole the materials in this study.

3.5.1 Corona Discharge Poling

In order reduce the likelihood of sample damage and achieve higher poling fields, a corona discharge poling method is often used [10, 11]. This utilizes the low surface conductivities of the polymer film. Corona discharge is the partial breakdown of air, usually at atmospheric pressure, that is initiated by a discharge in an inhomogeneous electric field. Such a field may be established when a sufficiently high potential difference exists between a pair of asymmetric electrodes, such as a needle and plate arrangement. The corona produced is a continuous, self-sustainable flow of ions.

An advantage of this type of poling is that the discharge is readily controlled by adjustments of the corona voltage. Since the field distribution is asymmetric, the ionization remains localized at the needle tip ensuring there is no catastrophic breakdown across the air gap. Instead, the ions drift towards regions of low potential and so become trapped on the sample surface causing a potential field to be set up across the sample thickness. Poling field strengths are limited only by the dielectric strength of the sample and the availability of surface traps at the poling temperature. Thus much higher fields may be established than in the fixed electrode procedures.

However, severe physical damage of the film surface caused by ion impact has been reported in connection with corona discharge poling [12]. Attempts to reduce this damage and electrical break-down have included introduction of a protective cladding layer [13] and use of a higher resistivity substrate [14]. Also, although high surface charges can be attained using corona charging, the final sample voltage and the surface uniformity are not easily identified. Knowledge of the applied poling field is of particular importance if quantitative analysis of the non-linear response of the sample is to be undertaken.

An important improvement was made by Moreno and Gross with the introduction of an electrically biased metallic grid between the needle and sample [15]. This three-electrode system was called a corona triode and became the hallmark of charge transport studies in polymers and in corona charging for non-linear optics [16]. The grid allows a uniform charge distribution to be achieved across the sample, thereby enabling determination of the surface potential and sample charging currents during poling [17]. Since constant voltages were applied to the grid and the corona tip, the sample current was seen to decrease as the sample became charged up to the potential of the grid.

The change in charging current was a limitation that prompted the development of new versions of the triode in which the current was controlled and maintained at a constant value. The constant current condition is essential for some charge transport equations to be solved and the sample potential accurately determined. At first, the corona current was increased by increasing the tip voltage to compensate for the decrease in charging current when the sample potential rose [18]. However, this method had limitations, and the grid could not be operated at high voltages due to grid emissions occurring at high potentials. This was overcome by operating the tip in constant current mode thus supplying a constant current of ions through the system and varying the grid voltage to compensate for the decreasing sample charging currents [19]. Since in this mode of operation the grid potential rises with that of the sample, the potential difference between the grid and sample is kept constant and so no grid emissions occur, even at high charging potentials. The characteristics of this constant current corona triode ensure that the sample potential can be determined directly during the charging process and when poling is complete. The constant current corona triode used in this work is of this type.

3.5.2 Constant Current Corona Triode

As considered in the previous section, the design of the constant current corona triode (CCCT) ensures that the charge is deposited evenly and enables the user to monitor and control the surface potential build up. A schematic diagram of the experimental set-up used, which is a modification of the charger designed by Giacometti and Campos, is shown Figure 3.5.

The rig consisted of a sharp steel needle, set at a negative potential of 8-10 kV with a Brandenberg Alpha III high voltage supply (V_c), operated in local mode. This high voltage supply had the facility to measure the corona current (I_c) by monitoring the output voltage using a 15 pin connector. This voltage was measured in mV (Thandar TM 355 digital multimeter) and is then related to the corona current by Ic (nA) = {(10 x *x*mV)/1.5}. The needle was positioned in the centre of PVC cylinder that was shielded by an earthed metal cylinder. The flow of ions onto the sample was controlled by means of a metal grid that was negatively biased using a high voltage amplifier (TREK, model 610C) operated in remote mode with the controller function selected. The grid (Goodman, Cat no: NI008711) had an approximate optical transparency of 0.8, and was placed roughly 5 cm from the needle tip at the end of the cylinder. The grid was made of a mesh of wires and the centre was forced slightly downwards relative to the sample such that the shape of a lens was formed. This shape introduces a small uncertainty in the grid-to-sample distance, but it has been shown that this shortcoming is amply compensated for by a greater uniformity of charge deposition [20].

The sample was placed on the movable heated stage, which was kept approximately 8 mm below the grid during charging, unless otherwise stated. The temperature of the sample was controlled using a Eurotherm temperature controller. A shielded thermocouple was located in a small hole near the top of the sample stage. All high voltage cables were electrically shielded using earthed foil covering.

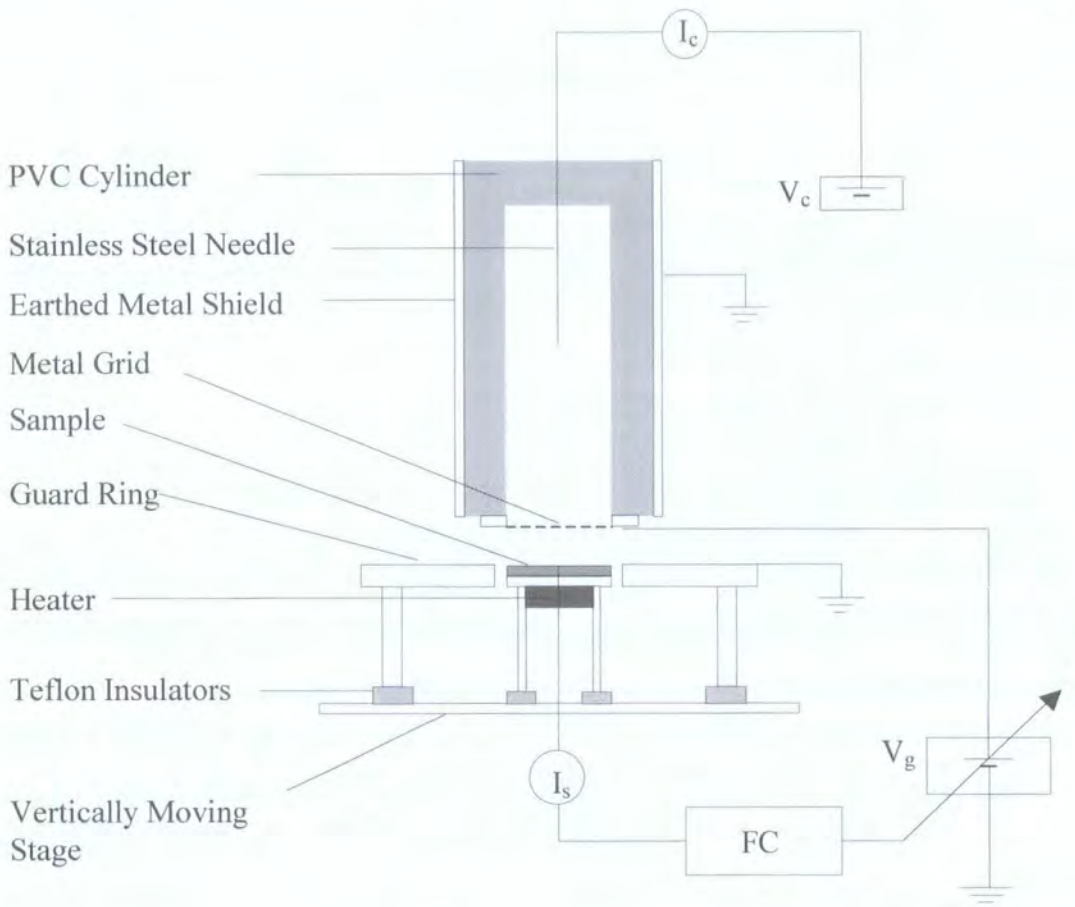

Figure 3.5: Schematic of Constant Current Corona Triode where FC is the Feed Back circuit

The thin film samples were made by spin coating onto ITO coated glass substrates as described in Section 3.2.2. The substrates were patterned by etching (as described in Appendix I) to include a guard ring arrangement as shown in Figure 3.6. This ensured that only currents passing through the film are measured by the feedback circuit, FC, and leakage currents, due to the migration of surface charge to earth, are not measured.

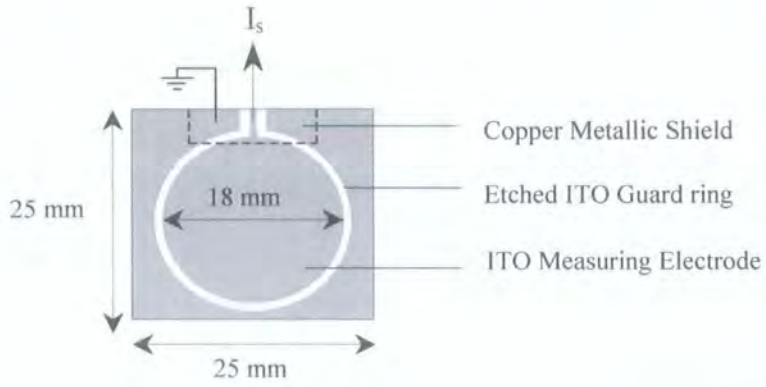

Figure 3.6: Substrate design

The sample current, I_s, was monitored with a picoammeter (Keithley model 485). The feedback circuit, shown in Figure 3.7, ensures that the flow of ions onto the sample and hence I_s remains constant by monitoring I_s and adjusting V_g accordingly. Typical charging currents (I_s) of 10 nA and corona currents (I_c) of 1.5 μA were used. Usually these conditions gave rise to a gap voltage between the grid and the sample of approximately 200 V. Poling was carried out some degrees below the T_g of the polymer host to allow high fields to be established across the sample. Low temperature poling is possible for the polymer films but simply takes longer because of increased material viscosity. However, lower temperatures allow higher fields to be established across the sample, as the conductivity remains low. It has been seen that corona poling may be effective several tens of degrees below the T_g of the system [21] and this was found to be the case for our material systems. When the grid voltage indicated that the charging was complete, the sample was cooled for 30 minutes whilst the constant charging current was maintained.

The advantages of keeping the charging current constant by varying the grid voltage have been outlined in the previous sections. The constant current corona triode used in this work was originally set up in 1994 by D.Healy *et al* [22]. Extensive modifications were necessary to achieve the required performance, and these modifications represented a significant part of this work. In addition, new equipment was purchased, namely a new picoammeter for the measurement of the sample current. This involved an input voltage into the feedback circuit instead of the sample current directly and so it was necessary to design a new feedback circuit.

A circuit was needed which responds to changes in the sample current; in order to keep the charging current constant, the grid voltage must be increased (i.e. become *more*

negative) if the sample current decreases (i.e. becomes *less* negative). Although the input into the picoammter is a negative current, the output is a positive voltage that is proportional to the input. Figure 3.7 shows the circuit that was designed to produce the required effect and a summary of its operation follows.

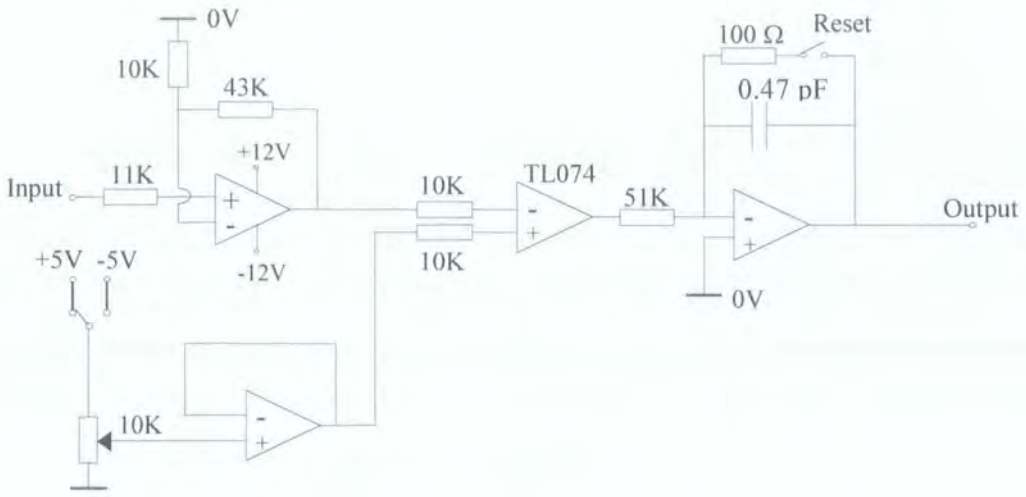

Figure 3.7: Feedback circuit used in CCCT

The input voltage is amplified, by a factor of 5, before it is compared to a reference voltage of the same polarity as the input voltage. The output of the comparator is then integrated over time (at a suitable time constant) in either a positive direction or a negative direction, depending on which input to the comparator is the larger. The output of this circuit is then fed directly into the input of the grid high voltage controller. Obviously, the rising (or falling) grid voltage will affect the sample current directly. The whole system is thus said to be in a dynamic equilibrium. The polarities of the reference voltage, grid voltage and corona voltages may be reversed such that samples can be poled with fields of both polarities.

3.5.3 Theory of CCCT Operation Procedure

Since it has now been shown how the sample charging current, I_s can be kept constant at a value I_0, the analysis presented here will show how the sample voltage can be inferred from measurement of the grid voltage, V_g. Figure 3.8 shows a schematic

diagram of the sample and the air gap region below the grid. One-dimensional geometry is assumed, i.e. that the electric quantities are independent of lateral position in the air gap. This is a reasonable assumption, since the PVC cylinder becomes charged and acts as a lens to collimate the ions uniformly onto the grid [17].

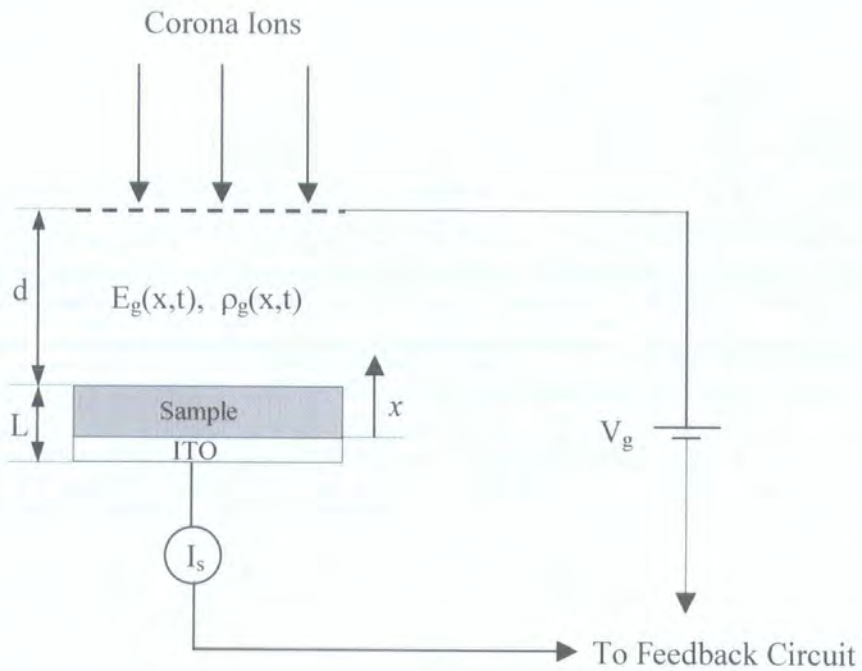

Figure 3.8: Schematic diagram of sample and air gap below the grid of CCCT.

The total charging current density, $J(t)$, in the air gap between the grid and the sample of thickness L is given by [19]:

$$J(x,t) = \frac{I(x,t)}{A} = [\, \nu + \mu E_g(x,t) \,] \rho_g(x,t) + \frac{\varepsilon_0 \delta E_g(x,t)}{\delta t}$$

Equation 3.4

Where $E_g(x,t)$, μ, $\rho_g(x,t)$, ν and ε are the gap electric field (V/cm), the ion mobility (cm^2/Vs), the charge density in the gap (C/cm^3), the velocity of the corona wind (cm/s) and the dielectric constant (F/cm) of the air respectively. The first term in Equation 3.4

is the conduction current density that includes the gas displacement by corona discharge (corona wind) and that due to corona ions. The second term represents the electric displacement current density. If Equation 3.4 is integrated over the gap distance the following equation is derived:

$$J(t) = \frac{1}{d}\int_{L}^{L+d}\left[v + \mu E_G(X,t)\right]\rho_g(x,t)dx + \frac{\varepsilon_0}{d}\frac{d}{dt}\left[V_g(t) - V_s(t)\right]$$

Equation 3.5

Where the gap potential drop due to the ionic space charge is given by $V_{gap} = V_g(t)-V_s(t)$, and V_s and V_g are the sample surface voltage and grid voltage respectively. Thus, when V_{gap} is kept constant, a stationary state for the ionic charge density and the electric field is reached in the air gap and so the charging current density becomes time independent [23]. In the inverse way, if the charging current is kept constant such that $J(t) = J_0$ then the voltage drop V_{gap} also remains constant. As a result, if V_{gap} is known then the sample potential, V_s, can be determined throughout the charging procedure by recording the values of the grid voltage, V_g, necessary to maintain a constant sample current, I_s. Experimentally a constant charging current is achieved by means of the feed back circuit described in section 3.5.2 and by operating the grid voltage supply in constant current mode. Since the amount of gap space charge is directly proportional to the corona current, I_c, it is necessary to maintain a constant corona current by operating the supply V_c in constant current mode.

Therefore, this set-up allows the control of the ion flux onto the sample surface and the determination of the sample potential during the charging by measuring the grid voltage, $V_g(t)$. In order to determine the sample potential it is necessary to know the air gap potential V_{gap} as a function of the system parameters and measurement conditions. If there is no polymer sample present (i.e. $V_s = 0$) then the measured V_{gap} equals the grid voltage value, V_g. This must be recorded prior to each poling experiment using a patterned substrate with no polymer film present.

From the calibration curves shown in Figure 3.9 and Figure 3.10 it can be seen that the sample current, I_s depends on both the corona current, I_c and the distance between the grid and the sample, d. This highlights the need to maintain I_c at a constant value and the fact that this calibration experiment must be carried out following any changes in d.

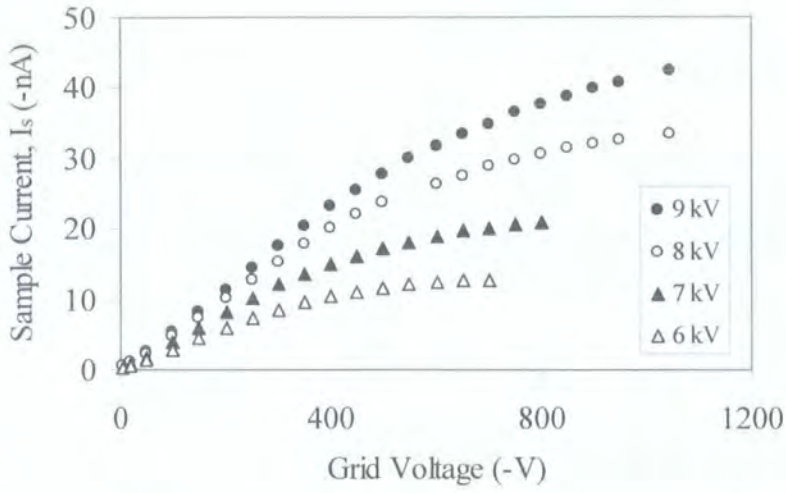

Figure 3.9: A typical set of calibration curves for CCCT varying the needle current, I_c; 9 kV (4.23 μA), 8 kV (3.77 μA), 7 kV (3.15 μA) and 6 kV (2.61 μA)

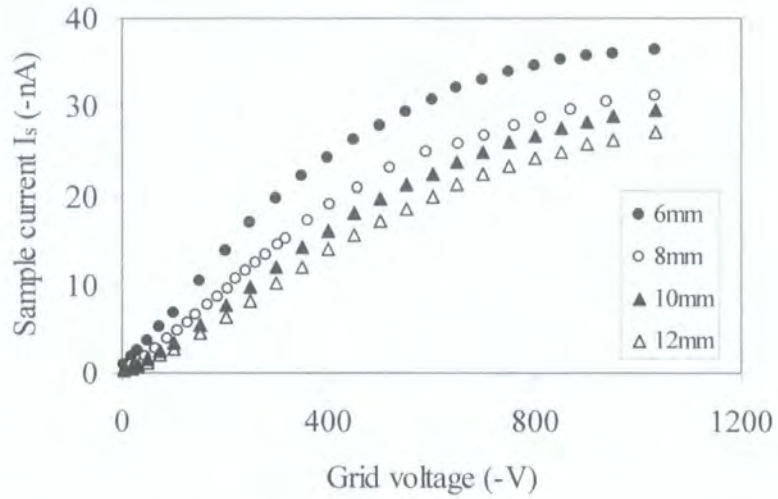

Figure 3.10: A typical set of calibration curves for varying grid-to-sample distance, *d*

3.5.4 In-situ Poling

Although the CCCT has many advantages already outlined; such as uniform charge distribution and the possibility of measuring the voltage across the sample it is also useful to perform poling "in-situ". In-situ poling enables the measurement of the second harmonic generation as a function of system poling parameters. The experimental arrangement of the in-situ poling and second harmonic generation measurements is shown in Figure 3.11. The intense electric field generated at the

needle tip during the corona process accelerates nearby free electrons to velocities high enough to impact-ionize gas molecules in their path, creating ions with the same polarity as the needle. Space charge is established by the ion current carriers between the needle and the sample, since the ambient air forms a relatively good insulator. The reactive ions accelerate toward the grounded film and accumulate near the surface region, generating a very high magnitude electric field across the film. This field orients the dopants thereby inducing second order nonlinear activity.

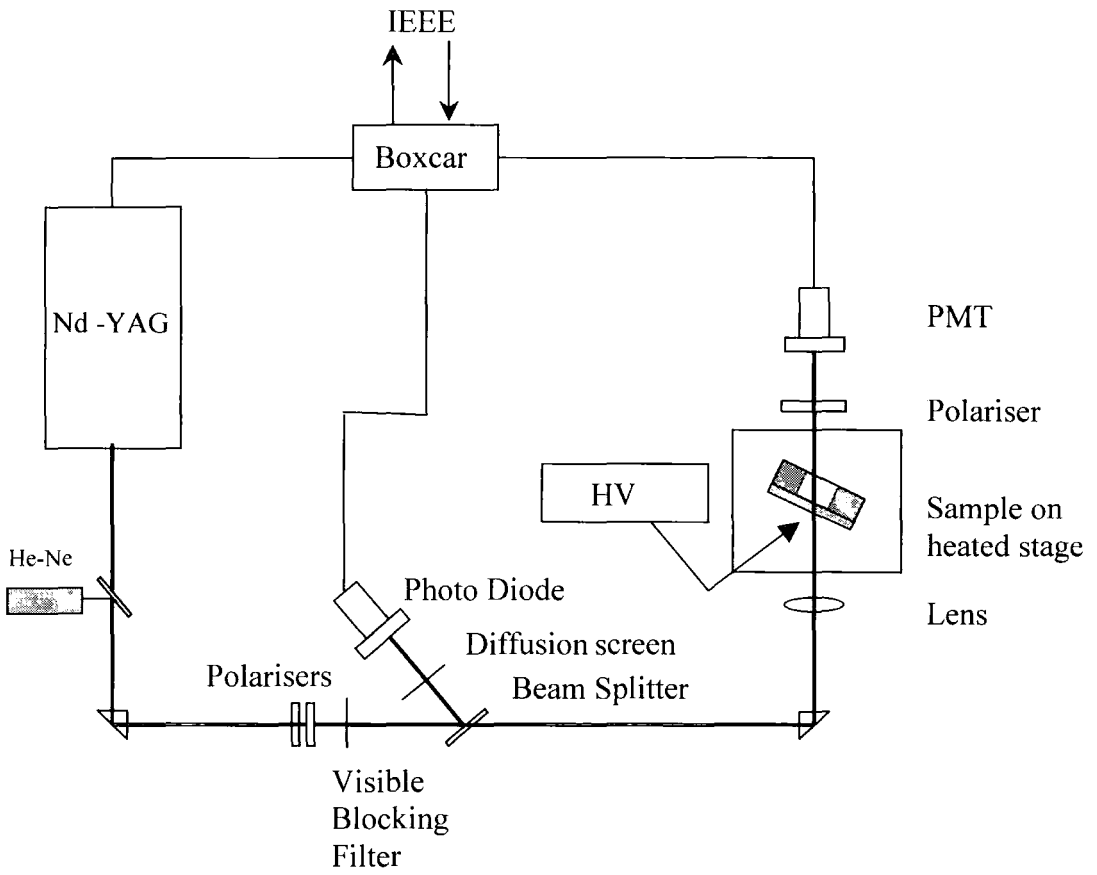

Figure 3.11: The Schematic layout of the experimental set-up for in-situ poling

The laser arrangement was the same as that used in second harmonic generation measurements and is described in the next section. The polarized beam of the Nd:YAG laser (Spectra-Physics Quanta-Ray DCR-11) was focused on the sample with an incident angle of $\theta = 45°$. A large voltage was applied (Brandenberg Alpha III HV supply) to a steel needle located approximately 15 mm above the film. The film was mounted on a heated copper plate that was controlled by means of a temperature controller (CAL 9900). The thermocouple (type K; nickel chromium/nickel aluminum) was located close to the film sample in a small hole in the heated stage. Measurements

were made to find the difference in temperature between the sample surface and the heated copper plate and the discrepancy taken into account on all subsequent readings. The whole rig was mounted in an isolated Perspex cage for safety.

3.6 Second Harmonic Generation Measurements

The theory of second harmonic generation has been described in chapter 2. A detailed description of the Maker Fringe technique [6] that was performed to determine the second harmonic non-linear optical coefficients, d_{ij} (where $d_{ijk} = \frac{1}{2}\chi_{IJK}$ and d_{ijk} is expressed in its contracted Voigt notation [24]) has been given by Jerphagnon and Kurtz in 1970 [8]. This technique utilises the difference in the velocities of the bound and free second harmonic waves, such that an interference pattern is produced when the optical path lengths of these waves is altered. This can be achieved by translating a wedge of material normal to the incident radiation or by simply rotating a film of the material about an axis perpendicular to the incident beam. However, in 1995 Herman and Hayden presented an analysis that accounted for the absorption at both the fundamental and second harmonic wavelengths. This factor was not originally considered as at that time transparent crystals, with no absorption at these wavelengths, were being studied. The analysis that will be used in this work is therefore based upon that of Herman and Hayden as described in Chapter 5.

3.6.1 Experimental Arrangement

The experimental arrangement used to monitor the second harmonic intensity and to measure the d_{eff} coefficient is shown in Figure 3.12. The fundamental beam from a Nd : YAG, Q - switched laser (Spectra-Physics Inc., DCR – 11) of wavelength 1064 nm and a pulse duration of approximately 7 ns was used as the source. The laser was operated at a repetition rate of 3-4 Hz and the beam energy was stopped down to about 0.1 mJ using a pair of polarisers which may either be crossed (maximum reduction in energy) or uncrossed (giving about 90 mJ of energy per pulse). The second polariser controlled the polarisation plane of the optical field incident on the sample.

A beam splitter positioned after the polarisers, was used to create a reference arm. A fast S1 response silicon photodiode (Instrument Technology Ltd. (UK), t ~ 500ps), pre-filtered with a diffusion screen, was used to monitor the fundamental intensity from the reference arm. The photodiode was operated at 3.0 kV from a standard HV supply (Thorn EMI, PM28A). A short focal length lens (approx. 30cm) was used to focus the fundamental beam onto the sample that was mounted on a stage such that the poling direction was in the plane of incidence.

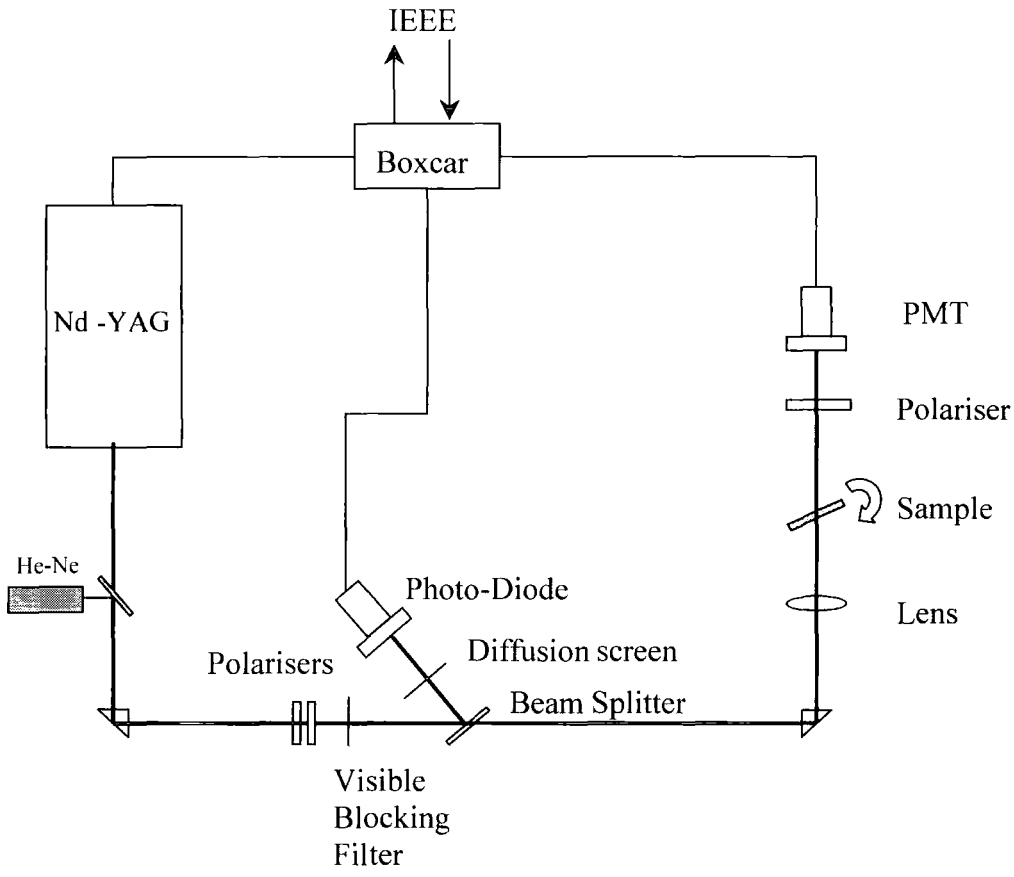

Figure 3.12: Experimental arrangement for second harmonic generation measurements

The intensity of the 532 nm second harmonic beam ($I_{2\omega}$), was measured using an uncooled photomultiplier tube (PMT) (Thorn EMI model 9658B) with a KG3 near infra-red blocking filter, to remove the fundamental radiation, and a 532 nm band pass filter mounted on the front. The PMT operates in a linear regime when between 1·1 - 1·3 kV is applied by the HV power supply (Thorn EMI, Electron Tubes Division, PM28B). The choice of voltage level must be made with care to avoid amplification of noise, whilst

using the gain to optimise the signal. It was found that 1·1 kV was the most effective supply voltage for the tube to detect the second harmonic signal. A polariser was placed between the sample and the PMT tube so that only "*p*-polarised" light was detected. Appropriate neutral density filters were used to reduce the intensity of the detected signal if necessary. The intensities of the reference beam and the second harmonic were measured with a Stanford Research Systems gated integrator and Boxcar averager (SR250) in conjunction with a computer, which normalised the signal by dividing the second harmonic by the square of the reference.

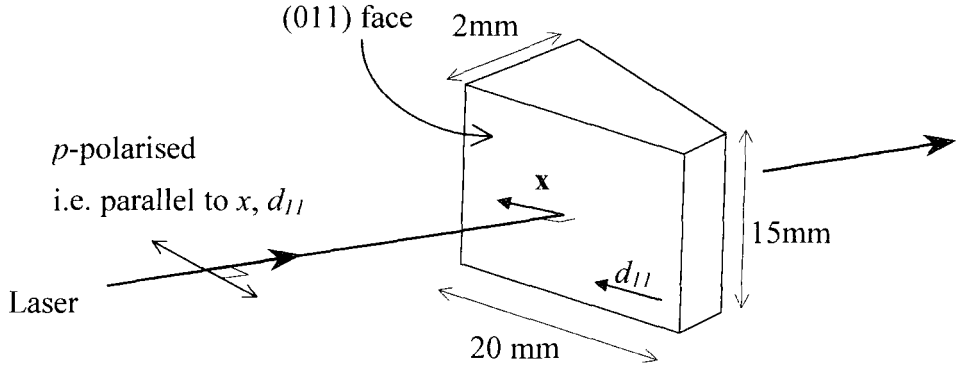

Figure 3.13: Schematic of Quartz wedge used for reference

In order that the collected data may be analysed quantitatively, the signal is referenced to quartz. The quartz was a wedge shape crystal of α-quartz cut to an angle of 1° along the (011) plane such that the d_{11} tensorial component of the non-linear coefficient is accessed when the incident beam is polarised in this direction. Maker fringes are produced when the incident radiation is "*p*-polarised" and the wedge is translated horizontally in the *x*-direction as shown in Figure 3.13.

3.7 Computational Methodology

The second order polarisabilities and dipole moments presented in Chapter 4 and Chapter 5 were calculated using the CS MOPAC PRO program in the CS ChemOffice PRO [25] package. CS ChemOffice PRO is an application specifically designed to aid scientists in modeling chemicals. This package provides computational tools based on

molecular mechanics and quantum mechanics for optimising model structures. CS MOPAC is an implementation of MOPAC, the well-known semi-empirical modeling application [26], which takes advantage of the interface in CS ChemOffice. The CS MOPAC PRO allows advanced energy minimizations and computing properties to be performed.

Computational methods calculate the potential energy surfaces of molecules. The potential energy surface can be considered as the embodiment of the forces of interaction among the atoms of a molecule. The potential energy surface may be used to derive structural and chemical information about the molecule. Different methods may be used to calculate the potential energy surface, but in general, there are a set of basic calculations that are performed for each method: Firstly, a single point energy calculation is performed to calculate the potential energy surface of a given set of atomic coordinates i.e. a given spatial arrangement of the atoms in a molecule. Then geometry optimization is performed. This involves the systematic modification of the atomic coordinates of a model resulting in a geometry where the forces on the atoms are zero. This represents a local energy minimum that is a stable molecular geometry. Finally, a property calculation can be executed to predict certain physical and chemical properties such as the dipole moment and polarisability.

The calculations performed in the work of this thesis use the CS MOPAC PRO program. Such quantum mechanical methods are concerned with the approximate solutions to Schrödinger's wave equation. The Hamiltonian operator contains information describing the electrons and nuclei in a system. Approximations to the Hamiltonian are made using the Born-Oppenheimer approximation, which allows separate treatment of the electronic and nuclear energies. This Hamiltonian is further simplified by if the electrons are assumed to act independently of one another such that the electronic Hamiltonian may be represented as a sum of 1-electron Hamiltonians. However, in molecular systems, this Hamiltonian does not account for the interaction between electrons with two or more different interaction centres or the interaction of two electrons. Thus, the Hamiltonian is further modified and renamed to the Fock operator which is supplemented by terms that describe the interaction between two electrons. The default method in CS MOPAC PRO uses the restricted form (RHF) of the Fock matrix in the quantum mechanical calculations. The RHF requires that spin up and spin down electrons have the same energy and occupy the same orbital. The

effects of electron repulsion are underestimated by this method, resulting in the overestimation of energies. For this reason the CS MOPAC PRO automatically invokes a configuration interaction to correct these errors. Repulsive interactions can be minimised by allowing electrons to exist in more orbitals, specifically termed virtual orbitals. The multi-electron configuration interaction method in MOPAC addresses this problem by allowing multiple electron configurations to be used in constructing molecular wavefunctions. Molecular wavefunctions, representing different configurations, are combined in a manner analogous to the linear combination of atomic orbital approach.

The computations reported here involved energies that were minimised with convergence criteria of a minimum RMS gradient of 0.100, the default setting in the package. The AM1 (Austin Model 1) method of approximating the Hamiltonian with the closed shell (restricted) wavefunction was employed. This potential energy function modifies the Hamiltonian by approximating and parameterising aspects of the Fock matrix. In this approximation the core electrons are not explicitly treated and are instead added to the nuclear charge. Under the "properties" tab the heat of formation, gradient norm, dipole and polarisability were selected and the default charges of Muliken were used. The energy minimisation was then performed with the PRECISE keyword added under the general tab. Following the energy minimisation, the "compute properties" program was run with the properties dipole and polarisability selected. The computations were performed using a PC. The output file gives values of β that must be scaled by a factor of 0.5 for comparisons with experimental data (this aspect is clarified in the later versions of MOPAC but not the earlier versions). The theoretical calculations employ atomic units and conversion factors are required to obtain SI and esu units [26]:

1 a.u. of elelctric field, E	$= 1.71514 \times 10^{7}$ esu
	$= 5.14192 \times 10^{11}$ V/m
1 a.u. of polarisability, α	$= 1.48176 \times 10^{-25}$ esu
1 a.u. of 2nd order polarisability, β	$= 8.63993 \times 10^{-33}$ esu
1.a.u. of 3rd order polarisability, γ	$= 5.03717 \times 10^{-40}$ esu

3.8 References

1. Tien, P.K. and Ulrich, R., *Theory of prism-film coupler and thin-film light guides.* Journal of the Optical Society of America, 1970. **60**(10): p. 1325-1337.

2. Kogelnik, H. and Ramaswamy, V., *Scaling rules for thin-film optical waveguides.* Applied Optics, 1974. **13**(8): p. 1857-1862.

3. Sherlock, T.W., *Mathematica*, 1988-1992, Wolfram Research.

4. Oudar, J.L., *Optical nonlinearities of conjugated molecules. Stilbene derivatives and highly polar aromatic compounds.* The Journal of Chemical Physics, 1977. **67**(2): p. 446-457.

5. Levine, B.F. and Bethea, C.G., *Second and third order hyperpolarizabilitlies of organic molecules.* The Journal of Chemical Physics, 1975. **63**(6): p. 2666-2682.

6. Maker, P.D., Terhune, R.W., Nisenoff, M., and Savage, C.M., *Effects of dispersion and focusing on the production of optical harmonics.* Physical Review Letters, 1962. **8**(1): p. 21-22.

7. Teng, C.C. and Garito, A.F., *Dispersion of the nonlinear second-order optical susceptibility of organic systems.* Physical Review B, 1983. **28**(12): p. 6766-6773.

8. Jerphagnon, J. and Kurtz, K., *Maker fringes: detailed comparison of theory and experiment for isotropic and unixial crystals.* Journal of Applied Physics, 1970. **41**(4): p. 1667-1681.

9. Thomas, P.R., *The molecular properties of zwitterionic, non-linear optical molecules and their evolution and their evolution with molecular environment*, in *Department of Physics*. Ph.D, 1998, University of Durham: Durham. p. 235.

10. Hampsch, H.L. and Torkelson, J.M., *Second harmonic generation in corona poled, doped polymer films as a function of corona processing.* Journal of Applied Physics, 1990. **67**(2): p. 1037-1041.

11. Mortazavi, M.A., Knoesen, A., Kowel, S.T., Higgins, B.G., and Dienes, A., *Second-harmonic generation and absorption studies of polymer dye films oriented by corona-onset poling at elevated-temperatures.* Journal of the Optical Society of America B-Optical Physics, 1989. **6**(4): p. 733-741.

12. Morichere, D., Chollet, P.A., Fleming, W., Jurich, M., Smith, B.A., and Swalen, J.D., *Electrooptic effects in two tolane side-chain nonlinear-optical polymers - comparison between measured coefficients and second-harmonic generation.* Journal of the Optical Society of America B-Optical Physics, 1993. **10**(10): p. 1894-1900.

13. Hill, R.A., Knoesen, A., and Mortazavi, M.A., *Corona poling of nonlinear polymer thin-films for electrooptic modulators.* Applied Physics Letters, 1994. **65**(14): p. 1733-1735.

14. Suzuki, A., Matsuoka, Y., and Ikushima, A.J., *Substrate effect on poling process of nonlinear optical polymer-films.* Japanese Journal of Applied Physics Part 2-Letters, 1991. **30**(8B): p. L1493-L1495.

15. Moreno, R.A. and Gross, B., *Measurement of potential buildup and decay, surface charge density, and charging currents of corona-charged polymer foil electrets.* Journal of Applied Physics, 1976. **47**(8): p. 3397-3402.

16. Giacometti, J.A. and Oliveira, O.N., *Corona charging of polymers.* IEEE Transactions On Electrical Insulation, 1992. **27**(5): p. 924-943.

17. Giacometti, J.A., *Radial current-density distributions and sample charge uniformity in a corona triode.* Journal of Physics D-Applied Physics, 1987. **20**(6): p. 675-682.

18. Gross, B., Giacometti, J.A., Ferreira, G.F.L., and Oliveira, O.N.J., *Constant current corona charging of PVF_2.* Journal of Applied Physics, 1984. **56**(5): p. 1487-1491.

19. Giacometti, J.A. and Campos, J.S.C., *Constant current corona triode with grid voltage control - application to polymer foil charging.* Review of Scientific Instruments, 1990. **61**(3): p. 1143-1150.

20. Oliveira, O.N. and Ferreira, G.F.L., *Grid-to-plate current-voltage characteristics of a corona triode.* Review of Scientific Instruments, 1985. **56**(10): p. 1957-1961.

21. Page, R.H., Jurich, M.C., Reck, B., Sen, A., Twieg, R.J., Swalen, J.D., Bjorklund, G.C., and Willson, C.G., *Electrochromic and optical waveguide studies of corona-poled electro-optic polymer films.* Journal of the Optical society of America B, 1990. **7**(7): p. 1239-1250.

22. Healy, D., *Solid solution studies of the molecular nonlinear optical properties of organic chromophores*, in *Physics Department*. PhD, 1996, Univeristy of Durham: Durham. p. 116.

23. Dao, P.T., Williams, D.W., McKenna, W.P., and Goppert-Berarducci, K., *Constant current corona charging as a technique for poling organic nonlinear optical thin films and the effect of ambient gas.* Journal of Aplied Physics, 1993. **73**(5): p. 2043-2050.

24. Prasad, P.N. and Williams, D., *Introduction to nonlinear optical effects in molecules and polymers.* 1991, New York: Wiley-Interscience. 306.

25. ChemOffice, C., *CS Chem 3D Pro*, 1999, www.camsoft.com: Cambridge.

26. Stewart, J., *CS MOPAC PRO: Semi-empirical computation*, 1993-1997, Fujitsu Limited.

Chapter 4 : Results and Discussion of Molecular Properties

4.1 Introduction

The design of organic molecules with high second order susceptibility, β, has been guided by theoretical calculations [1-3], experimental data [4-6] and various related models [1, 7-11]. Such studies have shown that the optimisation of β requires both a high degree of polarisability and electronic asymmetry within a molecule. The polarisability may be achieved using a molecule that contains a conjugated chain or ring system. If such a system is made from alternate single and double bonds, the π-electrons may become delocalised and move over the conjugation length. A scale for π-conjugation for a model molecule with a polyenic bridge has been defined by the average difference between the lengths of alternating single and double bonds, known as bond length alternation [12]. The electronic asymmetry is usually implemented by attaching donor and acceptor groups to opposite ends of a conjugated molecule, causing the molecule to exhibit a permanent dipole moment, μ. Indeed, it is the product of the molecular properties, $\mu\beta$, which is often cited as a "figure of merit" (FOM) when comparisons are made between different chromophores for second order NLO applications. Further, since sufficient $2p_z$ orbital overlap is required for delocalisation of π-electrons it follows that planar molecules should provide higher nonlinearities than nonplanar molecules.

It has generally been assumed that the macroscopic optical nonlinearity scales linearly with $N\beta\langle cos\theta\rangle$, where N is the chromophore number density, β is the molecular hyperpolarisability and $\langle cos\theta\rangle$ is the orientational averaging factor. According to the classical thermodynamic model [13-15] that has been outlined in Chapter 2, this averaging factor may be approximated by $\mu E/5kT$. This implies that the second order nonlinearity will scale linearly with the number density. One of the key assumptions of this model is that all chromophore-chromophore interactions are negligible. Thus the macroscopic nonlinearity is expected to be the orientational average of molecular nonlinearities of the constituent chromophores.

It has been described how the hyperpolarisability, β, vanishes by symmetry in a molecule with a centre of inversion. Thus, β is particularly sensitive to interactions that remove or create such a centre of symmetry. For a system of high $\mu\beta$ chromophores, any interaction that has the effect of reducing the β of the molecules will result in a decreased second order macroscopic nonlinearity. So for a high FOM, molecules are designed to be planar with large dipole moments and second order hyperpolarisabilities. However, the very same properties that create a large FOM are also likely to favour interactions between the highly dipolar chromophores to align head to tail, thus creating a symmetric system where β will vanish. In fact it is reasonable to suppose that noncentrosymmetric order (and hence the bulk second order nonlinearity) will be determined by the competition of ordering and disordering electrostatic forces. Ordering forces including the electric field used to align the chromophores and disordering forces such as thermal effects and chromophore-chromophore electrostatic interactions.

Whilst the main thrust of research has concentrated on the design of high "$\mu\beta$" chromophores for second order NLO [3, 16-18], until recently [19, 20], there has been comparatively little focus of attention to the macroscopic ordering or packing of such molecules.

Enhanced β values have been reported for molecules containing the tricyanoquinodimethane acceptor moiety [4]. This work uses highly polarisable molecules with dicyanoquinodimethane as acceptors to provide a high degree of electronic asymmetry within the molecule.

The molecules discussed in this chapter are all derivatives of 7,7,8,8 tetracyanoquinodimethane (TCNQ). The chemical structure of TCNQ, shown in Figure 4.1, was first reported in 1960 by two independent groups [21, 22]. However it was the researchers at Du Pont who went on to study more of the properties of TCNQ [23-27]. The molecule has a high electron affinity due to the presence of the four strong electron accepting cyano groups and its planar nature and hence it has been used to form stable charge transfer salts [22].

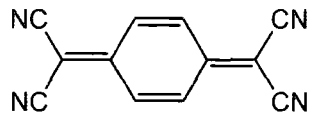

Figure 4.1: Molecular Structure of TCNQ

Although the chemistry of TCNQ has been known for the last forty years, there are relatively few reports of the nonlinear optical properties of TCNQ derivatives substituted with primary and secondary amines [27-32]. In 1984 it was discovered that TCNQ could be reacted to form a zwitterionic donor-π-acceptor adduct [33]. Since this discovery, other varieties of TCNQ-zwitterionic molecules have been synthesised for applications in nonlinear optics [34-37].

Tertiary amine TCNQ zwitterionic derivatives have been synthesised and characterised in Durham. These adducts, e.g. 4-[1Cyano-3-(diethylamino)-2-propenylidene]-2,5-cyclohexadiene-1-ylidenepropanedinitrile, (DEMI), illustrated in Figure 4.2, are highly charge separated in the ground state and thus exhibit extremely high values of ground state dipole moment, μ. They are also highly polarisable molecules and possess large second order hyperpolarisabilities, β [34]. The large dipole moment enables a high degree of polar order to be achieved by electric field poling of poly(methyl methacrylate) films containing these chromophores [38]. Investigations of the photostability of these molecules have indicated that they are prone to photo-oxidation [39]. The most probable source of the instability is the presence of double bonds in the substituents groups. Practical applications of these molecules are limited by visible wavelength absorption, to infrared wavelengths.

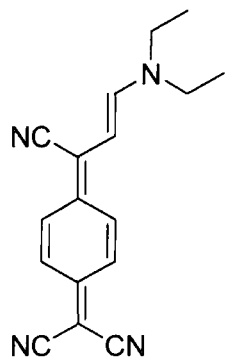

Figure 4.2: Chemical Structure of DEMI

In contrast, the adducts used in this thesis are simpler in that they have shorter conjugation lengths than the tertiary amine TCNQ derivatives. The molecules in this work contain few or no double bonds in the substituents. This class of chromophore is

easily synthesised (see Appendix II). The synthetic methods allow a variety of donor groups to be introduced. These comparatively small chromophores exhibit high thermal stability up to 250-350 °C and have optical transparency through most of the visible range.

In this chapter, the molecular properties of the materials used in this work are presented and discussed. The results from EFISH experiments and the corresponding first hyperpolarisabilities of nine 7,7,8,8-tetracyanoquinodimethane (TCNQ) derivatives are presented. The study of solvent dependence of the first hyperpolarisability for all the molecules and concentration dependence for a standard molecule are discussed. Dipole moments and optical spectroscopy data are also presented.

4.2 Materials

The molecular structures of the chromophores in this study are shown in Figure 4.3. All the molecules except RIGID (molecule **7**) are di-substituted dicyanoquinodimethanes and were synthesised in the laboratories in Durham by M. Ravi and M. Szablewski. The molecules in Figure 4.3 may be grouped into four sets based on the nature of the donor amino groups present, a more detailed discussion of the molecules follows.

Molecules in the first series (**1-3**) contain at least a single morpholine unit as an electron donor group. Crystal structure studies of molecules **2** and **3** have shown that these nonlinear optical chromophores adopt configurations such that the piperidino and morpholino groups are twisted out of the molecular plane [31]. The twist angle for MORPIP (Molecule **2**) in the crystal structure being 45.3°. MORPYROL (molecule **1**) contains a hydroxy group for chemical attachment to a polycarbonate polymer backbone [40]. The molecular structure of MORPYROL (molecule **1**) was studied using synchrotron x-ray diffraction techniques in order to elucidate the crystal structure which was obtained from single-crystal x-ray analysis. The x-ray structure was solved by J.M. Cole [41] and the crystal structure for MORPYROL (molecule **1**) is shown in Figure 4.4 revealing the twist between the morpholine unit and the quinoid ring. Selected bond lengths are shown in Table 4.1. These compounds exhibit a strong fluorescence, which is visible as an iridescent colouration of powder samples under daylight illumination [30].

The second series of molecules (**4-6**) also have a characteristic twist, or dihedral, between the diaminomethylene plane and the quinoid ring. This twist has been observed in all previously determined crystallographic structures of such materials and in the computational geometries [29, 42]. Studies have shown that this molecular twist is a sensitive structural feature that influences the molecular hyperpolarisability in these push-pull quinoid type molecules [43].

DMPDQ (molecule **5**) was first synthesised as part of a systematic study by M. Ravi *et al* to increase the SHG capability of these materials by the introduction of two rigid stereogenic centres close to the dipole axis [36]. It was noted that these molecules contained dipole vectors that deviated from an antiparallel orientation in the crystal structures. Consequently, larger powder second harmonic generation (SHG) was observed from this class of chromophore. These molecules also exhibit fluorescence although to a lesser extent compared to the first series of molecules.

RIGID, (Molecule **7**) was originally synthesised for potential use in polymer dispersed liquid crystal (PDLC) applications [44]. Liquid crystals often take the structural form of a rigid rod with long alkyl chains at one end. In order to make this molecule compatible with the liquid crystal host, a long flexible alkyl chain was added to the TCNQ adduct. The oxazolidine group in RIGID, (molecule 7) contains more asymmetric character than the morpholine or aminomethylene groups of the previous two series. Also, there is asymmetry in terms of the electron affinities of the two hetero atoms closest to the TCNQ residue and this may lead to molecule **7** having a lower dipole moment. It has been discussed in Chapter 2 that highly dipolar molecules may be expected to have a stronger tendency to form aggregates than molecules with lower dipole moments. Since this molecule is expected to have a lower dipole moment than the series above, this molecule was also studied for its second order nonlinear optical properties.

Molecules **8** and **9** were synthesised in an attempt to increase the solubility of these compounds by the addition of alkyl chains. No crystal structures for either of these compounds or molecule **7** have been determined.

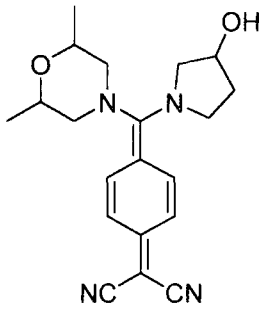

1. MORPYROL

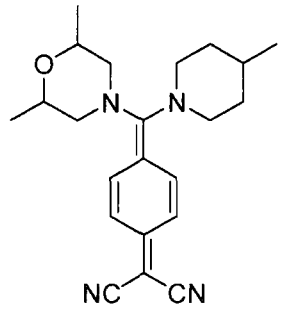

2. MORPIP

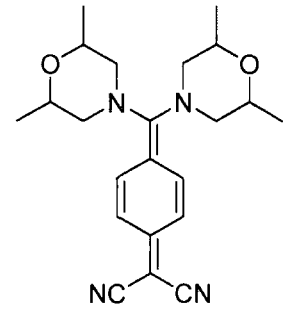

3. MOR2

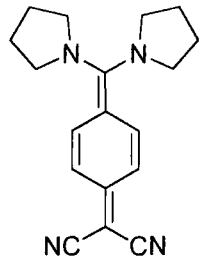

4. DPDQ

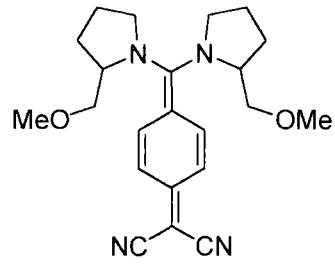

5. DMPDQ

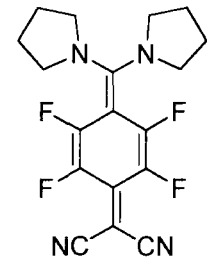

6. DPDQF

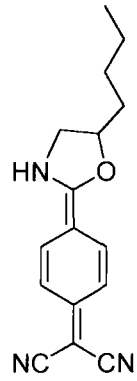

7. RIGID

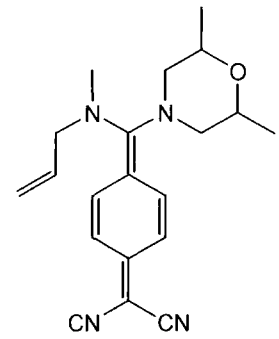

8. MOR2ALLYL

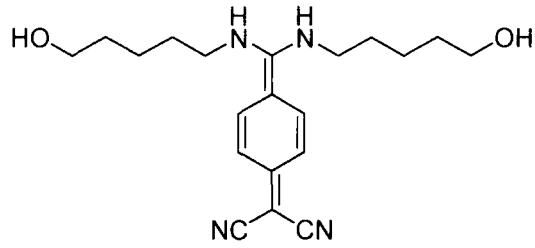

9. LCAT5OH

Figure 4.3: Chemical structures of molecules studied in this work

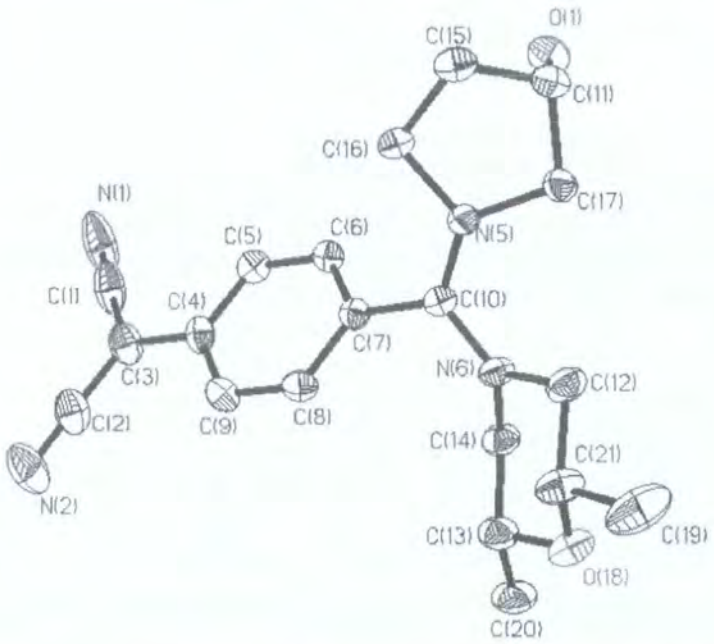

Figure 4.4: Structure of molecule 1, MORPYROL as a single molecule from crystal structure

Bond	Distance (Å)	Bond	Distance (Å)	Bond	Distance (Å)
N(5)-C(10)	1.323(3)	C(40)-C(38)	1.408(3)	C(39)-C(36)	1.395(3)
N(5)-C(17)	1.480(3)	C(4)-C(5)	1.405(3)	C(38)-C(33)	1.414(4)
N(5)-C(16)	1.494(3)	C(4)-C(9)	1.416(3)	C(38)-C(34)	1.438(3)
O(1)-C(11)	1.433(3)	C(4)-C(3)	1.444(3)	C(17)-C(11)	1.514(3)
N(6)-C(10)	1.345(3)	C(5)-C(6)	1.374(3)	N(3)-C(33)	1.150(3)
N(6)-C(12)	1.461(3)	C(7)-C(6)	1.393(3)	C(16)-C(15)	1.515(3)
N(6)-C(14)	1.474(3)	C(7)-C(8)	1.403(3)	C(37)-C(34)	1.405(4)
O(18)-C(21)	1.431(3)	C(7)-C(10)	1.469(3)	C(36)-C(32)	1.397(4)
O(18)-C(13)	1.444(3)	C(8)-C(9)	1.378(3)	C(36)-C(35)	1.476(3)
C(40)-N(4)	1.144(3)	C(39)-C(37)	1.375(3)		

Table 4.1: Bond Lengths for the x-ray crystal structure of Molecule 1, MORPYROL

4.3 Dipole Moment Measurements

The solution molecular dipole moments of all the compounds were measured in order to extract β values from EFISH measurements. The dipole moments were determined from the measurement of the capacitance and hence dielectric constant of liquid solutions of the molecules under investigation. The experimental method used to measure the dielectric constants was developed by P.R. Thomas during PhD work at Durham [45].

Solutions of successive dilutions were prepared and their dielectric constants calculated from the capacitance measurements. The experimental procedure and typical solution concentrations are described in Chapter 3. All experiments yield a linear increase in dielectric constant with concentration. A typical graph showing the dielectric constant obtained for solutions of one of the molecules is shown in Figure 4.5.

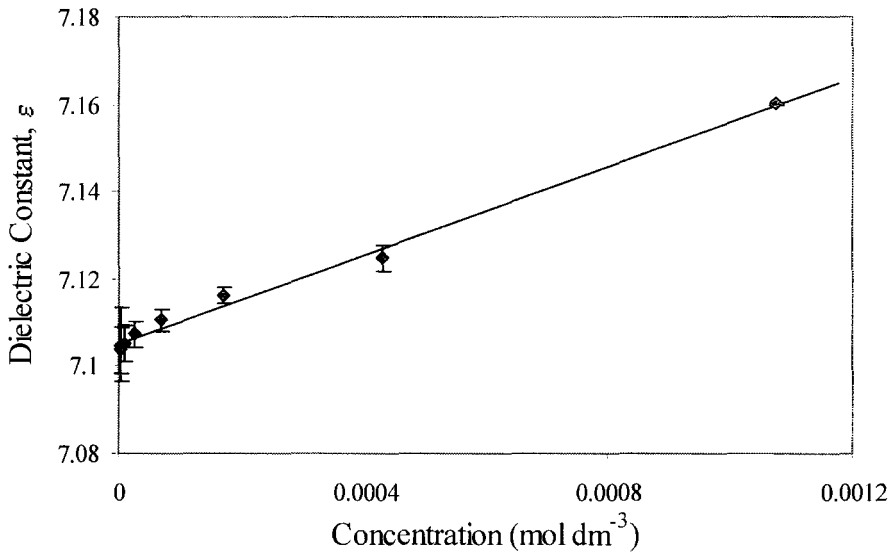

Figure 4.5: Typical graph showing dielectric constant obtained for a solution of molecule 9, LCAT5OH, in Tetrahydrofuran (THF). The straight line is a fit to the data.

The error bars show possible deviations in the dielectric constant. A straight line was fitted to the data points and the gradient calculated. Theory predicts that the intercept should give the dielectric constant of the solvent. However, all the measurements have lower than expected intercepts giving rise to erroneously low solvent dielectric constants. At low concentrations, larger errors are incurred, as the differences between the solution and solvent permitivity are small but this cannot wholly account for the discrepancy. Although the origin for the low intercept is not clear, one possible

explanation may arise from external factors such as the cell geometry. Nevertheless since the gradient of the slope gives the dipole moment, this error is inconsequential for the calculations. The most commonly used method for calculating dipole moments from solution dielectric constant experiments is based on the Guggenheim equation [46], Equation 4.1,

$$\mu_s = \sqrt{\frac{10^{36}}{N_a} \cdot \frac{9kT}{4\pi} \cdot \frac{3}{(\varepsilon+2)(n+2)} \cdot \frac{\partial\varepsilon}{\partial C}\Big|_0}$$

Equation 4.1

where μ_s is the solution dipole moment in Debyes, N_a is Avogadro's number, k is the Boltzman constant, T is the temperature, ε and n are the dielectric constant and refractive index respectively and $\partial\varepsilon/\partial C\,|_0$ is the experimental gradient at zero concentration.

The Guggenheim equation is derived from the Debye equation, which implicitly assumes that the internal field (or Lorenz field) and the directing fields are the same. One of the key assumptions made by Debye was that the molecular interaction energy is small compared to the thermal energy, and the effect of a reaction field that is produced by an isolated dipole on the surrounding medium is not considered. This latter effect was considered by Onsager.

The phenomenon of deviation of the solution dipole moment from the moment of the isolated molecule or the gas phase dipole moment is known as the solvent effect. This effect can be attributed to specific interactions between the solute molecule and the solvent molecules, and also the bulk properties of the solvent, particularly the dielectric constant. For this reason erroneously low dipole moments can be derived using the Debye model. This solvent effect may be accounted for using expressions based on the Onsager theory. Indeed, P.R. Thomas has shown, through thorough investigations of local field formalisms and molecular anisotropy, that the dipole moments derived are very sensitively dependent on the model used in the data analysis [45] and these issues will not be discussed further here. However, the more advanced models have the disadvantage of introducing many unknown parameters, such as cavity radius and polarisability, to the analysis leading to large uncertainties of the results. Moreover, since a solution measurement of $\mu\beta$ is generated by EFISH measurements, in this case, the dipole moment in solution is preferred to the use of gas phase dipole to derive β.

In general solvents of low polarity are chosen for these measurements to reduce the solvent-solute interactions. Chloroform was used due to its relatively low dielectric constant and, in addition, it was the solvent used in the EFISH measurements. However, the solubility of LCAT5OH (molecule **9**) in chloroform was found to be too low to conduct these experiments and so tetrahydrofuran (THF) was used.

The experimental and theoretical dipole moments for the nine molecules are shown in Table 4.2. The theoretical values of the ground state moment are calculated using MOPAC [47]. The AM1 Hamiltonian was used in the molecular geometry optimisation for these calculations. Table 4.3 is included for reference and shows the dielectric constants and refractive indices used in the calculations of the experimental dipole moments.

One disadvantage of this method is that reliable determinations of the dielectric constant are required at low concentrations where the difference between solution and solvent permittivity is small, and the experimental discrimination is correspondingly low. Nonetheless, the experimental solution dipole moments are within experimental error for the majority of the calculated values as shown in Table 4.2. There are a few notable exceptions, namely MOR2 (molecule **3**), DPDQ (molecule **4**) and RIGID (molecule **7**); the largest difference between the experimental and theoretical values being up to 50% for MOR2 (molecule **3**).

Molecule	Solvent	Dipole (D)	
		EXPERIMENTAL μ_s	THEORY μ_g
1 MORPYROL	Chloroform	11.4 ± 1.5	11.2
2 MORPIP	Chloroform	15.1[1] ± 1.0	14.9
3 MOR2	Chloroform	16.5 ± 2.3	7.9
4 DPDQ	Dichloromethane	19.8[2] ± 3.9	11.5
5 DMPDQ	Dichloromethane	13.2 ± 1.4	13.1
6 DPDQF	Dichloromethane	17.7[2] ± 3.5	16.3
7 RIGID	Chloroform	9.1 ± 1.4	13.2
8 MOR2ALLYL	Chloroform	10.8 ± 1.6	12.6
9 LCAT5OH	Tetrahydrofuran	14.2 ± 1.7	12.2

[1] Values from [31]
[2] Values from [29]

Table 4.2: Experimental and theoretical values of dipole moments

Solvent	Dielectric Constant, ε	Refractive Index, n_D (20 °C)
Chloroform	4.806	1.4459
Dichloromethane	8.93	1.42416
Tetrahydrofuran	7.58	1.40716

Table 4.3: Data for solvents used in dipole measurements [48]

The under estimation of theory compared to experimental values for MOR2 (molecule **3**) and DPDQ (molecule **4**) is most probably due to the gas phase nature of the theoretical calculation. In terms of the "bond length alternation (BLA) model" (see Chapter 2), the dipole moment will evolve with reaction field and the gas phase dipole moment, being defined as the value at zero reaction fields, is the minimum value. Thus when a molecule is placed in a medium, it experiences a reaction field that will have the effect of increasing the dipole moment relative to the gas phase. Furthermore, Rigid (molecule **7**) shows an over estimation of theory compared to the experimental value. This is most likely because the Guggenheim equation, (Equation 4.1) used to calculate the dipole moment does not account for all the interactions, such as hydrogen bonding and solvation effects, between the solute and the solvent and may not be strictly appropriate in this case.

4.4 EFISH Results

Hyperpolarisabilities of the molecules were determined by electric field induced second harmonic generation (EFISH) solution experiments. These experiments were performed as part of collaboration with Professor J. Zyss's group at the Laboratoire de Photonique Quantique et Moléculaire (LPQM) at the École Normale Supérieure de Cachan (ENS) in Cachan, Paris [49]. Experiments were conducted on all nine molecules at wavelengths of 1064 nm and 1907 nm and were conducted in two different solvent systems to determine the effect of solvent on the value of $\mu\beta$.

4.4.1 Solvent dependent EFISH studies

Experiments were performed to investigate the solvatochromic effect on the $\mu\beta$ of the molecules. Furthermore, the resonance enhancement was probed using two different wavelengths. For clarity, results for the two solvents will each be described separately before comparisons are made between the two.

The results from EFISH experiments in acetone are shown in Table 4.4. Acetone is a relatively polar solvent with a dipole moment of 2.69 D, dielectric constant, $\varepsilon = 20.7$ [48] and relatively small second order polarisability, $\beta_0 = 0.21 \times 10^{-30}$ esu [50]. The absorption maxima for these molecules in acetone range from 383 nm to 447 nm for

DPDQF (molecule **6**) to RIGID (molecule **7**) respectively. All $\mu\beta$ values shown are solution values, the extrapolated β_0 are shown and discussed in the next section, 4.4.2.

All the $\mu\beta$ results from experiments in acetone at 1064 nm are higher than those performed at 1907 nm. This effect may be explained in terms of resonant enhancement. According to the two level model [10], measurements at different frequencies would be expected to show resonant enhancement closer to the absorption maxima. In every case, resonance enhancement between the two wavelengths is clearly demonstrated.

In the second series, the peak absorption wavelength range from 383 nm (for DPDQF, molecule **6**) to 419 nm (for DMPDQ, molecule **5**). The $\mu\beta$ increases through the series following the order of: DPDQF < DPDQ < DMPDQ. The only difference between DPDQ and DPDQF is the substitution of the ring system with fluorine atoms. This suggests that the substituted ring system in the case of DPDQF reduces the $\mu\beta$ of the molecule. The fluorine atoms are highly electronegative and will therefore significantly affect the electron accepting properties of the TCNQ residue. Certainly the effect of the fluorine substituents has resulted in a blue shift of the absorption maximum indicating differences in the relative energies of the ground and excited states between DPDQ (molecule **4**) and DPDQF (molecule **6**). The electronic distribution of polar molecules is intimately related to the charge transfer and hyperpolarisability. A convenient scale for the relationship of the hyperpolarisability to the charge structure and π-conjugation is described by the bond length alternation model (BLA). The main aspects of the BLA model have been introduced in Chapter 2.

Molecule	λmax (± 2 nm)	EFISH $\mu\beta$ x10^{-48} esu 1064 nm	EFISH $\mu\beta$ x10^{-48} esu 1907 nm
1 MORPYROL	425	-1740 ± 98	-686 ± 122
2 MORPIP	433	-2080 ± 87	-726 ± 162
3 MOR2	436	NM	-473 ± 85
4 DPDQ	395	-1130 ± 41	-508 ± 86
5 DMPDQ	419	-2030 ± 63	-697 ± 68
6 DPDQF	383	-791 ± 32	-361 ± 47
7 RIGID	442	-1340 ± 54	-521 ± 50
8 MOR2ALLYL	437	NM	-945 ± 85
9 LCAT5OH	390	-988 ± 43	-725 ± 139

NM = Not measured

Table 4.4: EFISH data for molecules in acetone

The data for the EFISH measurements that were taken in chloroform are shown in Table 4.5. Chloroform is a less polar solvent than acetone with a dipole moment of 1.15 D, dielectric constant of $\varepsilon = 4.8$ [48] and second order polarisability, $\beta_0 = 0.49 \times 10^{-30}$ esu [51]. The absorption maxima range from 420 nm to 478 nm for RIGID (molecule **7**) to MOR2 (molecule **3**) respectively. Once again, resonant enhancement is clearly shown for all samples studied. However, although the results are higher for 1064 nm compared to 1907 nm, the difference is too great to be accounted for by resonant enhancement alone, as described by the two level model. This result is highlighted when the data are extrapolated to the static hyperpolarisability and so will be discussed in more detail in the next section.

Molecule	λmax (± 2 nm)	EFISH $\mu\beta$ x10^{-48} esu 1064 nm	EFISH $\mu\beta$ x10^{-48} esu 1907 nm
1 MORPYROL	465	-900 ± 288	-43 ± 9
2 MORPIP	471	-734 ± 198	-256 ± 75
3 MOR2	478	-4170 ± 1126	-379 ± 38
4 DPDQ	432	-603 ± 104	-159 ± 59
5 DMPDQ	447	-2530 ± 890	-399 ± 64
6 DPDQF	426	-153 ± 57	-37 ± 19
7 RIGID	420	NM	NM
8 MOR2ALLYL	478	-770 ± 100	-422 ± 123
9 LCAT5OH	NS	NS	NS

NS = Not soluble
NM = Not measured

Table 4.5: EFISH data for molecules in chloroform

As in the case of acetone, a trend may be seen in the second series of molecules. All the absorption maxima of this second series occur at significantly lower wavelengths than those of the first series. This implies that the electronic transition energy is greater for the second series. Both absorption maxima and $\mu\beta$ increase in the order DPDQF (molecule **6**) < DPDQ (molecule **4**) <DMPDQ (molecule **5**). Once again the effect of ring substitution has the effect of reducing the $\mu\beta$ of the system. The addition of the methoxy groups to the pyrolidine rings in DMPDQ (molecule **5**) enhances the $\mu\beta$ of this molecule relative to the others in the series. These bulky groups may help in the reduction of intermolecular interactions in solution. The effect of the methoxy groups has been described previously by Ravi *et al* in relation to powder SHG [42].

LCAT5OH (molecule **9**) was not soluble in sufficient quantities in chloroform to perform EFISH measurements at all. This was an unexpected result as the alkyl chains

were a deliberate addition to the molecule in an attempt to increase the solubility of this molecule.

Comparison of Table 4.4 and Table 4.5 reveals a negative solvatochromic effect in the optical absorption spectra, with a shift towards shorter wavelengths in acetone (λ_{max} = 433 nm, for MORPIP) compared to chloroform (λ_{max} = 471 nm, for MORPIP), which is characteristic of such dipolar molecules, and confirms a negative $\mu\beta$. This shift however is in the wrong direction for resonant enhancement to contribute to the higher values in acetone compared to chloroform. Indeed zero-field values of β_0 may be extrapolated to eliminate the effects of resonant enhancement and this is the subject of the following section, together with further discussion of the differences between acetone and chloroform.

4.4.2 Static Hyperpolarisabilties

The two-level model describes the contribution of the charge-transfer resonance to the first hyperpolarisability within a molecule. This model was first developed by Oudar and Chemla [10] and is often used in practice today to extrapolate zero field β_0 values from experimental values. This model has been outlined in Chapter 2.

In the case of sum-frequency generation and when only two levels are involved such that the transition dipole moments lie parallel to each other and only the single diagonal matrix element dominates the contribution to β, then β may be approximated by [52],

$$\beta_{zzz} = \left(\frac{\Delta\mu \cdot \mu_{eg}^2}{2\varepsilon_0 \hbar^2} \right) \cdot \left(\frac{\omega_{eg}^2 \left(3\omega_{eg}^2 + \omega_1\omega_2 - \omega_3^2 \right)}{\left(\omega_{eg}^2 - \omega_1^2 \right) \cdot \left(\omega_{eg}^2 - \omega_2^2 \right) \cdot \left(\omega_{eg}^2 - \omega_3^2 \right)} \right)$$

Equation 4.2

where ω_{eg} denotes the resonant frequency of the transition, ω_1, ω_2, ω_3 are the frequencies of the three interacting waves, $\Delta\mu = \mu_e - \mu_g$ is the difference between the excited and ground state electric dipole moments of the molecule and μ_{eg} is the transition dipole moment between the excited and ground state. If the dispersion free

hyperpolarisability β_0 (that is extrapolated to infinite optical wavelengths away from electronic resonance) is now introduced:

$$\beta_0 = \left(\frac{3}{2\varepsilon_0 \hbar^2}\right)\left(\frac{\Delta\mu \cdot \mu_{eg}^2}{\omega_{eg}^2}\right)$$

Equation 4.3

Then for frequency doubling the following equation may be obtained:

$$\beta_0 = \frac{\beta(\omega)}{\omega_{eg}^2}\left[\left(1-\frac{\omega^2}{\omega_{eg}^2}\right)\cdot\left(1-\frac{4\omega^2}{\omega_{eg}^2}\right)\right]$$

Equation 4.4

Equation 4.4 together with the dipole moments calculated from experimental measurements in Table 4.2 may then be used to extrapolate β_0 values from the $\mu\beta(\omega)$ results of EFISH experiments from Table 4.4 and Table 4.5. These zero field β_0 values are shown in Table 4.6. It can be seen that all molecules have experimental negative $\mu\beta$ values, agreeing with the theoretical predictions and is consistent with negative solvatochromism demonstrated by these molecules.

Table 4.6 shows that higher values are obtained in the more polar solvent acetone ($\varepsilon = 20.7$) than in the less polar solvent chloroform ($\varepsilon = 4.8$) at both wavelengths. In principle, neglecting different interactions and molecular conformations, the same β_0 should be obtained when the same solute is measured in the different solvents. However, it is well known that different solvents strongly effect β_0 through different solvent-solute interactions that will perturb the electronic configuration of the molecules in solutions. In this case, the quality of the recording (and thus the accuracy of the measurement) clearly depends on the nature of the solvent and the solute. Thus for acetone, stronger EFISH signals results in more precise determination of β_0.

Molecule	EFISH β_0 x10^{-30} esu 1064 nm		EFISH β_0 x10^{-30} esu 1907 nm	
	Acetone	Chloroform	Acetone	Chloroform
1 MORPYROL	-46 ± 9	-11 ± 5	-46 ± 14	-3 ± 1
2 MORPIP	-39 ± 4	-9 ± 3	-36 ± 10	-12 ± 4
3 MOR2	NM	-38 ± 15	-27 ± 8	-16 ± 4
4 DPDQ	-22 ± 3	-9 ± 3	-20 ± 5	-6 ± 3
5 DMPDQ	-49 ± 7	-46 ± 20	-41 ± 8	-23 ± 6
6 DPDQF	-19 ± 3	-3 ± 1.7	-16 ± 4	-1.5 ± 0.9
7 RIGID	-17 ± 3	NM	-20 ± 5	NM
8 MOR2ALLYL	NM	-11 ± 3	-39 ± 8	-27 ± 12
9 LCAT5OH	-28 ± 5	NS	-41 ± 12	NS

[1] Values from [31]
[2] Values from [29]

Table 4.6: Extrapolated β_0 values for nine molecules studied in EFISH measurements

A different β_0 value obtained from two solvents for the same solute demonstrates the effect of solvent on the hyperpolarisability of the molecules. Marder *et al* have shown that for a given molecule, the BLA and hence $\mu\beta_0$ may be tuned by varying the solvent polarity [6] since the polarity of the solvent will effect the electronic energy distribution of the molecule. The BLA model predicts that with the increase in polarity of the solvent (or reaction field) the zwitterionic nature of the molecule will be increased leading to an enhancement of the dipole moment. In particular for negative solvatochromic molecules, the theory predicts an increase in the magnitude β_0 with increasing polarity of the solvent.

It has been seen previously that tertiary amino TCNQ adducts measured at 1907 nm in chloroform have extremely low values of β_0 [45]. This was attributed to the fact that the geometry and electronic distribution of the tertiary amino TCNQ adducts are such that they reside close to the cyanine limit in this solvent. However in the case of tertiary TCNQ adducts, a reversal in the shift of the transition frequency as a function of solvent polarity was also observed. In this case, no such reversal in either solvent

dependent EFISH measurements or transition frequencies was observed. This leads to the conclusion that the low values in chloroform are not due to the electronic distribution of the dicyanoquinodimethane adducts residing close to the cyanine limit.

Since chloroform is less polar than acetone, it is possible that the hyperpolarisability increases with higher solvent dielectric constant through tuning of the bond length alternation parameter [6]. However, the increase in β_0 from chloroform to acetone is too large for solvatochromic effects to be the only origin of the discrepancy. Thus the existence of the discrepancy between β_0 in acetone and chloroform could be due to inadequacies in the static field models, which may be improved by using more appropriate theories. However, since the Lorenz local field proved to be adequate for the calculation of dipole moments in chloroform, any remaining discrepancies are more likely due to solute-solute interactions and solute-solvent interactions that occur in chloroform but not in acetone. Such interactions will affect the electronic energy states (for example the ground and first excited state) and involve both angular correlation and electronic dispersion effects due to *inter*molecular charge transfer.

Furthermore, the values of β_0 from chloroform obtained with 1064 nm do not agree with β_0 obtained at 1907 nm. The same values of β_0 for a solute in a particular solvent should be obtained regardless of the wavelength used and this is indeed the case for measurements in acetone (within experimental errors). The discrepancy in chloroform may be attributed to several factors.

One factor could be the fact that the solutions are absorbing at either the fundamental or the second harmonic frequencies. However, absorption spectra of the pure solvents, acetone and chloroform referenced to air indicate that there is negligible absorption due to the solvent at either the fundamental or second harmonic wavelengths. Moreover, absorption from the solvent at the fundamental or the second harmonic frequency is unlikely to effect measurements since each measurement was referenced to an experiment using the pure solvent. In addition, the dilute concentrations of the solutions used for these EFISH measurements show negligible absorption at the fundamental or the second harmonic and so should not be a significant problem here.

Another factor could be the inadequacy of the two level model in describing the dispersion of β for novel materials as has been previously demonstrated [53, 54] and thus care must be taken with the interpretation of the zero frequency results. As the

two level model is inadequate for extrapolation for chloroform, yet adequately projects the acetone β_0 values from the two wavelengths studied, the discrepancy between β_0 in acetone and chloroform may be real and could be due to the formation of aggregates in chloroform due to chromophore-chromophore interactions. In the less polar solvent, there may be more opportunity for solute - solute interactions to dominate solute - solvent interactions compared to a polar solvent. If aggregates exist in chloroform solution, they are likely to have higher order energy levels that may contribute significantly to the β of the system. This would not be accounted for in the two level model and this would be consistent with discrepancies in β_0 measured at different wavelengths in chloroform but not acetone. This provides evidence for the solvent effect on the hyperpolarisability of the molecule through different intermolecular interactions occurring in acetone to chloroform.

Ultraviolet absorption data may provide information of complex systems and these are studied for a number of the solutions in section 4.5. Since molecular interactions are an important consideration, concentration dependence of β_0 has been investigated in chloroform.

4.4.3 Concentration dependent EFISH studies

It is well established [50, 55] that the structure of solutions, depending on the nature of solvent-solute interactions, strongly influences nonlinear phenomena and, in particular, eventually limits the access of solute molecular nonlinearity. Often, an additive model such as that expressed in Equation 4.5 is used to describe the macroscopic nonlinearity,

$$\Gamma = f \sum_i N_i \gamma_i^0$$

Equation 4.5

where Γ is the total macroscopic liquid nonlinearity produced by the N molecules of type i per unit volume, f accounts for all the local field factors at the relevant wavelengths and the hyperpolarisability is,

$$\gamma^0 = \gamma_e + \frac{\mu \cdot \beta}{5kT}$$

Equation 4.6

where γ_e is the purely electronic average third order contribution (which does not vanish for centrosymmetric molecules) and the temperature dependent rotational term, $\mu\beta$ is the scalar product of the dipole moment, μ, with the vector part of the second order polarisability, β. When molecular interactions are present solvent and solute molecules can no longer be considered as behaving independently from each other; this departure from linearity is further enhanced in a solution where the solute-solute interactions dominate. The solute-solute interactions, or aggregation effects, are very complex and require a more detailed analysis.

In order to investigate the effect of aggregation, EFISH experiments were also carried out as a function of concentration using a representative molecule, MORPIP (molecule **2**). Molecule **2** was chosen as a representative molecule as it has a relatively simple synthesis route with fair yields and is more readily available than the other molecules. The procedure for the synthesis of this molecule may be found in Appendix II.

The peak position of the electronic absorption band, λ_{max} for MORPIP in chloroform was found to be 471 nm and this band extends to around 530 nm. Therefore for experiments at 1064 nm, there is little or no absorption at either ω or 2ω. Nonetheless, such experiments may benefit from the electronic resonant enhancement of β at 532 nm allowing larger signals to be observed. Thus, it was for this reason that experiments were conducted at 1064 nm. Chloroform was chosen as the solvent as it is relatively apolar and so this would limit the solvent-solute interactions present in solution. In this way the solute-solute interactions were studied.

In the absence of appreciable absorption at 2ω, and any intermolecular interactions, the amplitude of the signal from such EFISH experiments may be related directly to the macroscopic susceptibilities. The ratios of the amplitudes of the SHG signal obtained for the solution, $A_m^{2\omega}$ and that for the pure solvent, $A_s^{2\omega}$, may be related directly to the macroscopic susceptibilities, Γ_m and Γ_s for the solution and solvent respectively, may be expressed by Equation 4.7.

$$\frac{A_m^{2\omega}}{A_s^{2\omega}} \alpha \left(\frac{\Gamma_m}{\Gamma_s} \right)^2$$

Equation 4.7

Thus the square root of the amplitude of the second harmonic intensity is proportional to the non-linearity. The square root of the amplitude of the second harmonic intensity as a function of MORPIP concentration in chloroform is shown in Figure 4.6.

At the more dilute concentrations, a strong dependence is seen. This is mostly due to the binary mixture of nonlinear optical species. It is interesting to note that there is a reduction in signal strength at weak solute concentrations until a minimum zero value followed by an increase in signal strength at high concentrations. This phenomenon is seen more clearly in Figure 4.7, which show the dilute concentrations of MORPIP in chloroform solutions. Such behaviour is associated with molecules which possess a non-linearity which is opposite in sign to that of the solvent. This occurs when there is a negative contribution to the susceptibility, γ^0, from a solute dispersed in a solvent that only has positive contributions to γ^0. According to Oudar [56], the sign of the non-linearity of chloroform is positive, $\Gamma = 8.7 \times 10^{-14}$ esu at 1064 nm and the second order nonlinearity has been measured by Kajzar *et al* to be $\beta = 0.49 \times 10^{-30}$ esu [51]. Hence there occurs a point at which the total non-linearity of MORPIP is exactly equal and opposite to that of the chloroform solvent and consequently no fringes are seen at that point [50]. The signal strength increases at stronger concentrations when the macroscopic non-linearity of the solute is greater than the macroscopic non-linearity of the solvent.

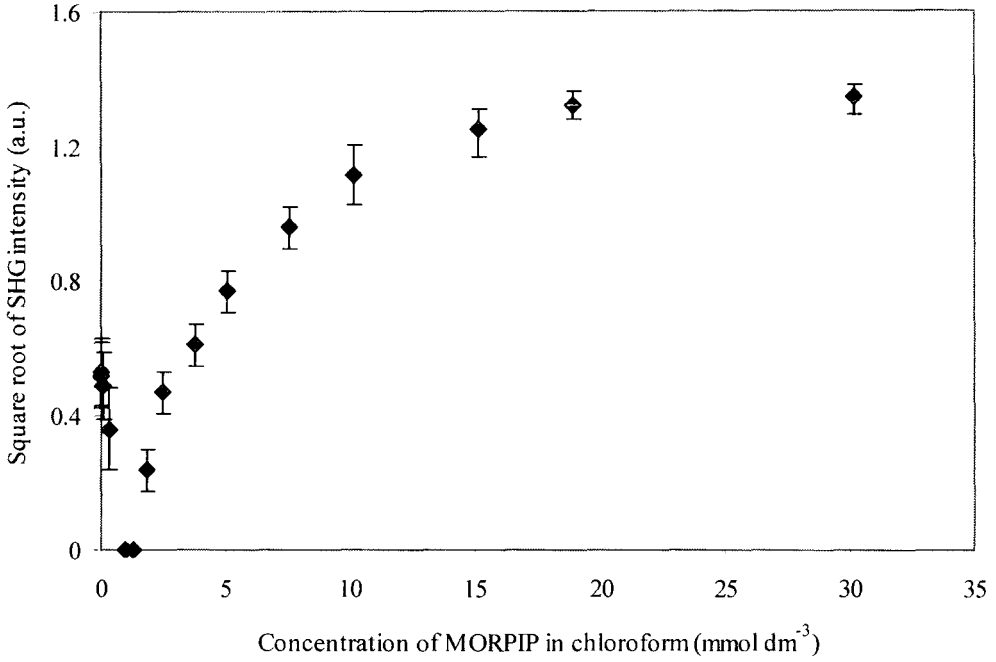

Figure 4.6: SHG intensity of MORPIP as a function of concentration in chloroform solution

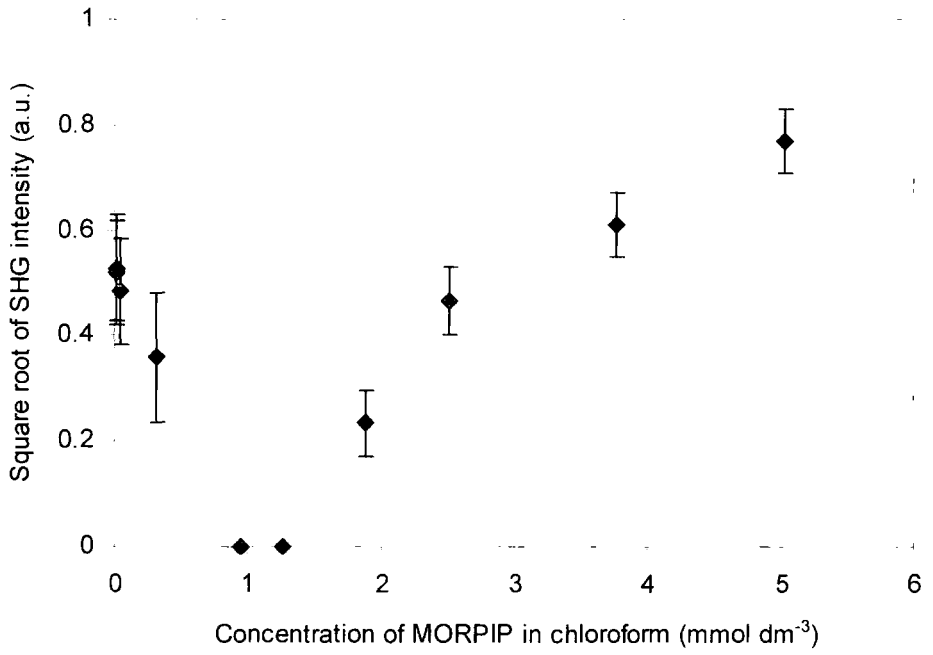

Figure 4.7: SHG intensity of MORPIP as a function of dilute concentration range in chloroform

For a solution of non-associating, non-absorbing molecules, the total non-linearity is expected to be the sum of the non-linearities of the constituents [57]. Therefore, beyond the zero-fringe concentration, the non-linearity of the solution in Figure 4.6 and Figure 4.7 is expected to be a linear function of MORPIP number density.

It can be seen that for increased concentrations of MORPIP in chloroform this is not the case and the non-linearity of the solution changes in gradient as a function of concentration. There may be several reasons for this deviation from linearity and the reduction in the gradient. One such reason is a drift in the power of the laser. However, since each measurement was immediately followed by a measurement of the reference solvent this can be ruled out. Limited solubility would also account for the deviation as a function of concentration. However, even the most concentrated solutions were transparent to the eye and no evidence of particulate scattering was observed. Also there could be an increase in the conductivity of the solutions or an increase in the absorption at 532 nm. Since the applied voltage and current were monitored throughout the experiment, increased conductivity was eliminated as the source of the deviation. Absorption spectra, as shown in section 4.5.1, show that the absorption does indeed increase with higher concentrations. Therefore the intensity at 532 nm may become a significant problem at the higher concentrations used in this experiment. Such an increase in absorption intensity would result in the second harmonic signal being overcome by the absorption at the concentration of measurement. Following the analysis of Levine and Bethea [58], if the liquid is absorbing at the second harmonic intensity with an absorption coefficient, $\alpha_{2\omega}$, and neglecting absorptions at the fundamental, the necessary data corrections are derived to be:

$$I_{2\omega}(\text{absorption}) = I_{2\omega}(0)\left[\exp\left(\frac{-\alpha_{2\omega}}{2}\ell\right)\right]$$

Equation 4.8

Where $I_{2\omega}(0)$ is the data corrected for absorption at the second harmonic frequency and l is the path length of the solution. The absorption corrected data, shown in Figure 4.8, clearly demonstrates a deviation from linearity. The line through the data is intended as a guide to the eye. The deviation occurs at higher concentrations than the uncorrected data implying that some absorption is contributing to the deviation. The residual

concentration dependence suggests the deviation is indeed due to strong solute-solute interactions. Concentration dependent solute-solvent interactions may also contribute to this trend [58].

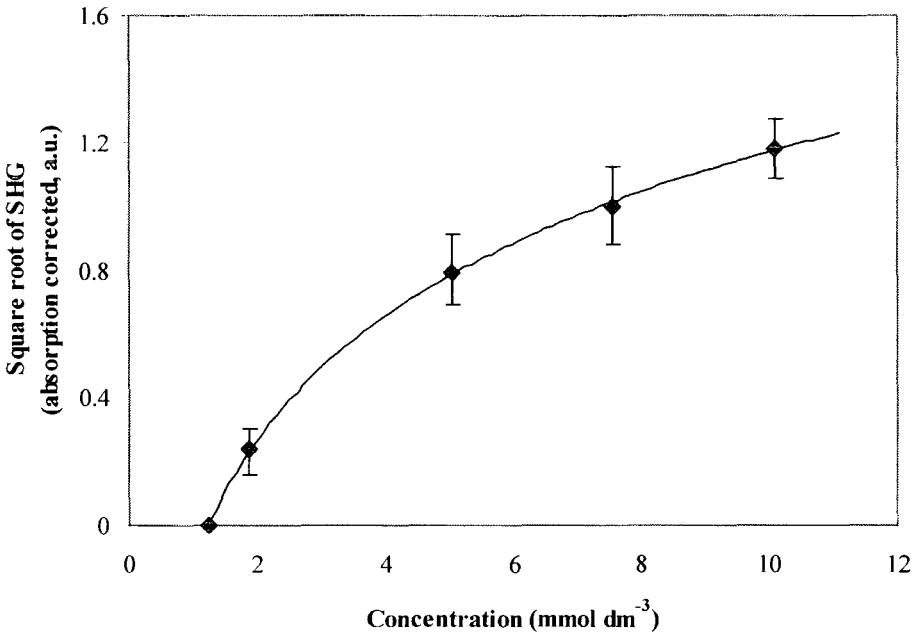

Figure 4.8: EFISH data corrected for absorption at 532 nm

The analysis described in Chapter 3 has been performed to calculate $\mu\beta(\omega)$ from the data in Figure 4.6, and the results are shown in Figure 4.9. For clarity, the concentration has been plotted as a log function. Figure 4.9 shows three regimes for this calculated $\mu\beta$. There is a region at low concentrations with large negative values of $\mu\beta \approx$ -5500 x 10^{-48} esu. Following this there is a middle section where the $\mu\beta$ appears to change with concentration. Whilst at higher concentrations the third portion shows positive values of $\mu\beta \approx$ 1000 x 10^{-48} esu. Since $\mu\beta$ is a molecular property, variation with number density for a particular molecule would not be expected. It has already been described how β vanishes by symmetry in a molecule with a centre of inversion (such as benzene) whereas α and γ do not. Thus, β is particularly sensitive to interactions that remove or create such a centre of symmetry. The decrease in non-linearity with increasing concentration, due to chromophore-chromophore interactions, is not accounted for in the usual analysis of the data and calculation of $\mu\beta$. At higher concentrations, there is a smaller signal for increasing number density and, since the

calculation involves dividing the signal by the number density, an erroneously small $\mu\beta$ is derived from this analysis.

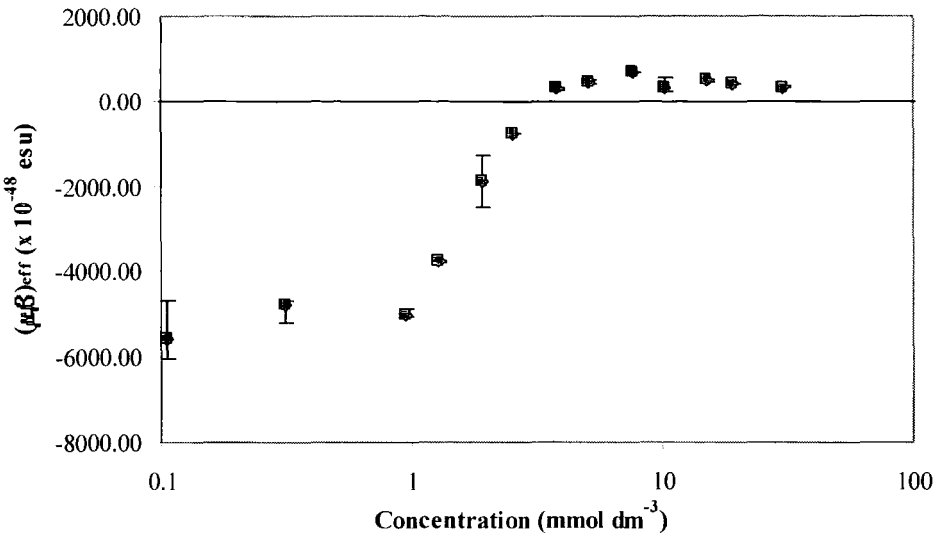

Figure 4.9: Calculated μβ of MORPIP in chloroform as a function of concentration

Figure 4.9 and Figure 4.8 both highlight the problems associated with single concentration measurements. The change in $\mu\beta$ is primarily due to solute-solute interactions. This occurs as the solute-solute separation decreases and thus the dipolar forces are increased.

4.4.4 "Zero-Fringe" Calculations

The EFISH measurements suggest that at higher concentrations, the molecules become aggregated and cannot contribute to the total non-linearity of the system in the same way as individual non-interacting molecules. It is possible to consider that at higher concentrations, a new species is present with the appearance of aggregates and the form of Equation 4.9 may be employed to describe the total macroscopic non-linearity of the system:

$$\Gamma = F\left[N^f\gamma_e^f + N^f\frac{\mu^f\beta^f}{5kT} + N^a\gamma_e^a\right] + F\left[N^s\gamma_e^s + N^s\frac{\mu^s\beta^s}{5kT}\right]$$

Equation 4.9

The first term in square brackets accounts for the non-linearity arising from the NLO molecule MORPIP and the second term is due to the contribution from the solvent. F denotes the field factors and N is the number density of the particular species. The superscripts a, f and s refer to the aggregate, single "free" molecule and solvent respectively. If the aggregate takes the expected form of an antiparallel dimer then the aggregate would not possess a net dipole moment. Since, in that case, the aggregate is not expected to possess a net dipole moment there is no $\mu\beta$ term relating to the orientation of the aggregate in the static electric field.

Initially, at low concentrations, there will be very few aggregates in the solution and so the number of aggregates, N^a will be negligible compared to the number of single MORPIP molecules, N^f. However, as the concentration increases, the number of aggregate species will increase and the number of free MORPIP molecules will decrease. Therefore, at high concentrations the total contribution to the macroscopic susceptibility will be dominated by the positive cubic non-linear γ_e terms in Equation 4.9. Since information about the number density and nature of the aggregates is not known this effect is not accounted for in the calculation of $\mu\beta$.

For this reason, advantage can be taken of the concentration dependent measurements carried out at 1064 nm in chloroform. Namely, since there occurs a concentration at which the non-linearity of chloroform is exactly equal and opposite to that of MORPIP as has been discussed, $\mu\beta$ can be calculated directly. The usual additive model is applied as shown in Equation 4.10,

$$\begin{aligned}\Gamma_L &= \Gamma_C + \Gamma_{MORPIP} \\ &= \Gamma_C + \left(NF\left[\frac{\mu\beta}{5kT} + \gamma_e \right] \right)\end{aligned}$$

Equation 4.10

where Γ_L is the total nonlinearity of the system, Γ_C is the nonlinearity of chloroform and is taken to be $\Gamma = 8.7\text{x}10^{-14}$ esu at 1064 nm after Oudar *et al* [56], F contains the local field factors, N is the number density of MORPIP in cm^{-3}. In the case where no fringes are seen, $\Gamma_L = 0$. The electronic contribution γ_e is assumed to be negligible compared with the rotational term in accordance with other experiments [53-56, 59]. There were a number of concentrations for which no fringes could be seen and this calculation was carried out for those concentrations shown in Table 4.7. By

comparison of this data with that in Table 4.6 it is clear that by neglecting the intermolecular interactions at higher concentrations, errors are introduced into the calculation of $\mu\beta$. In fact very dilute solutions should give the nearest value of $\mu\beta$ to that of MORPIP. Problems arise with large errors at these low concentrations and therefore the zero-fringe calculations have also been carried out. An improved correlation with theoretical β_0 values is obtained from this method. (β_0 = -53 x 10^{-30} esu from crystal structure calculations for MORPIP).

Concentration (mmol dm^{-3})	Calculated $\mu\beta$ (x 10^{-48} esu)	$\mu\beta_0$ (x 10^{-48} esu)	β_0 (x 10^{-30} esu)
1.26	-4830	-840	-55
1.20	-5071	-881	-59
0.94	-6447	-1120	-75

Table 4.7: Zero fringe calculations for MORPIP in chloroform at 1064 nm from EFISH data

4.4.5 Theoretical β_0 Calculations

In order to compare the β_0 values, theoretical β_0 values were also calculated. It was found that there is a considerable variation in the β_0 value obtained depending on the starting geometry used. Table 4.8 shows the calculated β_0 values for the four molecules whose crystal structures have been determined. All the calculations were performed using the MOPAC97 [47] package as described in Chapter 3. Different calculation methods involved the crystal structures run with no optimisation and with full AM1 geometry optimisations. Also structures that had been drawn using Chemoffice (thus having an arbitrary starting geometry) were minimised using the AM1 formalism. All calculations involving the AM1 optimisation give lower values for the static hyperpolarisability than the crystal structure with no further optimisation. The energy of the heat of formation for each molecule was compared for the different calculation

methods but there was no obvious correlation between the minimum energy and the method of calculation. However, by comparison of Table 4.6, Table 4.7 and Table 4.8 some interesting features can be seen. Firstly, the zero fringe calculation of the static hyperpolarisability agrees most closely to the crystal structure calculation with no further minimisation for MORPIP. However, since MOPAC with the AM1 optimisation, calculates reasonable ground state dipole moments in the gas phase, this may suggest that MOPAC is erroneous when calculating excited state characteristics of these molecules.

Molecule	Theoretical β_0 (x 10^{-30} esu) from CS		Purely Theoretical β_0 (x 10^{-30} esu)
	No optimisation	AM1	AM1
2 MORPIP	53.4	8.0	16.4
3 MOR2	48.4	2.5	2.51
4 DPDQ	39.5	52.6	7.94
6 DPDQF	20.2	33.6	20.4

Table 4.8: Calculated static hyperpolarisabilities (β_0) from crystal structure (CS) and AM1 optimised geomteries

These results imply that the geometry of the molecule plays an important role in the determination of β and that β is extremely sensitive to the molecular geometry. Thus any interactions that affect the molecular geometry will also affect the hyperpolarisability, β, of the molecule.

4.4.6 Discussion

When two polar molecules approach each other, there is a dipole-dipole interaction between them. This is often not accounted for when translating microscopic properties of nonlinearities to macroscopic nonlinearities in nonlinear optical materials. This electrostatic interaction becomes stronger the larger the dipole moments of the

molecules concerned. The evidence gathered for dipolar aggregates has been found in the concentration dependent EFISH studies (showing a decreasing signal for increasing concentration of chromophore). Recently, Dalton *et al* have proposed a model [20] for these intermolecular interactions and this will be discussed in the context of these new molecules.

The competition between chromophore-chromophore electrostatic interactions and chromophore-applied electric field interactions is modelled using a theory based on Van der Waals interactions and is termed a modified "London theory". The main aspects of Dalton's model have been outlined in Chapter 2. The interaction dispersion energy arises from dipole-dipole interactions between induced molecular dipoles and follows a $1/r^6$ dependence where r is the average intermolecular separation. Typical strengths of the London dispersion interaction are 2 kJ mol^{-1} [60]. At closer distances strong repulsive forces dominate that arise from Coulombic repulsions due to the overlap of electronic distributions of molecules. An empirical formula is often used to characterise this repulsive interaction, such as the Lennard-Jones potential which has a $1/r^{12}$ dependence. These simple expressions of the interaction potential are well suited for very simple gaseous species. Dalton's model neglects the repulsive forces between molecules and only considers the van der Waal interactions. If this model is applied to the calculations for EFISH, the main result is the modification of the usual model such that:

$$\Gamma = Nf_{\omega}^{2} f_{2\omega} \beta L_3(p)\left[1 - L_1^{\,2}\left(\frac{W_{VDW}}{kT}\right)\right]$$

Equation 4.11

Where p is the ratio of the poling orientation energy to thermal energy, $f_0\mu E_p/kT$, N is the number density of chromophores, L_1 and L_3 are the first order and third order Langevin functions previously described in Chapter 2, and the f's are the usual field factors. The W_{VDW} statistically averaged energy term includes induction interactions, orientation interactions and dipole-induced dipole contributions to the net van der Waals force. Figure 4.10 shows the non-linearity plotted as a function of the number density of NLO chromophores. The long-range van der Waals forces associated with polar and neutral molecules defines the form of this graph. The graph illustrates the basic features of this model. Namely it can be seen that initially there is a linear increase of Γ with increasing number density of NLO species followed by a predicted

maximum. Also, there is a shift of this maximum to lower chromophore number densities with increasing chromophore electrostatic interaction. In other words if the dipole moment of the individual molecules is increased, for example, the optimum value of loading is shifted towards lower number densities and the gradient thus becomes steeper. Clearly this is a disadvantage when trying to build devices and increase the total non-linearity of the system by increasing the number of active NLO species present.

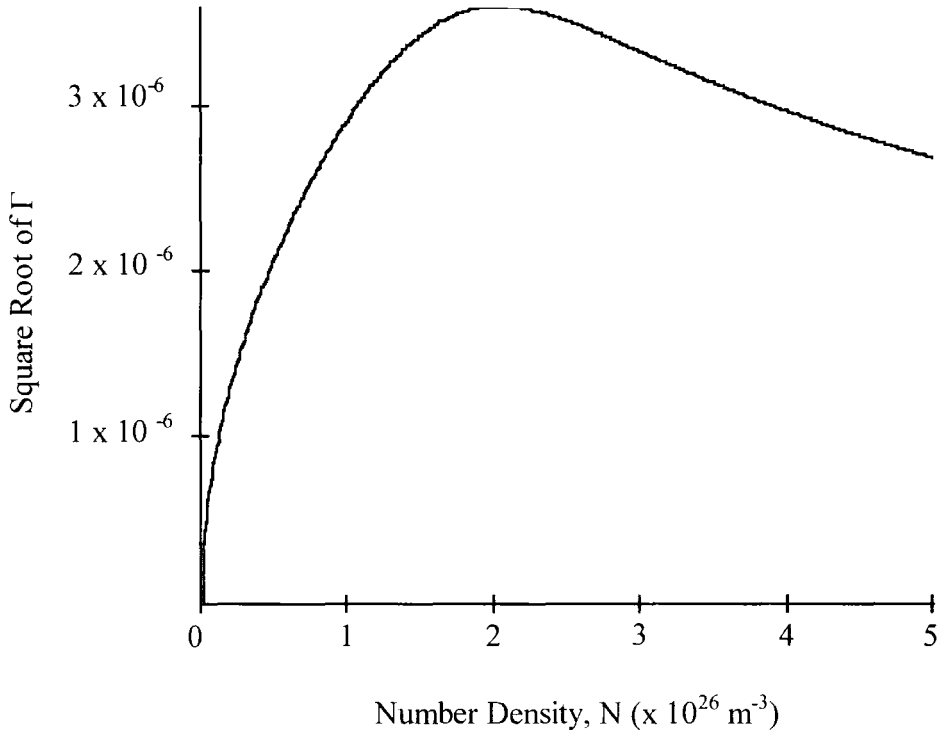

Figure 4.10: Plot of bulk nonlinearity, Γ as a function of number density, N of chromophore with dipole moment, μ = 15D

Figure 4.10 shows that for a molecule with dipole moment of 15 D, the optimum number density is approximately 2 x 10^{26} m^{-3}. If the concentrations in Figure 4.8 are converted to number densities, it can be seen that the deviation from linearity is observed to occur at between 2 and 5 mmol dm^{-3}, corresponding to $N \approx 1.51 \times 10^{24}$ m^{-3} and 3 x 10^{24} m^{-3}. Indeed the highest concentration used in EFISH experiments was about 30 mmol dm^{-3} which corresponds to a number density of 1.0 x ^{25} m^{-3}. At these levels of number density, Figure 4.10 indicates that the bulk nonlinearity should be a linear function of the number density. Thus the EFISH

experiments show a deviation from linearity at far lower concentrations than are predicted from a simple model that includes interacting dipoles subject to van der Waals interactions.

This discrepancy suggests that this model is inappropriate for the description of the molecular systems studied here. The reasons for this are not obvious. This model does not account for factors such as molecular shape or solvent-solute interactions. However, specific molecular interactions within the system, hydrogen bonding for example, are likely to increase the separation distances of the molecules and thus decrease the forces between them. Another factor not accounted for in this model is the fact that the local environment of associated molecules may be significantly different to that of a single molecule in a solvent. The reaction fields established when two molecules are brought closer together may strongly effect the electron distribution of the two molecules. Moreover, the model implicitly assumes a spherical geometry for the molecules. The approximations are not appropriate for real chromophores characterised by, for example, prolate ellipsoidal shapes. Dalton *et al* have shown that this more complicated treatment requires numerical methods to calculate full rotational matrixes and complex three-dimensional minimum energy surfaces [61]. Nevertheless, their work has shown that when this numerical analysis is applied, the optimum number density is indeed shifted to lower concentrations. The discrepancy in the data for the MORPIP molecule compared to this model suggests that the same prolate ellipsoidal molecular geometry may be more appropriate than the spherical shape assumed in the basic van der Waals formalism in Equation 4.11.

4.5 Optical Spectroscopy

The implications of this EFISH data are the presence of strong intermolecular interactions. Such interactions occur in luminescent polymers and their effect on photoluminescence can often be used as a tool for investigation of aggregates [62, 63]. For this reason, advantage was taken of the fluorescence property of the TCNQ adducts and this technique used to investigate the aggregation properties.

Absorption and photoluminescent spectra were taken to investigate the properties the molecule MORPIP in three solvents of differing polarities. Spectra of the molecules in solution exhibit a solvatochromic absorption band that is ascribed to the main intramolecular electronic excitation from the ground state to the excited state. For the highest concentration absorption measurements, very short path length cells were used. Each of the three solvents, chloroform ($\varepsilon = 4.806$), acetonitrile ($\varepsilon = 35.94$) and 1,1,2,2-tetrachloroethane ($\varepsilon = 8.20$) will be discussed separately in the following sections.

4.5.1 Measurements in Chloroform

Figure 4.11 shows the absorption spectra of molecule **2**, MORPIP, in the solvent chloroform at varying concentrations. At lower concentrations the absorption follows the normal linear relationship of the Beer-Lambert law [60] as shown by Figure 4.12.

$$A = \varepsilon C \ell$$

Equation 4.12

Where A is the absorbance, C is the concentration (mol dm^{-3}), ε is the molar extinction coefficient and l is the path length of solution.

At more concentrated solutions of MORPIP in chloroform, the absorption peak changes shape and an additional band can be observed in the blue edge of the spectra as shown in Figure 4.11. This new band is attributed to the presence of a new absorbing species present only in higher concentrations. This new band could be due to a transition within a physical aggregate. The term physical aggregate or physical dimer is used to describe the situation in which two (dimer) or more (aggregate) identical molecules are close together in a special spatial arrangement than other like molecules but do not form a chemical bond between themselves. These physical dimers often have different optical properties relative to the monomer.

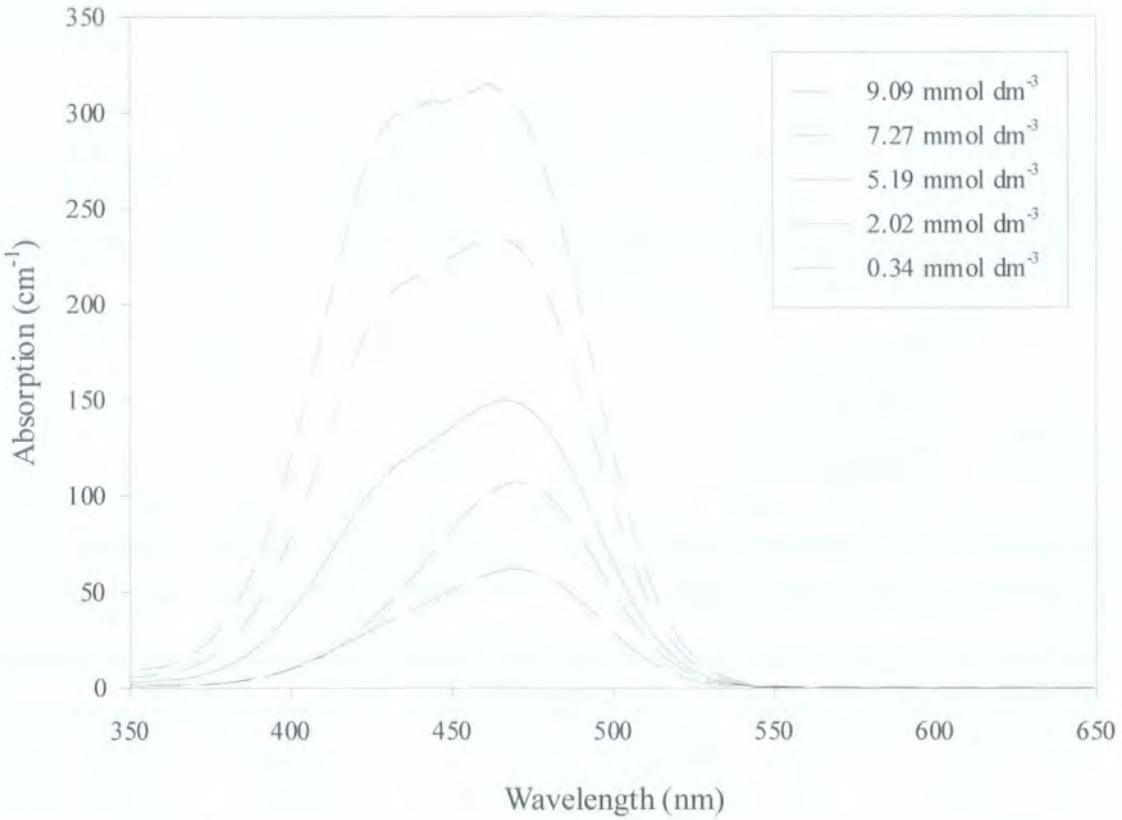

Figure 4.11: Absorption spectra of MORPIP in Chloroform solution as a function of concentration

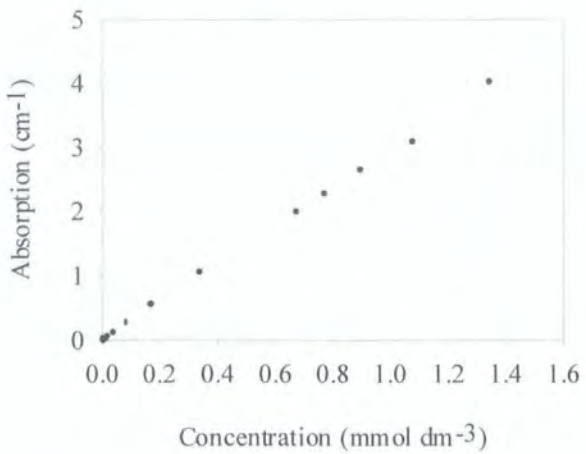

Figure 4.12: Peak absorption of MORPIP in chloroform at dilute concentrations

There is also the appearance of a shoulder in the concentration-dependent absorption spectra for molecule **1**, MORPYROL for low polarity solvents such as chloroform, as shown in Figure 4.13. Once again a distinctly hypsochromically shifted band can be seen occurring even in dilute solutions. The effect is more pronounced than in the case

of MORPIP and occurs at lower concentrations. Similar blue shifted absorption bands have also recently been attributed to the formation of physical dimer aggregates in merocyanine dyes [64].

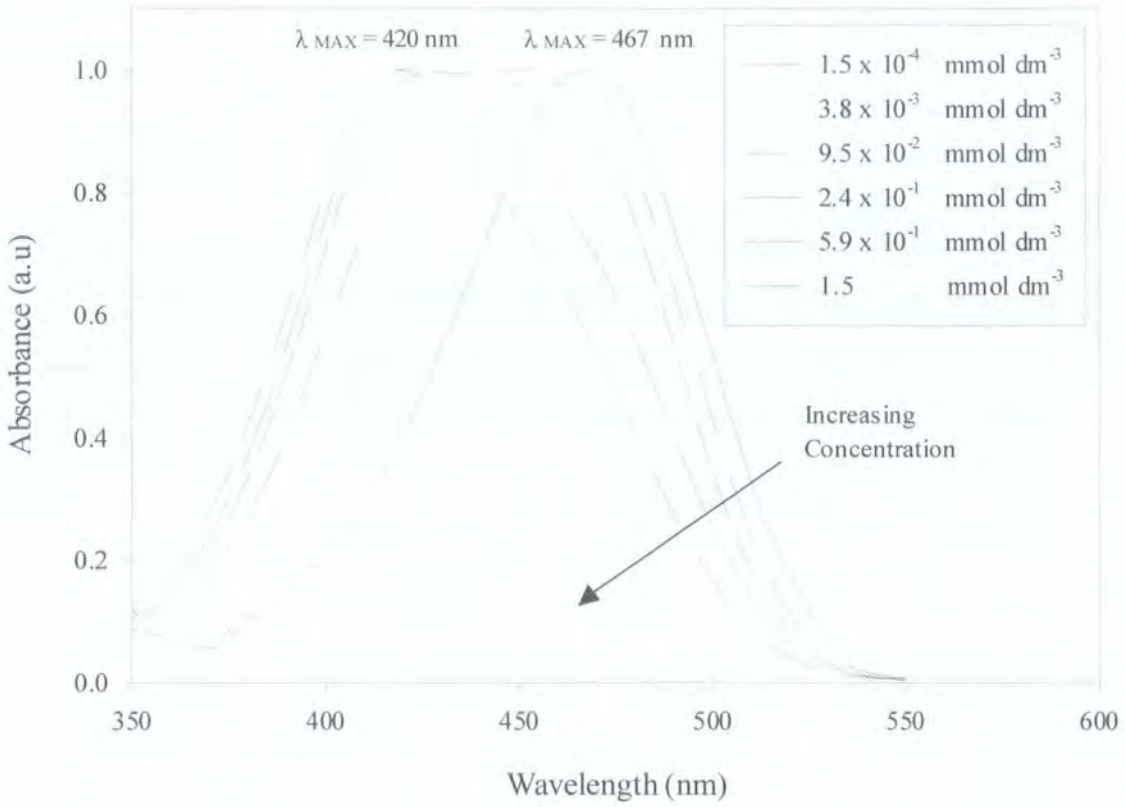

Figure 4.13: Absorption of MORPYROL in chloroform as a function of concentration

Solution photoluminescence spectra of the standard molecule MORPIP (compound **2**) in various solvents were taken as a function of concentration to investigate the aggregation properties of these molecules.

In the range of the concentrations where the new absorption band appears it was also important to probe the luminescence properties of the system, and in order to achieve this the excitation wavelength was chosen carefully. Namely the excitation wavelength was chosen to be slightly in the tail of the absorption (λ_{ex} = 500 nm) such that selective excitation in one absorption band could be achieved. Figure 4.14 shows the PL spectra of MORPIP in chloroform as a function of the concentration.

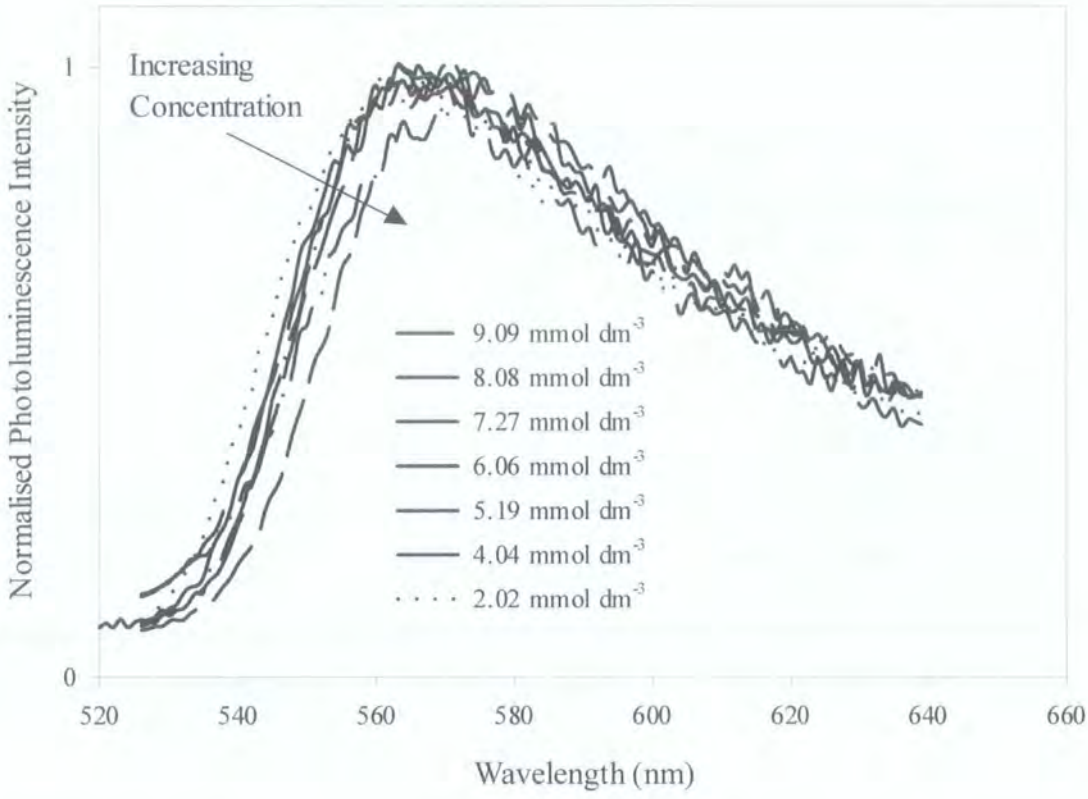

Figure 4.14: Normalised photoluminescent spectra of MORPIP in chloroform as a function of concentration. $\lambda_{ex} = 500$ nm

The peak of the PL spectra occurs at 560 nm and there is a small red shift as the concentration is increased. However it should be noted that the peak absorption wavelength occurs at $\lambda_{max} = 470$ nm. With high concentrations, the absorption at 520 - 540 nm becomes significant and some re-absorption of the photoluminescence will occur. This red shift is therefore characteristic of the absorption distorting the solution PL spectra. No change was observed in the PL spectra when the excitation wavelength was moved further into the tail of the absorption band. This result indicates that only one luminescent species was excited within the solution.

Thus combining the absorption with the PL data may suggest the presence of a new aggregated species at higher concentration whose fluorescence is quenched. However, in the more concentrated solutions the excitation wavelength would ideally have been around 420 nm, in an attempt to exclusively excite the new absorbing species. In fact, the optical density (OD) at these wavelengths and concentrations was too high for undistorted spectra to be obtained and shorter path-length cells were unavailable.

Nevertheless, even though direct excitation is not possible, it is unlikely that the aggregate fluorescence would not be detected when the excitation wavelength was near the peak absorption band, given the proximity of the aggregate band to the monomer absorption band. Thus it might be expected that some change would occur in the PL spectra when exciting at 500 nm because this excitation wavelength would be expected to contain some of the "tail" of the absorption of the aggregate, particularly at higher concentrations. The lack of any change in the PL may be an indication of fluorescence-quenched aggregates. Future experiments could be performed using very short path length cells in an attempt to excite into the second absorption band and fully investigate this new species.

Photoluminescence excitation experiments were attempted on these high concentration solutions. Once again the concentrations that show new absorbing species exhibit an OD that is too large for undistorted results to be obtained.

4.5.2 Measurements in Acetonitrile

Absorption spectra and photoluminescence experiments were also carried out on solutions of MORPIP in acetonitrile. This is a more polar solvent and allows the investigation of the impact of the solvent polarity on the molecular interactions. The absorption spectra as a function of concentration are shown in Figure 4.15. The absorption band remains a single smooth peak over a range of concentrations that exhibited the shoulder in chloroform. The linear relation of Beer Lambert, Equation 4.12, is also obeyed as shown by the inset in Figure 4.15.

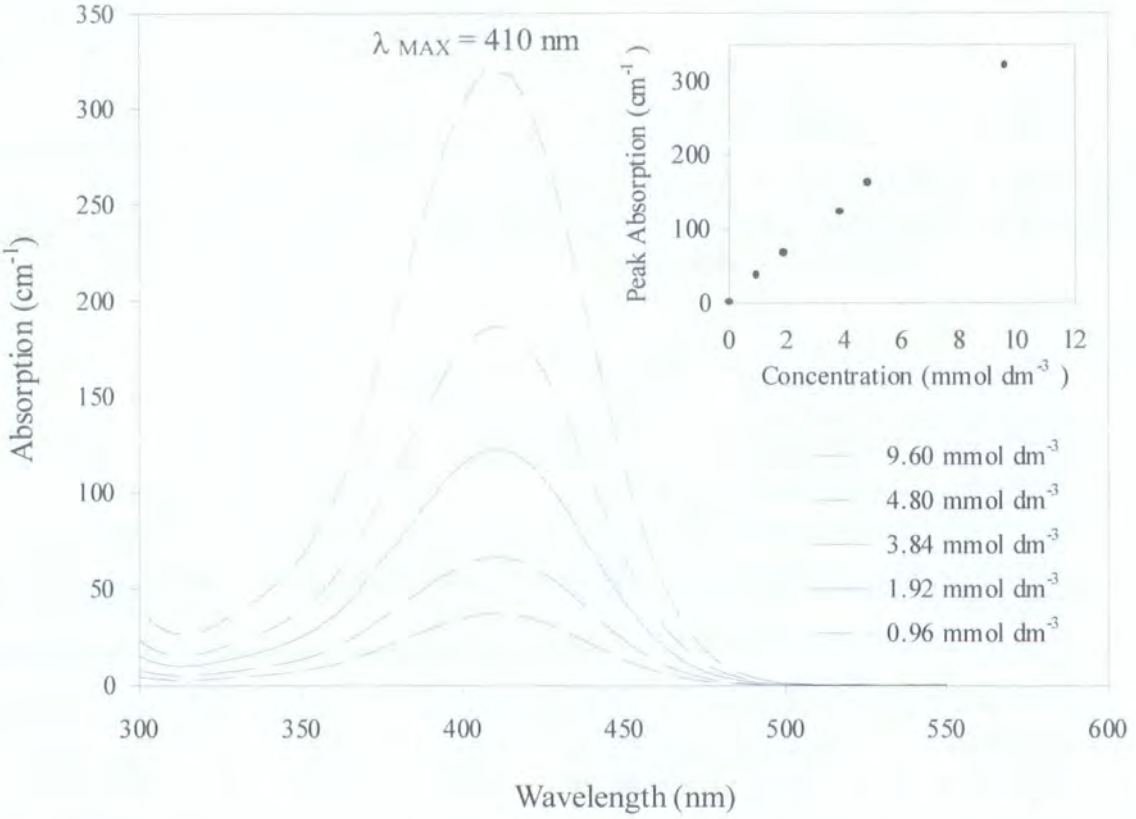

Figure 4.15: Absorption spectra of MORPIP in acetonitrile as a function of concentration

Photoluminescence spectra were also measured and are shown in Figure 4.16. Care was taken to use solutions where the OD of the peak absorption was below 0.3. At higher concentrations, and hence higher OD, there was a deviation from a linear relationship between the intensity and the absorption. This suggests quenching in the PL spectra but the peak shape did not change.

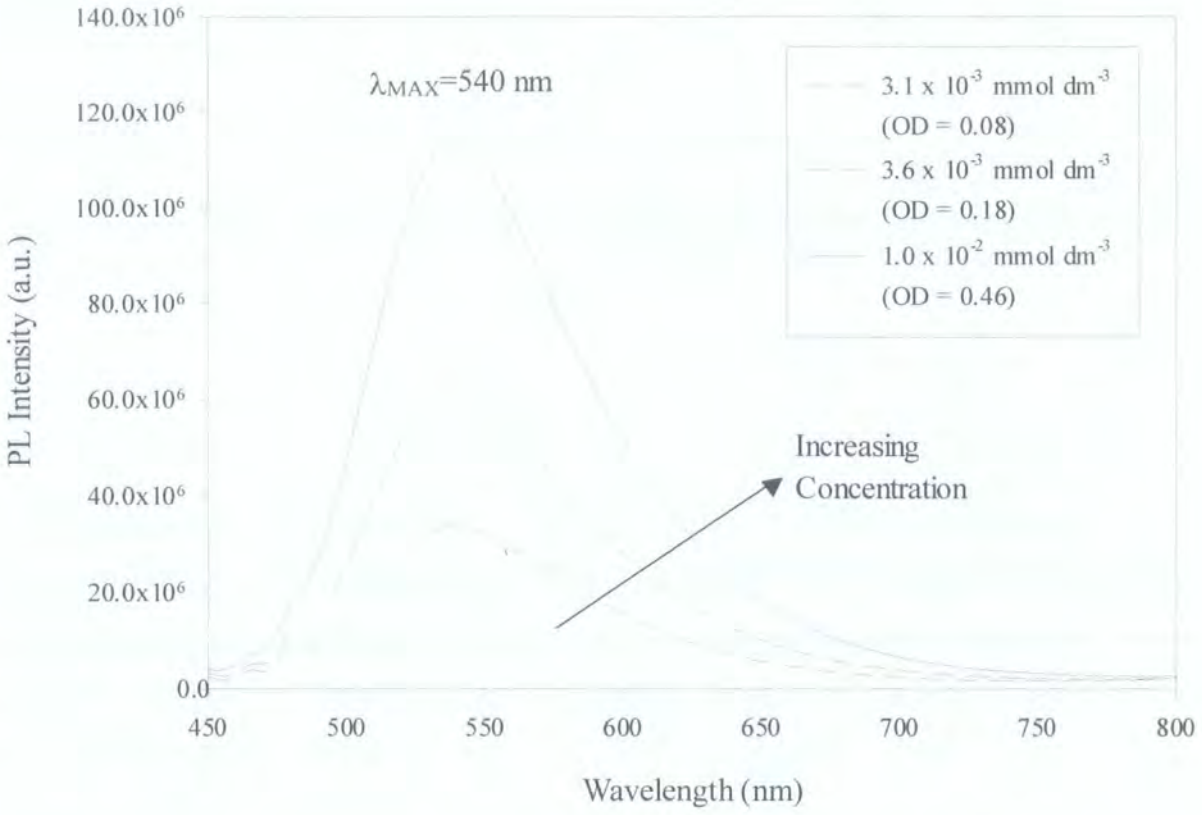

Figure 4.16: Photoluminescence spectra of MORPIP in acetonitrile solution as a function of concentration, λex = 410 nm (absorption peak)

Furthermore, the Stokes shift for MORPIP in acetonitrile was calculated to be $\Delta E = 0.66$ eV and this value did not change with increasing concentration.

Photoluminescence excitation (PLE) experiments were also carried out on the most concentrated solution (0.01 mmol dm^{-3}) that could be used in the luminescent experiments. In addition, the transmission spectra, T, were approximated from the absorption spectra and the plot of (1 - T) and the PLE spectra are shown in Figure 4.17. According to the Beer Lambert law, the PLE spectra should scale linearly with the (1 - T) spectra and the spectra should follow each other closely if the sample solution is homogenous. Figure 4.17 shows that the spectra follow each other, which suggests a homogenous solution containing only one absorbing and fluorescing species.

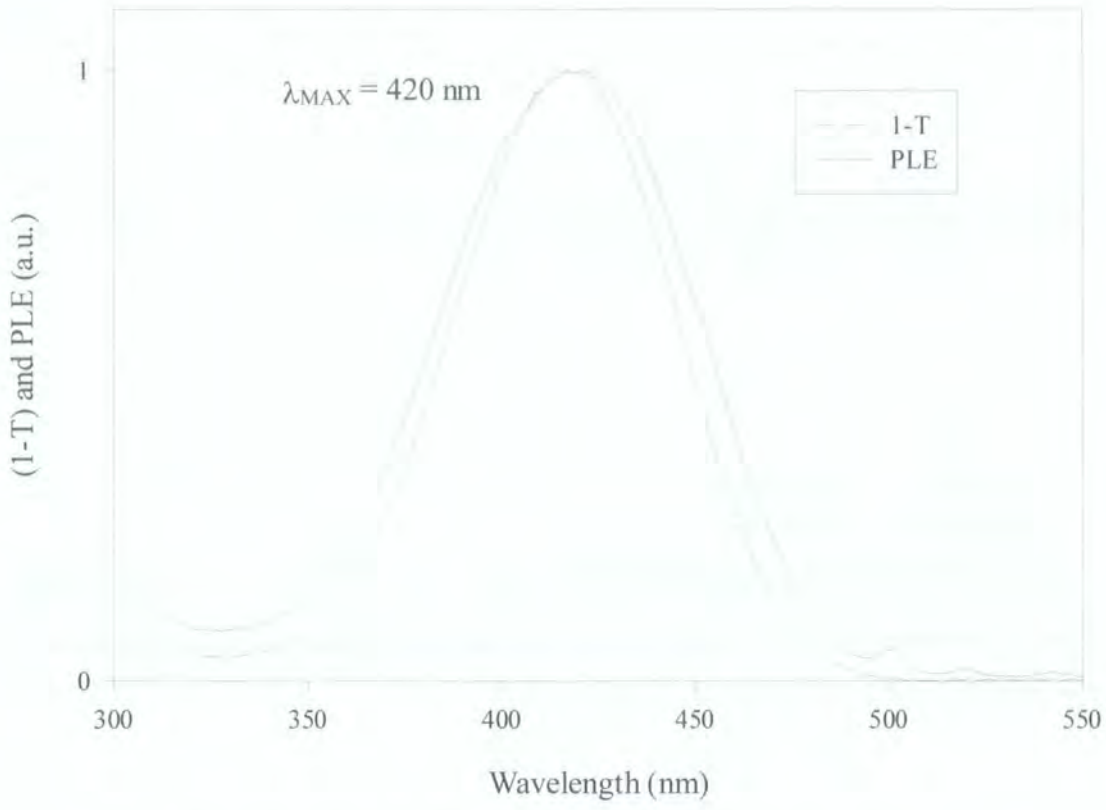

Figure 4.17: PLE and (1-T) spectra for MORPIP in acetonitrile solution, PLE detected at 590 nm, c = 0.01 mmol dm^{-3}

4.5.3 Measurements in Tetrachloroethane (TCE)

Absorption and PL measurements were also made in the solvent tetrachloroethane (TCE). This solvent has a polarity between that of acetonitrile and chloroform. TCE was used as the solvent for spin casting of MORPIP doped polycarbonate thin films and hence investigations of MORPIP in TCE are particularly relevant and were also performed.

Figure 4.18 shows the absorption spectra of MORPIP in TCE as a function of concentration. The spectra are broader than those taken in acetonitrile and there is a long tail that is finite even at wavelengths far away from the peak absorption. This tail is possibly due to light scattering from aggregates or other inhomogenieties in the solutions. A second band is observed at 310 nm that has not been shown in Figure 4.18, which is thought to be attributable to higher order excited states of MORPIP. In other solvents this band is thought to occur at wavelengths shorter than 300 nm and cannot be quantified due to the limited range of the spectrometer and the cells

available. As it has not been considered for any other materials in this study, it has been omitted from the plot.

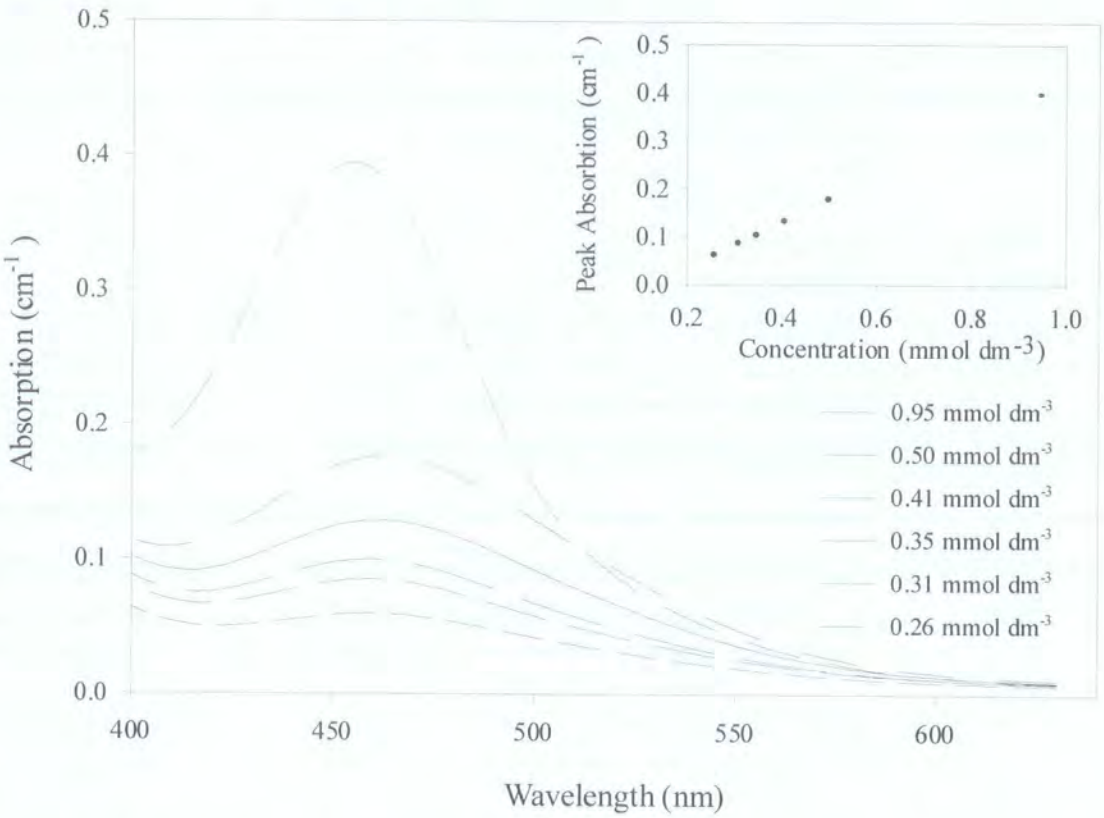

Figure 4.18: Absorption of MORPIP in Tetrachloroethance (TCE) as a function of concentration

PL experiments were carried out as a function of concentration. The spectra have been normalised to unity for clarity and are shown in Figure 4.19. At low concentrations, the PL peak occurs at 627 nm. As the concentration is increased, a distinct blue-shifted new band appears in the original PL spectra. This band increases in intensity with increasing concentrations and finally becomes the dominant PL peak at 547 nm. This suggests the presence of new species at high concentrations that have fluorescence at different wavelengths. These new species are likely to be physical dimers or higher order aggregates.

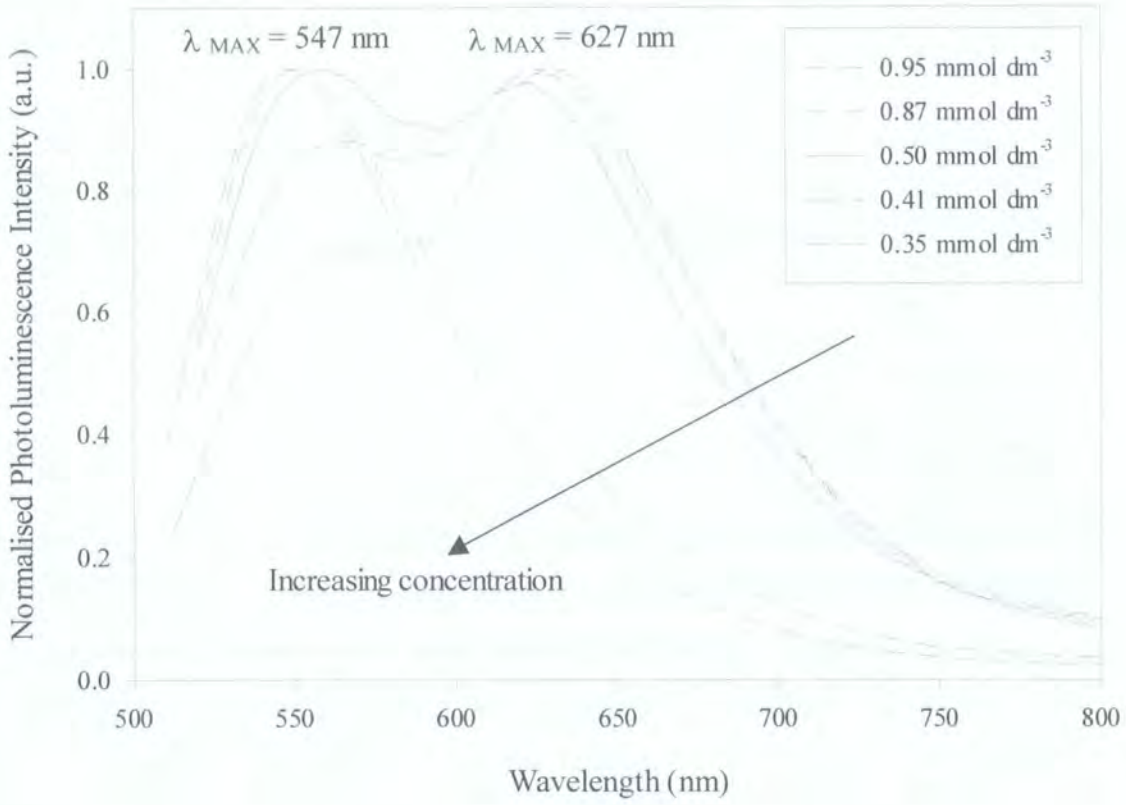

Figure 4.19: Normalised photoluminescence spectra of MORPIP in tetrachloroethane (TCE) solution as a function of concentration, λex = 500 nm

In addition to varying the concentration, the PL spectra were taken as a function of excitation wavelength and the results are shown in Figure 4.20. When the solution was excited in the peak of the absorption band (i.e. at 460 nm) the PL peak occurs at 547 nm. When the solution was excited at longer wavelengths into the tail of the absorption, a second band is seen to arise at the expense of the original band. This second band in the PL spectra has a peak at 642 nm. This case is quite unlike solutions of MORPIP in acetonitrile or chloroform where no effect was observed. These data show that at the higher concentrations there are two distinctly different fluorescing species. In other words, the existence of a second band at 642 nm suggests there is more than one luminescent species present in the solution.

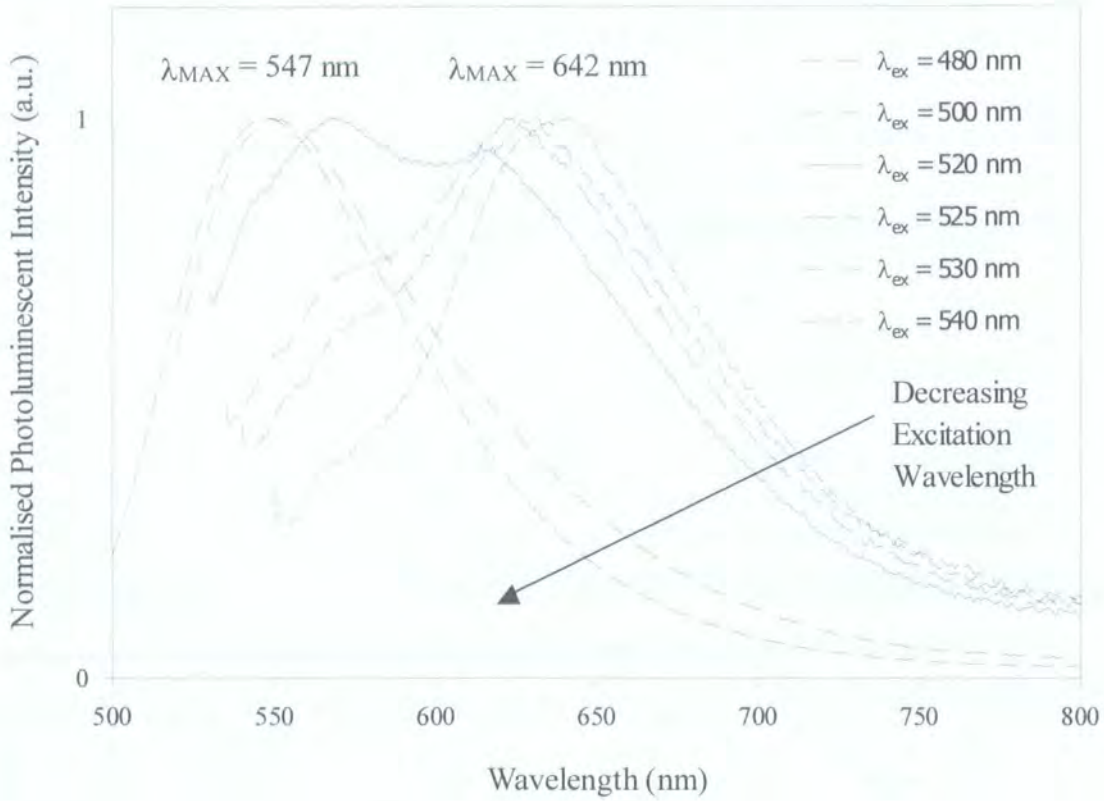

Figure 4.20: Normalised photoluminescent spectra for MORPIP in Tetrachlroethane solution as a function of excitation wavelength, concentration = 0.87 mmol dm^{-3}

The transmission (1-T) spectra were approximated from the absorption spectra and compared to the photoluminescent excitation (PLE) spectra. The results, shown in Figure 4.21, show the PLE spectra are slightly red shifted compared to the (1-T) spectra. In addition, the PLE spectra show a long red tail unlike the (1-T) spectra. Thus, unlike the case of MORPIP in acetonitrile, the two spectra do not show a close correlation as would be expected for a homogenous system. This strongly suggests the presence of aggregates in the solution.

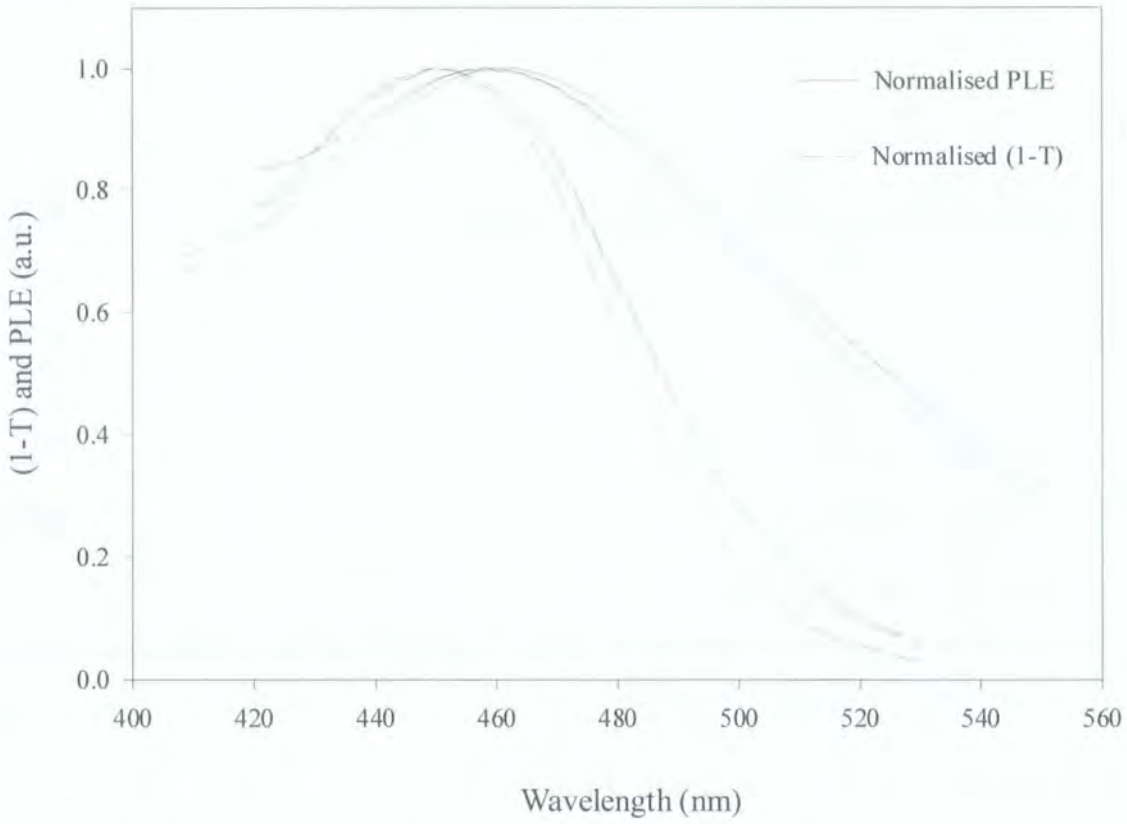

Figure 4.21: PLE and (1-T) spectra for MORPIP in tetrachloroethane solution, PLE detected at 550 nm, c = 0.42, 0.35 and 0.26 mmol dm^{-3}

4.5.4 Discussion

PL and absorption spectra were studied as a function of concentration in the three different solvents to investigate the different solvent effects. It was observed that when MORPIP is dissolved in solvents of different polarity, strong solvatochromic effects were observed in the absorption and PL spectra.

At lower concentrations, the absorption follows the Beer-Lambert law for all the solvents tested. At higher levels of MORPIP concentration in chloroform (ε = 4.806), the peak changes shape and a shoulder appears in the blue edge of the absorption band as shown in Figure 4.13. However, this effect is not observed in acetonitrile (ε = 35.94), as demonstrated in Figure 4.15. Absorption experiments were also performed with the solvent that was used in the preparation of films, namely TCE, (ε = 8.20). When dissolved in TCE, the absorption spectrum, shown in Figure 4.18, is broad compared to the other solvents with a peak wavelength at around 458 nm.

When these data are combined with the PL results some interesting trends may be seen. When MORPIP is dissolved in chloroform, there is no change in the PL spectra as the concentration is increased and in addition, there is no significant effect when excitation wavelength is changed. Since a blue shoulder appears in the absorption over the same concentration range (0.34 - 9.09 mmol dm^{-3}), it may be concluded that a new species is present whose fluorescence properties, although not directly probed, are likely to be quenched. The concentration dependent EFISH measurements indicate a deviation from linearity between 2 and 5 mmol dm^{-3} which is in exact agreement with the appearance of a new species in the absorption spectra. The nature of this new species is likely to be an aggregated form of the molecule MORPIP. Since the presence of this new species correlates with the reduction in signal of the EFISH data, it might be suggested that the aggregate either has a smaller β value than the single molecule or that the symmetry of the aggregate reduces the β of the aggregated system to zero.

An anomalous frequency dependence of β_0 from EFISH results of MORPIP in chloroform was observed. Other reports suggest that the presence of centrosymmetric chromophore aggregates may be responsible for anomalous dispersion effects in poled guest-host polymer systems [65]. Lundquist and co-workers observed a sharp resonance in the SHG response as a function of frequency near the chromophore absorption maximum for films of DANS in PMMA. It is reasonable to suggest that the irregular frequency dependence of EFISH observed in this study might be due to chromophore aggregates within solution, particularly in light of the new absorbing species present in solution.

Figure 4.19 shows a clear blue shifted band in the photoluminescent spectra of MORPIP in tetrachloroethane (TCE) solution with increasing concentration. This new band may again be attributed to the presence of aggregates within the solution. The aggregates in TCE show fluorescence at a distinctly blue-shifted wavelength.

However, the results are clearly very different when MORPIP is dissolved in acetonitrile. In this case, the absorption obeys the linear Beer Lambert law over the whole concentration range with peak absorption at 410 nm. The PL spectra exhibits one smooth peak with the peak at 540 nm and the PLE spectra follow the (1-T) calculations. These three observations suggest less of a tendency for the formation of aggregates in the concentration range studies (0.96-9.60 mmol dm^{-3}) in this more polar solvent. This may be explained in terms of the solvent interactions with the solute

reducing the likelihood of intermolecular interactions. If the solvent-solute interactions are sufficiently favourable compared to solute-solute interactions, they may dominate over aggregation effects.

4.6 Conclusions

New TCNQ derivatives have been studied by means of EFISH and optical spectroscopy measurements. High experimental hyperpolarisabilities predicted by theoretical calculations were confirmed by means of EFISH measurements in solutions of varying concentrations. When combined with optical spectroscopic data, overwhelming evidence has been collected that these compounds have a strong tendency to form aggregates in moderately dilute solutions. This is in agreement with expected behaviour for highly dipolar, molecules of a predominantly flat geometry. In addition, different β_0 values were obtained from EFISH experiments in different solvents. PL and absorption data showed the presence of new luminescent species at higher concentrations in TCE, a new non-luminescent species in chloroform at higher concentrations and a lack of any new species in acetonitrile at any concentration studied. This evidence strongly suggests that the intermolecular interactions and aggregates are different in different solvent environments.

4.7 References

1. Kanis, D.R., Ratner, M.A., and Marks, T.J., *Design and construction of molecular assemblies with large second order optical nonlinearities. Quantum chemical aspects.* Chemical Reviews, 1994. **1994**(94): p. 195-242.

2. Sheng, Y. and Jiang, Y., *AM1/C1 study of the first order hyperpolarizability for push-pull quinones and push-pull polyenes.* Journal of the Chemical Society, Faraday Transactions, 1998. **94**(13): p. 1823-1828.

3. Kamada, K., Ueda, M., Nagao, H., Tawa, K., Sugino, T., Shmizu, Y., and Ohta, K., *Molecular design for organic nonlinear optics: polarisability and hyperpolarisabilities of furan homologues investigated by ab initio molecular orbital method.* Journal of Physical Chemistry, 2000. **A 104**: p. 4723-4734.

4. Boldt, P., Bourhill, G., Brauchle, C., Jim, Y., Kammler, R., Muller, C., Rase, J., and Wichern, J., *Tricyanoquinodimethane derivatives with extremely large second- order optical nonlinearities.* Chemical Communications, 1996(6): p. 793-795.

5. Lambert, C., Stadler, S., Bourhill, G., and Brauchle, C., *Polarized π-electron systems in a chemically generated electric field: Second-order nonlinear optical properties of ammonium borate zwitterions.* Angewandte Chemie-International Edition in English, 1996. **35**(6): p. 644-646.

6. Bourhill, G., Bredas, J.L., Cheng, L.T., Marder, S.R., Meyers, F., Perry, J.W., and Tiemann, B.G., *Experimental demonstration of the dependence of the 1st hyperpolarizability of donor-acceptor-substituted polyenes on the ground-state polarization and bond-length alternation.* Journal of the American Chemical Society, 1994. **116**(6): p. 2619-2620.

7. Prasad, P.N. and Williams, D., *Introduction to nonlinear optical effects in molecules and polymers.* 1991, New York: Wiley-Interscience. 306.

8. Perry, J.W., Bourhill, G., Marder, S.R., Lu, D., Chen, G., and Goddard, W.A., *Hyperpolarizabilities of push-pull polyenes - experimental results and a new 2-state model.* Abstracts of Papers of the American Chemical Society, 1994. **208**: p. 218-POLY.

9. Marder, S.R., Gorman, C.B., Meyers, F., Perry, J.W., Bourhill, G., Bredas, J.L., and Pierce, B.M., *A unified description of linear and nonlinear polarization in organic polymethine dyes.* Science, 1994. **265**(5172): p. 632-635.

10. Oudar, J.L. and Chemla, D.S., *Hyperpolarisabilities of the nitroanilines and their relations to the excited state dipole moment.* The Journal of Chemical Physics, 1977. **66**(6): p. 2664-2668.

11. Oudar, J.L. and Chemla, D.S., *Theory of second-order optical susceptibilities of benzene substituents.* Optics Communications, 1975. **13**(2): p. 164-168.

12. Meyers, F., Marder, S.R., Pierce, B.M., and Brédas, J.L., *Electric field modulated nonlinear optical properties of donar-acceptor polyenes: sum-over-states investigation of the relationship between molecular polarizabilities (α, β, and γ) and bond length alternation.* Journal of the Chemical Society, 1994. **116**: p. 10703-10714.

13. Singer, K.D., Sohn, J.E., and Lalama, S.J., *Second harmonic generation in poled polymer films.* Applied Physics Letters, 1986. **49**(5): p. 248-250.

14. Burland, D.M., Miller, R.D., and Walsh, C.A., *Second-order nonlinearity in poled-polymer systems.* Chemical Reviews, 1994. **94**(1): p. 31-75.

15. Chemla, D.S. and Zyss, J., *Nonlinear optical properties of organic molecules and crystals.* Quantum Electronics - Principles and Applications, ed. D.S. Chemla and J. Zyss. Vol. 1 and 2. 1987, New York: Academic Press. 482.

16. Blanchard-Desce, M., Alain, V., Midrier, L., Wortmann, R., Lebus, S., Glania, C., Krämer, P., Fort, A., Muller, J., and Barzoukas, M., *Intramolecular charge transfer and enhanced quadratic optical non-linearities in push-pull polyenes.* Journal of Photochemsitry and Photobiology A: Chemistry, 1997. **105**: p. 115-121.

17. Verbiest, T., Houbrechts, S., Kauranen, M., Clays, K., and Persoons, A., *Second-order nonlinear optical materials: recent advances in chromophore design.* Journal of Materials Chemistry, 1997. 7(11): p. 2175-2189.

18. Meyers, F., Marder, S.R., Pierce, B.M., and Brédas, J.L., *Tuning of large second hyperpolarizabilities in organic conjugated compounds.* Chemical Physics Letters, 1994. **228**: p. 171-176.

19. Dalton, L.R., Harper, A.W., and Robinson, B.H., *The role of London forces in defining noncentrosymmetric order of high dipole moment high hyperpolarizability chromophores in electrically poled polymeric thin films.* Proceedings of the National Academy of Sciences of the United States of America, 1997. **94**(10): p. 4842-4847.

20. Harper, A.W., Sun, S., Dalton, L.R., Garner, S.M., Chen, A., Kalluri, S., Steier, W.H., and Robinson, B.H., *Translating microscopic optical nonlinearity into macroscopic optical nonlinearity: the role of chromophore-chromophore electrostatic interactions.* Journal of the Optical Society of America B-Optical Physics, 1998. **15**(1): p. 329-337.

21. Kepler, R.G., Bierstedt, P.E., and Merrifield, R.E., *Electronic conduction and exchange interaction in a new class of conductive organic solids.* Physical Review Letters, 1960. **5**(11): p. 503.

22. Acker, D.S., Harder, R.J., Hertler, W.R., Mahler, W., Melby, L.R., Benson, R.E., and Mochel, W.E., *7,7,8,8-Tetracyanoquinodimethane and its electrically conducting anion-radical derivatives.* Journal of the American Chemical Society, 1960. **85**: p. 6408.

23. Acker, D.S. and Blomstrom, D.C., *Derivatives of 1,4-bismethylene cyclohexane and 1,4-bismethylene cyclohexadiene and processes of preparation*, 1963, E. I. du Pont de Nemours and Company: US.

24. Acker, D.S., Waynesboro, V.A., and Blomstrom, D.C., *Charge-transfer compounds of 7,7,8,8-tetracyano-p-quinodimethan and c-cyano-p-quinodimthans with lewis bases*, 1964, E. I. du Pont de Nemours and Company: US.

25. Acker, D.S. and Hertler, W.R., *Substituted quinodimethanes I. Preparation and chemistry of 7,7,8,8-tetracyanoquinodimethane.* Journal of the American Chemical Soceity, 1962. **84**: p. 3370-3374.

26. Melby, L.R., Harder, R.J., Hertler, W.R., Mahler, W., Benson, R.E., and Mochel, W.E., *Substituted quinodimethanes II. Anion-radical derivatives and complexes of 7,7,8,8-tetracyanoquinodimethane.* Journal of the American Chemical Soceity, 1962. **84**: p. 3374-3387.

27. Hertler, W.R., Harzler, H.D., Acker, D.S., and Benson, R.E., *Substituted quinodimethans. III. Diplacement reactions of 7,7,8,8-tetracyanoquinodimethan.* Journal of the American chemical Society, 1962. **84**: p. 3387-3390.

28. Ravi, M., *A simple method for the estimation of hyperpolarisabilities: Application to diamino substituted dicyanoquinodimethane molecules.* Proceedings of the Indian Academy of Sciences-Chemical Sciences, 1998. **110**(2): p. 133-141.

29. Ravi, M., Szablewski, M., Hackman, N.-A., Cross, G.H., Bloor, D., Goeta, A.E., and Howard, J.A.K., *Crystal structures of amino substituted dicyanoquinodimethanes with potential nonlinear optical applications.* New Journal of Chemistry, 1999. **23**: p. 841-844.

30. Kagawa, Y., Szablewski, M., Ravi, M., Hackman, N.-A., Cross, G.H., Bloor, D., Batsanov, A.S., and Howard, J.A.K., *Polar TCNQ adducts for nonlinear optics.* Nonlinear Optics, 1999. **22**: p. 235-240.

31. Kagawa, Y., *New tetracyanoquinodimethane chromphores, synthesis and physical properties*, in *Department of Physics*. PhD, 1998, University of Durham: Durham. p. 160.

32. Lalama, S.J., Singer, K.D., Garito, A.F., and Desai, K.N., *Exceptional second-order nonlinear optical susceptibilities of quinoid systems.* Applied Physics Letters, 1981. **39**(12): p. 940-942.

33. Metzger, R.M., Heimer, N.E., and Ashwell, G.J., *Crystal and molecular structure and properties of picolyltricyanoquindimethan, the zwitterionic donor-pi-acceptor adduct between $Li^{+}TCNQ^{-}$ and 1,2,-dimethylpyridinium iodide.* Molecular Crystals and Liquid Crystals, 1984. **107**((1-2)): p. 133-149.

34. Szablewski, M., Thomas, P.R., Thornton, A., Bloor, D., Cross, G.H., Cole, J.M., Howard, J.A.K., Malagoli, M., Meyers, F., Bredas, J.-L., Wenseleers, W., and Goovaerts, E., *Highly dipolar, optically nonlinear adducts of tetracyano-p-*

quinodimethane: synthesis, physical characterisation and theoretical aspects. Journal of the American Chemical Society, 1997. **119**(13): p. 3144-3154.

35. Szablewski, M., *Novel reactions of TCNQ: formation of zwitterions for nonlinear optics by reactions with enamines.* The Journal of Organic Chemistry, 1994. **59**: p. 954-956.

36. Ravi, M., Rao, D.N., Cohen, S., Agranat, I., and Radhakrishnan, T.P., *Push-pull quinoid compounds: Enhanced powder SHG utilizing the effect of chiral centres on the dipole alignment.* Chemical Materials, 1997. **9**: p. 830-837.

37. Ashwell, G.J., Dawnay, E.J.C., Kuczynski, A.P., Szableweski, M., Sandy, I.M., Bryce, M.R., Grainger, A.M., and Hasan, M., *Langmuir-Blodgett alignment of zwitterionic optically non-linear D-π-A materials.* Journal of the Chemical Society of Faraday Transactions, 1990. **68**(7): p. 1117-1121.

38. Cross, G.H., Healy, D., Szablewski, M., Bloor, D., Malagoli, M., Kogej, T., Beljonne, D., and Bredas, J.L., *Highly polar chromophores in poled polymer films characterised by second harmonic generation.* Chemical Physics Letters, 1997. **268**(1-2): p. 36-42.

39. Ren, Y., Szablewski, M., and Cross, G.H., *Waveguide photodegradation of nonlinear optical organic chromophores in polymeric films.* Applied Optics, 2000. **39**(15): p. 2499-2506.

40. Ham, S.K., Choi, S.H., Lee, B.H., and Song, K., *Synthesis of nonlinear optical polycarbonate for optical device applications.* Polymer-Korea, 1997. **21**(2): p. 201-207.

41. Szablewski, M., Ravi, M., Cole, J.M., Teat, S.J., and Maclean, E.J., Unpublished.

42. Ravi, M., *Optical second harmonic generation studies on a new class of molecular materials: diaminodicyanoquinodimethanes*, in *School of Chemistry.* PhD, 1997, University of Hyderabad: Hyderabad. p. 216.

43. Gangopadhyay, P., Ravi, M., and radhakrishnan, *Hyperpolarisability - molecular twist correlation in diaminodicyanoquinodimethanes.* Indian journal of chemistry, 2000. **39A**: p. 106-113.

44. Masutani, A., *Guest-host effect of dyes in polymer dispersed liquid crystals*, in *Physics*. PhD, 2001, University of Durham: Durham. p. 100.

45. Thomas, P.R., *The molecular properties of zwitterionic, non-linear optical molecules and their evolution and their evolution with molecular environment*, in *Department of Physics*. Ph.D, 1998, University of Durham: Durham. p. 235.

46. Guggenheim, E.A., *A proposed simplification in the procedure for computing electric dipole moments.* Transactions of the Faraday Society, 1949. **45**: p. 714-720.

47. MOPAC, *CS MOPAC PRO: Semi-empirical computation*, 1993-1997, Fujitsu Limited.

48. Riddick, J.A., Bunger, W.B., and Sakano, T.K., *Organic Solvents Physical Properties and methods of purification.* Techniques of Chemistry Volume II. 1986, New York: Wiley-Interscience. 1325.

49. Hackman, N.A. *Alignment and aggregation studies of highly dipolar TCNQ adducts in guest-host systems.* in *SPIE, The International Society for Optical Engineering.* 2000. San Diego, USA: SPIE.

50. Ledoux, I. and Zyss, J., *Influence of the molecular environment in solution measurements of the second-order optical susceptibility for urea and derivatives.* Chemical Physics, 1982. **73**: p. 203-213.

51. Kajzar, F., Ledoux, I., and Zyss, J., *Electric-field-induced optical second-harmonic generation in polydiacetylene soluions.* Physical review A, 1987. **36**(5): p. 2210-2219.

52. Bosshard, C.H., Sutter, K., Prêtre, P.H., Hulliger, J., Flörsheimer, M., Kaatz, P., and Günter, P., *Organic nonlinear optical materials.* Advances in nonlinear optics, ed. A.F. Garito and F. Kajzar. Vol. Volume I. 1995, Postfach: Gordon and Breach.

53. Boyd, R.W., *Nonlinear Optics.* 1992, London: Academic Press Inc. 427.

54. Teng, C.C. and Garito, A.F., *Dispersion of the nonlinear second-order optical susceptibility of organic systems.* Physical Review B, 1983. **28**(12): p. 6766-6773.

55. Singer, K.D. and Garito, A.F., *Measurements of molecular second order optical susceptibilities using dc induced second harmonic generation.* Journal of Chemical Physics, 1981. **75**(7): p. 3572-3580.

56. Oudar, J.L., *Optical nonlinearities of conjugated molecules. Stilbene derivatives and highly polar aromatic compounds.* The Journal of Chemical Physics, 1977. **67**(2): p. 446-457.

57. Levine, B.F. and Bethea, C.G., *Molecular hyperpolarisabiliies determined from conjugated and nonconjugated organic liquids.* Applied Physics Letters, 1974. **24**(9): p. 445-447.

58. Levine, B.F. and Bethea, C.G., *Second and third order hyperpolarizabilitlies of organic molecules.* The Journal of Chemical Physics, 1975. **63**(6): p. 2666-2682.

59. Levine, B.F. and Bethea, C.G., *Effects on hyperpolarisabilities of molecular interactions in associating liquid mixtures.* The Journal of Chemical Physics, 1976. **65**(15): p. 2429-2438.

60. Atkins, P.W., *Physical Chemistry.* Fourth ed. 1990, Oxford: Oxford University Press. 992.

61. Dalton, L., Harper, A., Ren, A., Wang, F., Todorova, G., Chen, J., Zhang, C., and Lee, M., *Polymeric electro-optic modulators: From chromophore design to integration with semiconductor very large scale integration electronics and*

silica fiber optics. Industrial & Engineering Chemistry Research, 1999. **38**(1): p. 8-33.

62. Blatchford, J.W., Jessen, S.W., Lin, L.B., Gustafson, T.L., Fu, D.K., Wang, H.L., Swager, T.M., MacDiarmid, A.G., and Epstein, A.J., *Photoluminescence in pyridine-based polymers: Role of aggregates.* Physical Review B-Condensed Matter, 1996. **54**(13): p. 9180-9189.

63. Blatchford, J.W., Gustafson, T.L., Epstein, A.J., VandenBout, D.A., Kerimo, J., Higgins, D.A., Barbara, P.F., Fu, D.K., Swager, T.M., and MacDiarmid, A.G., *Spatially and temporally resolved emission from aggregates in conjugated polymers.* Physical Review B-Condensed Matter, 1996. **54**(6): p. R3683-R3686.

64. Würthner, F. and Yao, S., *Dipolar dye aggregates: a problem for nonlinear optics, but a chance for supramolecular chemistry.* Angewandte Chemie International Edition in English, 2000. **39**(11): p. 1978-1981.

65. Lundquist, P.M., Yitzchaik, S., Marks, T.J., Wong, G.K., DiBella, S., Cohen, R., and Berkovic, G., *Spectral characteristics of second-order optical nonlinearities in poled polymer films containing charged chromophore aggregates.* Physical Review B-Condensed Matter, 1997. **55**(21): p. 14055-14058.

Chapter 5 : Results and Discussion of Macroscopic Properties

5.1 Introduction

In poled polymer films, second order effects such as second harmonic generation (SHG) are generally considered to arise from non-interacting chromophores. The chromophore number density can limit the response of isolated dipolar chromophores in polymer systems because dipolar chromophores tend to form centrosymmetric aggregate species as the number density increases. These centrosymmetric species are forbidden by symmetry from contributing to conventional second order processes [1]. The possible contribution of aggregated chromophore species to poled polymer NLO characteristics has seldom been considered [1-6].

Indeed, the most severe, and unanticipated, problem encountered in fabricating polymeric devices (electro-optic modulators, or frequency modulators for example), is translating the large molecular hyperpolarisability of the organic chromophores into large macroscopic activity in the bulk materials.

This chapter focuses on the bulk results from solid-state measurements. Chromophores were doped into a polymer host in a guest-host system. Thin films of these guest-host systems were prepared by spin coating onto ITO coated glass substrates as described in Chapter 3. Typical concentrations of the guest molecules ranged from 1 wt% to 10 wt% in films approximately 3 μm thick. Samples for refractive index measurements were coated onto silica substrates. For SHG experiments, it was necessary to induce the non-centrosymmetry into the polymer samples and hence the samples were poled using applied DC fields in order to align the dipolar molecules. The poling was carried out using a constant current corona triode, (CCCT). The second order nonlinear optical coefficients of the molecular species were determined by angular second harmonic generation (SHG) measurements. Photoluminescence quantum yield experiments were used to investigate the aggregation properties of the chromophores.

5.2 Material Systems

The guest molecules have been described previously in some detail in Chapter 4. In addition to these new TCNQ adducts, some standard NLO materials were used; Disperse Red 1 (DR1) was used to characterise the CCCT rig and 2 - (N, N, dimethylamino) - 5 - nitroacetanilide (DAN) was used as a comparison for the new materials. The structure of these two guest chromophores may be seen in Figure 5.1. Poly(bisphenol A carbonate), (PC) was chosen as the host polymer. This polymer possesses a chain extended diphenylmethane structure as shown in Figure 5.2.

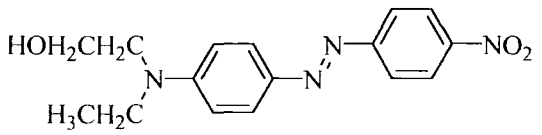

(a)

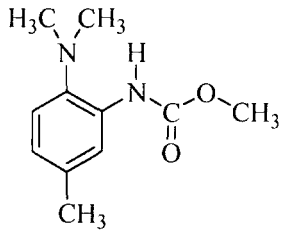

(b)

Figure 5.1: Structures of host chromophores used as standards (a) DR1, (b) DAN

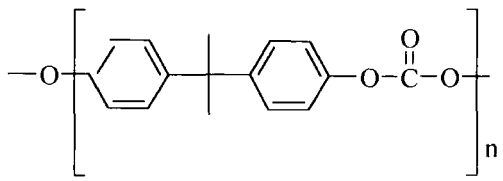

Figure 5.2: Chemical structure of the host polymer, Poly(bisphenol A carbonate), (PC)

It is a common observation that the dopant relaxation is related to the glass transition temperature (T_g) of the system [7]. This polymer has a relatively high T_g of 150 °C. The PC polymer has a high optical transparency (89%) in the visible region and good mechanical properties [8], which has led to applications such as lens coatings and substrates for optical disks. Thin films were prepared using the spin coating technique as described in Chapter 3.

5.2.1 Refractive Index Characterisation of Films

Refractive index measurements were carried out using the prism coupling technique as described in Chapter 3. Measurements were made at four wavelengths (633 nm, 780 nm, 940 nm and 1300 nm) on pure polycarbonate and MORPIP doped polycarbonate films. The results for transverse electric, TE, and transverse magnetic, TM, polarisations are displayed in the form of dispersion curves in Figure 5.3 and Figure 5.4, respectively.

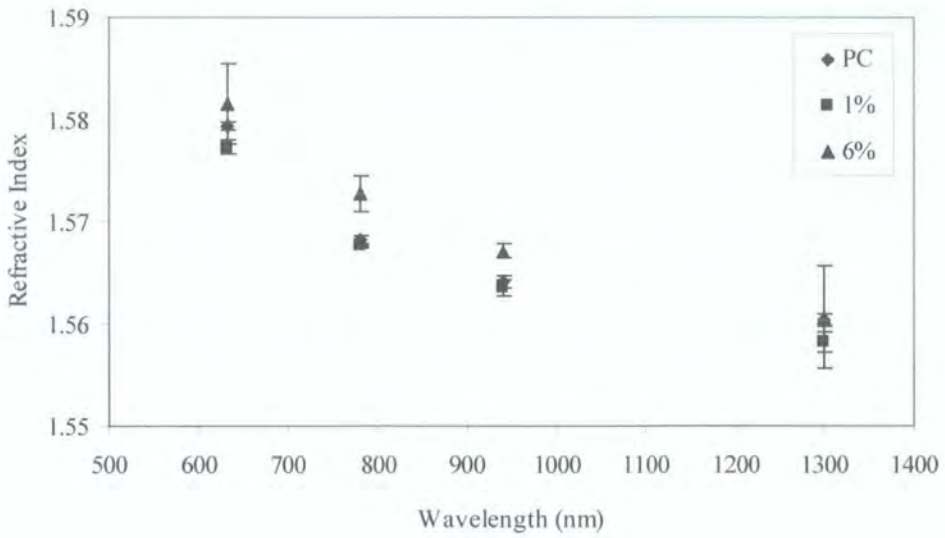

Figure 5.3: TM mode dispersion graph of polycarbonate films and MORPIP doped polycarbonate films.

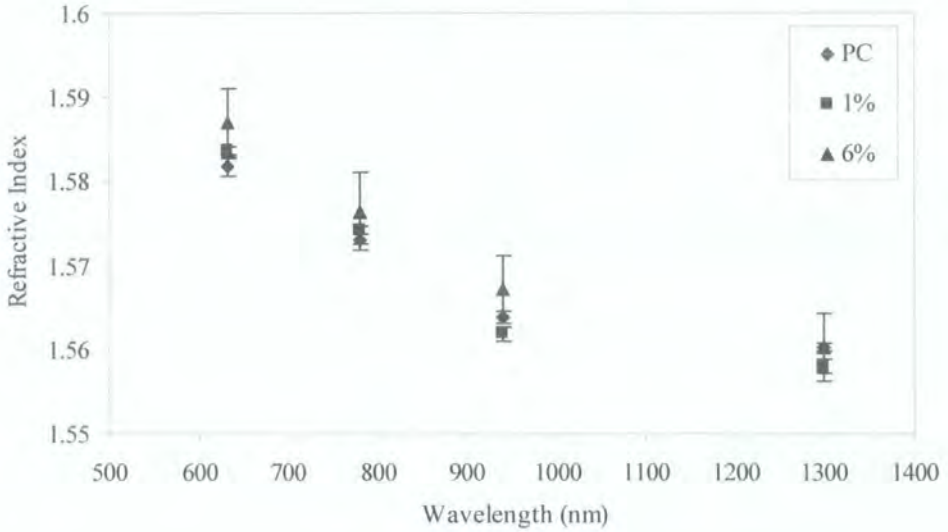

Figure 5.4: TE mode dispersion graph of polycarbonate films and MORPIP doped polycarbonate films.

The dispersion curves follow the normal dispersion for a dielectric medium. The results were used to determine the refractive indices at 1064 nm and 532 nm. These two wavelengths correspond to the fundamental and second harmonic wavelengths used in SHG experiments and therefore accurate determination of the refractive indices is necessary to obtain good fits to angular second harmonic data.

When a material has an absorption band within the visible spectrum, the minima and maxima for the refractive index dispersion curve occur at frequencies closely adjacent to the absorption band.

As absorption band frequencies are approached, the Sellmeier equation describes the relationship between the refractive index, $n(\omega)$, and the frequency, $\omega = 2\pi c/\lambda$, which in the case of one dominant oscillator is given by:

$$n^2(\omega) - 1 = A + \frac{\omega_p^2 \gamma_0}{(\omega_{eg}^2 - \omega^2)}$$

Equation 5.1

Where ω_p is the plasma frequency, γ_0 is a local field parameter, ω_{eg} is the oscillator frequency and A is a constant containing contributions of other excitations. This formula was sufficient to describe the dispersion of the materials since the measured

indices were adequately removed from the absorbing region so that no extra damping term was required. A typical fit to the refractive index data is shown in Figure 5.5 and the resulting Sellmeier parameters are listed in Table 5.1. The values of refractive index at 1064 nm and 532 nm were the same within errors for TE and TM polarisations. The values quoted in Table 5.1 are used in the SHG measurements.

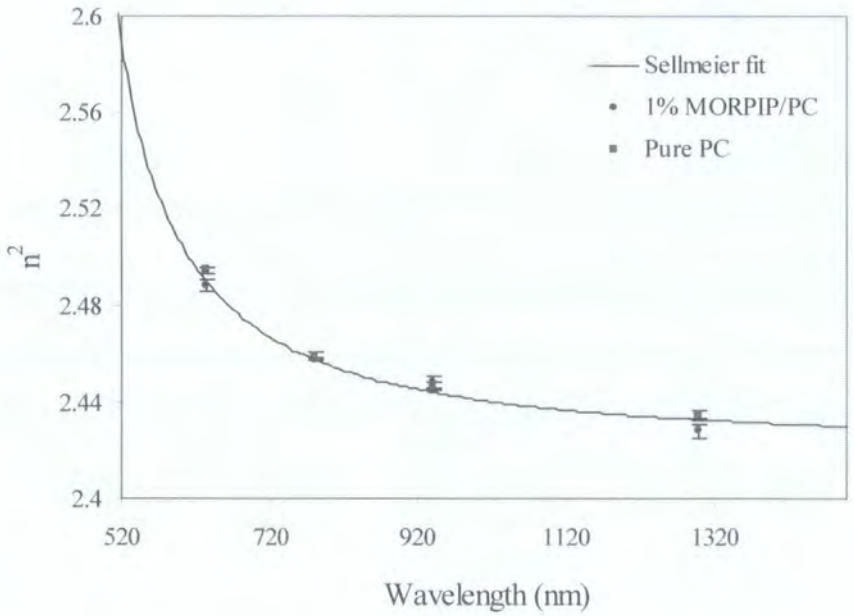

Figure 5.5: Sellmeier equation used to fit to refractive index dispersion

Sellmeier Parameters	
λ_{eg} (nm)	426
ω_{eg} (10^{15} s^{-1})	4.42
$\gamma_0\omega_p^2$ (10^{30} s^{-1})	1.60
A	1.34
n (1064 nm)	1.56 ± 0.01
n (532 nm)	1.60 ± 0.02

Table 5.1: Sellmeier parameters and refractive index

5.3 Electric Field Poling

As discussed in Chapter 2, a material must not possess a centre of symmetry if it is to exhibit a finite second order susceptibility, $\chi^{(2)}$. Often the active chromophore is dispersed in or chemically attached to polymer chains, either as part of the main chain or as a pendant side group. Such polymer systems are amorphous and do not possess three-dimensional order. To induce the necessary asymmetry into these systems, an electrical poling process must be carried out. The technique of electric field poling consists of heating the sample to near the glass transition temperature of the polymer whilst simultaneously applying a very high DC electric field. The dipolar nature of the chromophores is exploited and the dipole moments align in the direction of the applied field. Then, whilst maintaining the electric field, the sample is cooled to room temperature and the dipolar alignment is locked in.

5.3.1 Introduction

Two types of poling rig were used in the work, a constant current corona triode and an "in-situ" poling rig. The experimental descriptions for both of these set-ups may be found in Chapter 3. Since the constant current corona triode (CCCT) rig was used to obtain quantitative data, (such as d_{33} values) thorough checks of the system were undertaken. Thus this section confirms that the CCCT rig was working to the standard required.

5.3.2 Poling Uniformity

In order to verify that the CCCT rig was working correctly, a sample of a known material, DR1, was doped into poly (bisphenol A carbonate) and poled in the rig. The SHG of this poled sample was then compared to a second sample that had not been poled. The un-poled sample produced no signal whereas the poled sample gave a strong SHG signal that displayed angular dependency. This sample was then used to collect data and calculate a d_{33} value. These results will be discussed in section 5.4.1.

Once confirmation had been achieved that the CCCT was poling the samples, films were checked for homogeneity and uniformity of poling. These measurements were performed as part of a collaboration with Professor Eich's group in Hamburg by Robert Blum *et al.*

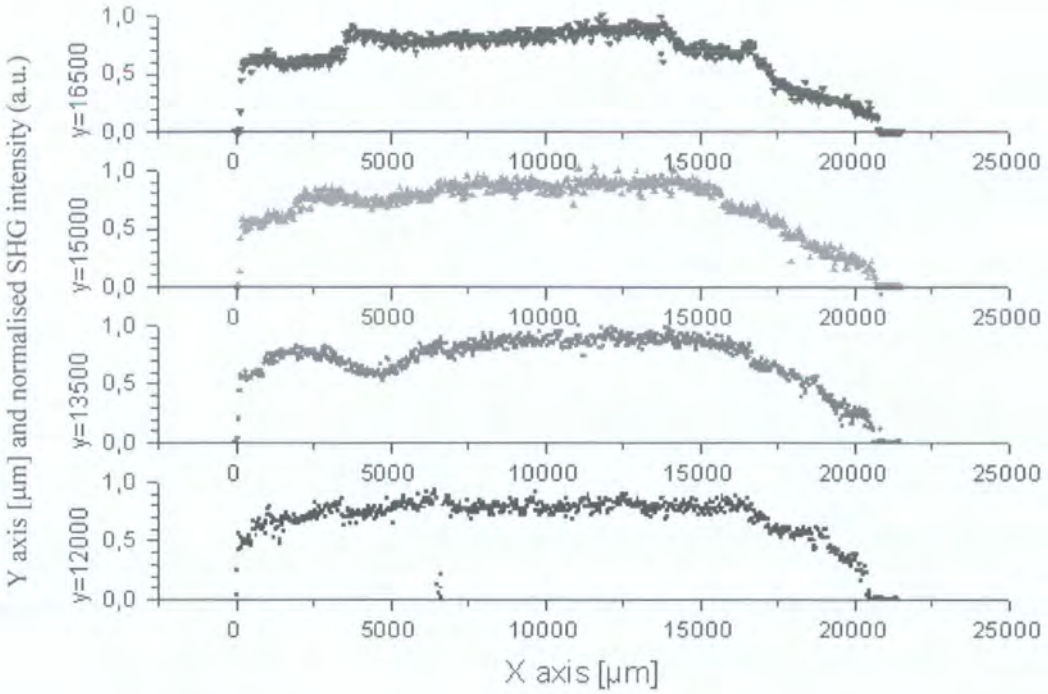

Figure 5.6: SHG spatial line scans across a sample to check poling uniformity

The SHG line scans across the sample surface are shown in Figure 5.6 and indicate that uniform poling is achieved across the centre section of the sample. The poling uniformity of the sample will be affected by factors such as temperature, electric field and thickness uniformities and film inhomogenieties.

As a further check of the field uniformity, a small 8 x 8 mm ITO coated glass square substrate was prepared to which a simple contact was attached. The spatial position of this "test" electrode was varied systematically across the heated stage and the field measured using the grid voltage. The results, shown diagrammatically in Figure 5.7, indicate that there is a uniform field across the whole sample area.

103	99	99
99	99	99
103	100	101

Figure 5.7: Diagram to show spatial variation of the electric field (as measured by the grid high voltage supply, in V) of the CCCT

5.4 System Characterisation

Once it had been established that the CCCT poling rig was working satisfactorily, the whole system was characterised using known standards. For this purpose, samples of known materials were prepared and poled in the CCCT and the SHG measured as a function of angle. The fitting procedure was then applied to obtain d_{33} values for these samples.

5.4.1 Comparison of Experimental with Standard Values

Although it is difficult to compare sets of data from different sources because of differences in the poling details and geometrical set up etc, the validation of the operation of the apparatus prior to the measurement of the new TCNQ derivatives is prudent. To this end, two different systems have been prepared and compared with literature values.

The first system to be studied was that of Disperse Red 1 (DR1) doped into PC films. The 95% pure guest DR1, obtained from Aldrich, was recrystalised from hot absolute alcohol and dried overnight in a vacuum oven at 75 °C. The films were prepared from solutions containing about 10 wt% ($\sim N = 2.23 \times 10^{20}$ cm^{-3}) of guest-host ratio and 10 ml of the solvent cyclohexanone. The mixture was heated and stirred at 70 °C for three hours to ensure that a homogeneous solution was produced. The hot solution was used to prepare spin-coated films on ITO coated glass substrates for use in the CCCT. The films were baked in a vacuum oven at 75 °C overnight. This recipe and procedure was performed in accordance with Wan *et al* [9]. The films were poled in the CCCT at 95 °C. These samples resulted in d_{33} values of 8 ± 1 pmV^{-1} when referenced to quartz

at 0.46 pmV^{-1} (following Wan *et al*). Accounting for a factor of 3.5 difference in the poling fields and linearly scaling d_{33} accordingly, the d_{33} values of 28.0 ± 3.5 $pmV^{-1}$are comparable to d_{33} = 31.6 pmV^{-1} obtained by Wan *et al* [9].

There have been extensive studies on DR1 incorporated into poly(methyl methacrylate), (PMMA), systems. For this reason, a second model system of DR1 doped PMMA was investigated to ensure agreement with literature values. Once again the 95% pure guest DR1, obtained from Aldrich, was recrystalised from hot ethanol solution. The films were spin cast from chlorobenzene solution (1 g of polymer to 6 ml solvent). Poling was carried out at 80 °C and fields of around 65 $V\mu m^{-1}$ were achieved. This poling resulted in d_{33} values of 9.5 ± 0.9 pmV^{-1}. These values are in excellent agreement with the values found elsewhere for films prepared with similar parameters (d_{33} = 9.0 pmV^{-1} [3] and d_{33} = 8.3 pmV^{-1} [4]). Singer *et al* also measured a value of d_{33} = 6.7 pmV^{-1} of DR1 doped PMMA films at a fundamental wavelength of 1.58 μm [5].

Absorption measurements have also been performed by Mortazavi *et al* on corona poled DR1 doped PMMA films [4]. These measurements were used to estimate d_{33} values by scaling with d_{33} values from Hayden and co-workers [3] at the same doping density to obtain d_{33} = 8.3 pmV^{-1}, which is consistent with the results from this work.

5.4.2 Contribution of Pure Polymer

Since this work involves films of composite systems, the total measured susceptibility is simply the sum of the susceptibilities of the polymer and the chromophore. The second-harmonic coefficient is expected to be linear in the number density [5] and does not extrapolate to d_{33} = 0 at zero chromophore concentrations. The nonzero intercept represents the contribution to d_{33} of the host polymer. The chromophores in this work were all doped into PC films and so the contribution from the pure polymer was determined. Films of pure PC were spin coated from tetrachloroethane solutions (1 g of polymer to 6 ml of solvent, spin speed of 2000 rpm for 10 s). These samples were poled at a temperature of 130 °C achieving poling fields of 140 $V\mu m^{-1}$ and SHG results gave d_{33} = 0.05 ± 0.02 pmV^{-1}. This data is in good agreement with similar studies

carried about by Gulotty *et al* [10] who obtained d_{33} values ranging from 0.033 to 0.044 pmV^{-1}.

5.4.3 Contribution of ITO Coating

It has been shown that indium tin oxide (ITO) thin films on glass substrates produce a small second harmonic signal [11]. In order to eliminate the influence of the ITO substrate on the optical second harmonic characterisation of guest/host polymer films, d_{33} values from poled films on substrates of different ITO resistivities were measured. Samples were produced on high (130 Ω /square) and low (12 Ω /square) resistivities. Poling was performed on samples with the same doping levels and under identical conditions. Ghebremichael *et al* [12] have showed that when isotropic PMMA thin films are deposited onto ITO coated surfaces, the resulting SHG intensity is larger than the SHG intensity from either ITO or polymer when measured separately. However, in this case no distinction was observed between the SHG intensities or measured d_{33} values for ITO samples of different resistivities. This is most likely to be a consequence of the ITO layer being negligibly thin compared to the polymer films such that the ITO did not contribute significantly to the SHG signal. Indeed, when blank (i.e. substrates without polymer) ITO substrates were measured, the signal to noise ratio was too low for any meaningful results to be obtained.

5.5 Second Harmonic Generation (SHG) Measurements

Second harmonic generation is very sensitive to molecular orientation. The intensity of the second harmonic generation is dependent, among other factors, on the coherence length, angle of incidence and the direction of the polarisation of the light. At the molecular level, the second harmonic radiation is produced predominantly as a result of the charge transfer through the conjugated pathway along the length of the molecule. Consequently the maximum second harmonic intensity will be obtained when the electric field vector of the incident radiation is parallel to dominant direction of the nonlinearity of the molecule. In the ideal case the poled films are expected to contain chromophores that are aligned with uniaxial symmetry. Thus this section presents data collected from angular scans of second harmonic generation (SHG) from samples poled using the CCCT.

5.5.1 Introduction

For the measurement of the second order susceptibility of the system a Maker fringe-type technique was employed. This technique was first introduced by Maker and co workers in 1962 [13] and was subsequently discussed in detail by Jerphagnon and Kurtz [14]. The fundamental laser beam of angular frequency ω was incident on a nonlinear polymeric film at an angle of θ. Inside the film, the electric field E_ω induces a non-linear polarisation that radiates electromagnetic waves of angular frequency 2ω. As the harmonic wave propagates through a non-linear medium, light is coupled from the fundamental wave to the second harmonic wave, resulting in a build-up of second harmonic intensity. This coupled wave is known as the second harmonic bound wave. The analysis used is presented here as a summary of that introduced by Herman and Hayden [15] who refined the theory of Jerphagnon and Kurtz [14] for thin polymeric films on a substrate. The theory takes into account the absorption of the material, the second harmonic wave reflected from the film-substrate interface and the dispersive nature of the medium. This analysis uses the geometrical arrangement shown in Figure 5.8, and results in the following relation between the observed second harmonic intensity, $I_{2\omega}$, and the fundamental pump intensity, I_ω:

$$\frac{I_{2\omega}}{I_\omega^2} = \left(\frac{128\pi^3}{c}\right)\left(\frac{t_\omega^4 t_{2\omega}^2 t_0^2}{n_2^2 c_2^2}\right)\left(\frac{2\pi L}{\lambda}\right)^2 d_{eff}^2 \exp[-2(\delta_1+\delta_2)]\left(\frac{\sin^2\Psi+\sinh^2\Phi}{\Psi^2+\Phi^2}\right)$$

Equation 5.2

Where:

$$\delta_m = \left(\frac{2\pi L}{\lambda}\right)\frac{n_m \kappa_m}{c_m}$$

Equation 5.3

$$\Psi = \left(\frac{2\pi L}{\lambda}\right)(n_1 c_1 - n_2 c_2)$$

Equation 5.4

$$c_m = \left[1 - \left(\frac{\sin\theta}{n_m}\right)^2\right]^{\frac{1}{2}}$$

Equation 5.5

$$\Phi = \delta_1 - \delta_2$$

Equation 5.6

$$\kappa_m = \frac{\alpha_m}{k_m} = \frac{\alpha_m \lambda_m}{2\pi n_m}$$

Equation 5.7

where L is the film thickness, λ is the fundamental wavelength, α_m is the absorption coefficient, K_m is the extinction coefficient of the film and t_ω, $t_{2\omega}$ and t_0 are the standard Fresnel transmission coefficients at the air-film, film-substrate and substrate-air interface respectively for the appropriate polarisations and frequencies. The subscript m (m = 1 or 2) refers to the value at frequency $m\omega$. Thus by monitoring the SHG signal with respect to the incident angle of the fundamental beam, elements of the second order susceptibility tensor can be evaluated using Equation 5.2 through to Equation 5.7.

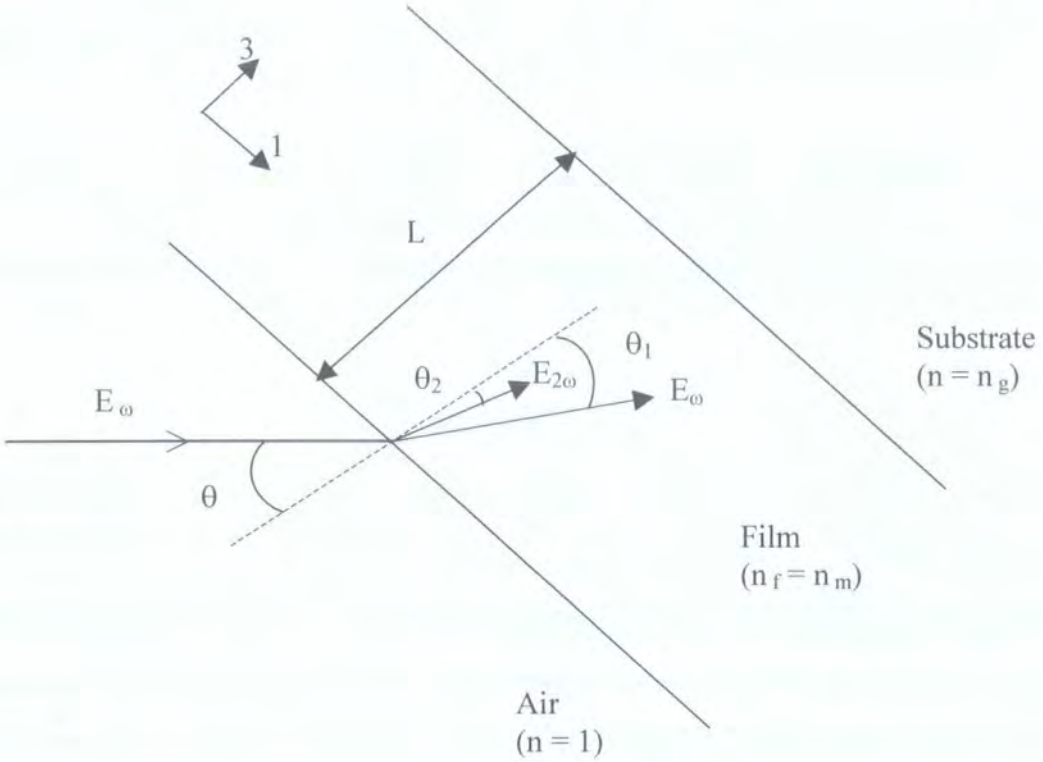

Figure 5.8: Optical geometry used in SHG measurements

The effective second harmonic coefficient of the film, d_{eff}, is dependent on the polarisation plane of the incident optical field and the symmetry of the nonlinear medium. If the incident beam is polarised in the plane of incidence it is said to be *p*-polarised. Similarly, if the incident beam is polarised perpendicular to the plane of incidence, then the light is said to be *s*-polarised.

In the case of *s*-polarised incident light on a poled polymer film, d_{eff} is given by:

$$d_{eff} = d_{31} \sin\theta_2$$

Equation 5.8

If the incident beam is *p*-polarised and there is no in-plane anisotropy, then d_{eff} is given by:

$$d_{eff} = d_{33}\left[R\cos\theta_2 \sin 2\theta_1 + \sin\theta_2\left(R\cos^2\theta_1 + \sin^2\theta_1\right)\right]$$

Equation 5.9

Where R is the ratio d_{31}/d_{33}. For the purpose of these experiments, the second harmonic beam is always *p*-polarised and as such only the t_ω transmission coefficient needs to be adjusted to take into account the polarisation of the incident beam. When Equation 5.9 is substituted into Equation 5.2, the only unknown parameter among the angular dependent terms is R. The value of R is then determined by fitting the angular dependent terms into the second harmonic intensity recorded as a function of rotation angle.

In order that exact values of d_{eff} are calculated, the output second harmonic intensity is compared with the second harmonic of a reference crystal whose nonlinear optical coefficient is known. In this work a quartz wedge was used where d_{11} was taken be 0.3 pmV^{-1} according to recent measurements [16], unless otherwise stated. Therefore, the value of the d_{eff} and hence the d_{33} coefficient may be determined.

In order to analyse the SHG data produced from angular scans a nonlinear regressional analysis program [17] was employed in conjunction with the program shown in Appendix III. A typical set of data and the fitted curve is shown in Figure 5.9. At normal incidence (i.e. 0°), there is no second harmonic intensity because there is no projection of the optical electric field along the d_{33} tensor element.

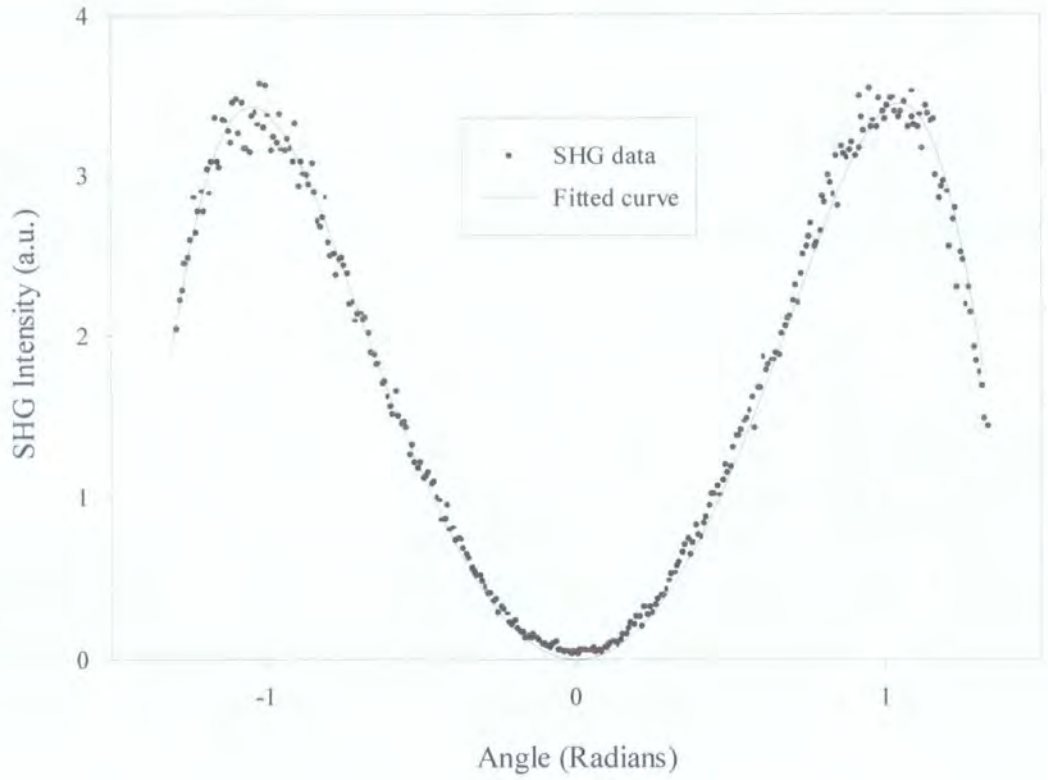

Figure 5.9: Typical curve fit for SHG of a DAN doped polycarbonate film

5.5.2 Results and Comparison with Theoretical Calculations

For each film the poling temperature was below its T_g, and the ability to successfully align the chromophores was probably aided by molecular backbone motion occurring well below T_g [18]. Comparison of the temperature dependence of the dielectric constant and low frequency mechanical measurements of polycarbonate have shown two major relaxation process above room temperature [19]; a process associated with large scale motion of the polymer chain and a process ascribed to more local reorientation of the phenyl ring structure. An additional relaxation process has been detected in certain samples and is attributed to either changes in morphology or relaxation of strained regions within the sample. More discussion of PC relaxations will follow in section 5.6.2.

The data for the molecules that were available in sufficient quantities for polymeric guest host films to be prepared are summarised in Table 5.2. The CCCT rig enabled

high poling fields to be established across the samples and all the measurements were made within a few minutes of the removal of the field.

Chromophore	MW	N ($x\ 10^{25}\ m^{-3}$)	Host	E_p ($V\mu m^{-1}$)	λ_{max} ($\pm$ 4 nm)	d_{33} (exp) (pmV^{-1})
2 MORPIP	364.48	7.90	PC	96	426	0.19 ± 0.03
1 MORPYROL	352.43	8.17	PC	80	416	0.04 ± 0.02
4 DPDQ	292.38	9.85	PMMA	200	372	0.45 ± 0.09
6 DPDQF	364.34	7.90	PMMA	60	391	0.09 ± 0.04
7 RIGID	267.33	8.08	PC	286	418	0.60 ± 0.20
8 MOR2ALLYL	336.43	10.70	PC	56	435	0.22 ± 0.05

Table 5.2: SHG results for TCNQ derivatives

The experimental d_{33} values were found to be very small which correlates with the low SHG intensities measured in the in-situ poling rig, see section 5.6. In order that comparisons could be made, calculations were performed to estimate the expected d_{33} values for these molecules poled in a PC film.

Chromophore	d_{33} (pmV^{-1}) Experimental	d_{33} (pmV^{-1}) Calculated with CS β_0	d_{33} (pmV^{-1}) Calculated with β_0 (1064 nm) from EFISH	
			$\beta_{0\ acetone}$	$\beta_{0\ chloroform}$
2 MORPIP	0.19 ± 0.03	2.996	2.2 ± 0.2	0.5 ± 0.2
1 MORPYROL	0.04 ± 0.02	NA	1.5 ± 0.3	0.3 ± 0.1
4 DPDQ	0.45 ± 0.09	5.288	2.9 ± 0.4	1.2 ± 0.4
6 DPDQF	0.09 ± 0.04	0.656	0.6 ± 0.1	0.1 ± 0.05
7 RIGID	0.60 ± 0.20	NA	1.6 ± 0.3	NM
8 MOR2ALLYL	0.22 ± 0.05	NA	NM	0.3 ± 0.08

CS = Crystal Structure

NA = Not Available

NM = Not Measured

Table 5.3: Experimental and theoretical d_{33} values of doped films

The two level model [20] was used to extrapolate the $\beta(\omega)$ values expected at 1064 nm from the β_0 value obtained in EFISH experiments and hence calculate the d_{33} values at this wavelength using the orientated free gas model. The experimental poling fields and number densities were employed in the calculation. All the experimental values

were found to be significantly smaller than the calculated values using the free gas model, as shown in Table 5.3. It is also clear that the calculated values of d_{33} are very sensitive to the choice of β_0 employed in the calculations since d_{33} scales linearly with β_0 in the oriented gas model. Calculations involving the crystal structure β_0 show the greatest differences compared to experiment. In the crystal structure, the molecules will experience a large reaction field due to the electrostatic nature of the surrounding molecules in the crystal. It has been shown that β is extremely sensitive to reaction fields in particular and hence the dielectric nature of the environment of the molecule in more general terms. The peak of the absorption band in the UV-Visible spectra of MORPIP in acetone and chloroform are 433 nm and 471 nm respectively. The resonance of the MORPIP doped PC films at 426 nm is closer to the absorption peak in acetone than chloroform. This suggests that, to a rough approximation, the local environment of the MORPIP molecules in PC is more similar to those in acetone and less similar to those in chloroform. Healy *et al* have found that the high reaction fields in the PC host environment may enhance the β of the guest chromophores [21]. It might therefore be expected that comparable hyperpolarisability values will be obtained in acetone and PC. Conversely, Table 5.3 indicates that the d_{33} values obtained from calculations employing the β_0 from EFISH measurements in acetone are not closer in agreement with the experimental values. This would suggest the free gas model does not strictly apply to these systems. The free gas model implicitly neglects all chromophore-chromophore interactions. These types of interactions will become increasingly dominant at larger concentrations of chromophores and hence closer intermolecular distances, and their effects will be more pronounced. Thus concentration dependent studies were performed to investigate the scaling of the nonlinearity with chromophore number density.

5.5.3 Concentration Dependent Studies of Poled Films

In order to compare the maximum weight loading of one of the new TCNQ derivatives with that of a well known material a concentration dependence study for each was carried out. Samples of DAN and MORPIP doped PC films of varying concentrations up to 20 %wt were prepared. MORPIP was chosen as a typical representative of the new TCNQ derivatives. DAN was chosen as its characterisation is well documented

[21-25] and will have similar dispersion characteristics to MORPIP in terms of the two level model.

DAN doped PC films show a linear dependence of d_{33} as a function of concentration as shown in Figure 5.10. The oriented gas model has been used to calculate the expected values of d_{33} as described in Chapter 2, using equation 2.27 where $\chi^{(2)} = 2d_{33}$. For this calculation a value of β_0 for DAN was required. The dipole moment and hyperpolarisability of DAN has been measured by EFISH experiments by Gray *et al* [26]. The measurements were made in the solvent 1,4 dioxane and the EFISH measurements were referenced to a quartz value of 1.1 x 10^{-9} esu (= 0.46 pmV^{-1}) [27]. The results obtained gave a dipole moment of $\mu = 9.2$ D and hyperpolarisability of $\beta_0 = 17 \times 10^{-30}$ esu. However, more recent work has shown the value of quartz susceptibilities to be $d_{11} = 0.3$ pmV^{-1} [16] and this value was used in the SHG of poled polymer films in this work. Therefore the β_0 value had to be scaled according to the different quartz reference measurements. Since EFISH gives susceptibilities that are proportional to the square root of the signal, and directly proportional to the quartz susceptibilities, the β_0 may be scaled according to 0.3/0.46, giving $\beta_0 = 11 \times 10^{-30}$ esu. Using the two level model, the β at 1064 nm was calculated and this was then used to calculate the theoretical d_{33} values according to equation 2.27.

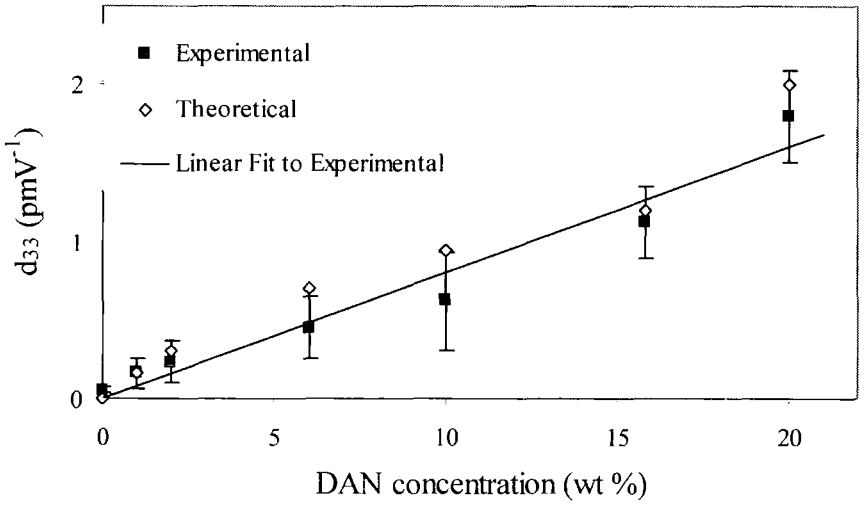

Figure 5.10: d_{33} as a function of weight loading for DAN doped PC films

A good agreement is achieved between the experimental data with this calculation as shown in Figure 5.10. In order that comparisons may be seen between d_{33} values directly, values have not field normalised. However the same poling fields that were achieved in the experiential were used in the calculation of d_{33}. Moreover, the fields were similar for all samples as is demonstrated by the linear fit in Figure 5.10.

The situation is somewhat different however for the MORPIP doped PC films as shown in Figure 5.11. The experimental values are dramatically lower than the calculated values; there an order of magnitude discrepancy between the experimental and the expected value from the free gas model. This may be seen clearly by the different scales used in Figure 5.11. These observations are associated with the effect of dipole-dipole interactions which form aggregate species whose symmetry render them inactive with regard to a second order NLO responses, effectively reducing the active chromophore concentration of the samples.

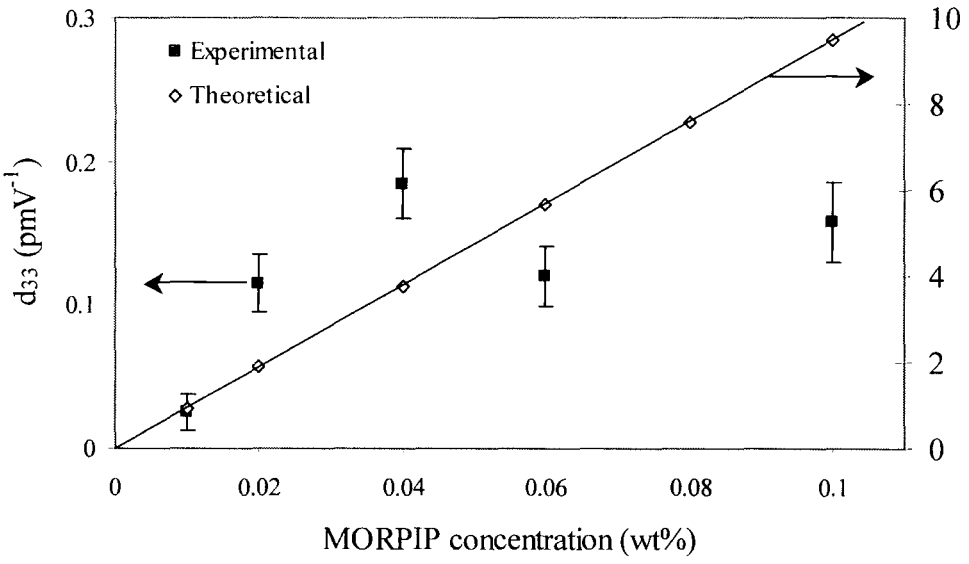

Figure 5.11: d_{33} as a function of weight loading for MORPIP doped PC films

A model for intermolecular interactions proposed by Dalton *et al* [28] has been described in Chapter 2 and applied to EFISH measurements in Chapter 4. This model uses attractive Van der Waals interaction forces to describe the chromophore-chromophore electrostatic interactions. This type of model predicts a deviation from linearity at higher number densities than is shown by experimental data. In the case of

the highly dipolar molecules used in this work, the attractive dispersion interactions in a polymer film are likely to be overwhelmed by stronger electrostatic interactions and the formation of dimers or aggregates.

5.5.4 Alternative Host Studies

In an attempt to address the issue of aggregation, a more polar host was used. EFISH and optical spectroscopy experiments have shown that chromophore-chromophore interactions may be reduced when the molecules are in polar environments. The aim of the study was to attempt to reduce the aggregation effects by increasing the chromophore-host interactions relative to the chromophore-chromophore interactions within the polymer film. Specific interactions between guest and host may increase the magnitude and stability of d_{33} [29] by improving the miscibility and homogeneity of chromophore distribution and poling efficiency. To this end a commercially available polymer, poly 4-vinylpyridine, P-4VP, was studied. P-4VP is a side chain polymer that contains a polar pyridine group directly bonded to the backbone by a single C-C bond and the structure is shown in Figure 5.12. The glass transition temperature of P-4VP has been reported to be 145° C and the dielectric constant has been measured to be $\varepsilon = 2.7$ at room temperature [22]. Thus this polymer has a similar glass transition temperature to poly(bisphenol A carbonate) at 150° C and has a slightly increased polarity relative to poly(bisphenol A carbonate) which has $\varepsilon = 2.5$.

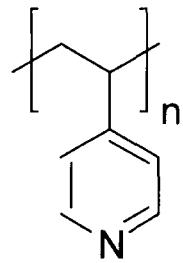

Figure 5.12: Chemical structure of P-4VP

The pyridine group in P-4VP is susceptible to hydrogen bonding with any free hydroxyl group [30]. Since all the TCNQ derivatives studied gave lower d_{33} coefficients than expected from theory, MORPYROL (molecule **1**) was chosen as the test molecule for this study. The structure of MORPYROL contains a hydroxyl group

attached to a pyridine moiety as one of the electron donating groups of the molecule (see Figure 5.3 for the structure). Since hydrogen bonding enhances chromophore separation it was expected that this system would show a decrease in the detrimental effect of dipole-dipole interactions between chromophores at higher concentrations. In addition, since the polymer host is field responsive, coupling of the chromophore to the polymer chain may improve poling efficiency thereby producing an increase in the measured d_{33} coefficient.

A similar study by Banach *et al* [29] has shown an enhancement in the electrooptic coefficient at higher number chromophore density of DR1 doped P-2VP films compared to DR1 doped PMMA films. This was attributed to specific hydrogen bonding interactions between the host and polymer reducing the dipole-dipole interactions of the chromophore.

Thin films of MORPIP doped P-4VP were prepared by spin casting from tetrachloroethane solution (1g of polymer to 5 ml solvent). The samples were then poled in the CCCT rig. However the poling efficiencies were too low at any temperature for any significant SHG intensity to be measured. The low poling efficiency of P-4VP samples by corona poling is not understood although has been reported previously [22]. One possible explanation for the low poling efficiencies may be due to the penetration of ions through the sample such that high fields cannot be obtained. Karakus *et al* [22] have conducted careful poling studies of thin films of P-4VP and have concluded that an increase in the current density of the P-4VP samples leads to a reduction in the effective poling fields and so reduced poling efficiencies.

5.6 In-situ Poling Experiments

The ability to monitor the NLO activity of a polymer film during poling process is an efficient means to learn more about the poling and relaxation processes. The "in-situ" SHG measurement involves measurement of the SHG from the polymer film whilst voltage and heat are applied. One of the main advantages of in-situ poling experiments over the CCCT rig is that this technique allows the SHG to be monitored during the entire poling process and so the poling parameters may be optimised for maximum poling efficiency. The immediate effect of removing the field may also be monitored.

Polymer film samples were prepared as described in Chapter 3 on ITO coated glass slides. Since the sample current was not measured in these in-situ measurements, these substrates were not patterned. The sample under investigation was placed in the corona holder at an angle of 45° between the plane of normal incidence of the sample and the incident laser beam. The laser beam was polarised in the plane of incidence (i.e. *p* - polarised) and the power of the beam was arranged such that adequate SHG was generated without destroying the polymer film. The analyser was arranged so that the SHG was collected in the plane of incidence of the sample (i.e *p* to *p* polarisation geometry was used). Several different experiments were carried out; room temperature experiments where the SHG was monitored as a function of the needle voltage and power of the incident beam and experiments that monitored the SHG as a function of temperature.

5.6.1 Room Temperature Experiments

Glassy polymer films can be poled either above or below the glass transition temperature T_g, if there is sufficient segmental mobility or local free volume in the polymer matrix to allow dopants to orient freely with their dipole moments along the electric field vector. In-situ poling was carried out at room temperature to gain an insight into the different poling characteristics of PC samples doped with different chromophores. Samples of MORPIP and DAN doped PC were prepared to approximately the same concentrations of 4 wt%. In addition a polar polysulphone (polymer 2 in [31]) host was kindly provided by Wang *et al* [31] for these experiments. All the samples were prepared by spin coating from tetrachloroethane (TCE) solutions.

At the outset the optimum needle voltage was determined by measuring the SHG intensity as a function of needle current. A typical plot of the square root of the SHG signal as a function of corona current, I_c, is shown in Figure 5.13. Initially, there is a small offset signal that remains constant until the needle voltages are sufficiently high to produce a corona current. Then the signal is seen to increase in the usual quadratic manner.

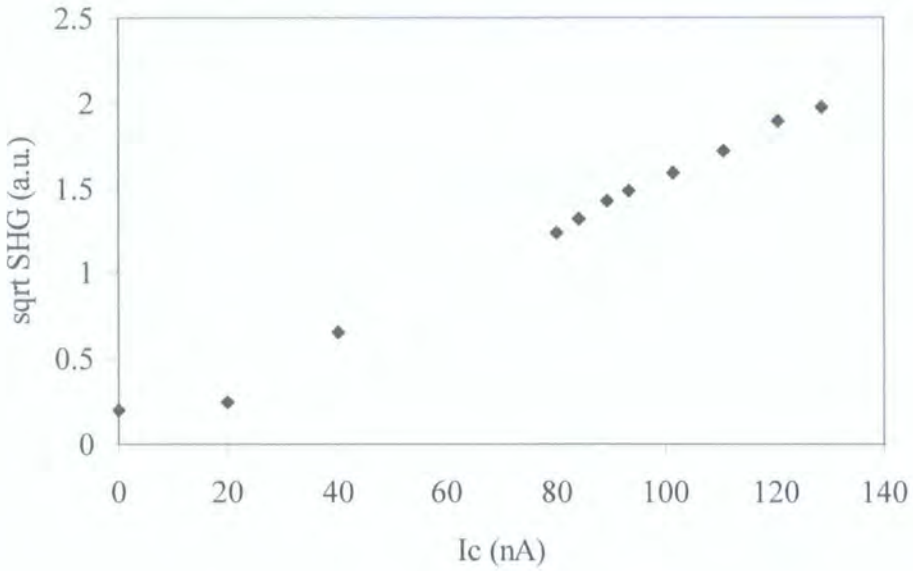

Figure 5.13: SHG signal as a function of corona current for a 4.4% MORPIP doped PC film in-situ experiment

Then the needle voltage was set to an optimum value, typically around 4.5 kV, and the SHG signal monitored as a function of incident power. Once again a linear relationship of the square root of the SHG as a function of incident intensity was observed. The incident intensity and needle voltage were maintained at the optimum values determined in these experiments and a final decay measurement was performed for all the samples.

After 10 minutes of poling at room temperature, the electric field was removed. Removal of the electric field effectively removes the applied driving force for chromophore orientation. Thus chromophores that are located in regions of sufficient mobility are able to rotate out of the imposed orientation and hence a decrease of the SHG intensity was observed. The shapes of the normalised decay curves once the electric field has been removed as shown in Figure 5.14 are significantly different, implying that there is a change in the mechanism of chromophore rotation.

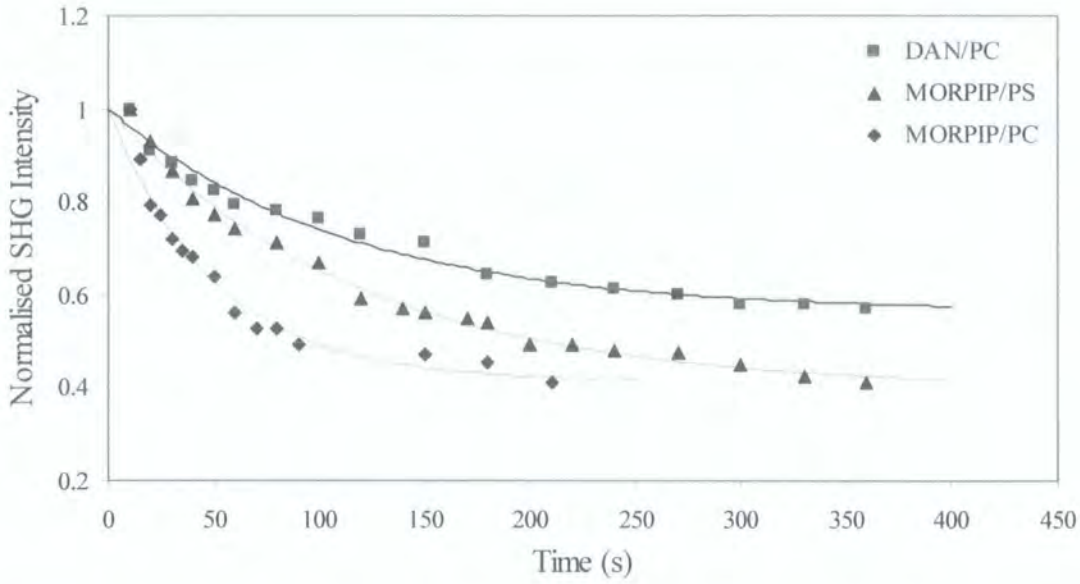

Figure 5.14: Decay of SHG intensity from room temperature poling for three different systems after field is removed. A biexponential decay function, Equation 5.11, was used to fit to the data

Since the decays are highly nonexponential, a single decay time cannot be defined. The decays can generally be described by a stretched exponential [32] (Kohlrausch-Williams-Watts) equation:

$$\left(\frac{I}{I_0}\right)^{\frac{1}{2}} = \exp\left(-\frac{t}{\tau}\right)^{\beta} \qquad 0 < \beta < 1$$

Equation 5.10

Where $(I/I_0)^{1/2}$, is the square root of the normalised SHG intensity and τ is the characteristic relaxation time required for the system to decay to *1/e* of it's initial value. The stretched exponential coefficient β measures the width of the distribution of relaxation times about some central value. A simple exponential decay corresponds to $\beta = 1$. This functional form does not uniquely describe the decays. They can in general be described equally well using the sum of two exponentials [33-35]. Thus, to a first approximation, the decay of the normalised SHG signal can be described by the following biexponential decay:

$$\left(\frac{I}{I_0}\right)^{\frac{1}{2}} = \alpha \exp\left(-\frac{t}{\tau_1}\right) + (1-\alpha)\exp\left(-\frac{t}{\tau_2}\right)$$

Equation 5.11

where $(I/I_0)^{1/2}$, is the square root of the normalised SHG intensity, τ_1 and τ_2 are the relaxation time constants for the fast and slow components and α is a decay constant. Curves based on Equation 5.10 and Equation 5.11 were fitted to the data by a least squares routine. It was found that the biexponential equation gave a better fit and these curves are shown in Figure 5.14. Biexponential equations are often found to give better fits than stretched exponentials when the decay process of the system does not involve many different decay mechanisms. For reference, the constants in Equation 5.11 were found to be $\alpha = 0.563, 0.397, 0.413$, $\tau_1 = 8 \times 10^{10}, 1 \times 10^{11}, 1 \times 10^{13}$ and $\tau_2 = 110, 116, 49.8$ for the DAN/PC, MORPIP/PS and MORPIP/PC films respectively.

The shapes of the decay curves of the SHG intensity vary according to the guest and the host. Firstly, there is a striking difference in the decay of the MORPIP doped PC films to the DAN doped PC films. The films doped with DAN show an increased temporal stability over those doped with MORPIP. Since the polymer host is identical, the differences must be due to the guest chromophores. Previous reports have indicated that enhanced stability of DAN doped PC films may be due to the presence of hydrogen bond formation between the carbonyl moieties of DAN and poly(bisphenol A carbonate) [22, 36]. The MORPIP molecules have no such ability to form hydrogen bonds and thus this may account for the increased decay rate of the signal from MORPIP doped films.

It has also been suggested that hydrogen bonds are not the only source of the temporal stability in DAN doped PC films and that differences in the alignment mechanisms of the polymer also plays an important role [21]. In the study by Healy *et al* [21], restricted motion of dipolar species in PC compared to PMMA was attributed to the slower compensation rate of deposited surface charge by polarisation currents in PC compared to PMMA. The polarisation currents may be dependent not only on the polymer structure but also on the nature of the dipolar species present within the film. Further experiments, such as surface potential, or thermally stimulated discharge current measurements would need to be performed to provide conclusive evidence of differences in charge build up on the polymer films.

The difference in rates of decay for the MORPIP doped into different polymer hosts may be explained in terms of differences in the glass transition temperatures of the two systems. A connection between the chromophore relaxation time and T_g has been suggested such that lifetimes can be improved by higher T_g polymer hosts [7, 37, 38]. The polysulphone, PS, has a relatively high $T_g = 218°$ C [31] compared to PC which has $T_g = 150°$ C. The reason for this phenomenon is generally explained in terms of free volume.

The free volume of a polymer is defined as the unoccupied space in a sample arising from the inefficient packing of disordered chains in the amorphous regions [39]. The free volume is a measure of the empty space available for the polymer to undergo rotation and translation and when the polymer is in a liquid or rubber-like state the amount of free volume will increase with temperature as the molecular motion increases. Conversely, as the free volume collapses with decreasing temperature, the molecular mobility decreases until a critical volume is reached where there is insufficient free space to allow large-scale segmental motion to take place. The temperature at which this critical volume is reached is the glass transition temperature, T_g. Thus in general, the greater the difference between the T_g and the sample temperature, the smaller the amount of free volume present within the sample. However different polymers with similar glass transition temperatures may contain different quantities of free volume even at same the same temperature because free volume partially arises from the disorder and vibrational and rotational motion of the segmental polymer chains. Malhortra *et al* have measured the free volume of polycarbonate and polysulphone by positron annihilation studies [40]. They suggest that the beta and alpha relaxation processes in PC are intimately connected and that the polymer can sustain a larger free volume than found in PS and other glassy polymers.

Another contributing factor to the faster decay of MORPIP in PC than PS may be due to the different conducting properties between the two polymers and differences in the decay of surface charges after field is switched off. Again further experiments of simultaneous measurement of both the SHG signal and the surface potential, as a function of time would give clearer indications of these factors.

5.6.2 Experiments at Increased Temperature

During the electrical poling process dipolar molecules or polymer backbone segments will experience a torque, $\mu E sin\theta$, which tends to align the dipole moments, μ of the polymer segments and the chromophores in the direction of the applied field. As the temperature of the polymer film is raised the viscosity is lowered and various motions and rotations of the polymer and dipolar dopants become possible, depending on the polymer structure and the dipolar nature of the species under torque. Near the polymer T_g the increased torque and reduced viscosity become sufficient for large-scale motions of the polymer chains and for orientation of the NLO chromophores to occur.

Since temperature is clearly an important factor in determining the ease of orientation of the chromophores, experiments were performed to establish the temperature for optimum poling conditions. The SHG intensity indicates that the maximum polar alignment occurs at a temperature below the T_g of the pure polymer host as shown in Figure 5.15. There are two explanations for this phenomenon; firstly doping polymers with guest molecules reduces the T_g of the system by the plasticising effect [22], and secondly as the temperature approaches the T_g, the conductivity of the sample increases [41]. The increased conductivity decreases the effective poling field. Since the doping concentrations were at reasonable levels for these experiments the former description is favoured over the later to explain the lower poling temperatures.

The reduction of T_g due to the plasticising effect is well documented [7, 34, 42, 43]. In particular, Boyd *et al* [44] reported a plasticising effect in azo dye doped PC. They have found that the doping of 30% DR1 into PC depresses the T_g of the host by 85 °C. Similar experiments performed by Healy *et al* result in the T_g reducing from 155 °C to 82 °C for a 20%wt DAN doped PC film. Comparable results were obtained by doping by DAN with weight fractions 5, 10, 15 and 20% in PC reducing the T_g from 150 °C for pure PC, down to 118 °C, 100 °C, 93 °C, 90 °C, respectively [22]. In addition, Karakus *et al* observed that doping PC with the same amount of different size guest molecules (DAN and NMBA) reduces the T_g of the host polymer to the same level [22, 36, 45].

In light of these studies, it seems reasonable to assume that doping PC with MORPIP will also have a plasticising effect on the T_g of the host polymer films. Indeed Figure

5.15 suggests that the maximum SHG intensity is reached well below the T_g of pure PC at around 90° C, which is in accordance with the reduced T_g of DAN doped PC films of similar weight loading. At temperatures close to and above the T_g of the chromophore doped PC the mobility and maximum current flow will occur. Consequently the SHG intensity is seen to fall in Figure 5.15 to near zero due to the increased conductivity. Also, the dipolar guest molecules gain thermal energy as the temperature of the system is increased. At 180° C the induced polar alignment is overcome by the thermal energy of the dipoles. Thus in order to achieve high poling fields the temperature must be optimised. The dipoles must be mobile and able to rotate in high electric fields without the motion being dominated by the randomising thermal effects or the conductivity of the system becoming too great.

Furthermore, dynamic mechanical studies have shown that PC exhibits three relaxation peaks, α, β and γ at 155° C, 80° C and -97° C respectively [46]. The prominent α-relaxation is undoubtedly due to the glass transition. The small broad band β-relaxation is ascribed by Yee and Smith [46] to packing defects or changes in morphology while Reding *et al* attribute motion of the phenyl groups as the origin of the effect. [47]. It has been suggested that γ-relaxation arises from motions involving the displacement of the entire monomer unit [46, 48]. Thus the β-relaxation is probably partly responsible for increased SHG in this study as shown in Figure 5.15. The optimum poling temperature was thus determined to be 90° C and a needle voltage of -4 kV for the MORPIP doped PC samples studied in-situ.

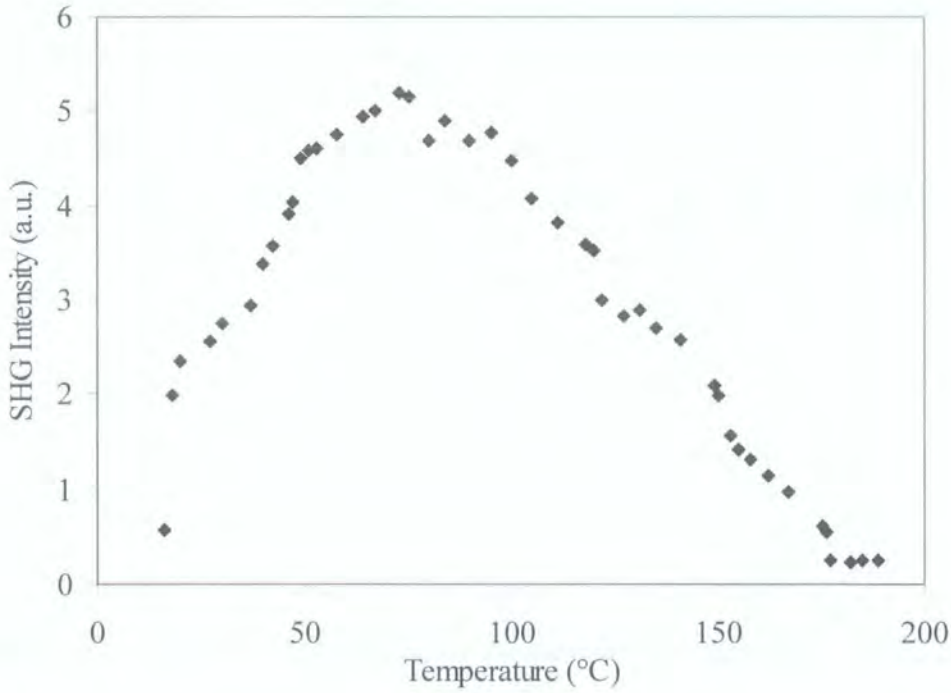

Figure 5.15: Typical curve of SHG intensity as a function of temperature for 8.5 wt% MORPIP doped PC film

Once the optimum poling conditions were established, poling was performed and the SHG intensity monitored in-situ. The shapes of growth of the SHG intensity during the poling for three different films as a function of time are shown in Figure 5.16. At short times, the signal increases as the electric field causes the polar dopants to orient along the field vector. Poling was carried at 90° C for all the samples since this temperature is expected to be near or slightly below the glass transition temperature for these doped systems. The maximum SHG intensity was reached within two minutes of poling for all of the samples.

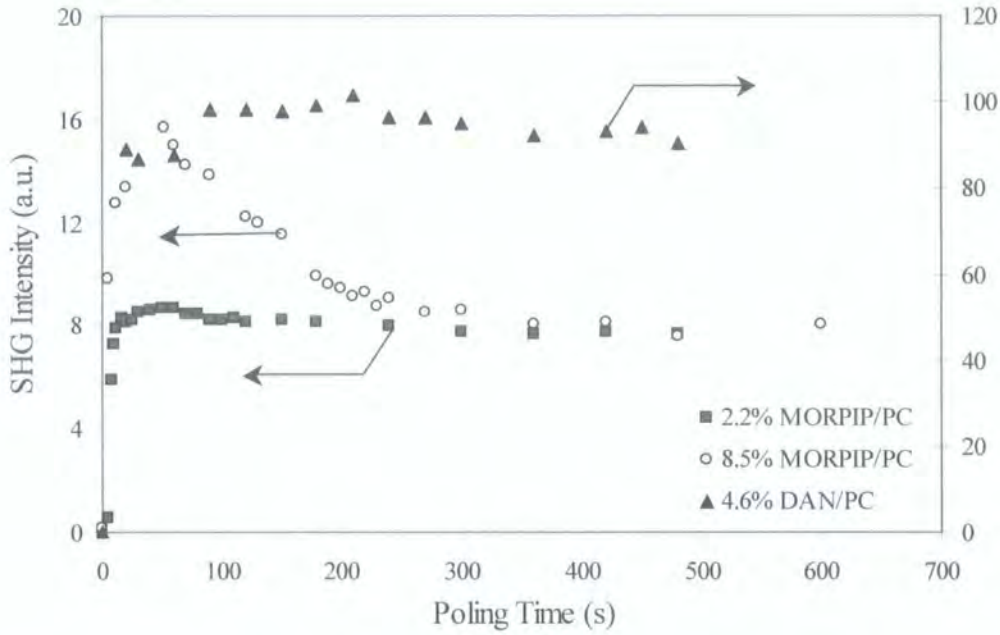

Figure 5.16: In-situ growth of observed SHG intensity of corona poled MORPIP and DAN doped PC films poled at 90 °C.

The growth of the SHG intensity with time is similar during the first two minutes for all three chromophores, with the DAN poling to far higher intensities as shown by the different scale on the second axis of Figure 5.16. This rapid growth of the SHG signal is attributed to the chromophore rotation to align with the electric field.

The magnitude of the SHG intensity from the 8.5% film should be roughly 16 times that of the 2.2 % film if the signal according to standard thermodynamic models where,

$$I \alpha \left[\chi^{(2)}\right]^2 \alpha N^2$$

Equation 5.12

Figure 5.16 shows that the relative intensities between the two films after a few minutes poling is only a factor of two. In addition, the 8.5% doped MORPIP samples showed a very different temporal behaviour during poling: After the initial rise in SHG intensity, a decrease in the signal is observed. The signal continues to decrease until the intensity is the same as that for the 2.2% MORPIP doped film. This feature suggests the poling mechanism is different for the two samples. This may be explained by two processes. The fist process may be charge trapping occurring in the film doped to higher concentrations that lowers the internal poling fields and affects the poling induced alignment. An alternative explanation may suggest the dipolar species are able to

interact over time and dimerisation takes place in the 8.5%film after a few minutes of poling. Such a dimerisation interaction process would render more of the species inactive to second harmonic generation because of symmetry considerations, effectively reducing the number density of active species.

Since the square root of the SHG intensity is proportional to $\chi^{(2)}_{33} = 2d_{33}$, the theoretical d_{33} values for MORPIP and DAN films have been calculated as shown in Table 5.4. As different β_0 were obtained from EFISH measurements for MORPIP, depending on the environment, the values obtained from experiments in acetone and chloroform together with the crystal structure values have been included. The two level model [20] was used to extrapolate the $\chi^{(2)}$ value expected at 1064 nm. For the sake of the calculation, the poling fields, E_p were assumed to be 96 $V\mu m^{-1}$ as in the case of MORPIP films poled in the CCCT rig. The calculations suggest that the SHG intensities of MORPIP will strongly depend on the value of β_0 of MORPIP in the film environment. Indeed theoretical calculations have shown that the nonlinear response of a molecule shows a marked dependence on the dielectric nature of its environment [49]. Previous studies have suggested that the high reaction field present in PC may enhance the molecular properties of the dopants [21].

Dopant	λ_{MAX} (nm)	MW	Wt %	N (x 10^{26} m^{-3})	μ (D)	β_0 (x10^{-30} esu)	$\chi^{(2)}_{33} = 2d_{33}$ (pmV-1)
DAN	373	208.26	4.6	1.6	9.2[a]	11[a]	0.5
MORPIP	426	364.48	8.5	1.7	15.1	54 39 9	12.7 9.3 2.2

(a) Scaled from [26]

Table 5.4: Calculated d_{33} values for DAN and MORPIP doped PC films

The calculations show that even if the lowest β_0 is assumed (from chloroform EFISH data), the SHG signal should be approximately 4 times greater in magnitude for the MORPIP films compared to the DAN films. However the scales in Figure 5.16

indicate that the MORPIP films show intensities that are approximately six times *less* than the DAN doped films. This discrepancy provides evidence of strong aggregation effects in the MORPIP films. The SHG intensity is proportional to the square of the number of nonlinearly active chromophores (for film thickness less than the coherence length) oriented along the field direction. The unexpected lower SHG intensities from the MORPIP doped films may suggest that there are fewer nonlinearly active chromophores in the MORPIP doped films compared to the DAN doped films. Since the poling conditions were identical in all cases, this is attributed to chromophore-chromophore interactions.

The temporal stability of the SHG intensity, shown in Figure 5.17 reflects complex reorientational processes by which chromophore orientations relax to thermodynamic equilibrium or to minimum free volume. Immediately after cooling and removal of the applied electric field all the films showed an initial rapid decay. The origin of the rapid decay may be due to the fast chromophore reorientation [35] or to the dissipation of surface charge thus reducing the field across the sample.

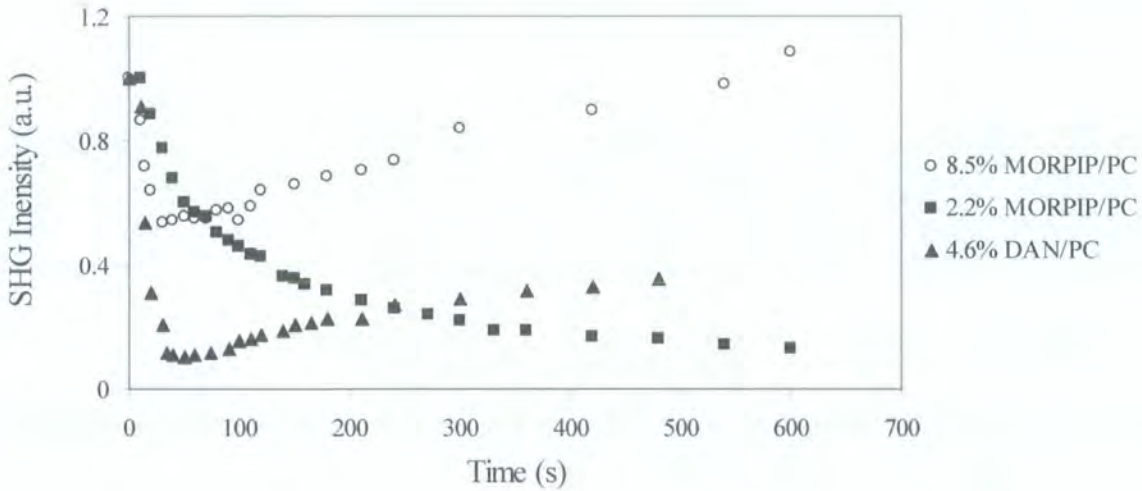

Figure 5.17: Normalised SHG decay curves for MORPIP and DAN doped PC films

These decay curves are different from those at room temperature, in Figure 5.14 compared to Figure 5.17, as there is a steady increase in the SHG after the field is switched off when poled above room temperature. The origin of the steady rise is not clear since it did not occur in all samples as shown in Figure 5.17. The strength of the net poling field gradient may be changing as a function of time due to the decay of sample currents due to trapped charges in the bulk.

The electric fields generated during corona poling arise from the accumulation of free charge trapped on the surface and in the bulk of the film. Pauley *et al* have shown that the lifetimes of charge traps in poling can vary considerably depending on the on the sample poling history [50]. As a result the decay of the poling field after the corona discharge is removed is not instantaneous and, due to the many decay processes involved, can be complicated and prolonged. Remnant fields are therefore common in corona poled samples and can affect the stability of the polar order.

5.7 Optical Spectroscopy of Films

The SHG data suggest that the TCNQ derivative, MORPIP, is prone to strong intermolecular interactions. However, the evidence is not conclusive since the in-situ measurements suggest that the stability of the polar order decays rapidly and depends strongly on the poling conditions. Since these molecules show strong fluorescence that is extremely sensitive to molecular geometry and environment, this was used as a tool to probe the properties of the molecules at increasing concentrations [51].

In general, the excited state of an organic molecule can be created by photoexcitation and fluorescence occurs when radiation is emitted from the excited, E_1 to the ground state, E_0. A schematic shown in Figure 5.18 shows the basic principle of absorption and fluorescence.

The absorption of photons with an energy equal to the resonance condition E_1-E_0 generates a concentration of electronically excited molecules in the sample. This concentration decays to zero as a result of spontaneous emission in the absence of other luminescence quenching processes.

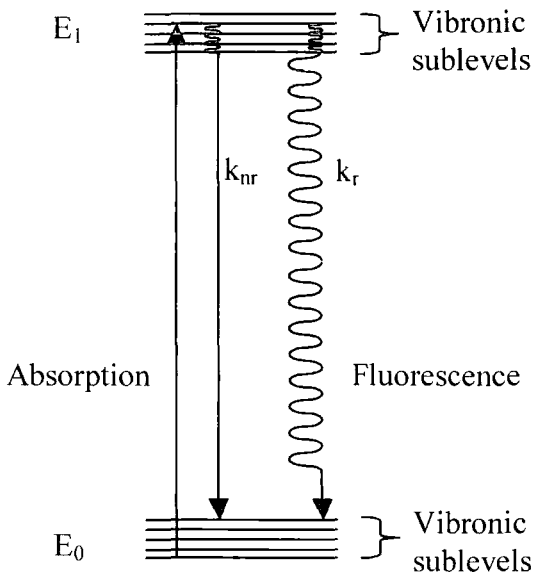

Figure 5.18: Schematic diagram of absorption and fluorescence processes

The spontaneous emission is a random process that follows first order time dependent kinetics [52, 53]. k_r denotes the radiative decay rate constant and k_{nr} includes all other non-radiative decay processes. The rate constants are related to the absorbance properties and the refractive index of the material [52]. All the decay processes follow fist order kinetics so the entire decay process is an exponential decay.

Non-radiative decay processes include internal conversion and intersystem crossing to triplet states. Both of these mechanisms for non-radiative decay are intramolecular transitions. A further mechanism for non-radiative decay is that of intermolecular electronic energy transfer in which an excited sate is transferred from one molecule to another. The dominant mechanism, and probably the most relevant in this case is due to dipole-dipole interactions [54].

The photoluminescent quantum yield, ϕ_f may be defined as [52]:

$$\phi_f = \frac{\text{Number of molecules flourescing per unit time per unit volume}}{\text{Number of quanta absorbed per unit time per unit volume}}$$

Equation 5.13

In terms of intensity this may be re-written as;

$$\phi_f = \frac{I_f}{I_{abs}}$$

Equation 5.14

In turn this may be expressed in terms of rate constants as:

$$\phi_f = \frac{k_r}{k_r + k_{nr}}$$

Equation 5.15

Thus it may be seen that when the non-radiative decay processes are negligible, the photoluminescent quantum yield, ϕ_f will be close to unity (assuming there are no other decay processes) and should not change with the number density of molecules present. However, if the non-radiative decay constant increases with increasing concentration, then according to Equation 5.15, the photoluminescent quantum yield will decrease as a function of number density.

MORPIP doped polycarbonate films of around 3 μm in thickness were spin coated onto quartz substrates for optical spectroscopy. When measuring the photoluminescent quantum yields (PLQY) of films an integrating sphere must be used since excitations can result in waveguide modes within the film. A consequence of this is that the luminescence is not isotropically distributed in all directions. An integrating sphere will collect all the luminescence and overcome this problem of angular distribution of the emission. An integrating sphere is a hollow sphere that has the inner surface coated with a diffusely reflecting material (such as barium sulphate). When a light source is placed in an ideal integrating sphere, the light will be redistributed isotropically over the entire sphere interior surface, regardless of the angular dependence of the emission.

For this reason, PLQY measurements were made using an integrating sphere and a charged couple device and camera spectrograph (CCD). A helium-cadmium laser was used giving an excitation wavelength of 425 nm into the peak of the absorption band for MORPIP doped polycarbonate films. The PLQY's were subsequently measured according to the technique developed by de Mello *et al* [55].

Figure 5.19 shows the photoluminescent quantum yields of the MORPIP doped polycarbonate films as a function of concentration. The line is shown as a guide to the eye. It can be seen clearly that there is a quenching of the PLQY with increasing doping concentration of the guest chromophore, MORPIP. This quenching implies that the films of higher concentrations must posses non-radiative decay mechanisms that are less prevalent in the films of lower concentrations. Since intersystem crossing and triplet states are less likely to change with concentration (as they are intramolecular processes), non-radiative decay mechanisms may result from energy transfer allowing the exciton to recombine non-radiatively at an impurity site [54] caused by aggregates present in the sample. Furthermore, at the low intensities used in this experiment, no triplet states were observed at lower energies.

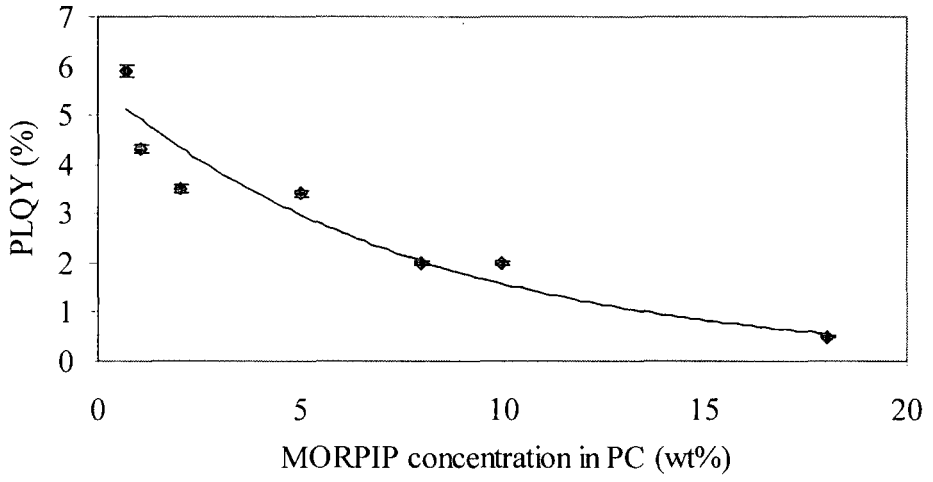

Figure 5.19: Concentration dependent photoluminescent quantum yields (PLQY, % values) of MORPIP doped polycarbonate films

Non-radiative decay mechanisms may occur as a consequence of the presence of dimers or higher order aggregates of the single molecule MORPIP [56]. Since exciton diffusion occurs at a very fast rate ($\sim 10^{-14}$s) compared to the luminescence rate ($\sim 10^{-12}$s), this would allow energy transfer to a defect site. Thus the PLQY experiments as a function of concentration have provided strong evidence for the presence of aggregates forming within the polymer film samples even at low doping levels such as one percent weight loading.

5.8 Summary and Conclusion

New TCNQ derivatives have been studied by means of SHG, electric field poling "in-situ" and PLQY experiments. A constant current corona triode rig has been modified and refined such that uniform fields were distributed over the sample area and accurate determination of the samples current was possible.

According to the free gas model, if electrostatic interactions do not occur, macroscopic optical nonlinearity should scale with $N\beta_{zzz}\langle\cos\theta\rangle$, which is approximated by $N\beta_{zzz}\mu E/5kT$ where μ is the dipole moment, E is the poling field at temperature T, N is the number density of NLO species and β is the molecular hyperpolarisability. d_{33} values obtained from angular SHG scans reveal lower values than those predicted by standard thermodynamic models. In addition the d_{33} values did not increase linearly with number density as expected if no interactions are present. The fundamental nature of the problem of translating microscopic β into large macroscopic nonlinearity has been illustrated in chapter 5 and in figure 5.10.

The molecules in this work have very large dipole moments and have a planar conformation at the TCNQ residue end of the molecule in an attempt to increase the second order FOM. However, the SHG experiments suggest that these are strong contributing factors to the aggregation effect, which reduces the effective active chromophore concentration in the bulk. When comparisons are made with a chromophore with similar dispersion effects and lower $\mu\beta$, these dramatic effects were not observed. The SHG data for MORPIP may be explained in terms of chromophore orientation occurring such that the contribution to the second-order susceptibility is partially cancelled, such as an antiparallel molecular alignment. This configuration minimises the electrostatic energy and results in a cancellation of the second harmonic signal. It is also possible that the molecular hyperpolarisability is diminished on aggregation as a result of electronic coupling of the separate molecules. Since this effect was not observed for a chromophore of lower $\mu\beta$, and the electrostatic dipole-dipole interactions show a μ^4 dependence, it can be seen that the dipolar nature is a strong contributing factor to the aggregation phenomena.

Similar effects have been observed in monolayers of LB films of a hemicyanine dye [57] [58]. In this work, an unexpected large enhancement of SHG from the dye was observed on dilution with an optically passive fatty acid. Girling and co-workers discounted dynamic local field effects and changes in dye orientation as causes for this effect. It was concluded that the larger second order efficiency was related to the film structure. A year later, additional absorption spectra data of these systems indicated a distinct hypsochromically shifted peak in the concentrated films [58]. This band was attributed to H aggregates of the monomer species. Enhanced signals were attributed in part to the resonant enhancement of the monomer compared to the aggregate. Further frequency dispersion measurement studies confirm the presence of these H aggregates and suggest that the aggregate has a much lower intrinsic nonlinearity than the monomer, such that β_0(aggregate) << β_0(monomer) [59]. H aggregation has also been reported in LB films of dyes such as stilbenes and azobenzenes [60, 61]. Chapter 4 has shown that the TCNQ derivatives tend to show a distinctly hypsochromically shifted absorption band on increasing concentration in solution. This may also be attributed to H aggregation occurring in solution. Film spectra did not show such a distinct shift. One suggestion may be the number densities in the film are sufficiently high that molecules are closely packed and interactions dominate even at low film concentrations. The number densities of the films are all much higher than those in the solution measurements. Moreover, since the molecular hyperpolarisability is particularly sensitive to the electronic distribution, an electronic coupling will directly affect the molecular hyperpolarisability of the molecules, thus reducing the second harmonic signal as described.

In addition, in-situ poling experiments suggest that the orientational order decreases rapidly after the field is removed. Polycarbonate is exceptional in that it possess a free volume which is 1.5 times greater than that observed for the majority of polymers [19]. As a consequence, molecules that do not have any guest-host interactions with the polymer may reorient more easily thus allowing the SHG signal to decay rapidly. It has been shown that for hemicyanine dyes the monomer-aggregate varies with processing conditions [59]. It would therefore be plausible to expect that the monomer-aggregate equilibrium of our systems may vary with poling conditions at increased temperatures, further complicating the in-situ experiments.

Finally, PLQY experiments reveal a concentration depended quenching that provides strong evidence that intermolecular energy transfer mechanisms occur in films of moderate concentrations. This further confirms the strong tendency for aggregation formation in these molecules. Such electronic coupling interactions are likely to affect the molecular nonlinearity and the SHG data suggest that the nonlinearity is reduced in the aggregate compared to the monomer species.

5.9 References

1. Burland, D.M., Miller, R.D., and Walsh, C.A., *Second-order nonlinearity in poled-polymer systems.* Chemical Reviews, 1994. **94**(1): p. 31-75.

2. Khanarian, G., Che, T., DeMartino, R.N., Haas, D., Leslie, T., Man, H.T., sansonce, M., Stamatoff, J.B., Teng, C.C., and Yoon, H.N., *Characterization of polymeric nonlinear optical materials.* Proceeding SPIE Advances on Nonlinear Polymers and Inorganic Crystals, Liquid Crystals, and Laser Media, 1987. **824**: p. 72-78.

3. Hayden, L.M., Sauter, G.F., Ore, F.R., Passillas, P.L., Hoover, J.M., Lindsay, G.A., and Henry, R., A, *Second order nonlinear optical measurements in guest host and side chain polymers.* Journal of Applied Physics, 1990. **68**(2): p. 456-465.

4. Mortazavi, M.A., Knoesen, A., Kowel, S.T., Higgins, B.G., and Dienes, A., *Second-harmonic generation and absorption studies of polymer dye films oriented by corona-onset poling at elevated-temperatures.* Journal of the Optical Society of America B-Optical Physics, 1989. **6**(4): p. 733-741.

5. Singer, K.D., Kuzyk, M.G., and Sohn, J.E., *Second-order nonlinear-optical processes in orientationally ordered materials: relationship between molecular and macroscopic properties.* Journal of the Optical Society of America B, 1987. **4**(6): p. 968-976.

6. Sohn, J.E., Singer, K.D., Kuzuk, M.G., Holland, W.R., Katz, H.E., Dirk, C.W., and Schilling, M.L., *Materials for nonlinear optics - orientationally ordered polymer films.* Polymer Engineering and Science, 1989. **29**(17): p. 1205-1208.

7. Stähelin, M., Burland, D.M., Ebert, M., Miller, R.D., Smith, B.A., Twieg, R.J., Volksen, W., and Walsh, C.A., *Reevaluation of the thermal-stability of optically nonlinear polymeric guest-host systems.* Applied Physics Letters, 1992. **61**(14): p. 1626-1628.

8. Freitag, D., Fengler, G., and Morbitzer, L., *Routes to new aromatic polaycarbonates with special material properties.* Angewente Chemie International Edition in English, 1991. **30**: p. 1598-1610.

9. Wan, F., Carlisle, G.O., Koch, K., and Martinez, D.R., *Enhanced 2nd-harmonic response and stability of corona-poled guest-host polycarbonate thin-films.* Journal of Materials Science-Materials in Electronics, 1995. **6**(4): p. 228-234.

10. Gulotty, R.J., Langhoff, C.A., and Bales, S.E., *Nonlinear optical activity of bisphenal A polycarbonate and related copolymers.* SPIE, 1990. **1337**: p. 258-270.

11. Wang, W., Xu, J., Liu, X., Wang, G., and Lu, X., *Second harmonic generation investigation of indium tin oxide thin films.* Thin Solid Films, 2000. **365**: p. 116-118.

12. Ghebremichael, F., Poga, C., and Kuzyk, M.G., *Optical 2nd-Harmonic Characterization of Spontaneous Symmetry- Breaking At Polymer Transparent Conductor Interfaces.* Applied Physics Letters, 1995. **66**(2): p. 139-141.

13. Maker, P.D., Terhune, R.W., Nisenoff, M., and Savage, C.M., *Effects of dispersion and focusing on the production of optical harmonics.* Physical Review Letters, 1962. **8**(1): p. 21-22.

14. Jerphagnon, J. and Kurtz, K., *Maker fringes: detailed comparison of theory and experiment for isotropic and unixial crystals.* Journal of Applied Physics, 1970. **41**(4): p. 1667-1681.

15. Herman, W.N. and Hayden, L.M., *Maker fringes revisited - 2nd-harmonic generation from birefringent or absorbing materials.* Journal of the Optical Society of America B-Optical Physics, 1995. **12**(3): p. 416-427.

16. Shoji, I., Kondo, T., Kitamoto, A., Shirane, M., and Ito, R., *Absolute scale of second-order nonlinear-optical coefficients.* Journal of the Optical Society of America B-Optical Physics, 1997. **14**(9): p. 2268-2294.

17. Sherrod, P.H., *Nonlinear Regressional Analysis Program, NLREG, http://www.nlreg.com/*, . regressional analysis, 1992-1998, Shareware.

18. Hara, T., *Dielectric property of some polymers in low temperature region.* Japanese Journal of Applied Physics, 1967. **6**(2): p. 147-150.

19. Allen, S.G. and Bevington, J.C., *Comprehensive polymer science.* Polymer Properties, ed. S.G. Allen and J.C. Bevington. Vol. Volume 2. 1989, Oxford: Pergamon. 791.

20. Oudar, J.L. and Chemla, D.S., *Hyperpolarisabilities of the nitroanilines and their relations to the excited state dipole moment.* The Journal of Chemical Physics, 1977. **66**(6): p. 2664-2668.

21. Healy, D., Bloor, D., Gray, D., and Cross, G.H., *Stabilized nonlinear optical chromophore alignment in high-Tg guest- host polycarbonates.* Journal of Physics D-Applied Physics, 1997. **30**(22): p. 3079-3084.

22. Karakus, Y., *Second order nonlinear optical properties of poled polymeric thin films*, in *Applied Physics Group*. Ph.D, 1993, Univeristy of Durham: Durham. p. 128.

23. Norman, P.A., Bloor, D., Obhi, J.S., Karaulov, S.A., Hursthouse, M.B., Kolinsky, P.V., Jones, R.J., and Hall, S.R., *Efficient 2nd-harmonic generation in single-crystals of 2-(N,N- dimethylamino)-5-nitroacetanilide.* Journal of the Optical Society of America B-Optical Physics, 1987. **4**(6): p. 1013-1017.

24. Kolinsky, P.V., Chad, R.J., Jones, R.J., Hall, S.R., Norman, P.A., Bloor, D., and Obhi, J.S., *2nd-harmonic generation in single-crystals of 2-(N,N-dimethylamino)-5-nitroacetanilide (Dan) At 1.3 μm.* Electronics Letters, 1987. **23**(15): p. 791-792.

25. Healy, D., Thomas, P.R., Szablewski, M., and Cross, G.H. *Molecular mubeta figure-of-merit studies of solid solutions.* in *SPIE Nonlinear Optical Properties of Organic Materials VIII.* 1995. San Diego.

26. Gray, D., *Molecular organic photonics*, in *Department of Physics*. Ph.D, 1994, Univeristy of Durham: Durham. p. 138.

27. Jerphagnon, J. and Kurtz, S.K., *Optical nonlinear susceptibilities: Accurate relative values for quartz, ammonium dihyrogen phosphate, and potassium dihydrogen phosphate.* Physical Review B, 1969. **1**(4): p. 1739-1744.

28. Harper, A.W., Sun, S., Dalton, L.R., Garner, S.M., Chen, A., Kalluri, S., Steier, W.H., and Robinson, B.H., *Translating microscopic optical nonlinearity into macroscopic optical nonlinearity: the role of chromophore-chromophore electrostatic interactions.* Journal of the Optical Society of America B-Optical Physics, 1998. **15**(1): p. 329-337.

29. Banach, M.J., Alexander, M.D., Caracci, S., and Vaia, R.A. *Enhancement of the electro-optic coefficient of doped films through optimization of chromophore environment.* in *SPIE Conference on Organic Photonic Materials and Devices.* 1999. San Jose, California.

30. Cesteros, L.C., Meaurio, E., and Katime, I., *Miscibility and specific interactions in blends of poly(hydroxy methacrylates) with poly(vinylpyridines).* Macromolecules, 1993. **26**: p. 2323-2330.

31. Douglas, J.E. and Wang, Z., Yuan, *Unsymmetric 1,4-naphthylene-containing polysulfones.* Macromolecules, Rapid Communication, 1996. **17**: p. 795-803.

32. Williams, G. and Watts, D.C., *Non-symmetrical dielectric relaxation behaviour arising from a simple emprical deacy function.* Transactions of the Faraday Society, 1970. **66**: p. 80-85.

33. Hampsch, H.L. and Torkelson, J.M., *Second harmonic generation in corona poled, doped polymer films as a function of corona processing.* Journal of Applied Physics, 1990. **67**(2): p. 1037-1041.

34. Stähelin, M., Walsh, C.A., Burland, D.M., Miller, R.D., Twieg, R.J., and Volksen, W., *Orientational decay in poled 2nd-order nonlinear-optical guest-host polymers - temperature-dependence and effects of poling geometry.* Journal of Applied Physics, 1993. **73**(12): p. 8471-8479.

35. Lindsay, G.A., Henry, R.A., Hoover, J.M., Knoesen, A., and Mortazavi, M.A., *Sub-T_g relaxation behavior of corona-poled nonlinear optical polymer films and views on physical aging.* Macromolecules, 1992. **25**: p. 4888-4894.

36. Karakus, Y., Bloor, D., and Cross, G.H., *Enhanced linear electro-optic response and enhanced stabilitly of thermo-poled "guest-host" polycarbonate thin films.* Journal of Physics D: Applied Physics, 1992. **25**: p. 1014-1018.

37. Weder, C., Neuenschwander, P., Suter, U.W., Prêtre, P., Kaatz, P., and Günter, P., *Orientational relaxation in electric-field poled films from main chain nonlinear optical polyimides.* Macromolecules, 1995. **28**: p. 2377-2382.

38. Man, H.-T. and Yoon, H.N., *The stability of poled nonlinear optical polymers.* Advanced Materials, 1992. **4**(3): p. 159-167.

39. Turnbull, D. and Cohen, M., *Free-volume model of the amorphous phase: glass transition temperature.* The Journal of Chemical Physics, 1961. **34**(1): p. 120-125.

40. Malhortra, B.D. and Pethrick, R.A., *Positron annihilation studies of polycarbonate, polyethersulphone and polysulphone.* Journal of European Polymer, 1983. **19**(6): p. 457-459.

41. Ren, W., Bauer, S., Yilmaz, S., Wirges, W., and Gerhard-Multhaupt, *Optimised poling of nonlinear optical polymers based on dipole-orientation and dipole-relaxation studies.* Journal of Applied Physics, 1994. **75**(11): p. 7211-7219.

42. Wu, J., Valley, J., Ermer, S., Binkley, E., Kenney, J., Lipscomb, G., and R., L., *Thermal-stability of electrooptic response in poled polyimide systems.* Applied Physics Letters, 1991. **58**(3): p. 225-227.

43. Boyd, R.W., *Nonlinear Optics*. 1992, London: Academic Press Inc. 427.

44. Maki, J., J., Malcuit, M.S., Sipe, J.E., and Boyd, R.W., *Linear and nonlinear optical measurements of the lorentz local field.* Physical Review Letters, 1991. **67**(8): p. 972-975.

45. Cross, G.H., Karakus, Y., Gray, D., and Bloor, D., *Cooperative processes in polar ordered polymers.* SPIE vol 1775 Nonlinear optical Properties of Organic Materials V, 1992. **1775**: p. 144-153.

46. Yee, A.F. and S.A., S., *Molecular structure effects on the dynamic mechanical spectra of polycarbonates.* Macromolecules, 1981. **14**: p. 54-64.

47. Reding, F.P., Faucher, J.A., and Whitman, R.D., *Mechanical behaviour of polycarbonates.* Journal of polymer science, 1961. **54**(160): p. S56-S58.

48. O'Gara, J.F., Dejardins, S.G., and Jones, A.A., *Spin relaxation and local motion in four structurally related dissolved polycarbonates.* Macromolecules, 1981. **14**: p. 64-68.

49. Meyers, F., Marder, S.R., Pierce, B.M., and Brédas, J.L., *Tuning of large second hyperpolarizabilities in organic conjugated compounds.* Chemical Physics Letters, 1994. **228**: p. 171-176.

50. Pauley, M.A., Wang, C.H., and Jen, A.K.Y., *Poling dynamics and effects of trapped charge in poled polymer films for nonlinear optical applications.* Macromolecules, 1996. **29**(22): p. 7064-7074.

51. Kagawa, Y., *New tetracyanoquinodimethane chromphores, synthesis and physical properties*, in *Department of Physics*. PhD, 1998, University of Durham: Durham. p. 160.

52. Gilbert, A., Baggott, J., and Wagner, P., J, *Essentials of molecular photochemistry*. 1991, Oxford: Blackwell Scientific Publications. 537.

53. Barltrop, J.A. and Coyle, J.D., *Principles of photochemistry*. 1975, Chichester: John Wiley and Sons. 213.

54. Förster, T.H., *Delocalised excitation and excitation transfer*, in *Light and Organic Crystals*. 1965. p. 55.

55. de Mello, J.C., Wittmann, F.H., and Friend, R.H., *An improved experimental determination of external quantum efficiency.* Advanced Materials, 1997. **9**(3): p. 230-232.

56. Davydov, A.S., *The radiationless transfer of energy of electronic excitation between impurity molecules in crystals.* Phsyics Stat. Sol., 1968. **30**: p. 357-366.

57. Girling, I.R., Cade, N.A., Kolinsky, P.V., Jones, R.J., Peterson, I.R., Ahmad, M.M., Neal, D.B., Petty, M.C., Roberts, G.G., and Feast, W.J., *2nd-Harmonic generation in mixed hemicyanine - fatty-acid langmuir-blodgett monolayers.* Journal of the Optical Society of America B-Optical Physics, 1987. **4**(6): p. 950-955.

58. Schildkraut, J.S., Penner, T.L., Willand, C.S., and Ulman, A., *Absorption and second harmonic generation of monomer and aggregate hemicanine dye in langmuir-blodgett films.* Optics Letters, 1988. **13**(2): p. 134-136.

59. Carpenter, M.A., Willand, C.S., Penner, T.L., Williams, D.J., and Mukamel, S., *Aggregation in hemicyanine dye langmuir-blodgett films: ultraviolet-visible absorption and second harmonic generation studies.* Journal of Chemical Physics, 1992. **96**: p. 2801-2804.

60. Heesemann, J., *Studies on monolayers. 1. Surface tension and absorption spectroscopic measurements of monolayers of surface-active azo and stilbene dyes.* Journal of the American Chemical Society, 1980. **102**(7): p. 2167-2176.

61. Mooney, W.F., Brown, P.E., Russell, J.C., Costa, S.B., Pedersen, L.G., and Whitten, D.G., *Photochemical-reactions in organized assemblies .37. Photochemistry and photophysics of surfactant trans-stilbenes in supported multilayers and films at the air water interface.* Journal of the American Chemical Society, 1984. **106**(19): p. 5659-5667.

Chapter 6 : Conclusions and Closing Remarks

This work contributes to the optimisation of NLO properties of organic chromophores through experimental studies of these properties of a new class of organic chromophore, providing insight into the relationship between the molecular properties and measured macroscopic characteristics.

The dipole moments of these chromophores were measured in dilute chloroform solutions and were found to be very large (8-17 D) which confirmed the highly dipolar nature of these molecules. EFISH measurements of $\mu\beta_0$ were combined with the measured dipole moments to extract β_0 values that in acetone yielded moderate negative values (-17 to -49 x 10^{-30} esu) in agreement with theoretical predictions and resonant enhancement was demonstrated between two wavelengths. In chloroform, however, the extracted β_0 values varied widely (-3 to -46 x 10^{-30} esu) for the molecules studied. Moreover, in terms of the two-level model, resonant enhancement could not account for the discrepancy of the measured $\mu\beta$ between two wavelengths. This anomalous resonance is interpreted in terms of aggregates in solution. Such aggregates are likely to be centrosymmetric and have a zero contribution to the SHG unless the symmetry is broken. The trapping of localised charge by one of the chromophore molecules within the aggregate may break the symmetry. In addition, aggregate species are most likely to have higher order energy levels such that the two-level approximation is no longer valid.

The results of concentration dependent EFISH experiments of MORPIP in chloroform solutions, corrected for absorption, show deviations in linearity of the signal at relatively low concentrations (~2 mmol dm^{-3}). This suggests the presence of aggregates, even within dilute solutions, that do not contribute to the signal in the same way as the free molecules. Indeed when β_0 values are calculated across the concentration range, three distinct regions are observed. Often, β_0 values are merely quoted in the literature with no mention of the concentration. However, the results of

this work suggest that for highly dipolar molecules this approach may not be appropriate and highlights the need for an entire concentration range to be studied if accurate determination of molecular properties is required.

A novel "zero-fringe" calculation has been performed to elucidate values of β_0 that agree with those predicted by theory. This calculation requires a concentration (~1 mmol dm^{-3} of MORPIP in chloroform) for which no fringes could be observed and this method provides an insight into the true magnitude of β_0 of the single molecule. In practice there is a narrow range of concentrations for which no fringes were observed, leading to a range of calculated β_0 values. However, this method is simple and direct and allows calculation from very dilute solutions were the aggregation is expected to be at a minimum.

A model of intermolecular interactions based on van der Waals dispersion interactions has been modified to apply to the EFISH results. The model predicts deviations to occur at higher concentrations than observed by experiment. This would suggest that the interactions occurring in solution for these molecules is extremely strong and cannot be explained in terms of van der Waals forces of attraction alone.

In addition, optical spectroscopy measurements have suggested the presence of a new H-aggregated species in the absorption spectra. The nature of the aggregate has also been shown to be solvent dependent, showing fluorescent properties in tetrachloroethane, but not in chloroform. This suggests different conformational properties of the molecules in different solvents. It is suggested that solvatochromic experiments utilising binary mixtures should be conducted. Such experiments may indicate how the solvents interact with the solute molecules as well as to how the geometry of the molecule and aggregate evolve with increasing solvent polarity.

Since the NLO properties of these TCNQ compounds has not previously been reported, new equipment was first characterised with materials that are well-known and have been studied extensively. Measurements of second harmonic generation of one of the TCNQ derivatives, MORPIP, reveal a strong number density dependence that is not observed for the comparative study of a standard NLO molecule, DAN over the same concentration range. In addition the measured d_{33} values are considerably smaller for

MORPIP than DAN chromophores even though the theoretical molecular hyperpolarisability, β_0, is greater. The dispersion characteristics of the two molecules are similar, however, MORPIP possess a dipole moment that is approximately twice as large as DAN. Since this dramatic effect was not observed for DAN, which is a chromophore of lower $\mu\beta$, and the electrostatic dipole-dipole interactions show a μ^4 dependence, it can be seen that the large dipoles are a strong contributing factor to the aggregation phenomena. Thus, it is suggested that the highly dipolar nature is a strong contributing factor to the aggregation properties of the molecules.

In summary, the magnitude of the SHG response of doped films and EFISH measurements in solution as a function of concentration cannot be explained in terms of electric field induced alignment of isolated chromophore molecules. This leads to the conclusion that the design of organic NLO chromophores is not a matter of synthesising molecules with the correct transparency, high μ and high β. Instead the value of $\mu\beta$ should be optimised to allow efficient poling in polymer films, yet small enough that aggregation is not encouraged to a sever extent. In addition, chromophore shape is expected to play an important role in aggregation effects and the design of future chromophores may include bulky substitituents that do not contribute to the β, but encourage steric hindrance such that aggregation is less energetically favourable.

Fast decay of the orientational order, which is typical of guest-host polymeric systems, has been observed through in-situ poling measurements. If the NLO chromophores were chemically attached to the polymer backbone, this would increase the thermal stability of poled systems. Such polymer systems would also be expected to increase the number density of active NLO species since steric hindrance would help to prevent chromophore-chromophore interactions.

It is clear that further investigation is required before the high nonlinearities of these chromophores may be realised in devices. As such, further characterisation of their properties should continue. Further studies of this aggregation phenomenon should be performed to fully understand the nature of the interactions and so elucidate the necessary steps to avoid such difficulties. Thus, chromophore design is expected to play a major role in these interactions. A natural extension of this fundamental work would be to perform further EFISH experiments that may prove to be insightful if

concentration dependent studies were systematically performed on a variety chromophores with different dipole moments and shapes in different solvents. Circular dichroism experiments would reveal more about the exact nature of the aggregates in solution, such as molecular orientation within the aggregate. Finally light scattering experiments would provide information of the aggregate size.

If these obstacles were to be overcome, the class of materials investigated during the course of this research would be strong contenders for possible device applications such as electro-optic modulators in local area networks.

Publication List

Hackman, N.A. *Alignment and aggregation studies of highly dipolar TCNQ adducts in guest-host systems*. in *SPIE, The International Society for Optical Engineering*. 2000. San Diego, USA.

Kagawa, Y., Szablewski, M., Ravi, M., **Hackman, N.-A**., Cross, G.H., Bloor, D., Batsanov, A.S., and Howard, J.A.K., *Polar TCNQ adducts for nonlinear optics.* Nonlinear Optics, 1999. **22**: p. 235-240.

Ravi, M., Szablewski, M., **Hackman, N.-A**., Cross, G.H., Bloor, D., Goeta, A.E., and Howard, J.A.K., *Crystal structures of amino substituted dicyanoquinodimethanes with potential nonlinear optical applications.* New Journal of Chemistry, 1999. **23**: p. 841-844.

Appendix II

Substrate Preparation

The conductive coated indium tin oxide (ITO) glass substrates were patterned to give a circular ground plane area of diameter 18 mm with a surrounding guard ring, to ensure accurate determination of the sample current. Glass sheets coated with ITO were cut into 25 x 25 mm squares and washed with acetone. The substrates were covered in a photo-resist through a mask pattern, defined by photolithography, of the guard ring arrangement. The guard ring pattern is shown in Chapter 3, Figure 3.7. The substrates were then etched, before being cleaned prior to sample preparation. The photo-resist patterning procedure will now be described.

AI.1 ITO Patterning Procedure

The ITO coated glass squares were dried on a hot plate at 120 °C for 30 minutes. Then a photo-resist was spin coated onto the substrate (Shipley, microposit S1813) at 4000 rpm for 30 seconds to give a thickness of approximately 1.3 μm. A hotplate was then used to bake the substrate for 30 minutes at 80 °C. A mask was made from a Kodak high resolution glass plate patterned using red coated "cut and strip" acetate. The photo-resist coated sample was then exposed through the mask to a 200W mercury arc lamp for 10 seconds. The light from the lamp softens the exposed photo-resist. The sample was then developed for 20 seconds (Hoechst , AZ351 B developer) before drying with a hot air gun.

AI.2 ITO Etching Procedure

The etching solution was prepared according to the Balzers catalogue, coatings for flat panel displays, ref. no. FO3O Rev. (951004), p.11. However, a series of trial and error experiments had to be performed before the correct conditions for complete, but not over etching were determined: Any excess photo resist was removed prior to etching with a scapal blade to ensure that the outer ring was separate from the inner. The following solution was made up and then gently heated to around 60°C:

200 ml Concentrated hydrochloric acid > 32%
10 ml Nitric acid vol. 70% AR Grade.
250 ml Deionised water

The photo-resist coated substrates were then submerged in the heated etching solution for 50 seconds. No agitation was required. A multimeter was used to check that the inner and outer rings of ITO were completely separated before removing the photo resist with acetone.

AI.3 Substrate Cleaning Procedure

In order to produce films of a high optical quality, the substrates must be completely free of all contaminants and so a procedure was developed for the cleaning of substrates. Firstly, polymer was removed from 're-used' substrates by placing them in a solution of the original solvent used in the sample preparation in a sonic bath for 10 minutes. This was followed by a second 'base bath' solution consisting of a saturated solution of sodium hydroxide and water with ethanol and left in a sonic bath for 30 minutes. Once this had been completed it was possible to remove any remaining polymer by washing the substrates with soap and de-ionized water. Acetone was then used to remove any grease that was left on the substrates and they were wiped with a piece of lint free cloth. The final cleaning procedure which was performed just before the sample preparation. Silica substrates were immersed in concentrated sulfuric acid for a few minutes before rinsing with de-ionized water and drying with a nitrogen gun. However, the ITO coated substrates needed a different procedure as the acid reacts with ITO layer. This second procedure involved the substrates being immersed in a fresh solution of the 'base bath' and left in the sonic bath for about 15 minutes. Upon removal from the bath, the substrates were given a final rinse with de-ionized water and were dried using a nitrogen gun.

Appendix II

Procedure for synthesis of 7-(2,6, dimethylmorpholino)-7-(4-methyl piperidino)-8,8, -dicyanoquinodimethane, MORPIP (molecule 2)

The synthetic procedures for all the TCNQ derivatives described in this work were developed by M. Szablewski and M. Ravi in Durham. Both NMR and mass spectroscopy confirmed the structure of the chromophores and their purity was estimated by thin layer chromatography. Once the procedure had been established and the elemental analysis completed, the representative molecule MORPIP (molecule **2**) could be synthesised by myself and the method is described here.

3.020 g (0.048 moles) of TCNQ powder was added to 500 ml tetrahydrafuran (THF) in a 2 neck round bottom flask fitted with a water condenser. The solution was stirred with heating at ~50 °C for 2 hours to allow full dissolution of the TCNQ resulting in a greenish yellow solution.

1.734 g (0.015 moles) of 2,6, dimethylmorpholine (Aldrich) was weighed out and mixed with a few ml of THF. The solution was carefully added to the warm TCNQ solution using a dropping pipette. After about 30 minutes of continued heat and stirring the solution turned a purple colour and was left to stir whilst heating for a further 2 hours, before the heat was switched off and the solution was allowed to cool to room temperature overnight. The inky purple solution was then evaporated under vacuum. After about 15 minutes a green powder coated the inside of the flask. This was subsequently dissolved in acetonitrile and the solution was recrystallised from a minimum volume. The purple crystals (0.8g, 18% yield) were thoroughly washed in ether before drying under vacuum over night.

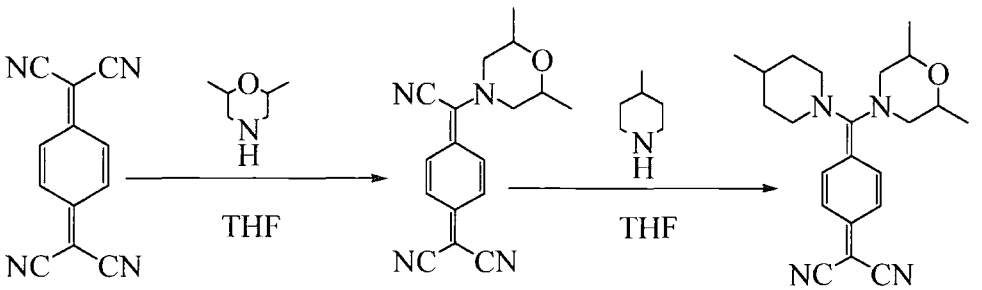

TCNQ | ***Mono-Morpholine*** | ***MORPIP***

$C_{12}H_4N_4$
Exact Mass: 204.04
Mol. Wt.: 204.19
C, 70.59; H, 1.97; N, 27.44

$C_{17}H_{16}N_4O$
Exact Mass: 292.13
Mol. Wt.: 292.34
C, 69.85; H, 5.52; N, 19.17; O, 5.47

$C_{22}H_{28}N_4O$
Exact Mass: 364.23
Mol. Wt.: 364.48
C, 72.50; H, 7.74; N, 15.37; O, 4.39

Figure 1: Schematic of synthesis of MORPIP

A solution of (cis/trans) 7-(2,6, dimethylmorpholino)-7,8,8,-tricyanoquinodimethane, monomorpholine, (0.4g, 1.36 mmol) in THF (30 ml) was warmed in a two-necked flask with a water condenser at 50 °C for 30 minutes to ensure complete dissolution. 4-methyl piperidine (0.2g, 2 mmol) was then carefully added and the solution was left to stir for a further 30 minutes at 50 °C. The yellow product was observed to precipitate and the solution was cooled to room temperature and stirred for a minimum of one hour or ideally overnight. The yellow precipitate was collected by filtration and dried under vacuum. Recrystallisation of the yellow solid was carried out with hot acetonitrile. The yellow crystals (0.24g, 33% yield) were washed with ether and allowed to dry overnight under vacuum.

Appendix III: Fitting Program for SHG Data

The theoretical analysis of the second harmonic generation is based upon that of Herman and Hayden [1]. To analyse the data, a nonlinear regressional analysis [2] program was developed. This program fits data from the angular scan to extract the physical quantities. As the mathematics has been dealt with, this section will present the non-linear regression program that has been developed to fit data. The second harmonic intensity was recorded as a function of sample rotation angle. A typical set of data and fit is shown in Chapter 5, Figure 5.9. This program finds $R=d_{31}/d_{33}$ by fitting angular dependent term in Equation **8** in reference [1] to the data. A similar program was then used with this value of R to evaluate the d_{33} value by comparison with quartz standard d_{33} and measured quartz peak intensities.

```
TITLE "Maker Fringe Fitting Program";

                                        ANGLETYPE Radians;

VARIABLE THETAD;
VARIABLE I;
                                                    //Values set by
                                                    experiment//

CONSTANT n1 = 1.495;
                                                    //Refractive index of
                                                    film at 1064 nm//

CONSTANT n2 = 1.510;
                                                    //Refractive index of
                                                    film at 532 nm, i.e. SH//
CONSTANT n2S = 1.51947;

                                                    //Refractive index of
                                                    glass substrate at SH//
CONSTANT L = 0.0000033;

CONSTANT nd=2;                                      //Film thickness (m)//
```

```
CONSTANT LAMBDA = 0.000001064;                    //ND_Filter in front of
                                                  PMT during quartz
                                                  reading//

CONSTANT a1 = 0;                                  //Fundamental λ (m)//
CONSTANT a2 = 3030;

PARAMETER A;
Parameter R=0.2;                                  //Absorption
Constrain R=0.001, 0.333333333;                   coefficient. At
                                                  1064nm//

ITERATIONS = 100;
SWEEP R = 0.001,0.4,0.01;

DOUBLE
tw,t0,t2w,THETA,THETA1,THETA2,C1,C2,C2S,d1,d2,PSI,CHI;

#INCLUDE "THETA.NLR";
#INCLUDE "FUNC1.NLR";
#INCLUDE "FUNC2S.NLR";
#INCLUDE "FUNtw.NLR";
#INCLUDE "FUNt0.NLR";
#INCLUDE "FUNt2w.NLR";
#INCLUDE "THETA1.NLR";
#INCLUDE "THETA2.NLR";
#INCLUDE "FUNC2.NLR";
#INCLUDE "FUNd1.NLR";                             //Function statements
#INCLUDE "FUNd2.NLR";                             found in separate files//
#INCLUDE "FUNPSI.NLR";
#INCLUDE "FUNCHI.NLR";


FUNCTION I =                                      // Fitting equation 8. //
A*(((tw)^4)*((t2w)^2)*((t0)^2)*(R*COS(THETA2)*SIN(2*THETA1)+R
*SIN(THETA2)*(COS(THETA1))^2+SIN(THETA2)*(SIN(THETA1))^2
)^2*EXP(-2*d1-2*d2)*((SIN(PSI))^2+(SINH(CHI))^2)/((
(C2)^2)*((PSI)^2+(CHI)^2)) );

RPLOT;
NPLOT;
```

POUTPUT "C:/nancy/fitting/bm2pp.dat";	**// Output Data files //**
OUTPUT TO "C:/nancy/fitting/bm2pp.out" THETA,I,PREDICTED;	**// Output Curve files //**
DATA "C:/nancy/fitting/bm2pp.TXT";	

AIII.1References

1. Herman, W.N. and Hayden, L.M., *Maker fringes revisited - 2nd-harmonic generation from birefringent or absorbing materials.* Journal of the Optical Society of America B-Optical Physics, 1995. **12**(3): p. 416-427.

2. Sherrod, P.H., *Nonlinear Regressional Analysis Program, NLREG, http://www.nlreg.com/*, . regressional analysis, 1992-1998, Shareware.